AD-A274 639

FERRITE PHASE SHIFTERS USING STRESS INSENSITIVE MATERIALS

FINAL REPORT

PERIOD COVERED:   JULY 1991 TO JULY 1993

CONTRACT NO. N00014-91-C-2202

CDRL B003

EMS JOB NO. 15638

PREPARED FOR:

NAVAL RESEARCH LABORATORY
4555 OVERLOOK AVENUE, S.W.
WASHINGTON, D.C.  20375-5000
DR. DENIS WEBB, COTR

DTIC
ELECTE
JAN 10 1994
S B D

PREPARED BY:

EMS TECHNOLOGIES, INC.
AN ELECTROMAGNETIC SCIENCES COMPANY
P. O. BOX 7700
660 ENGINEERING DRIVE
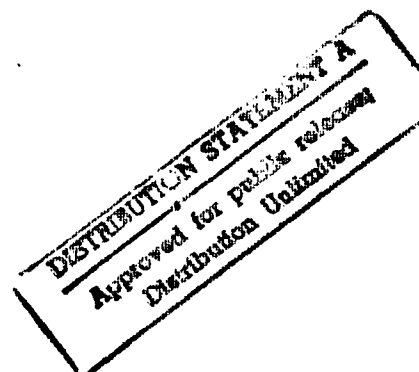TECHNOLOGY PARK / ATLANTA
NORCROSS, GA 30091-7700

94-00888

OCTOBER 1993

EMS
EMS TECHNOLOGIES, INC.
An Electromagnetic Sciences Company

94 1 7 325

# REPORT DOCUMENTATION PAGE

| 1a. REPORT SECURITY CLASSIFICATION <br> UNCLASSIFIED | | 1b. RESTRICTIVE MARKINGS | |
|---|---|---|---|
| 2a. SECURITY CLASSIFICATION AUTHORITY | | 3. DISTRIBUTION / AVAILABILITY OF REPORT <br><br> UNLIMITED | |
| 2b. DECLASSIFICATION / DOWNGRADING SCHEDULE | | | |
| 4. PERFORMING ORGANIZATION REPORT NUMBER(S) <br> EMS Job No. 15638, CDRL B603 | | 5. MONITORING ORGANIZATION REPORT NUMBER(S) | |
| 6a. NAME OF PERFORMING ORGANIZATION <br> EMS Technologies Inc. | 6b. OFFICE SYMBOL <br> (If applicable) | 7a. NAME OF MONITORING ORGANIZATION <br> Naval Research Laboratory | |
| 6c. ADDRESS (City, State, and ZIP Code) <br> P. O. Box 7700 <br> Norcross, Georgia 30091-7700 | | 7b. ADDRESS (City, State, and ZIP Code) <br> 4555 Overlook Avenue, S.W. <br> Washington, D. C. 20375-5000 | |
| 8a. NAME OF FUNDING / SPONSORING ORGANIZATION | 8b. OFFICE SYMBOL <br> (If applicable) | 9. PROCUREMENT INSTRUMENT IDENTIFICATION NUMBER <br> Contract No. N00014-91-C-2202 | |

| 8c. ADDRESS (City, State, and ZIP Code) | 10. SOURCE OF FUNDING NUMBERS | | | |
|---|---|---|---|---|
| | PROGRAM ELEMENT NO. | PROJECT NO. | TASK NO. | WORK UNIT ACCESSION NO |
| | | | | |

**11. TITLE (Include Security Classification)**
Ferrite Phase Shifters Using Stress Insensitive Materials

**12. PERSONAL AUTHOR(S)**
Todd Vaughn, Paul Cox, Gordon Harrison, Pete Rodrigue

| 13a. TYPE OF REPORT <br> Final | 13b. TIME COVERED <br> FROM 7-91 TO 7-93 | 14. DATE OF REPORT (Year, Month, Day) <br> 1993, July | 15. PAGE COUNT |
|---|---|---|---|

**16. SUPPLEMENTARY NOTATION**

| 17. COSATI CODES | | | 18. SUBJECT TERMS (Continue on reverse if necessary and identify by block number) |
|---|---|---|---|
| FIELD | GROUP | SUB-GROUP | Ferrite Phase Shifters, Stress Insensitive Materials |
| | | | Manganese Substitution in Garnets, Magnetostrictive, |
| | | | Stresses in Ferrite Phasers. |

**19. ABSTRACT (Continue on reverse if necessary and identify by block number)**
This R&D program sponsored by the Naval Research Laboratory and being conducted by EMS Technologies, Inc., Norcross, Georgia, is focused toward achieving improved performance in microwave switching components via use of "stress insensitive" microwave ferrite materials for applications where stable hysteresis characteristics of the materials are critical to the RF performance. The program, therefore, primarily addresses how to relieve or improve the magnetostrictive characteristics of the materials with emphasis on the specific application and demonstration of these materials in microwave switching components, particularly ferrite toroidal phase shifters. Material investigations were focused on $Mn^{+3}$ substitutions in Yttrium-gadolinum iron garnet. These compounds were evaluated in dual toroid waveguide phase shifter structures with temperature, pressure & Rf power as variables. Manganese substitution per formula unit for $Fe^{+3}$ of 0.11 to 0.13 (2.2 to 2.6%) produced compounds which exhibited stable performance from magnetostrictive stresses in phaser structures.

| 20. DISTRIBUTION / AVAILABILITY OF ABSTRACT <br> ☒ UNCLASSIFIED/UNLIMITED ☐ SAME AS RPT. ☐ DTIC USERS | 21. ABSTRACT SECURITY CLASSIFICATION <br> UNCLASSIFIED | |
|---|---|---|
| 22a. NAME OF RESPONSIBLE INDIVIDUAL | 22b. TELEPHONE (Include Area Code) <br> 404-263-9200 | 22c. OFFICE SYMBOL |

**DD FORM 1473, 84 MAR**                83 APR edition may be used until exhausted. <br> All other editions are obsolete.

**FERRITE PHASE SHIFTERS USING STRESS INSENSITIVE MATERIALS**


FINAL REPORT

PERIOD COVERED:   JULY 1991 TO JULY 1993

CONTRACT NO. N00014-91-C-2202


CDRL B003

EMS JOB NO. 15638


PREPARED FOR:

NAVAL RESEARCH LABORATORY
4555 OVERLOOK AVENUE, S.W.
WASHINGTON, D.C.   20375-5000
DR. DENIS WEBB, COTR


PREPARED BY:

EMS TECHNOLOGIES, INC.
AN ELECTROMAGNETIC SCIENCES COMPANY
P. O. BOX 7700
660 ENGINEERING DRIVE
TECHNOLOGY PARK / ATLANTA
NORCROSS, GA 30091-7700


OCTOBER 1993

## PREFACE

This R&D program has been conducted as a Phase I (first year) and Phase II (second year) effort. A Final Report, dated June 11, 1992, was generated to document the investigations and results of Phase I. This report covers the entire two year R&D program but, where appropriate, only summarizes some of the data and results presented in detail in the Phase I Final Report.

DTIC QUALITY INSPECTED 8

# TABLE OF CONTENTS

## 1.0    INTRODUCTION AND PROGRAM OBJECTIVES

### 1.1    INTRODUCTION

This R&D program sponsored by the Naval Research Laboratory and conducted by Electromagnetic Sciences, Inc., Norcross, Georgia, focused on achieving improved performance in microwave switching components via use of "stress insensitive" microwave ferrite materials for applications where stable hysteresis characteristics of the materials are critical to the RF performance. The program therefore primarily addressed how to relieve or improve the magnetostrictive characteristics of the materials with emphasis on the specific application and demonstration of these materials in microwave switching components, particularly ferrite toroidal phase shifters.

### 1.2    PROGRAM OBJECTIVES

The overall technical objective of this program was to improve the performance of microwave switching components using stress insensitive ferrite materials. Ferrite compounds exhibiting minimum stress sensitive hysteresis properties were to be "molecularly engineered" and processed into toroidal structures to demonstrate improved performance in high power, high accuracy microwave ferrite toroidal phase shifters.

The investigative program included further analysis of the molecular and physical mechanisms which appear to influence and/or control the stress sensitive characteristics of the cubic ferrimagnetic compounds of interest (emphasis focused on the ferrimagnetic garnet compounds). The magnetostrictive characteristics were related to the molecular crystalline structure and "molecular engineering" techniques were utilized to minimize (compensate) the dominant magnetostrictive constants. The analysis included the relative importance and magnitude of the magnetocrystalline anisotropy to magnetostrictive anisotropy. Compounds formulated were based on these analyses, and the material compositions prepared, processed and evaluated. Iteration of this cycle was implemented where appropriate. The material

- 4 -

properties were evaluated not only for stress insensitive hysteresis characteristics but also for acceptable microwave and magnetic properties supportive to toroidal phase shifter applications. A specific compound was generated as optimized for high power phase shifter application and demonstrated in the X-band frequency region.

The goal of the investigative effort was to demonstrate high power, high accuracy, stress insensitive dual toroid waveguide ferrite phase shifters over the 7 to 11 GHz frequency region with results applicable to structures covering the 6 to 18 GHz frequency region. A breadboard model of the X-band phaser was fabricated to demonstrate performance advancements achieved. Stress sensitivity was fully evaluated for phase states corresponding to minor hysteresis loop operation.

## 1.3    PROGRAM TECHNICAL TASKS

### 1.3.1    Selection of Baseline Test Vehicle

An existing X-band phase shifter was selected as a test vehicle with the concurrence of the NRL COTR. The stress sensitivity of the RF performance of this phase shifter was to be characterized and improved. Typical performance goals for this baseline phase shifter are as follows:

| | |
|---|---|
| Frequency: | 7 to 11 GHz |
| RF power (peak/average): | 5 kW/300 watts |
| Temperature range: | -10 to 80 °C |
| Accuracy: | four bits |

### 1.3.2    Analytical Phaser Model Studies

An analytical phaser model was to be established and utilized to predict performance with stress insensitive materials.

### 1.3.3  Materials Preparation and Characterization

Promising stress insensitive materials compositions were prepared and the physical, magnetic and electrical properties of these compounds characterized. "Static" stress sensitivity tests with both near-saturated and minor loop operation were conducted.

### 1.3.4  RF Evaluation

The most promising materials were selected for RF evaluation. These materials were characterized in an RF waveguide phaser structure as a function of frequency, temperature and RF power. The performance achieved was compared with that of the baseline test vehicle.

This phase shifter test vehicle with driver was provided to NRL for evaluation.

## 2.0  BACKGROUND DISCUSSION ON REMANENT STATE FERRITE PHASERS, REMANENT MAGNETIZATION AND MAGNETOSTRICTION

## 2.1  REMANENT STATE FERRITE PHASERS

Microwave ferrite digital phase shifters utilize ferrite toroidal structures and the hysteresis properties (square loop characteristics) of the ferrite for their operations.

The phase shifters are constructed in waveguide using either a single toroid or a dual toroid configuration. These structures are shown in Figures 2-1, 2-2, and 2-3.

The ferrite toroid fully fills the waveguide from top to bottom. The designs must include features that prevent any gaps at the top or bottom of the waveguide-ferrite interface. This generally requires that the ferrite toroid be captured in the structure with a slight "crush" from top to bottom. This is often implemented in a structure by a design approach referred to as a "soft" top. The top of the waveguide channel is either made from soft metal or is thin enough to flex slightly, or both.

The insertion phase length of the structure is dependent on the remanent magnetization of the ferrite (see the hysteresis loop shown in Figure 2-4). The toroids are threaded with a switching wire as shown in Figures 2-2 and 2-3, and the insertion phase length is changed by switching the ferrite to different remanent states. This switching operation provides a controlled differential phase shift. A 360 degree differential phase shift is achieved by selecting the magnetization of the material and the length of the toroid used.

The remanent magnetization ($4\pi M_r$) and the saturated value ($4\pi M_s$) change with temperature, and the RF design and material are selected for operation over a specified temperature range. The RF power of operation is also an influence on the design and resultant performance.

- 7 -

HI DIELECTRIC CENTER SLAB

FERRITE SLABS

M

M

H

H
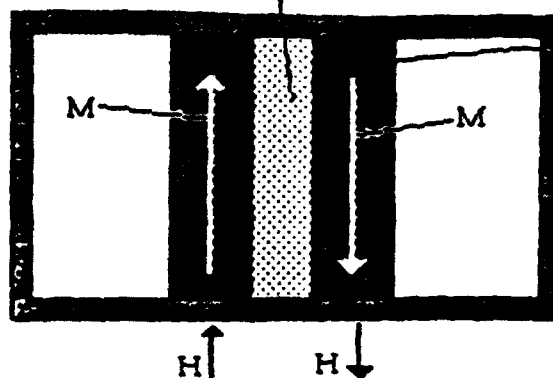
## a. TWIN SLAB PHASE SHIFTER

SWITCHING WIRE

HI DIELECTRIC CENTER CORE

FERRITE TOROID
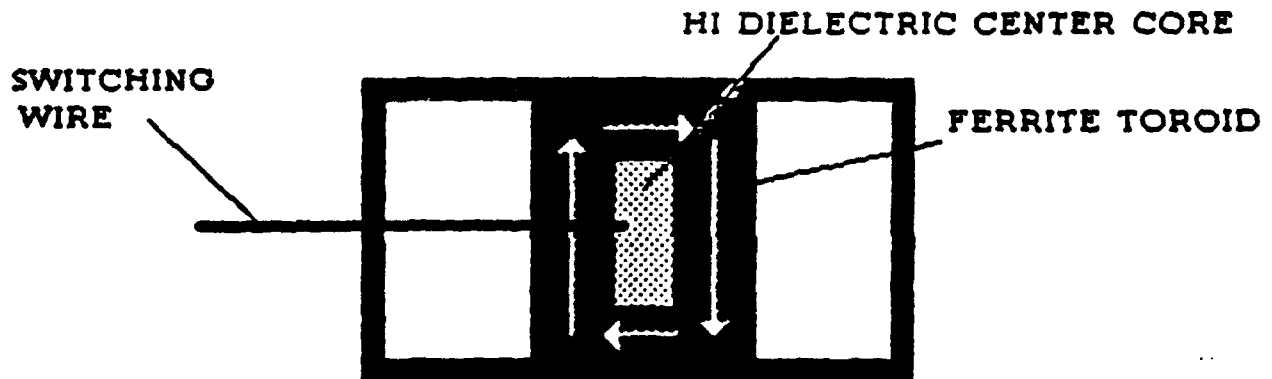
## b. SINGLE TOROID PHASE SHIFTER
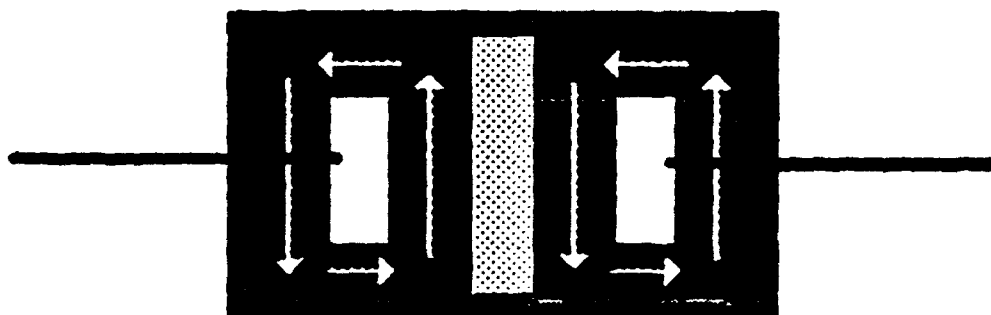
## c. DUAL TOROID PHASE SHIFTER

FIGURE 2-1: Phase Shifter Configurations
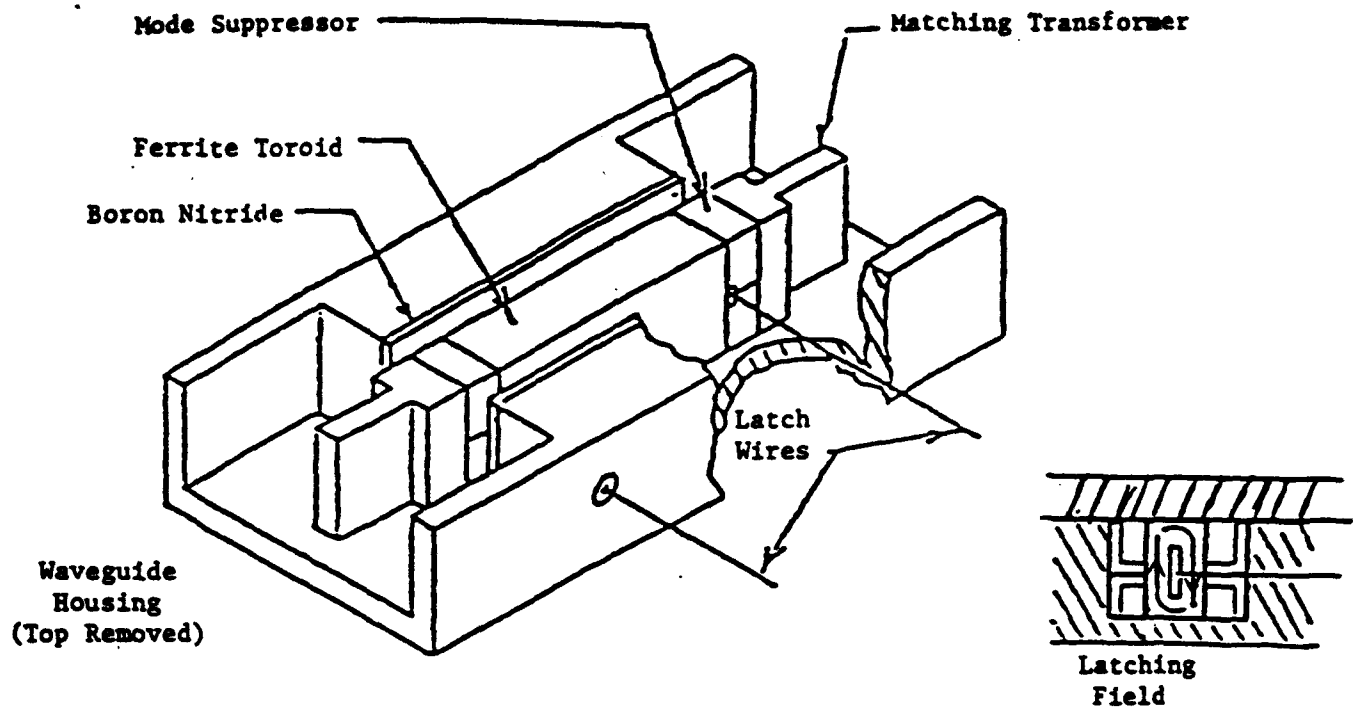
FIGURE 2-2:   Single Toroid Design
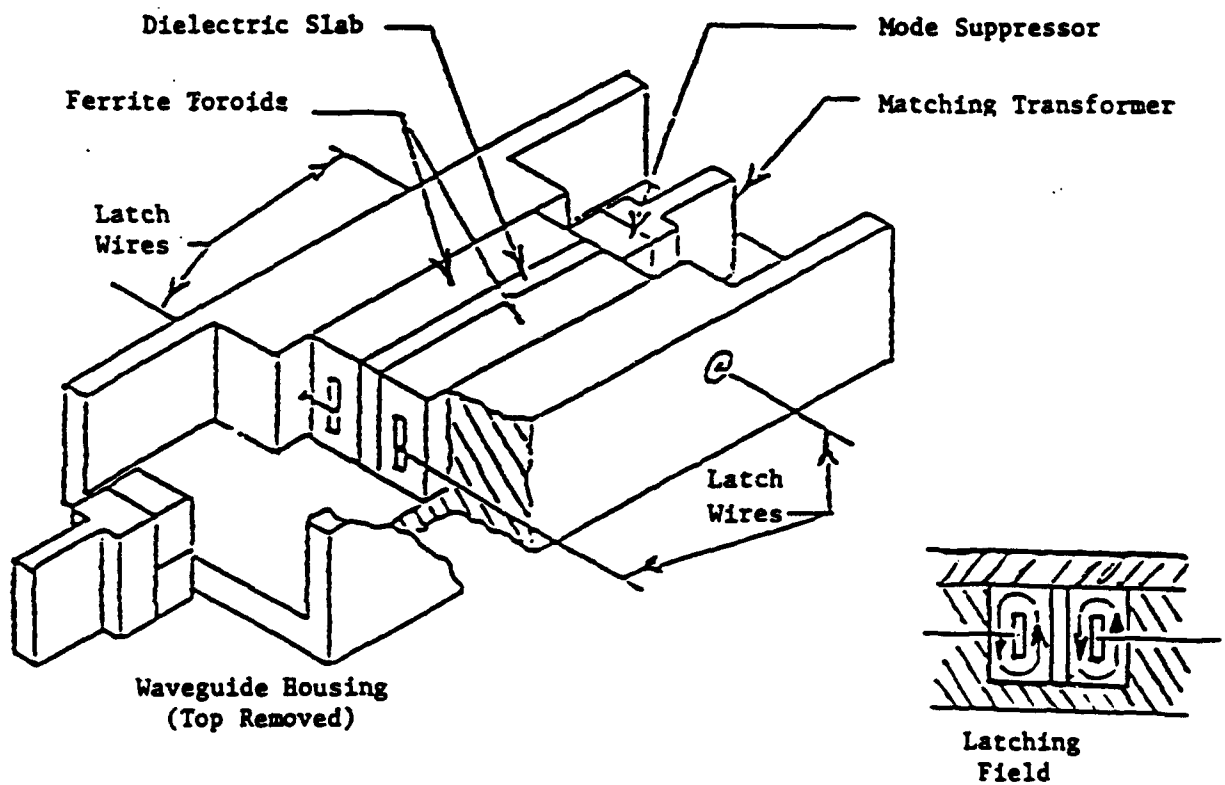


FIGURE 2-3:   Dual Toroid Design
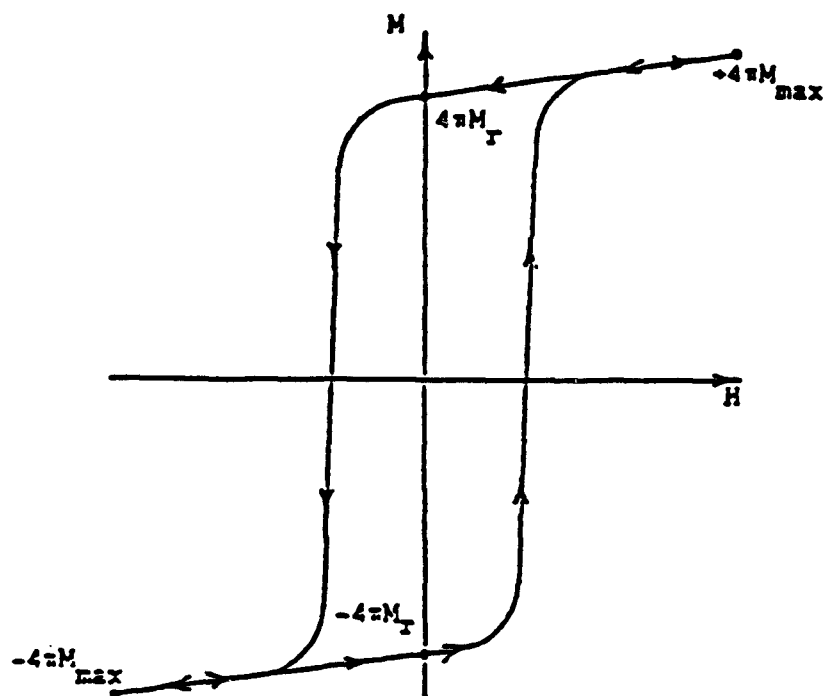
FIGURE 2-4: Typical Hysteresis Loop of a Latching Phase
Shifter Operating With Major Loop Switching

One characteristic of the ferrite material that often impacts observed performance is "stress sensitivity" which is related to the magnetostrictive properties of the ferrite. Stress sensitivity, in this case, is evident by changes in the shape of the hysteresis curve and, in particular, the value of the remanent magnetization and thus phase shift, as a function of external or internal stress. The ferrite material, as implied previously, is captured in the waveguide structure with some controlled top to bottom "crush." The crush may change with temperature since the ferrite and metallic housing expand and contract at different rates. The thermal expansion characteristics of the ferrite and metal housing are different and this can lead to significant (and often dominant) longitudinal stresses. Thus with changes in temperature both top to bottom (transverse) stress and longitudinal stress will occur. Similarly non-uniform RF heating in the ferrite can generate some internal stress. If the hysteresis properties of the material are stress sensitive, such effects cause erratic phase changes that severely impact on phase shifter performance; thus, materials with hysteresis properties (particularly the value of remanent magnetization) are desired that exhibit minimum sensitivity to stresses.

## 2.2 REMANENT MAGNETIZATION

The relative acceptability of a ferrite material for use in a digital phase shifter depends strongly on the material's ratio of remanent magnetization to saturation magnetization, its coercive field, and time required for switching it from one remanent state to the other. In general, a "good" ferrite for digital phase shifter applications will have a high remanence ratio, a low coercive field, and a small switching time.

The remanence ratio is probably the single most important square loop property as far as microwave applications of ferrite toroids is concerned. Ideally, the remanent magnetization should equal the saturation magnetization, i.e., the remanence ratio $R_r$ should be 1.0. This ideal situation is never attained in practice. Remanence ratios of 0.6 to 0.7 are more normally encountered.

In a polycrystalline ferrite or garnet material, the magnetization in the individual crystallites will, due to crystalline anisotropy, prefer to be aligned along the easy (111) directions (body diagonals of the cubic structure) of the crystallites. If magnetocrystalline anisotropy were the only factor influencing the magnetization in individual crystallites, the remanence ratio for a cubic material would be approximately 0.87. This result assumes that in the saturated state the magnetization in all crystals is parallel to the applied field and relaxes to the nearest easy direction, or body diagonal, when the field is removed. This ideal value is difficult to realize in practice because of unfavorable contributions from other anisotropies (stress anisotropy or magnetostriction and shape anisotropy). The existence in polycrystalline materials of pores or voids and corners in the material also gives rise to local demagnetizing fields which will lower the resultant remanence ratio (see Figure 2-5). Thus, magnetocrystalline anisotropy will tend to favor a high remanence ratio while porosity and other anisotropies tend to decrease remanence ratio. If the magnetocrystalline anisotropy is large compared to other anisotropies and demagnetizing fields arising at magnetic discontinuities in the materials, the remanence ratio can approach the theoretical limit of 0.87. Thus, highest remanence ratios will be realized in materials having low magnetostriction, low unfavorable internal stresses, and a dense, homogenous magnetic structure with a relatively high magnetocrystalline anisotropy (relatively high to other unfavorable anisotropies).

A unidirectional anisotropy favoring high remanence ratio can sometimes be built into a material by controlling its shape and internal stresses. Quenching, lattice deformation, applied pressure, etc., are techniques sometimes used.

In actual phase shifter applications, the ferrite materials are not driven into saturation with available drive fields. The hysteresis loop on which operation is based is then not the saturated loop, but rather minor hysteresis loops. This is particularly true with the "flux controlled" phase shifter where phase states are changed by switching a controlled amount of flux and thus changing the value of the resultant remanent magnetization.
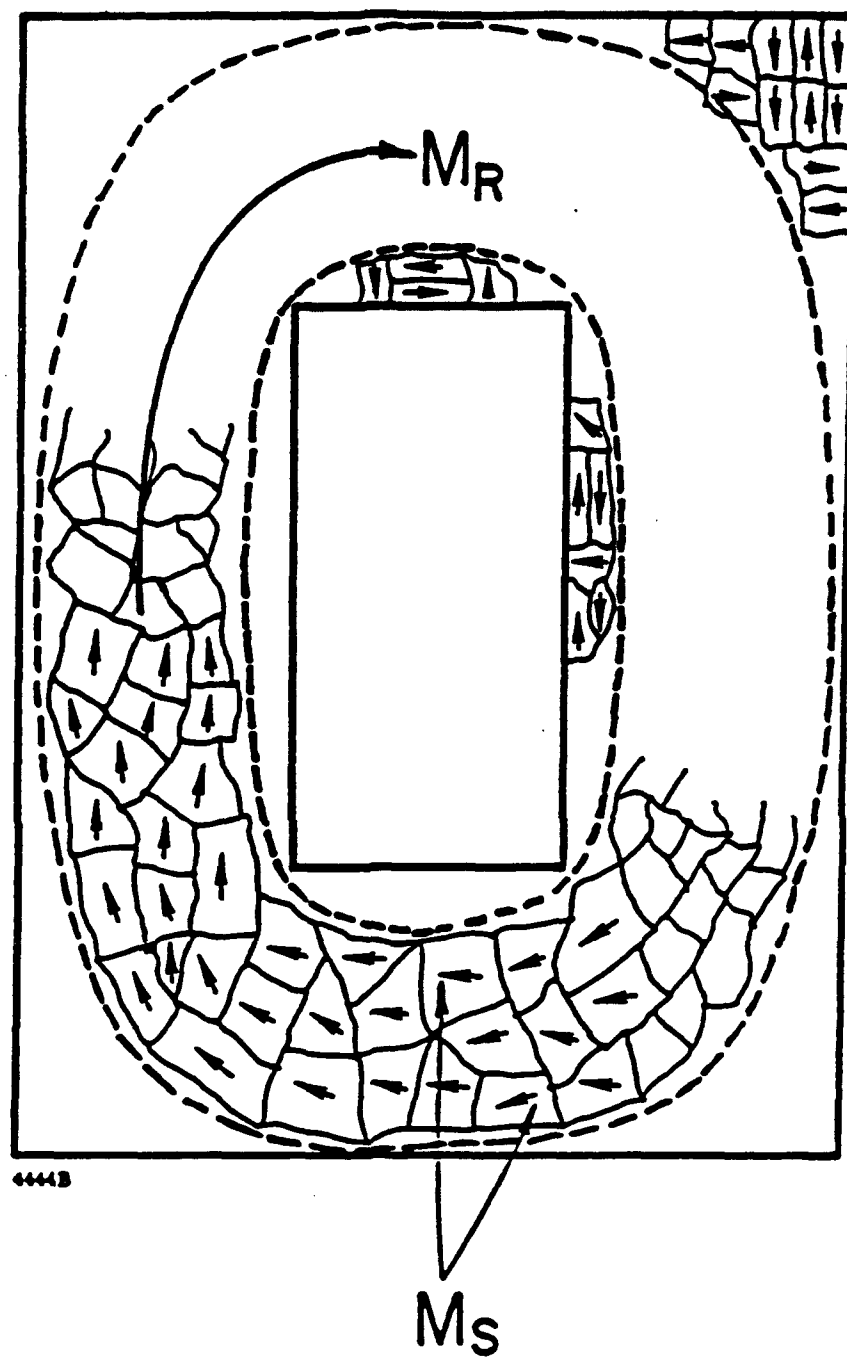
FIGURE 2-5:  Possible Domain Configurations in Remanent Toroids

The important (and measured) characteristics of toroidal ferrite materials are presented in Figure 2-6. The remanence ratio is the ratio of the remanent magnetization to the saturated magnetization ($4\pi M_r / 4\pi M_s$).

In Figure 2-6 ($4\pi M_D$), the drive magnetization is considerably less than $4\pi M_s$. The drive field for $4\pi M_D$ is typically five times the coercive field ($H_C$). The $4\pi M_{RD}$ is the remanent magnetization at the drive field used. At a drive field of $5H_C$, $4\pi M_{RD}$ is very nearly equal to the remanent magnetization. The squareness ratio (indicating the squareness of the hysteresis loop) is the ratio of $4\pi M_{RD}$ to $4\pi M_D$ or $4\pi M_{RD}/4\pi M_D$. If the material is stress sensitive, all of these measured parameters will change with stress.

To achieve a desired square hysteresis loop, the material should possess a dense homogenous magnetic structure, a high magnetocrystalline anisotropy and low magnetostriction and unfavorable internal stresses. A remanence ratio as high as possible and low $H_C$ are desired with a uniform microstructure.

## 2.2.1 Magnetostriction

### Theory

Magnetostriction describes the experimental fact that magnetic materials will become deformed (change their physical length) when they are magnetized. The deformation is measured along the direction of magnetization. Magnetostrictive constants are measured along crystalline axes. In cubic materials this is along the 111 (body diagonal) and 100 (cube edge) direction. Chikazumi [1] states that as the magnetization goes from 0 to $M_s$, the length of the sample will change by:

$$\frac{\Delta l}{l} = \frac{3}{2}\lambda_{100}\left(\alpha_1^2\beta_1^2 + \alpha_2^2\beta_2^2 + \alpha_3^2\beta_3^2 - \frac{1}{3}\right)$$

$$+ 3\lambda_{111}\left(\alpha_1\alpha_2\beta_1\beta_2 + \alpha_2\alpha_3\beta_2\beta_3 + \alpha_3\alpha_1\beta_3\beta_1\right),$$
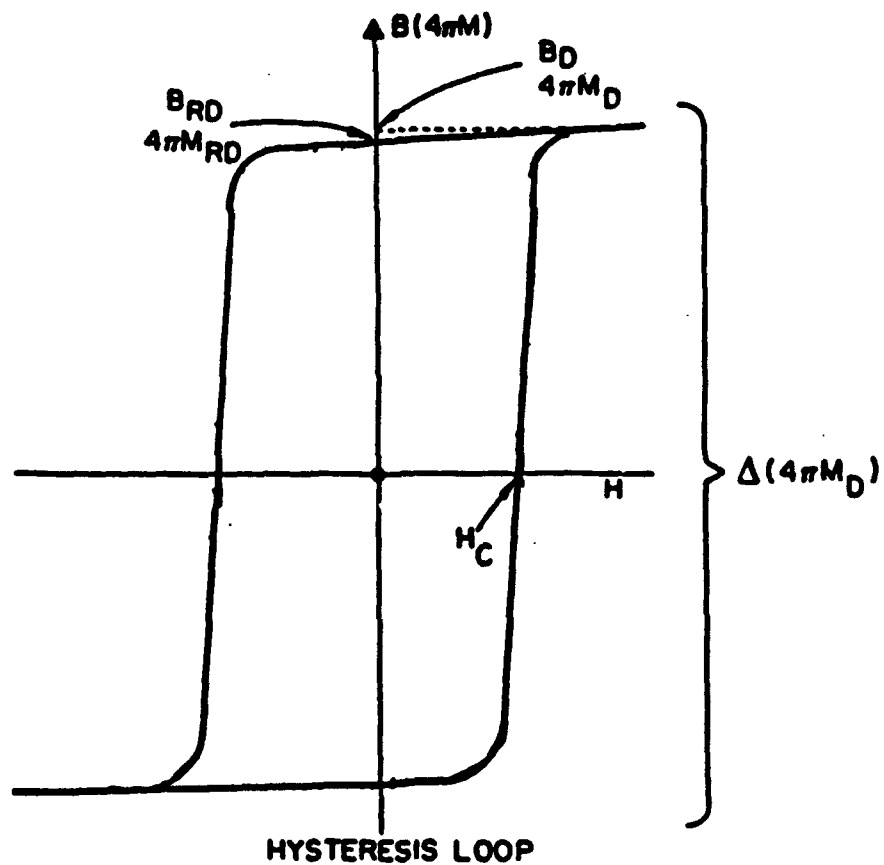
FIGURE 2-6:  Hysteresis Curve of a Ferrite Toroidal Material
Indicating Measured Characteristics

where $\Delta l/l$ is the fractional change in length, the $\alpha_i$'s are direction cosines between M and the x, y, and z crystal axes, and the $\beta$'s are the direction cosines between the measured deformation and the x, y, and z crystal axes. $\lambda_{100}$ is the magnetostrictive constant along the 100 direction, and $\lambda_{111}$ is the magnetostrictive constant along the 111 direction.

For example, if the material becomes saturated along the cube edge, [100], of a single crystal and the deformation is measured along this same direction, then $\alpha_1 = \beta_1 = 1$ and all others $= 0$ so that:

$$\left.\frac{\Delta l}{l}\right]_{100} = \frac{3}{2}\lambda_{100}\left(1 - \frac{1}{3}\right) = \lambda_{100}.$$

If the material were saturated along the body diagonal, [111], of a single crystal and the deformation measured along this same direction, then each $\alpha$ and $\beta$ become $1/\sqrt{3}$ so that:

$$\left.\frac{\Delta l}{l}\right]_{100} = 3\lambda_{111}\left(\frac{1}{3}\right) = \lambda_{111}.$$

For a polycrystalline material the random alignment of crystallites requires that an average be taken over various directions. When this is done (under the assumption that $\beta_i = \alpha_i$), the effective magnetostrictive constant for a polycrystalline material is found to be:

$$\lambda_s = \frac{2}{5}\lambda_{100} + \frac{3}{5}\lambda_{111},$$

where the deformation is measured along the direction of M. Then a polycrystalline material with $\lambda_{100} = -1.5\lambda_{111}$ would show no deformation along the direction of applied field as it is brought from a demagnetized state to saturation. Internally some crystallites are elongated and others shortened, but the net effect is compensated.

- 16 -

If a material possesses a negative $\lambda \left( \lambda - \dfrac{\Delta l}{l} \right)$, then the material contracts in the direction of magnetization. (Corollary) Physically compressing the material would cause the magnetization to more favorably align in the direction of the compression. Physically stretching the material would cause the magnetization to become less aligned with the direction of the stretching.

If a material possesses a positive $\lambda \left( \lambda - \dfrac{\Delta l}{l} \right)$, then the material elongates in the direction of magnetization. (Corollary) Physically stretching the material in this direction would cause the magnetization to favorably align in the stretching direction. Physically compressing the material would cause the magnetization to become less aligned with the direction of the compression.

Gerald Dionne [2,3,4] at MIT Lincoln Labs has studied magnetostrictive effects on remanence extensively. These studies have sought answers to two questions:

1) What effect does magnetostriction have on remanence ratios of ferrites (under no external stress)?

2) How does magnetostriction influence the effects of externally or internally applied stress on remanent magnetization?

The answer to question #2 is needed in order to make stress insensitive phase shifters. Dionne's paper [4] treats this problem for stress applied both parallel and perpendicular to the magnetization, and the paragraphs below summarize his findings.

In each grain the direction of magnetization (in the absence of an applied field) is determined by the combined effects of magnetocrystalline anisotropy ($K_1$) and magnetostriction ($\lambda_{100}$, $\lambda_{111}$). The magnetostrictive contribution will depend directly on the mechanical stress ($\sigma$) that is applied to that grain. The combined anisotropy stress energy is given by:

$$E_{K\sigma} = K_1 \left( \alpha_1^2 \alpha_2^2 + \alpha_2^2 \alpha_3^2 + \alpha_3^2 \alpha_1^2 \right)$$

$$+ \frac{3}{2} \sigma \lambda_{100} \left( \alpha_1^2 \beta_1^2 + \alpha_2^2 \beta_2^2 + \alpha_3^2 \beta_3^2 \right)$$

$$+ 3 \sigma \lambda_{111} \left( \alpha_1 \alpha_2 \beta_1 \beta_2 + \alpha_2 \alpha_3 \beta_2 \beta_3 + \alpha_3 \alpha_1 \beta_3 \beta_1 \right),$$

where

$K_1$ is the first order anisotropy constant in units of energy/volume,

$\lambda_{100}$, $\lambda_{111}$ are the magnetostriction coefficients,

$\sigma$ is the mechanical stress in units of energy/volume,

the $\alpha_i$'s and $\beta$'s are the direction cosines as defined previously.

For a given set of $K_1$, $\lambda_{100}$, $\lambda_{111}$, and $\sigma$, some direction for M will result in a minimum energy, $E_{K\sigma}$. This direction will be the "easy" direction. Note that when $\sigma \neq 0$, the "easy" direction is determined by the <u>combined</u> effects of $K_1$, $\lambda_{100}$, and $\lambda_{111}$. (If $\sigma = 0$, the usual "easy" directions due to anisotropy alone prevail.) Thus the applied stress, $\sigma$, can cause a rotation of M within each grain.

The remanence ratio, R, is the cosine of the angle between the easy direction of that grain and the applied field or average, macroscopic, magnetization. For a polycrystalline material the remanence ratio is the average of this cosine over all individual grains. Of particular interest is the sensitivity of remanence ratio to stress, or

$$\frac{\delta R}{\delta \sigma} = \text{stress sensitivity of remanence ratio.}$$

The results of stress sensitivity (as reported by Dionne)[4] for several particular cases are given below. (Dionne simulated a polycrystalline material by considering only the principal symmetry axes <100>, <110>, <111>, and weighted them by their frequency of occurrence 3, 6, and 4, respectively. These results represent somewhat of an approximation, and therefore there is little concern for numbers carried to three decimal places.)

A)  Stress applied parallel to M

  a)  For $K_1 < 0$ (all useful ferrites and garnets):

$$\frac{\delta R}{\delta \sigma}|| = 0.34 \frac{\lambda_{100}}{K_1} + 0.14 \frac{\lambda_{111}}{K_1} .$$

There will be no sensitivity to stress for $\lambda_{100} = -0.4\lambda_{111}$, or $\lambda_{100} = \lambda_{111} = 0$ or if $|K_1| >> \sigma\lambda_s$. Further, $\lambda_{100}$ would appear to be more important than $\lambda_{111}$.

  b)  For $K_1 > 0$ (no practical ferrites or garnets);

$$\frac{\delta R}{\delta \sigma}|| = -0.44 \frac{\lambda_{111}}{K_1} .$$

No stress sensitivity for $\lambda_{111} = 0$ or $|K_1| >> \sigma\lambda_{111}$.

B)   Stress applied perpendicular to M

       a1)   For $K_1 < 0$ and $\lambda_{111} < 0$ (most garnets and nickel ferrites)

$$\frac{\delta R^{\perp}}{\delta \sigma} = -0.13 \frac{\lambda_{100}}{K_1} \quad -0.15 \frac{\lambda_{111}}{K_1} \; .$$

No stress sensitivity if $\lambda_{100} = -\lambda_{111}$ or $\lambda_{100} = \lambda_{111} = 0$
or $|K_1| >> \sigma \lambda_s$.
Both $\lambda$'s are equally important.

       a2)   For $K_1 < 0$ and $\lambda_{111} > 0$ (lithium ferrites and MgMn ferrites)

$$\frac{\delta R^{\perp}}{\delta \sigma} = -0.13 \frac{\lambda_{100}}{K_1} \quad -0.05 \frac{\lambda_{111}}{K_1} \; .$$

No stress sensitivity if $\lambda_{100} = -0.38 \lambda_{111}$, or $\lambda_{100} = \lambda_{111} = 0$
or $|K_1| >> \sigma \lambda_s$.

In this case $\lambda_{100}$ is the dominant term.

     b)   For $K_1 > 0$ (No practical ferrites)

$$\frac{\delta R^{\perp}}{\delta \sigma} = 0.56 \frac{\lambda_{111}}{K_1} \qquad \text{for } \lambda_{111} < 0$$

$$\frac{\delta R^{\perp}}{\delta \sigma} = 0.46 \frac{\lambda_{111}}{K_1} \qquad \text{for } \lambda_{111} > 0$$

No stress sensitivity for $\lambda_{111} = 0$ in either case.

Note:   For $K_1 > 0$, $\frac{\delta R}{\delta \sigma} || = -0.44 \frac{\lambda_{111}}{K_1}$; therefore materials would be
stress insensitive when $K_1 > 0$ and $\lambda_{111} = 0$, for stress applied both
parallel and perpendicular to M.

In accordance with this theory, to get insensitivity to stress in both the parallel and perpendicular cases would require a material with

$$K_1 < 0, \quad \lambda_{111} > 0$$

and with

$$\lambda_{100} = -.4\lambda_{111} .$$

"Molecular engineering" techniques can be used to alter the magnetostrictive constants. For example, within a particular class of materials, a compound with a positive $\lambda_{111}$ can be mixed (reacted) with a compound of negative $\lambda_{111}$ to generate a resultant compound (solid solution of the two compositions) with a weighted average of these two values of magnetostriction. In this case a compound with zero value for $\lambda_{111}$ could be formulated.

As an example, consider a solid solution of yttrium-iron garnet (YIG) and gadolinium-iron garnet (GdIG) such as

$$Y_{2.6}Gd_{0.4}Fe_5O_{12} \text{ or } [YIG (13.3\%Gd)].$$
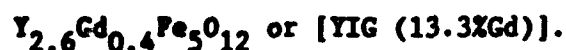
This compound is a mixture of

$$86 \ 2/3\% \text{ YIG and } 13 \ 1/3\% \text{ GdIG.}$$

The measured magnetostrictive constants of YIG and GdIG are as follows;

|  | $\lambda_{100}$ | $\lambda_{111}$ | $\lambda_s$ |
|---|---|---|---|
| YIG | $-1.3 \times 10^{-6}$ | $-2.7 \times 10^{-6}$ | $-2.14 \times 10^{-6}$ |
| GdIG | $0 \times 10^{-6}$ | $-3.1 \times 10^{-6}$ | $-1.86 \times 10^{-6}$ |
| YIG (13.3%Gd)* | $-1.13 \times 10^{-6}$* | $-2.75 \times 10^{-6}$* | $-2.1 \times 10{-6}$* |

*Values computed from weighted average for the solid solution of the two compositions.

- 21 -

Dionne reported [4] that the substitution of $Mn^{+3}$ for $Fe^{+3}$ in the garnet structure produces a change in the magnetostrictive constants as follows:

Change in magnetostrictive constant in garnet based on one $Mn^{+3}$ ion per formula unit:

|  | $\lambda_{100}$ | $\lambda_{111}$ | $\cdot\lambda_s$ |
|---|---|---|---|
| $Mn^{+3}$ | $+67.3 \times 10^{-6}$ | $+14.6 \times 10^{-6}$ | $+35.7 \times 10^{-6}$ |

Therefore substituting the appropriate amount of $Mn^{+3}$ into the YIG (13.3%Gd) compound can alter the magnetostrictive constant accordingly. Suppose that it is desired that $\lambda_{100}$ be zero via $Mn^{+3}$ substitution; the amount of $Mn^{+3}$ would be 0.017 $Mn^{+3}$ ions per formula unit $[(1.13/67.3) = 0.0168]$.

Further considerations of the various substitutions are as follows:

| $Mn^{+3}$ Ions/Formula Unit | $\lambda_{100}$ | $\lambda_{111}$ | $\lambda_s$ |
|---|---|---|---|
| 0.0168 $(\lambda_{100} = 0)$ | 0 | $-2.5 \times 10^{-6}$ | $-1.5 \times 10^{-6}$ |
| 0.188 $(\lambda_{111} = 0)$ | $+11.52 \times 10^{-6}$ | 0 | $+4.61 \times 10^{-6}$ |
| 0.059 $(\lambda_s = 0)$ | $+2.84 \times 10^{-6}$ | $-1.89 \times 10^{-6}$ | 0 |
| 0.047 $(\lambda_{100} \sim -\lambda_{111})$ | $+2.06 \times 10^{-6}$ | $-2.06 \times 10^{-6}$ | $-0.4 \times 10^{-6}$ |

The above illustrates the use of molecular engineering to alter magnetostrictive characteristics; however it should be noted that the substitution of $Mn^{+3}$ produces no compositions with zero magnetostriction $(\lambda_{100} = \lambda_{111} = \lambda_s = 0)$ or $\lambda_{111} > 0$ and $\lambda_{100} = -0.4\,\lambda_{111}$.

## Experimental Studies (Selected Data Summary)

Dr. S. Iida [5] measured the magnetostrictive constants for various rare earth garnets in the early 1960's while he was at Bell Labs. His data are presented in Table 2-1.

In the cubic garnet lattice and under remanent magnetization conditions, the magnetic moments are aligned (without other stresses) with a [111] direction; therefore with the magnetic moment aligned in the [111] direction, it would appear that $\lambda_{100}$ is less important than $\lambda_{111}$ and $\lambda_s$. While this may be a bad assumption based on Dionne's work, examination of Dr. Iida's data suggests that a solid solution of YIG and TbIG could provide a compound with $\lambda_{111} = 0$ at 25°C. Figure 2-7 shows the variation of $\lambda_{111}$ with terbium content in YIG. $\lambda_{111} \sim 0$ for a compound composed of a solid solution of 16.7% TbIG and 83.3% YIG.

A series of compositions were prepared with Tb content as a compositional variable at 5 different firing temperatures [6]. Measured data on these compositions are presented in Figures 2-8(a) and 2-8(b). [Data from Technical Report, "Advanced Ferrimagnetic Materials Applied to Digital Phase Shifters," RADC Contract No. AF30(602)3490, conducted by Sperry Microwave Electronics Company, August, 1965.] These data clearly indicate improved square loop properties and minimized stress sensitivity for the composition expected to provide $\lambda_{111} \sim 0$. While the magnetostriction is greatly reduced with terbium substitution, the microwave properties, particularly linewidth and therefore loss are not acceptable to support applications.

Russell West of Trans-Tech Inc. and Dionne [4,7] have reported the results of studies of magnetostrictive constants for $Mn^{+3}$ doped YIG. Measured magnetostrictive constant data taken on single crystals of YIG (doped with Mn) are presented in Figure 2-9. Using these values of $\lambda_{100}$ and $\lambda_{111}$, the theory predicts

$$\frac{\delta R||}{\delta \sigma} = 0 \text{ for } x = 0.05, \text{ and } \frac{\delta R\perp}{\delta \sigma} = 0 \text{ for } x = 0.07.$$

TABLE 2-1

## Magnetostrictive Constants For Various Rare Earth Garnets
(Data obtained by Private Communication, Dr. S. Iida,
University of Tokyo, Tokyo, Japan)

| | | 78°K | 196°K | 298°K(25°C) |
|---|---|---|---|---|
| YIG | $\lambda_{100}$ | $-1.0 \times 10^6$ | $-1.1 \times 10^6$ | $-1.4 \times 10^6$ |
| | $\lambda_{111}$ | $-3.6 \times 10^6$ | $-3.9 \times 10^6$ | $-2.4 \times 10^6$ |
| SmIG | $\lambda_{100}$ | $+159 \times 10^6$ | $+49 \times 10^6$ | $+21 \times 10^6$ |
| | $\lambda_{111}$ | $-183 \times 10^6$ | $-28.1 \times 10^6$ | $-8.5 \times 10^6$ |
| EuIG | $\lambda_{100}$ | $+86 \times 10^6$ | $+51 \times 10^6$ | $+21 \times 10^6$ |
| | $\lambda_{111}$ | $+9.7 \times 10^6$ | $+5.3 \times 10^6$ | $+1.8 \times 10^6$ |
| GdIG | $\lambda_{100}$ | $+4.0 \times 10^6$ | $+1.7 \times 10^6$ | $0 \times 10^6$ |
| | $\lambda_{111}$ | $-5.1 \times 10^6$ | $-4.5 \times 10^6$ | $-3.1 \times 10^6$ |
| TbIG | $\lambda_{100}$ | $+67 \times 10^6$ | $-10.3 \times 10^6$ | $-3.3 \times 10^6$ |
| | $\lambda_{111}$ | $+560 \times 10^6$ | $+65 \times 10^6$ | $+12 \times 10^6$ |
| DyIG | $\lambda_{100}$ | $-254 \times 10^6$ | $-46.6 \times 10^6$ | $-12.5 \times 10^6$ |
| | $\lambda_{111}$ | $-145 \times 10^6$ | $-21.6 \times 10^6$ | $-5.9 \times 10^6$ |
| HoIG | $\lambda_{100}$ | $-82.2 \times 10^6$ | $-10.6 \times 10^6$ | $-3.4 \times 10^6$ |
| | $\lambda_{111}$ | $-56.3 \times 10^6$ | $-7.4 \times 10^6$ | $-4.0 \times 10^6$ |
| ErIG | $\lambda_{100}$ | $+10.7 \times 10^6$ | $+4.1 \times 10^6$ | $+2.0 \times 10^6$ |
| | $\lambda_{111}$ | $-19.4 \times 10^6$ | $-8.8 \times 10^6$ | $-4.9 \times 10^6$ |
| TmIG | $\lambda_{100}$ | $+25.0 \times 10^6$ | $+4.9 \times 10^6$ | $+1.4 \times 10^6$ |
| | $\lambda_{111}$ | $-31.2 \times 10^6$ | $-11.3 \times 10^6$ | $-5.2 \times 10^6$ |
| YbIG | $\lambda_{100}$ | $+18.3 \times 10^6$ | $+5.0 \times 10^6$ | $+1.1 \times 10^6$ |
| | $\lambda_{111}$ | $-14.4 \times 10^6$ | $-7.1 \times 10^6$ | $-4.5 \times 10^6$ |

NOTE: Powers of 10 should be $10^{-6}$.
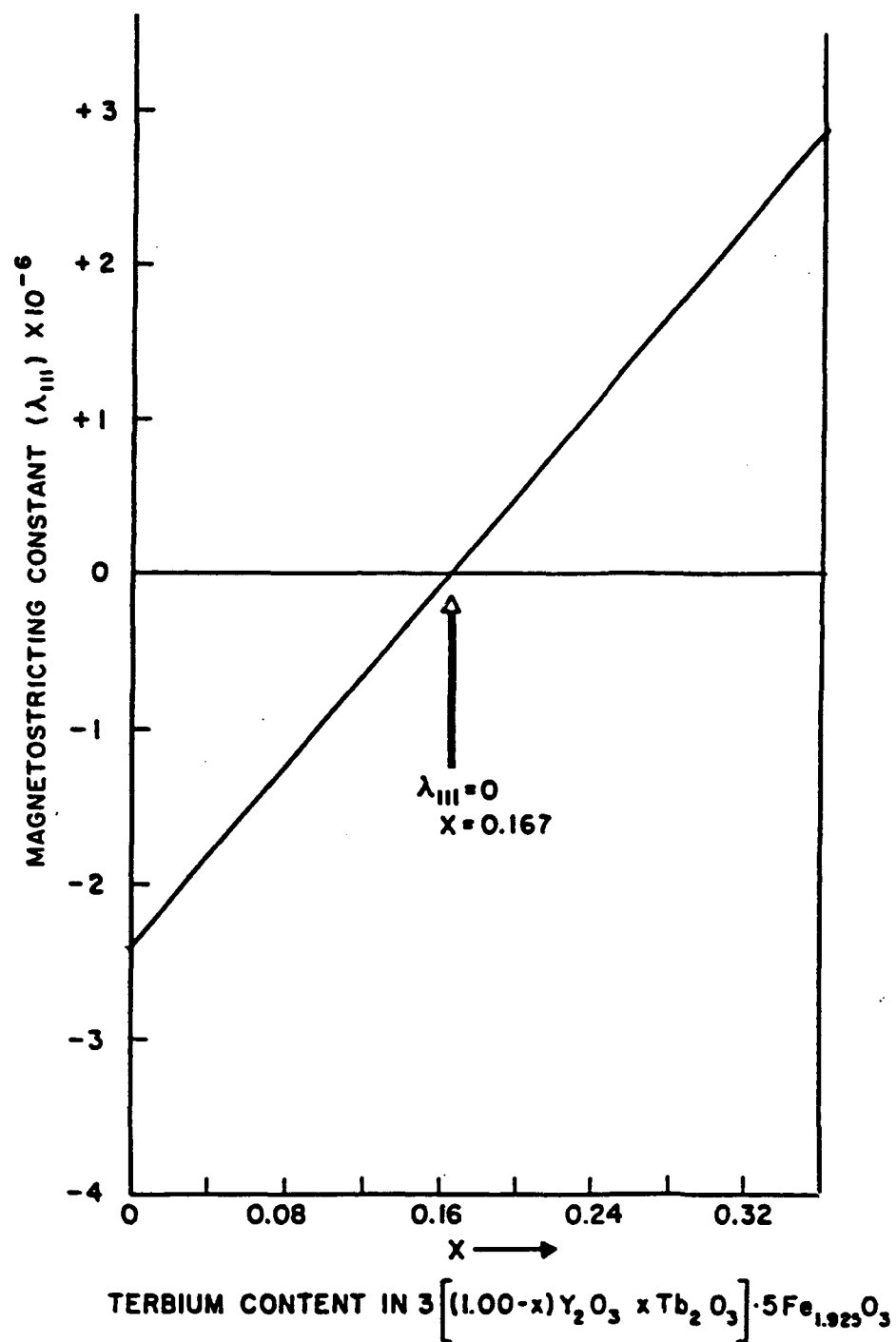
FIGURE 2-7: Magnetostrictive Constant $(\lambda_{111})$ as a Function of Terbium Content in YIG-TbIG

FIGURE 2-8(b): Change in Squareness and Coercive Field for an Applied Pressure of 20kg as a Function of Terbium Content in Yttrium-Terbium Iron garnet
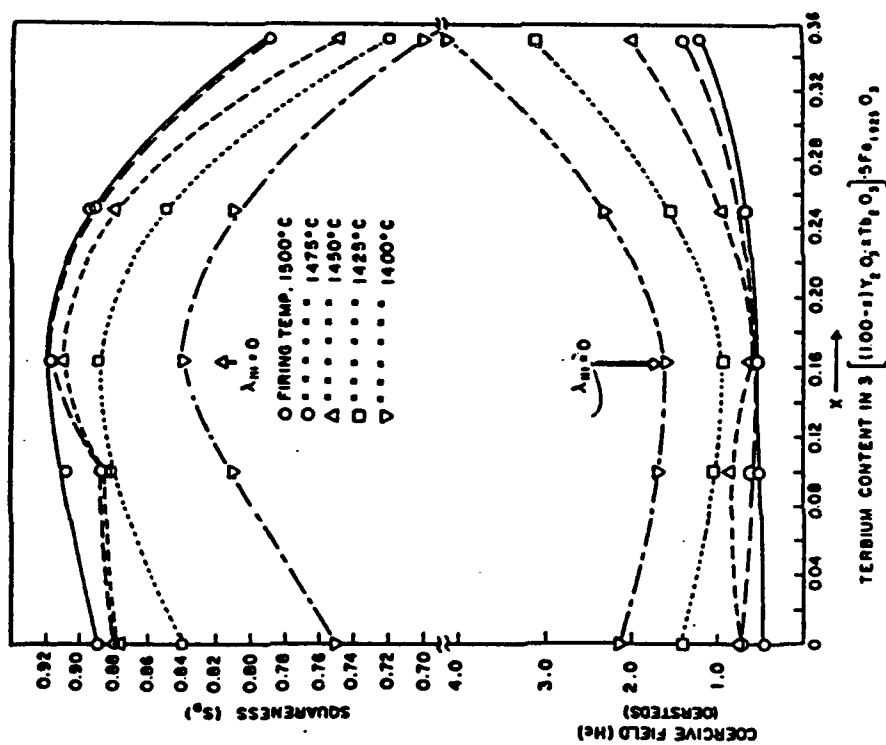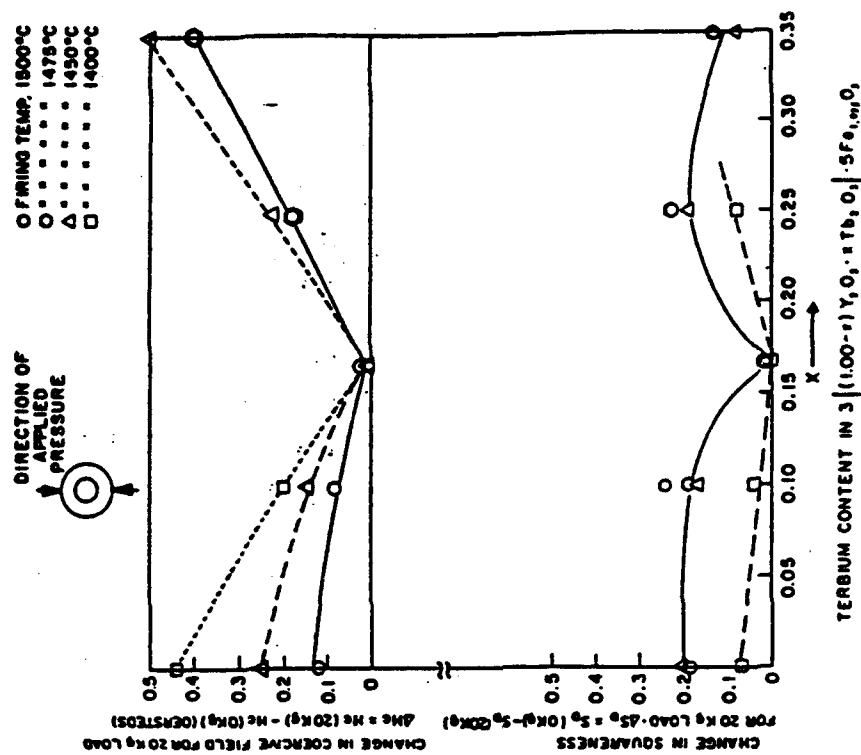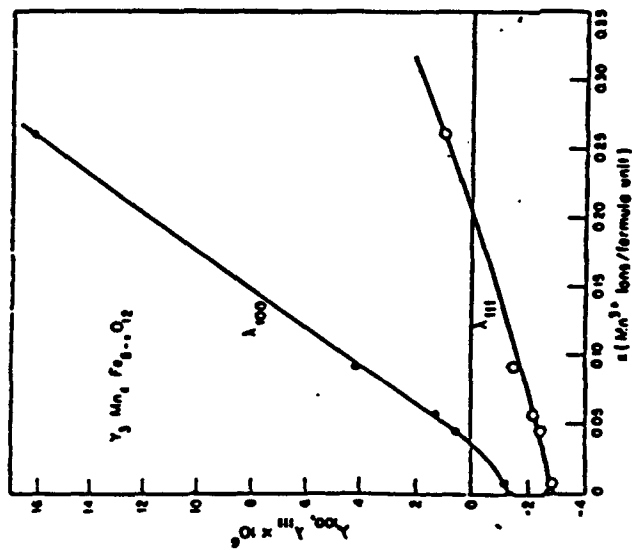
FIGURE 2-8(a): Squareness and Coercive Field for Various Firing Temperatures versus Terbium Content in Yttrium-Terbium Iron garnet
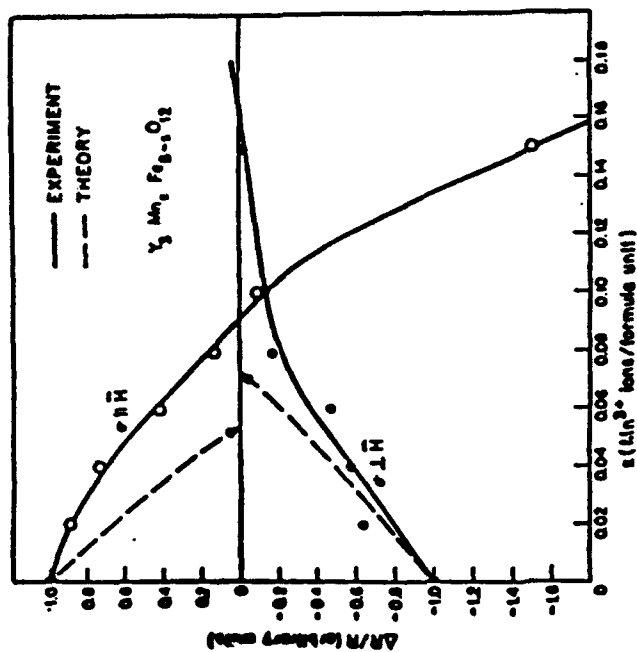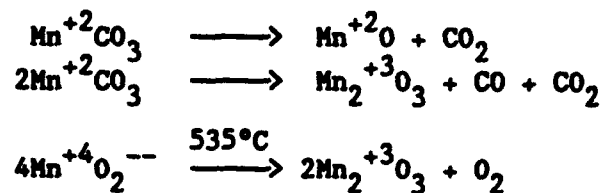
FIGURE 2-10: Fractional Change in Remanence Ratio as a Function of $Mn^{3+}$ Content for Compressive Stress Both Parallel and Perpendicular to Magnetic Field (After Dionne) 4.



FIGURE 2-9: Room Temperature Magnetostriction Constants $\lambda_{100}$ and $\lambda_{111}$ for Family $Y_3Mn_xFe_{5-x}O_{12}$ (After Dionne) 4.

Experimental measurements presented in Figure 2-10 indicate insensitivity at $x = 0.09$ and $x = 0.16$, respectively. Qualitatively, the agreement is fairly good, i.e., a higher manganese content for $R_\perp$ correction than for $R_{||}$ correction, and the orders of magnitude are correct. But detailed, quantitative agreement is missing; experimentally it takes about twice the Mn predicted theoretically.

Mn substituted in the amount of 0.09 per formula unit is utilized commercially for most garnet materials. This substitution level is a result of the data in Figure 2-10. The materials are improved but still exhibit considerable stress sensitivity.

It should be noted that Dionne's [4] theory is built around a $Mn^{+3}$ ion in the garnet structure which is substituted for $Fe^{+3}$. However, the carbonate $(Mn^{+2}CO_3)$ or oxide $(Mn^{+4}O_2)$ used as a raw material puts Mn in the structure as +2 or +4. $Mn^{+3}$ does not exist in stable form as a free oxide. Therefore appropriate and controlled solid state chemical reactions must take place to convert the Mn in the structure to the $Mn^{+3}$ state. Some of the chemical reactions of importance are as follows:

$$Mn^{+2}CO_3 \longrightarrow Mn^{+2}O + CO_2$$
$$2Mn^{+2}CO_3 \longrightarrow Mn_2^{+3}O_3 + CO + CO_2$$
$$4Mn^{+4}O_2^{--} \xrightarrow{535°C} 2Mn_2^{+3}O_3 + O_2$$

From these reactions it is evident that Mn can exist in the structure as a +2, +3, or +4 ion and therefore one cannot be certain that the desired +3 state is reached . Large substitutions (0.2) of Mn appears to alter the measured properties of the compound to indicate second phase formation.

Nonetheless, Mn, even with these uncertainties is presently the substitution most often used to reduce stress sensitivity in garnets and spinels.

Figure 2-11 presents data on the variations of the magnetostrictive constants of lithium ferrite (spinel) with $Mn^{+3}$ concentration. In this magnetic
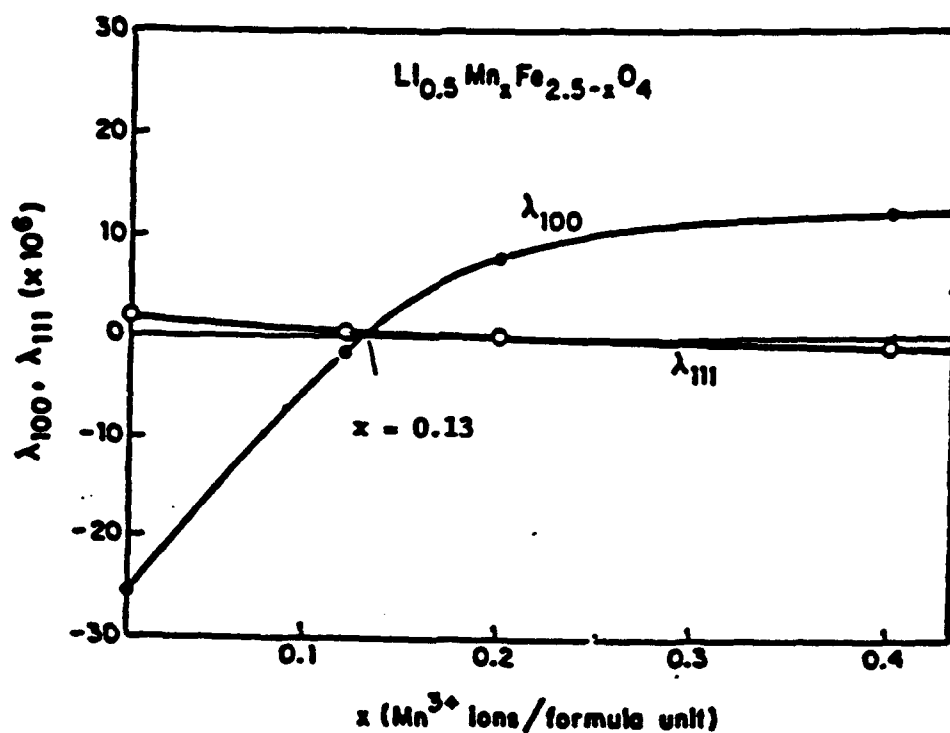
FIGURE 2-11: Variation in the Room-Temperature Magnetostriction Constants of Lithium Ferrite with $Mn^{3+}$ Concentration (After Van Hook and Dionne) [8].

compound, a $Mn^{+3}$ concentration of 0.13 $Mn^{+3}$ ions per formula unit appears to be ideal to adjust the magnitudes of both $\lambda_{100}$ and $\lambda_{111}$ to near zero values. This is a unique and valuable situation for these widely used spinels.

Dionne's work points out some interesting facts about the influence of small quantities of $Mn^{+3}$, $Co^{+2}$, and $Fe^{+2}$ ions on magnetostriction [7]. His June 1979 "Journal of Applied Physics" paper offers an explanation for the occurrence of these effects. The explanation is based on the effects of crystalline electric fields on energy levels of these ions, all of which are non-S-state and therefore have spin orbital coupling.

$\underline{Mn^{+3}~ions}$ produce large positive changes in magnetostriction when they occur in octahedral sites of either spinels or garnets. Divalent manganese ($Mn^{+2}$) is an S-state ion and would not show such an effect. Manganese doping does not appear to strongly affect magnetocrystalline anisotropy.

$Co^{+2}$ ions on octahedral sites appear to produce large negative changes in $\lambda_{100}$ and negligible changes in $\lambda_{111}$. (See Reference 9).

$Fe^{+2}$ ions produce large positive changes in $\lambda_{111}$ and negligible changes in $\lambda_{100}$.

Since the occurrence of $Fe^{+2}$ in either spinels or garnets is disastrous for dielectric loss tangents, divalent Fe cannot be considered to improve magnetostrictive characteristics.

The magnetostrictive effects of cobalt are of some interest since it will appear as a side effect in materials whose $\Delta H_k$ is controlled by cobalt additions. Cobalt additions will also change spinwave linewidth and anisotropy. Manganese additions seem to provide control of magnetostriction with minimal side effects.

For reference purposes, Table 2-2 lists the magnetostrictive constants and anisotropy fields for many garnet and spinel compounds. The garnet compounds (YIG and hybrid YIG materials) exhibit prominent magnetostrictive (or stress sensitive) characteristics. Since these compounds are otherwise extremely valuable and important to phase shifter applications, reducing and controlling the stress sensitivity of these materials would be a major technical advancement.

Many of the spinel compounds are stress insensitive particularly the MgMn ferrites.

It is noted however from the data in Table 2-2 that the magnetostrictive constants of these spinels are often much larger than the garnet materials. Why then are the spinels less stress sensitive and is it really desirable and necessary to dope the magnetostrictive constants to zero?

It was previously pointed out that the combined anisotropy ($K_1$) and stress ($\sigma$) energy collectively act on the magnetic moments in the materials. If the anisotropy energy (field) is much larger than the stress (magnetostrictive) energy, then the materials would exhibit low stress sensitivity regardless of the value of the magnetostrictive constants. This is believed to be the situation in spinels (anisotropy energy, $K_1$ is much larger than stress energy, $\sigma\lambda_{100}$ or $\sigma\lambda_{111}$).

The anisotropy field in garnets is much lower than that of the spinels and thus stress energy is more evident and sometimes dominant. The following table (Table 2-3) lists values to compare these anisotropies in YIG with lithium ferrite and MgMn ferrite. In this table, a 400 kg weight on one $cm^2$ is used as a stress. This corresponds to approximately 137 psi or a $\sigma$ of $3.92 \times 10^7$ joules/$M^3$. It is noted that the ratio of $K_1$ to $\sigma \lambda_s$ is much lower for YIG than the spinels.

These numbers reinforce the idea that magnetocrystalline anisotropy ($K_1$) overrides the effects of magnetostriction in some materials. Most spinels have

## TABLE 2-2

### Reported Magnetostrictive Constants and Anisotropy Fields for Some Garnet and Spinel Compounds at 25°C

| Garnets | $\lambda_{100}$ $(10^{-6})$ | $\lambda_{111}$ $(10^{-6})$ | $\lambda_s$ $(10^{-6})$ | $K_1$ ergs/cm$^3$ $(10^3)$ | $\frac{K_1}{M}$ (oe) | Ref |
|---|---|---|---|---|---|---|
| $Y_3Fe_5O_{12}$ (YIG) | -1.3 | -2.7 | -2.1 | -6.0 | -43.0 | 1 |
| $Y_3Fe_{4.74}Mn_{0.26}O_{12}$ | +16.2 | +1.1 | +7.1 | - | - | 1 |
| $Y_3Fe_{4.36}Ga_{0.64}O_{12}$ | -1.4 | -1.7 | - | - | - | 2 |
| $Gd_3Fe_5O_{12}$ | - | -3.1 | -1.9 | -7.0 | - | 3 |
| $Dy_3Fe_5O_{12}$ | -12.5 | -5.9 | -8.5 | -10.0 | - | 3 |
| EuIG | +21.0 | +1.8 | +9.5 | -3.0 | -350.0 | 3 |
| TbIG | -3.3 | +12.0 | +5.9 | -10.0 | - | 3 |
| $Yb_3Fe_5O_{12}$ | +1.1 | -4.5 | - | -7.0 | -41.5 | 3 |
| $Er_3Fe_5O_{12}$ | +2.0 | -4.9 | - | -7.0 | -100.0 | 3 |
| 50%YIG·50%GdIG | -0.65 | -2.9 | -2.0 | - | - | |
| $Mn^{+3}$ Substitution | +69.0 | +14.0 | +36.0 | | | |

### Spinels

| Spinels | | | | | | |
|---|---|---|---|---|---|---|
| $NiFe_2O_4$ | -45.9 | -21.6 | -31.0 | -63.0 | -200.0 | 4 |
| $MgFe_2O_4$ | -11.1 | +2.3 | -3.0 | -25.0 | -226.0 | 5 |
| $MnFe_2O_4$ | -26.0 | +4.5 | -7.7 | -29.0 | -53.0 | 6 |
| $Li_{0.5}Fe_{2.5}O_4$ | -25.6 | +2.3 | -8.9 | -90.0 | - | 7 |
| $Ni_{0.65}Zn_{0.35}Fe_2O_4$ | -33.7 | -13.2 | -21.4 | -25.0 | - | 8 |
| 80%Li·20%ZnFe | -22.4 | +4.5 | -6.3 | - | - | |
| 36%Li·64%ZnFe | -11.1 | +2.3 | -3.1 | - | - | |
| $Mn^{+3}$Substitution in | | | | | | |
| Spinels | +215.0 | -10.0 | +80.0 | - | - | |
| $Fe_3O_4$ | -20.0 | +78.0 | +39.0 | - | -230.0 | |
| $CoFe_2O_4$ | -730.0 | +130.0 | -214.0 | - | - | |

**TABLE 2-2 (Continued)**

**Reported Magnetostrictive Constants and
Anisotropy Fields for Some Garnet and Spinel Compounds
at 25°C**

| | $\lambda_{100}$ $(10^{-6})$ | $\lambda_{111}$ $(10^{-6})$ | $\lambda_s$ $(10^{-6})$ | $K_1$ ergs/cm$^3$ | $\frac{K_1}{M}$ (oe) |
|---|---|---|---|---|---|
| $Co_{0.8}Fe_{2.2}O_4$ | -590.0 | +120.0 | -164.0 | - | - |
| $Co_{0.3}Zn_{0.2}Fe_{2.2}O_4$ | -210.0 | +110.0 | -18.0 | - | - |
| $Co_{0.3}Mn_{0.4}Fe_{2.0}O_4$ | -200.0 | +65.0 | -41.0 | - | - |
| $Mn_{0.98}Fe_{1.86}O_4$ | -35.0 | 1.0 | -14.6 | - | - |
| $Mn_{0.6}Zn_{0.1}Fe_{2.1}O_4$ | -14.0 | +14.0 | +2.8 | - | - |
| $Ni_{0.8}Fe_{2.2}O_4$ | -36.0 | -4.0 | -16.8 | - | - |
| $Ni_{0.3}Zn_{0.45}Fe_{2.25}O_4$ | -15.0 | +11.0 | +0.6 | - | - |
| $Mn_{0.1}Fe_{2.9}O_4$ | -16.0 | +75.0 | +38.6 | - | - |
| $MnO.6Fe2.4O4$ | -5.0 | +45.0 | +25.0 | - | - |
| $Mn_{0.96}Fe_{2.05}O_4$ | -22.0 | +5.0 | -5.8 | - | - |
| MgMnFe | -10.0 | +2.4 | -2.6 | - | - |

==========================================

### References for Table 2-2

1. G.F. Dionne, IEEE Trans Mag. 7, p.715 (1971)

2. G.F. Dionne, J. Appl. Phys., 40, p.4486 (1969)

3. S. Iida (See Table 2-1)

4. E.V. Lee, Repts. Proj. Phys. XVIII, 184, (1955)

5. A.B. Smith and R.V. Jones, J. Appl. Phys. 37, p.1001 (1966)

6. Migata and Funatogava

7. H.J. Van Hook and G.F. Dionne, AIP Conf. Proc. 24, p.487 (1975)

8. G.F. Dionne, Lincoln Lab TR-737, Nov. 1985

## TABLE 2-3
### Comparison of Anisotropies in YIG with Lithium and MgMn Ferrite

| Material | $K_1$ $(J/m^3)$ | $\lambda_{100}$ | $\lambda_{111}$ | $\lambda_s$ | $\|\lambda_s \sigma\|$ $(\sigma=3.92 \times 10^7 J/M^3)$ | $\frac{K_1}{\lambda_s \sigma}$ |
|---|---|---|---|---|---|---|
| YIG | ~600 | $-1.3 \times 10^{-6}$ | $-2.7 \times 10^{-6}$ | $-2.1 \times 10^{-6}$ | ~80 | ~7.5 |
| Li-Fe | ~9000 | $-26.0 \times 10^{-6}$ | $+2.3 \times 10^{-6}$ | $-8.9 \times 10^{-6}$ | ~350 | ~26 |
| MgMn-Fe | ~2000 | $-10 \times 10^{-6}$ | $2.4 \times 10^{-6}$ | $-2.6 \times 10^{-6}$ | ~100 | ~20 |

large anisotropy as evidenced by their relatively broad linewidths. In these situations little is gained by reducing the magnitudes of magnetostrictive constants. However, if techniques are available to molecular engineer $\lambda_{111}$ and $\lambda_{100}$ to near 0, such low values would provide stress insensitive ferrimagnetic materials and perhaps improve the hysteresis characteristics toward higher values of remanent magnetization (hysteresis loops would be more square).

## Summary

The hysteresis properties of the garnet compounds exhibit considerably more stress sensitivity than do the ferrite spinels. This is believed to be due to the dominance of magnetocrystalline anisotropy relative to magnetostrictive anisotropy in the spinels. In the hybrid YIG compounds these anisotropy stresses are more comparable in value and thus these materials more readily exhibit sensitivity to stress.

Ferrimagnetic compounds and associated substitutions have been identified with a wide range of magnetostrictive constants.

In the microwave cubic compounds (both garnets and spinels) when the magnetic moments are "latched" to the remanent state of magnetization, the magnetic moments relax to the closest [111] (body diagonal) crystallographic direction. Since the magnetic moments are more likely to be aligned with these crystallographic directions, this would suggest the magnetostrictive characteristics in this direction ($\lambda_{111}$) would be most important and molecular engineering techniques should be utilized to adjust $\lambda_{111} \sim 0$. In YIG (according to the data of Dionne presented in Figure 2-9) this requires a $Mn^{+3}$ ion per formula unit of 0.2. (This assumes that the Mn substituted into the garnets as $Mn^{+2}$ or $Mn^{+4}$ ions is reacted to reach the $Mn^{+3}$ desired state.) Higher Mn substitutions (0.15 to 0.18) in hybrid YIG compounds do appear to reduce the stress sensitivity of these materials; however difficulty is encountered in achieving good single phase compounds with these higher levels of Mn. The improvements observed therefore may be due to altering other properties (such as magnetocrystalline anisotropy and microstructure) rather than magnetostriction.

In a phase shifter, stresses due to heating and cooling the structure will most likely not be along the direction of the remanent magnetization, thus the potential importance in this situation of $\lambda_{100}$ rather than $\lambda_{111}$. It would appear that to totally compensate magnetostrictive effects that both $\lambda_{100}$ and $\lambda_{111}$ should possess values as close to zero as possible.

## 3.0    PROGRAM PLAN

## 3.1    BASELINE TEST VEHICLE

An existing X-band dual toroid test structure [see Figure 2-1(c) and Figure 2-3]
was selected as the baseline test vehicle.

This structure had previously been developed for utilization as a phase shifter
in an earlier NRL program. The garnet material used in this baseline phaser was
Trans-Tech G-1002* with a 0.09 Mn substitution. This structure uses a "drum"
top to capture the ferrite material. RF input and output ports are double
ridged waveguide.

Excellent room temperature RF performance was achieved in this structure.
However, Figure 3-1 illustrates the typical differential phase shift observed as
a function of temperature. A phase hysteresis is observed with over 10° change
between increasing temperature and decreasing temperature. In this material a
clockwise hysteresis response is observed. This hysteresis response is due to
the material possessing stress sensitive characteristics and the stress being
experienced is due to the differences in the thermal expansion coefficients of
the metallic housing and garnet material. The elimination of this effect is the
prime thrust of the program.

This undesirable characteristic is very detrimental to differential phase shift
type RF switches where the phasers are utilized in a differential phase bridge
configured as a switch. The structure utilizes magic tees as the input and
output terminals with a phase shifter in each arm as shown schematically in
Figure 3-2.

* G-1002 is a standard garnet compound manufactured by Trans-Tech, Inc.,
  Adamstown, Maryland. G-1002 is a gadolinium doped yttrium iron garnet (a
  mixed GdlG-YIG compound) with a room temperature $4\pi M_s$ of 1000 gauss. A
  substitution of 0.09 Mn in garnet materials is an often used recommendation by
  Trans-Tech to improve the hysteresis characteristics and reduce
  magnetostriction.

TEMPERATURE HYSTERESIS OF PHASER STRUCTURE WITH TT G1002 (0.09Mn)
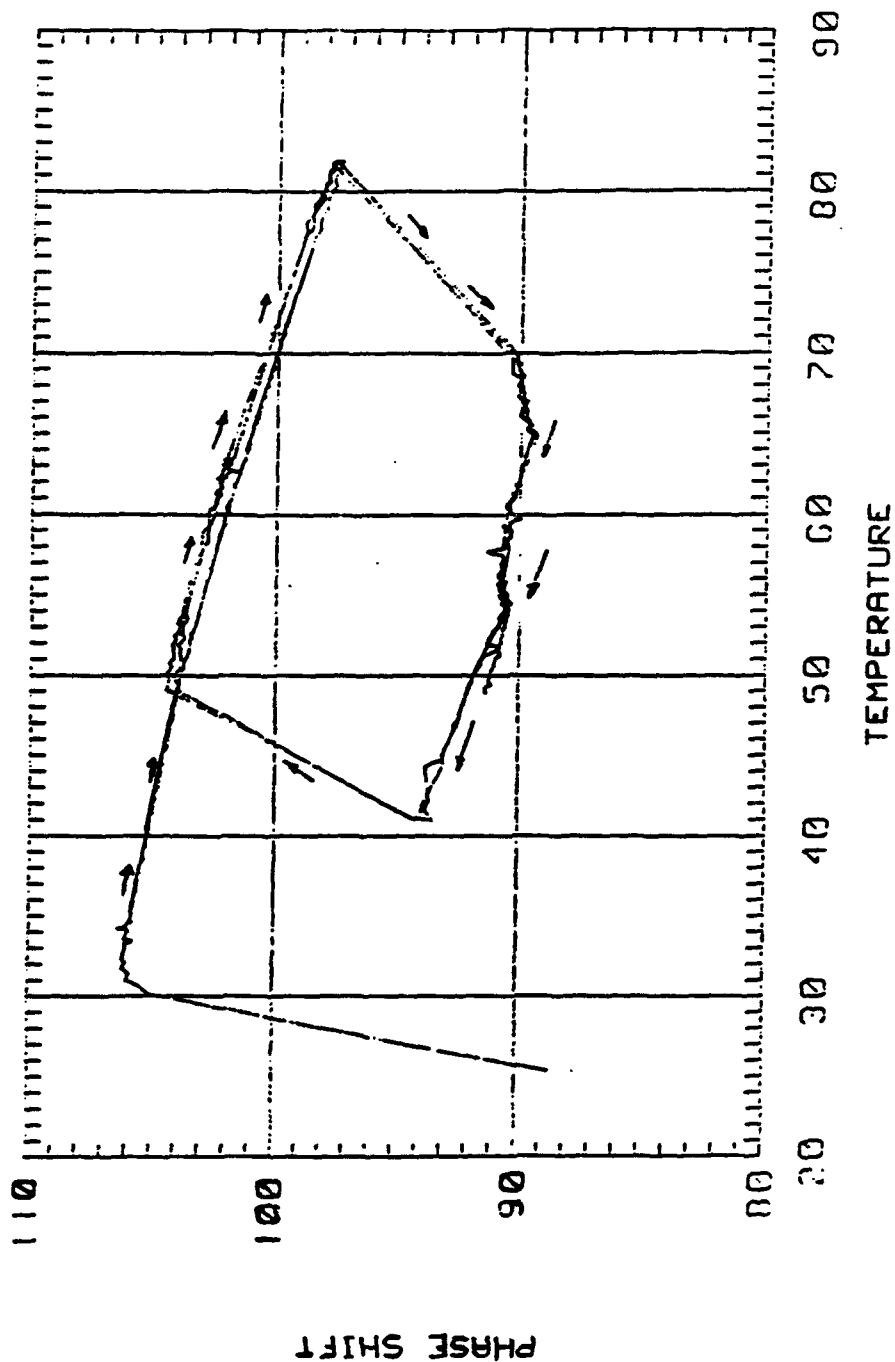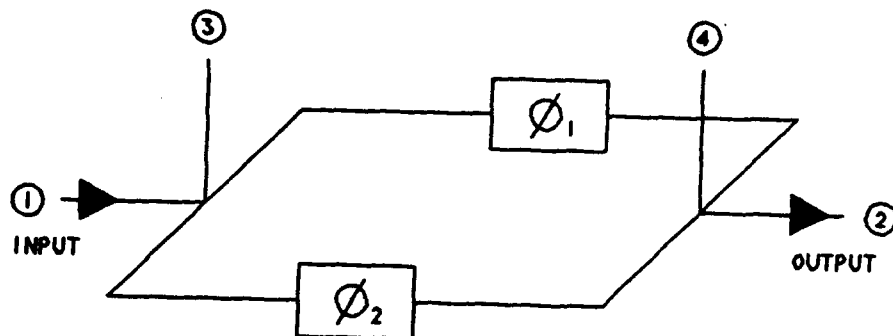
TT G1002 (0.09 Mn)

Figure 8.1

FIGURE 3-2    SCHEMATIC OF DIFFERENTIAL PHASE SHIFT CIRCULATOR

For operation, 180° degrees of differential phase shift is required.  Often 90°
phasers are used with a "designed in" 90° offset.  Figure 3-3 presents
the total available relative insertion phase shift in each channel with the 90°
offset between channels.  Note the hysteresis with temperature observed
in each phase state (long and short) of the phasers.  The short states exhibit
clockwise hysteresis and the long states exhibit counterclockwise
hysteresis.  This hysteresis effect is further noted in Figure 3-4 which plots
the phase difference (90° desired) between the short and long state for each
channel.  In channel B a phase hysteresis with temperature of nearly 20° was
observed.  Channel A is much better with about 8° of hysteresis.  This type
performance related to stress sensitivity of the material is extremely
detrimental to the desired and required RF performance of high power switches.

These data illustrate the problems arising from stress sensitive materials and
associated RF structures.  This is the problem that this program has addressed.

3.2       FERRITE MATERIAL STRESSES IN WAVEGUIDE PHASER STRUCTURES

The various potential stresses that a ferrite toroid may experience in a
waveguide phaser structure are illustrated in Figure 3-5.  Some of the stresses
are due to physical dimensions and associated tolerances; some result from
structural/assemble requirements of the phaser and others result from
environmental performance requirements (structural changes with ambient
temperature and RF power heating).

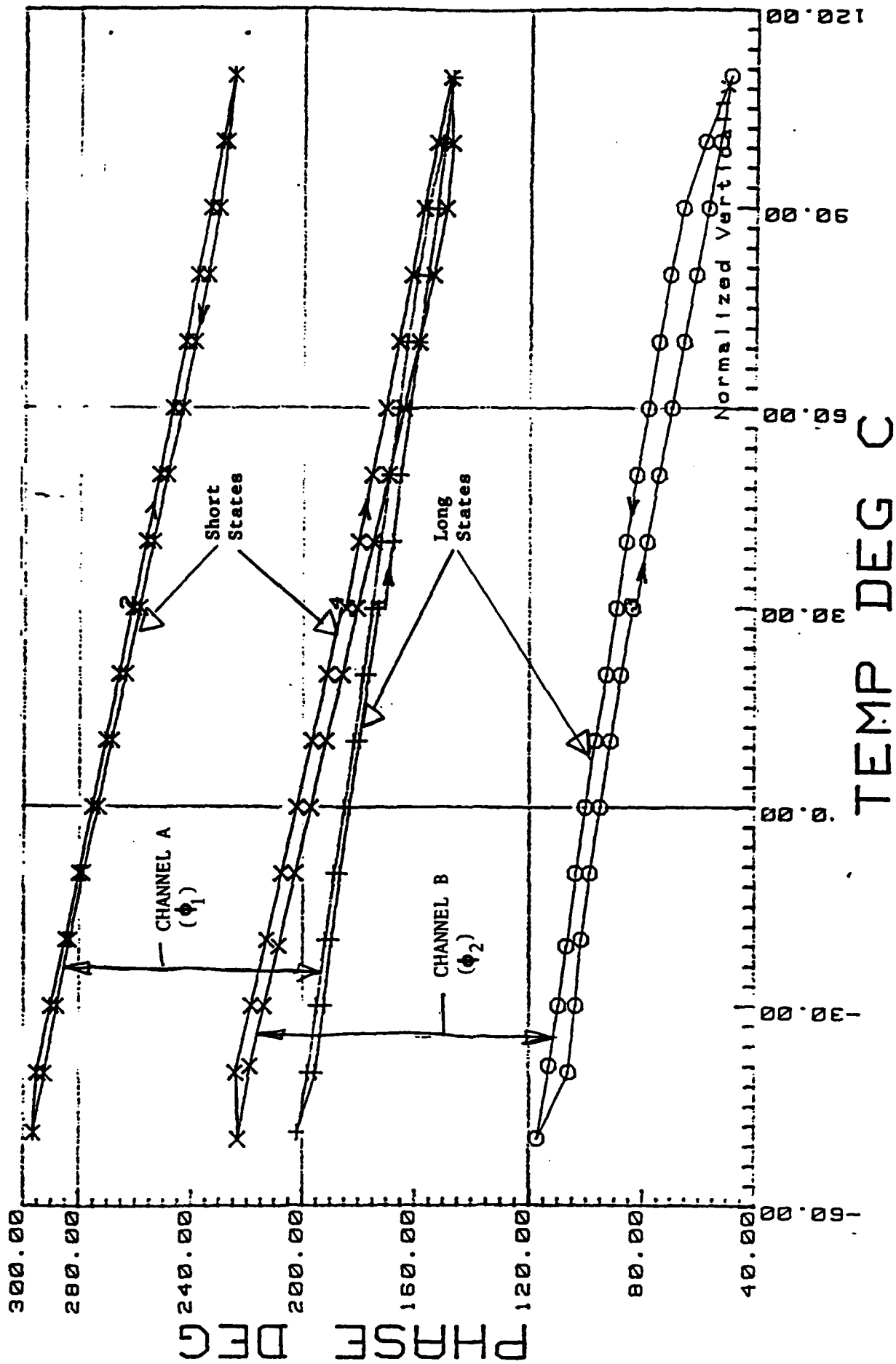Each of these are listed and illustrated in Figure 3-5.

FIGURE 3-3  TOTAL AVAILABLE PHASE SHIFT IN EACH CHANNEL OF SWITCH
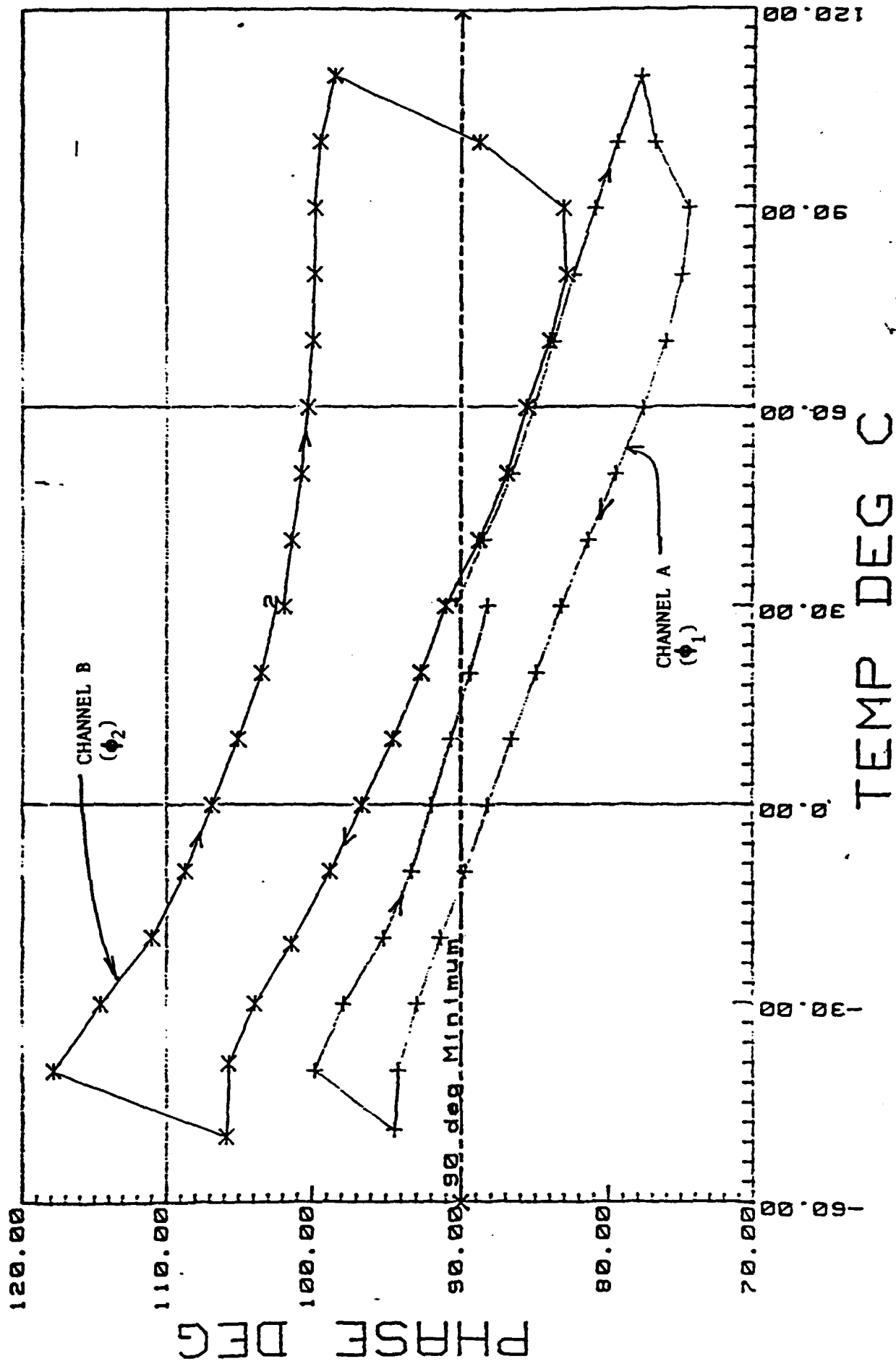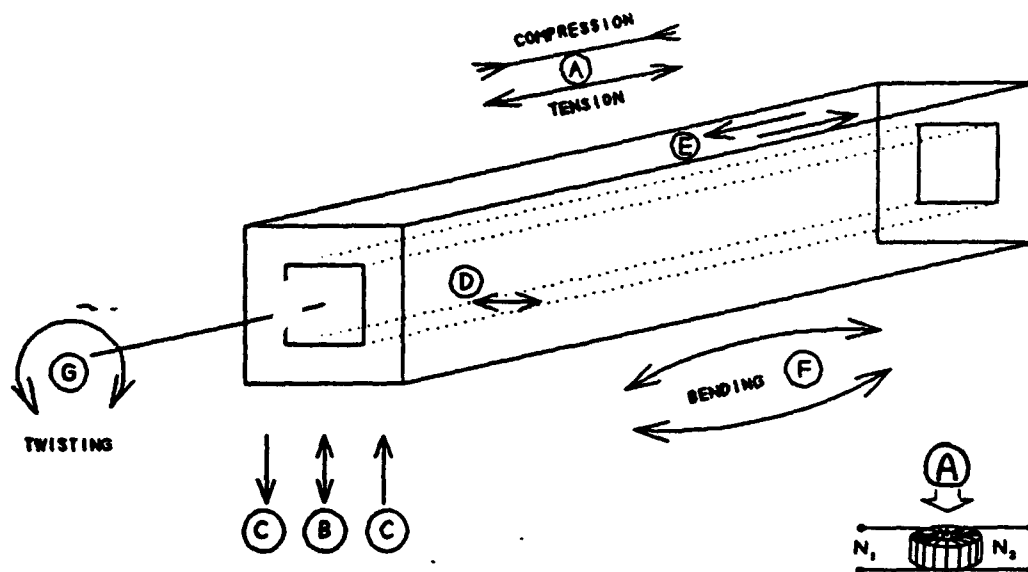SCHEMATIC SHOWN IN FIGURE 3-2 WITH "DESIGNED IN" 90°
OFF SET.

FIGURE 3-4   PHASE DIFFERENCE (90° DESIRED) BETWEEN SHORT AND LONG
STATE EACH CHANNEL AS A FUNCTION OF TEMPERATURE.

# POTENTIAL STRESSES



(A) Compression/Tension along the length occurs from differential expansin of the housing and ferrite material with temperature. Extremely Detrimental to phase shifters.

(B) Crush Compression and Relief: top to bottom of Phase Shifter: Necessary for good RF performance: can be very detrimental to phase shifter performance with temperature.

(BC) Differential Stress from soft top RF structures (more stress on outside leg than center leg in dual toroid structures.

(D) Side to side stress - not believed to be a major stress problem in phase shifters.

(E) Differential Expansion of ferrite material due to RF heating - (more in center leg than in outside leg): may be detrimental to performance at high RF power.

(F) Bending from tolerances in structure: Ferrite hysteresis properties very sensitive to this type of stress.

(G) Twisting - Structure related - not believed to be a major stress problem in phasers.

FIGURE 3-5

## 3.3    STATIC STRESS TEST FIXTURES

The program included both static and RF tests with stress. Comparative
evaluation of these data hopefully would provide for full stress sensitivity
assessment from only static tests of materials.

A standard test fixture in the ferrite lab was available to stress thin walled,
square cross section, round toroid samples (standard material test samples in
the Ferrite Lab). Figure 3-5 (inset A) shows this configuration.
A special test fixture was designed and fabricated to perform controlled static
stress tests on the specific square toroids to be used in the dual toroid phaser
structure. Schematics of this structure are shown in Figures 3-6 and 3-7. The
S-shaped component in this fixture is a pressure (strain) gauge with a voltage
output calibrated in pounds of pressure. With knowledge of the dimensions of
the samples a pressure in pounds per square inch (PSI) could be computed.

Rather thin walled toroids were to be evaluated and it was observed in
experimenting with this fixture that any distortion of the sample (bending,
twisting, bulging out of the side walls) severely distorted the observed
hysteresis loop. The desire was to provide a unidirectional stress (relative to
M) without sample distortion. Sample flatness was very important. It was
observed that the test fixture was best suited for longitudinal compressive
stress on the phaser toroids. This stress direction is perpendicular to the
average direction of the remanent magnetization in the toroid sample. The
"crush" direction (top to bottom, partially parallel to M) was studied on many
of the samples; however flatness and wall distortion of the toroids appeared to
negate the intrinsic value of these transverse stress measurements; thus
longitudinal stress measurements were primarily conducted.

The level of stress in pounds per square inch (PSI) experienced by the toroids
in phase structures was initially unknown. Therefore, tests were initially
conducted from 0 to 4000 PSI.

The test fixture was initially evaluated using the YIG-TbIG samples previously
discussed in Section 2. Both thin walled square and round cylindrical toroids
were available for evaluation. Figure 3-8 lists the anticipated
magnetostrictive constants for the compounds available. These results are for
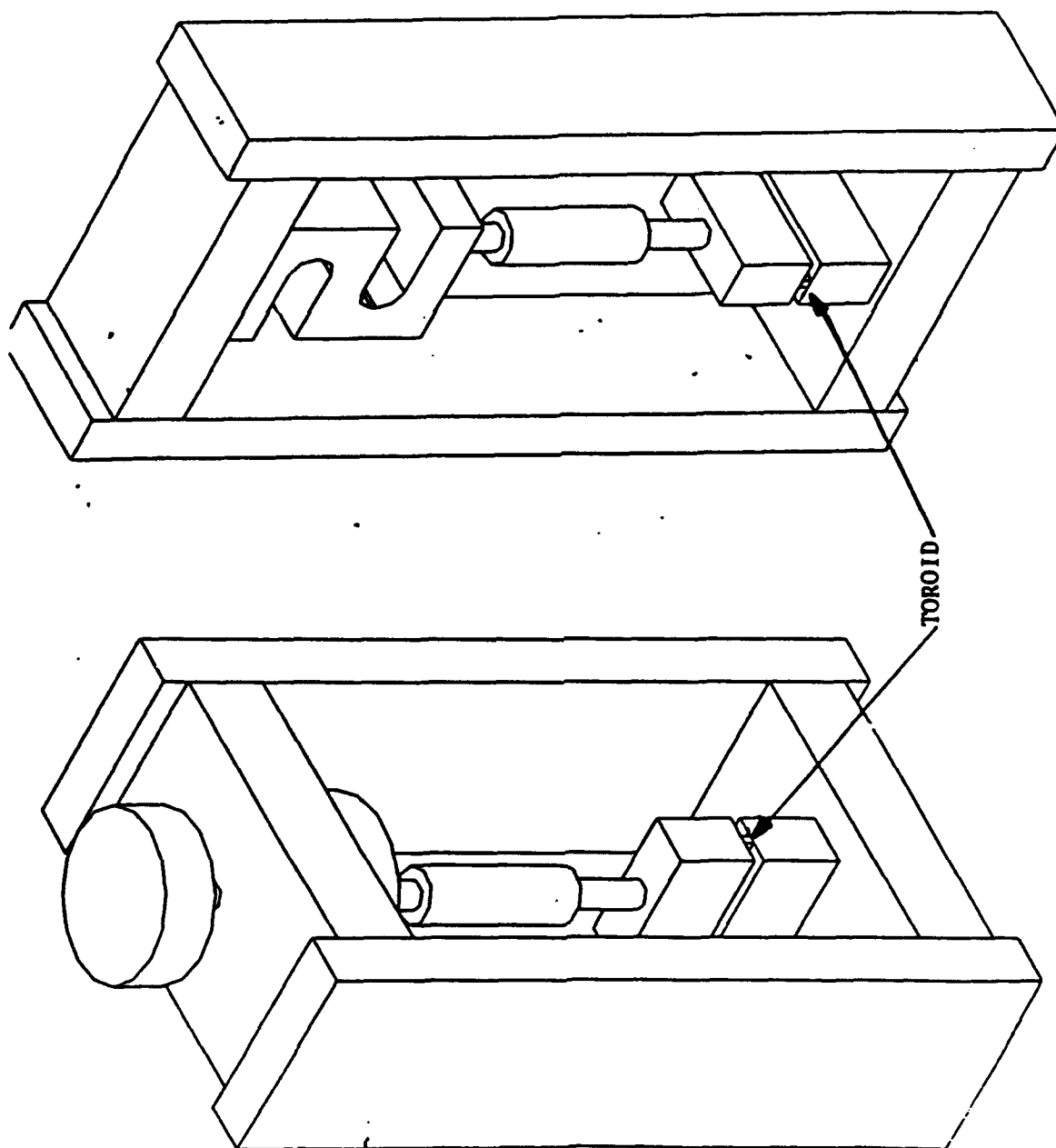solid solutions of YIG and TbIG using the single crystal

FIGURE 3-6

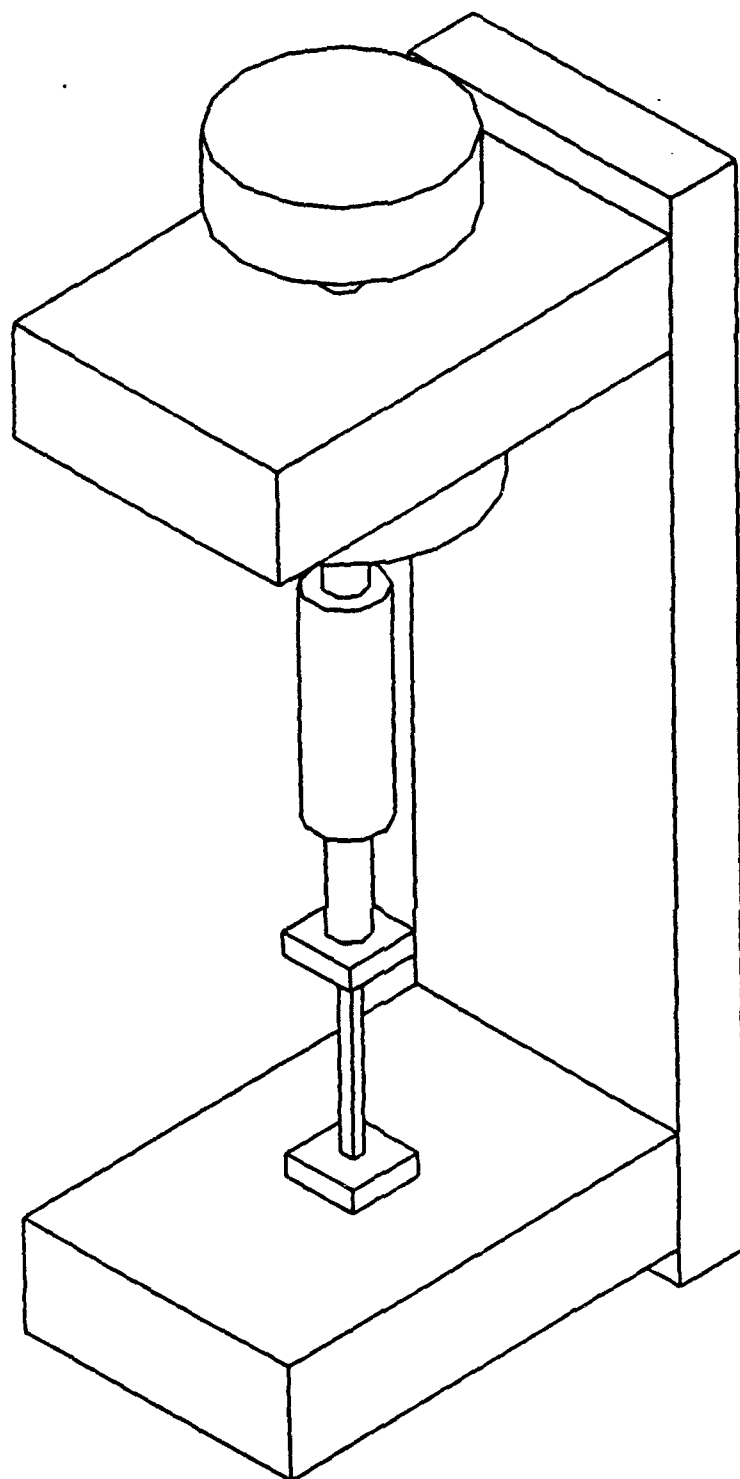SCHEMATIC OF FIXTURE FOR STATIC STRESS TESTS
(Top to Bottom Stress on Toroid)

TOROID

**FIGURE 3-7**

SCHEMATIC OF FIXTURE FOR STRESS TESTS
(Longitudinal Stress)

| Material | | Magnetostrictive Constants | Expected Changes in Hysteresis Properties With Stress |
|---|---|---|---|
| G-352 | YIG | $\lambda_{100} = -1.4 \times 10^{-6}$ | Top to Bottom Br ↑ |
| | | $\lambda_{111} = -2.4 \times 10^{-6}$ | End to End Br ↓ |
| | TbIG | $\lambda_{100} = -3.3 \times 10^{-6}$ | |
| | | $\lambda{111} = +12 \times 10^{-6}$ | |
| G-353 | 90% YIG · 10% TbIG | $\lambda_{100} = -1.6 \times 10^{-6}$ | Top to Bottom Br ↑ |
| | | $\lambda_{111} = -0.96 \times 10^{-6}$ | End to End Br ↓ |
| G-354 | 83.3% YIG · 16.7% TbIG | $\lambda_{100} = -1.72 \times 10^{-6}$ | |
| | | $\lambda_{111} = 0$ | 0 |
| G-355 | 75% YIG · 25% TbIG | $\lambda{100} = -1.88 \times 10^{-6}$ | Top to Bottom Br ↓ |
| | | $\lambda{111} = +1.2 \times 10^{-6}$ | End to End Br ↑ |
| G-356 | 65% YIG · 35% TbIG | $\lambda_{100} = -2.07 \times 10^{-6}$ | Top to Bottom Br ↓ |
| | | $\lambda_{111} = +2.64 \times 10^{-6}$ | End to End Br ↑ |

FIGURE 3-8

$\lambda_{100}$ and $\lambda_{111}$ data reported by Iida (see Table 2-1). These test samples were polycrystalline, and the expected changes in remanent magnetization with stress are noted in Figure 3-8. Figure 3-9 lists the observed changes in the hysteresis loops with stress. These observations are fully consistent with expected changes and the G-354 compound (16.7% TbIG) with a $\lambda_{111}$ computed to be zero, exhibited no observable stress sensitivity to both top to bottom and longitudinal compressive stress.

Photographs of the hysteresis characteristics with longitudinal compressive stress are presented in Figures 3-10, 3-11 and 3-12. Figure 3-10 is YIG which is very stress sensitive. Figure 3-11 is the 16.7% Tb substituted YIG. This compound exhibits no observable stress sensitivity. Figure 3-12 is a 35% Tb substituted YIG. In this compound $\lambda_{111}$ has been molecularly changed to a positive value. Longitudinal compressive stress should support magneto-crystalline anisotropy in this case (tendency to increase Br and increase Hc).

These photos do not indicate any significant observed increase in Br, but the loop does appear to be ballooned out, perhaps as a result from Hc increasing.

These data are significant in encouraging molecular engineering techniques to reduce stress sensitivity in garnets and the ability to observe improvements in static stress tests.

During Phase I (first year of the program) the static test fixture shown in Figure 3-6 and 3-7 was used extensively to characterize the stress sensitivity of the materials up to 4000 PSI. Considerable data taken using this fixture were presented in the Phase I report. By comparing the static stress response from this fixture with that observed from the actual phaser structure (top to bottom crush characteristics) in tests performed during Phase I, it was apparent that the top to bottom stress applied to the toroids in the phaser dual toroid structure was considerably less than 1000 PSI. More careful investigations indicated that the top to bottom crush stress never appeared to exceed 100 PSI. This observation suggested that if materials were to be fully evaluated from static tests only, that much lower stress levels should be used than initially anticipated.

| FINGER APPLIED STRESS | G-352 YIG | G-353 90% YIG · 10% TbIG | G-354 83.3% YIG · 16.7% TbIG | G-355 75% YIG · 25% TbIG | G-356 65% YIG · 35% TbIG |
|---|---|---|---|---|---|
| | $\lambda_{100} = -1.4$ <br> $\lambda_{111} = -2.4$ | $\lambda_{100} = -1.6$ <br> $\lambda_{111} = -0.96$ | $\lambda_{100} = -1.75$ <br> $\lambda_{111} = 0$ | $\lambda_{100} = -1.88$ <br> $\lambda_{111} = +1.2$ | $\lambda_{100} = -2.07$ <br> $\lambda_{111} = +2.64$ |
| **SQUARE TOROIDS** <br> Stress Top to Bottom <br> Expected Change in Hysteresis loop | Br ↑ | Br ↑ | 0 | Br ↓ | Br ↓ |
| Observed | Br ↑; Hc ↑ | Br ↑; Hc ↑ | Br –; Hc – | Br ↓; Hc ↓ | Br ↓; Hc – |
| **SQUARE TOROIDS** <br> Stress End to End <br> Expected | Br ↓ | Br ↓ | 0 | Br ↑ | Br ↑ |
| Observed | Br ↓; Hc ↓ | Br ↓; Hc ↓ | Br –; Hc – | Br ↑; Hc ↑ | Br ↑; Hc ↑ |
| **ROUND TOROIDS** <br> Stress Top to Bottom <br> Expected | ? | ? | ? | ? | ? |
| Observed | Br ↓; Hc ↑ | Br ↓; Hc ↑ | Br –; Hc – | Br ↓; Hc – | Br ↓; Hc – |
| **ROUND TOROIDS** <br> Stress End to End <br> Expected | Br ↓ | Br ↓ | 0 | Br ↑ | Br ↑ |
| Observed | Br ↓; Hc ↓ | Br ↓; Hc ↓ | 0 | Br ↑; Hc ↑ | Br ↑; Hc ↑ |

OBSERVED CHANGES IN HYSTERESIS LOOP WITH STRESS IN YIG–TbIG COMPOUNDS
(Square and Round Thin Walled Tubular Samples)
FIGURE 3-9

ILLUSTRATION OF HYSTERESIS CHARACTERISTIC OF YIG TOROID
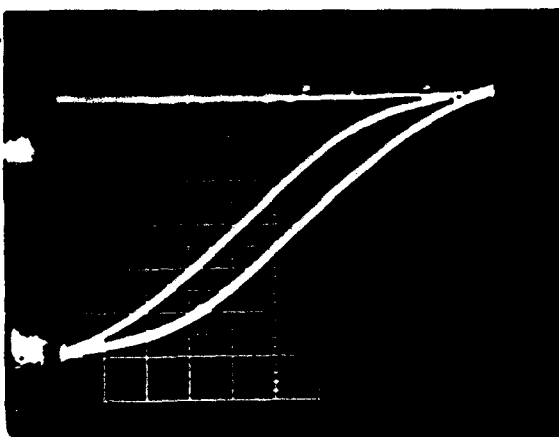UNDER LONGITUDINAL COMPRESSIVE STRESS

$\lambda_{100}$ AND $\lambda_{111}$ ARE BOTH NEGATIVE FOR YIG.
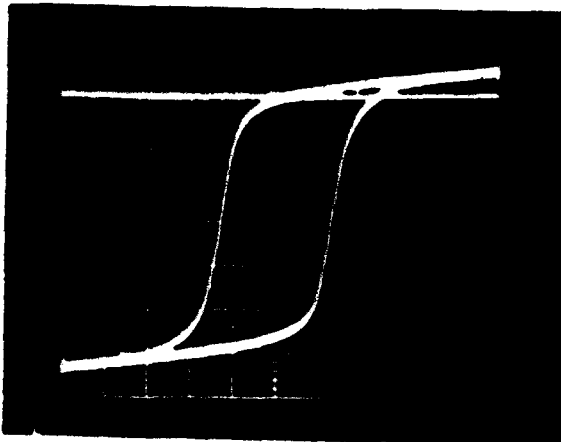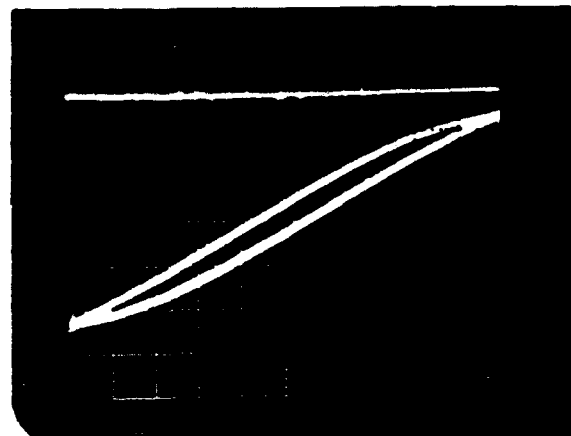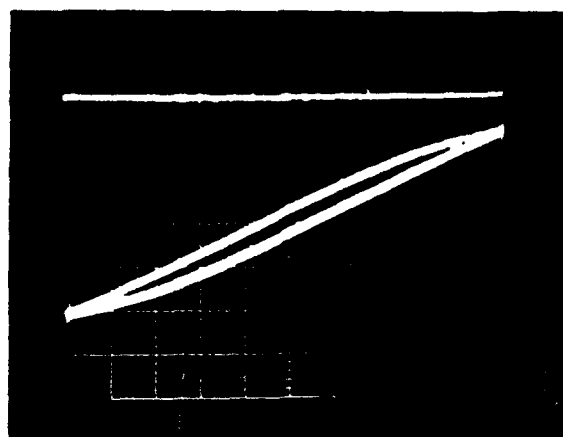


352 - YIG 0 PSI
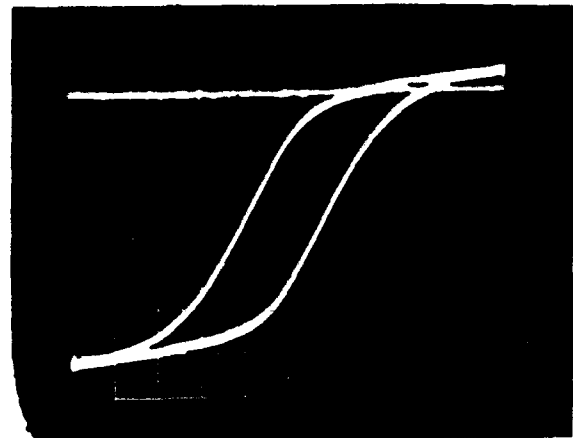
352 - YIG 1000 PSI
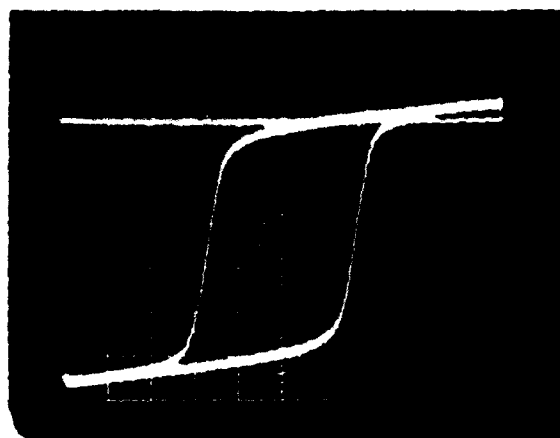
352 - YIG 2000 PSI

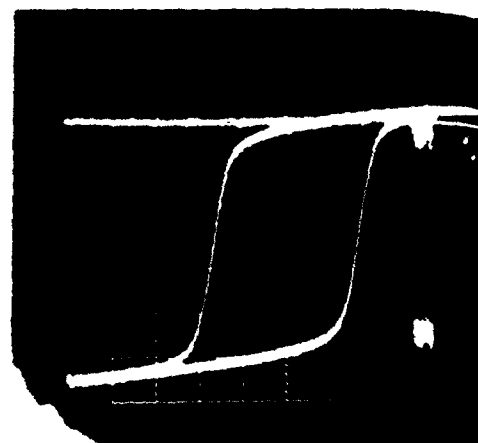352 - YIG 3000 PSI

352 - YIG 4000 PSI

FIGURE 3-10

ILLUSTRATION OF HYSTERESIS CHARACTERISTIC OF (YIG . 16.7% TbIG) UNDER
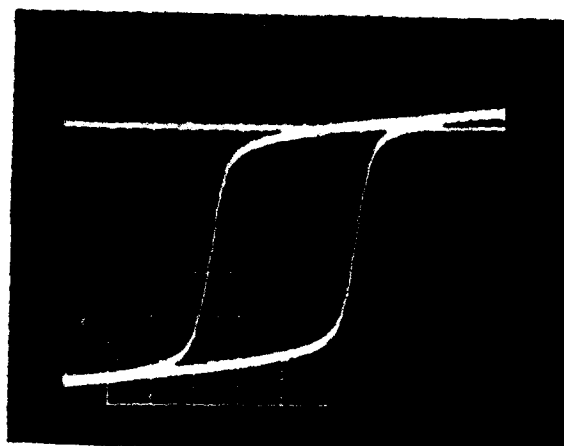LONGITUDINAL COMPRESSIVE STRESS

$\lambda_{100}$ IS NEGATIVE; $\lambda_{111} = 0$
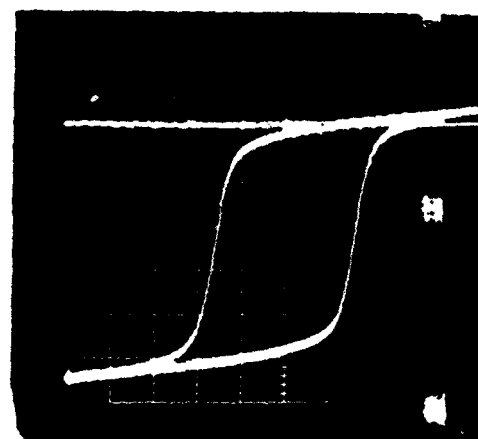


354 - YIG .167 Tb     0 PSI
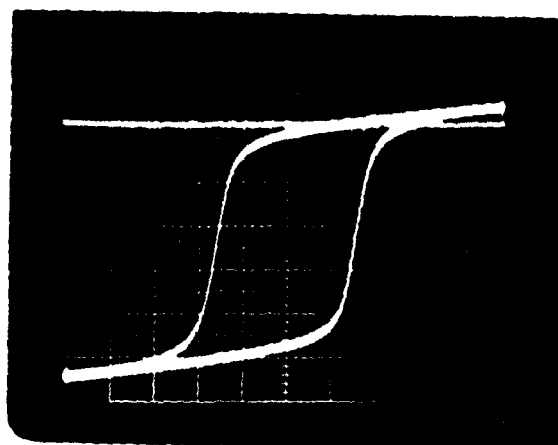
354 - YIG .167 Tb     1000 PSI

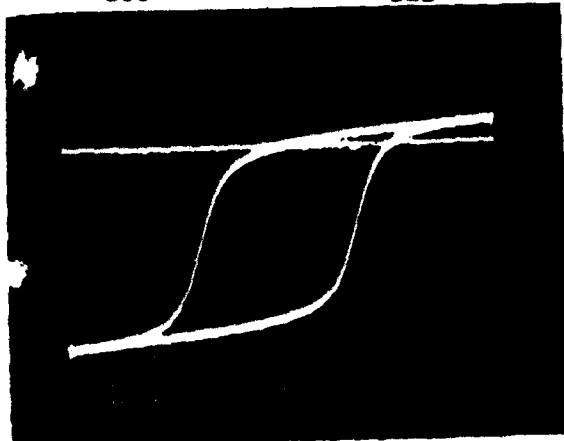354 - YIG .167 Tb     2000 PSI

354 - YIG .167 Tb     3000 PSI

354 - YIG .167 Tb     4000 PSI
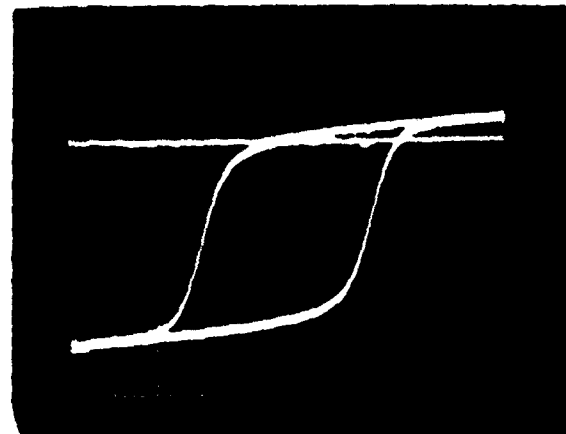
FIGURE 3-11

ILLUSTRATION OF HYSTERESIS CHARACTERISTIC OF (65% YIG . 35% TbIG) UNDER
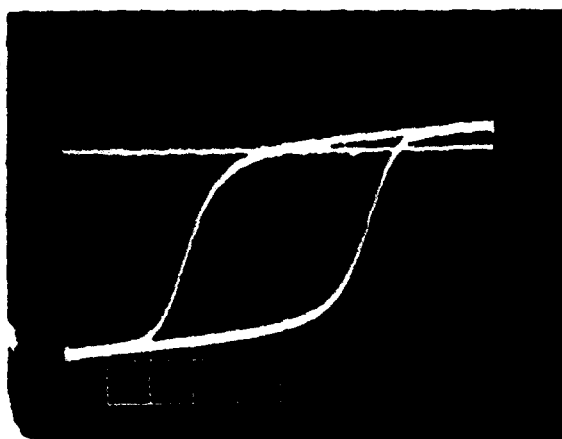LONGITUDINAL COMPRESSIVE STRESS

$\lambda_{100}$ IS NEGATIVE; $\lambda_{111}$ IS POSITIVE
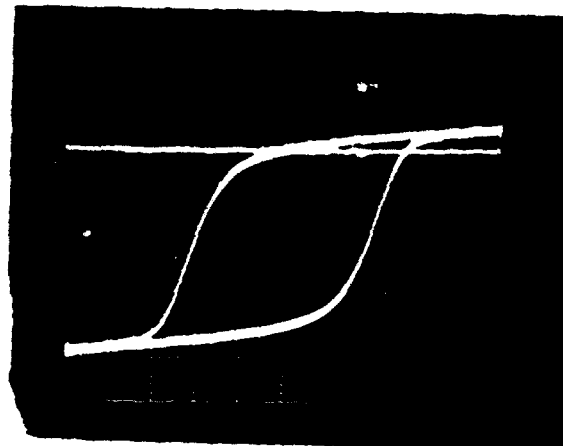


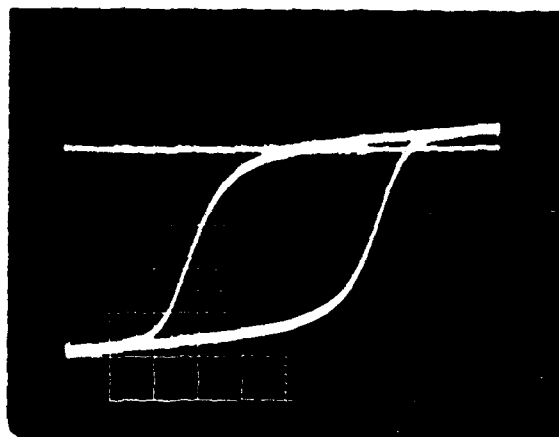356 - YIG .35 Tb     0 PSI

356 - YIG .35 Tb     1000 PSI

356 - YIG .35 Tb     2000 PSI

356 - YIG .35 Tb     3000 PSI

356 - YIG .35 Tb     4000 PSI

FIGURE 3-12

After considerable tests of materials at much lower stress using the fixture shown in Figure 3-6 and 3-7, it was concluded that this test fixture was not suitable for reproducible static evaluation of materials at stresses below 500 PSI. Stress levels could not be reproduced and the low pressure levels desired changed with time apparently from creep and thermal expansion associated with the test fixture.

A number of new static test fixtures were evaluated and the fixture yielding best correlation of static tests with RF phaser performance is shown in Figure 3-13. This test fixture is similar to the phaser structural environment. The fixture can accommodate four toroids at once. One inch long toroids were used; however, the fixture could be readily adapted for any size and shape toroid. Stress (pressure) was controlled through the use of metal shims, and rubber stress relief was incorporated in a similar fashion to that used in the phaser housing. This test fixture is referred to as the Phaser Simulator Test Fixture (PSTF).

Two such fixtures were used allowing for the evaluation of eight toroids (materials) during the same test run. Four one inch long toroids with the same cross sectional dimensions were mounted in each test structure. Stress was adjusted via shims to 100 PSI as determined by compression characteristics of the rubber in the stress path. This test fixture allowed for generation of repeatable stress levels and also created a static stress environment very similar to phaser structure. The entire test fixture was placed into an environmental chamber for the measurement of hysteresis characteristics as a function of temperature.

The PSTF structure utilizes the same silicone solid rubber material used in the soft top phase shifter housings. The typical rubber thickness used was 1/32 inch (measured to be 0.034" thick). The force in PSI required to compress the rubber was supplied by the manufacturer (CHR Industries, COHR lastic 300). For example, to compress the rubber 40% required 90 PSI. This requires the rubber thickness to be compressed to a thickness of 0.0204". The amount of compression (in mils) was controlled by varying the dimensions of the steel plate shown in Figure 3-13. The compressed response data supplied is linear. By controlling the compression of the rubber, the stress on the ferrite toroid could be varied and controlled. Typical procedure was to measure the hysteresis properties
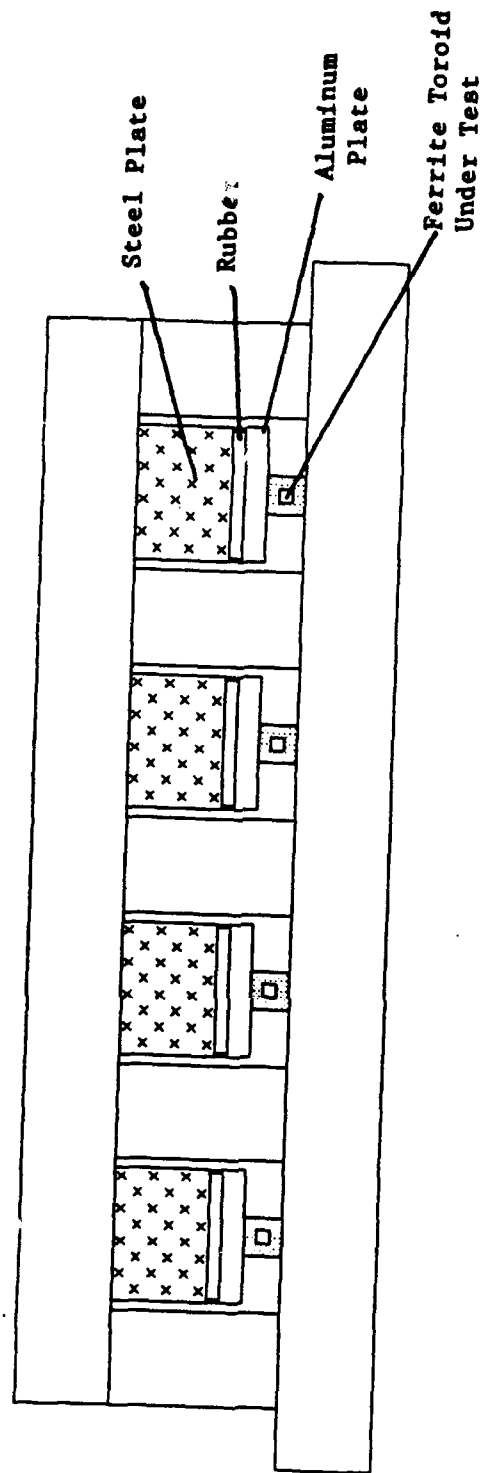
FIGURE 3-13   STATIC TEST FIXTURE (PHASER SIMULATION TEST
FIXTURE, PSTF)

of the material in the PSTF with no stress at 25°C. The rubber requires a compression set after pressure is applied that is achieved by 12 hour temperature soak at 110°C. The compression set reduces the stress to 85% of its initial value. For a desired PSI stress on the ferrite material, the required rubber compression was computed and implemented in the PSTF accounting for the 85% compression set. Hysteresis properties were again measured before and after the compression set. These known and measured characteristics allowed the PSTF to be used successfully up to stress levels of 500 PSI. In addition, the computed stress characteristics of the structure considering the coefficient of thermal expansion of each component indicated constant stress ($\pm 5$ PSI) up to 100°C.

Considerable time and effort were devoted to this area. It is believed that the accuracy and reproducibility of the PSI levels resulting from this procedure were never worse than $\pm 10\%$.

The PSTF structure was used to evaluate the stress characteristic of all the materials studied during the program. The data from the PSTF correlated well with that collected from actual dual toroid phase shifter structures. Data collected using the PSTF are presented in Section 7.

## 3.4    MANGANESE CHEMISTRY

As discussed in Section 2, $Mn^{+3}$ substitution in garnets has been observed to reduce the stress sensitivity of these compounds. $Mn^{+3}$ has been successfully substituted for $Fe^{+3}$ in the structure in amounts up to 0.1 ions/formula unit without second phase detection. In amounts above this level, second phase formation is likely. The garnet structure readily accepts only +3 ions unless valence compensation is otherwise planned, such as in the bismuth-calcium vanadium iron garnets.

Two areas of concern in studies regarding $Mn^{+3}$ substitutions are the need to prepare single phase compounds with $Mn^{+3}$ substitutions up to 0.2 ions/formula unit and the assurance that $Mn^{+3}$ is actually the ion in the final garnet structure. Manganese can possess a valence from +2 to +7 as noted in Figure 3-14. Manganese in a +3 valence is not available in a stable oxide as a

| Valance | Compound | Mol. Wt | Comments |
|---|---|---|---|
| +2 | $Mn^{+2}CO_3$ | 114.94 | Density 3.125 gm/cm$^3$<br>Decomposes with heat<br>Solubility in $H_2O$-<br>    .0065 gms/100 ml of Cold $H_2O$<br>Color: Rose pink or Light brown<br>        Powder |
| +2 | $Mn^{+2}O$ | 70.93 | Density 5.45 gm/cm$^3$<br>Melting Point 1650°C<br>Stable<br>Color: Green |
| +2, +3 | $Mn_3O_4$<br>$Mn^{+2}Mn_2^{+3}O_4$ | 228.79 | Density 4-85.6 gm/cm$^3$<br>Melting Point 1705°C<br>Color: Black |
| +3 | $Mn_2^{+3}O_3$ | 157.86 | Density 4.5 gm/cm$^3$<br>Decomposes with loss of $O_2$ at 1080°C<br>$2Mn_2O_3 \longrightarrow 1080°C\ 4MnO+O_2$?<br>Color: Black |
| +4 | $Mn^{+4}O_2$ | 86.93 | Density 5.026 gm/cm$^3$<br>Decomposes with loss of oxygen at<br>535°C $2MnO_2 \longrightarrow 535°C\ 1MnO+O_2$?<br>Color: Brown/Black |
| +6 | $MnO_3$ | | |
| +7 | $Mn_2O_7$ | | |

FIGURE 3-14

Some Characteristics of Manganese Compounds

starting compound. Starting manganese compounds available are $MnCO_3$ ($Mn^{+2}$), $MnO_2$ ($Mn^{+4}$) and $MnO$ ($Mn^{+2}$). Therefore to reach the $Mn^{+3}$ ion desired in the structure, some solid state chemical reactions must take place to create this ionic state by forming $Mn_2^{+3}O_3$.

Some attention was given to this area in an effort to produce the $Mn^{+3}$ substitution desired. Some of the characteristics of the various manganese compounds are listed in Figure 3-14. Figure 3-15 lists some of the possible solid state chemical reactions (under heat treatment) that may be encountered with starting compounds of $MnCO_3$, $MnO_2$ and $MnO$. Since the desired valence is +3, those reactions resulting in the possible formations of $Mn_2O_3$ are of prime interest for enhancement.

Manganese carbonate ($MnCO_3$) is the compound containing manganese that is most commonly used for substitution into ferrites and garnets. $MnO_2$ is also available but is a less pure, more coarse compound and thus less desirable to process.

Some heat treatment studies were conducted on $MnCO_3$ as outlined in Figure 3-16. $MnCO_3$ is a light brown powder. As noted in Figure 3-16, after a heat treatment to 600°C this powder turned black with a weight loss of 32.5%. This suggests the formation of $Mn_2O_3$. Additional heat treatment at 800°C did not significantly change the result and powder. Further heat treatment at 1200°C resulted in a brown/black powder and a weight loss of 10.1%. This suggests the decomposing of $Mn_2O_3$ to $MnO$ and a $Mn$ valence of +2.

This observation is of some concern since the garnet compounds are sintered at temperature above 1400°C. However, presintering of the mixed oxides is conducted near 1200°C and, at this point in the present study, it is assumed that the desired $Mn^{+3}$ ion is locked into the garnet compound and thus not free to be reduced to $Mn^{+2}$. This possibility may also suggest that sintering should be conducted in an oxygen environment to enhance the possibility of maintaining the manganese in a +3 valence state.

Desire/Require $Mn^{+3}$ in Garnet Structure

Oxides/Carbonates Available

$Mn^{+2}CO_3$         Molecular Wt. 114.94

$Mn^{+4}O_2$         Molecular Wt.  86.93

$Mn_3^{+2, +3}O_4$      Molecular Wt. 228.79

$Mn^{+2}O$          Molecular Wt.  70.93

$Mn_2^{+3}O_3$        Molecular Wt. 157.86

Possible Reactions:

1) $Mn^{+2}CO_3 \xrightarrow{\text{heat}} Mn^{+2}O + CO_2$

2) $2 Mn^{+2}CO_3 \xrightarrow{\text{heat}} Mn^{2+3}O_3 + CO + CO_2$

$\xrightarrow{600°C}$

$\longrightarrow 2Mn^{+2}O + 2CO + O_2$

$\longrightarrow 2Mn^{+2}O + 2CO_2$

3) $4Mn^{+2}O + O_2 \longrightarrow 2Mn_2^{+3}O_3$

4) $2Mn^{+4}O2 + O_2 \longrightarrow Mn_2^{+3}O_3$

5) $2Mn^{+4}O_2 \longrightarrow 2Mn^{+2}O + O_2$

6) $4 Mn O + O_2 \longrightarrow 2Mn_2^{+3}O_3$
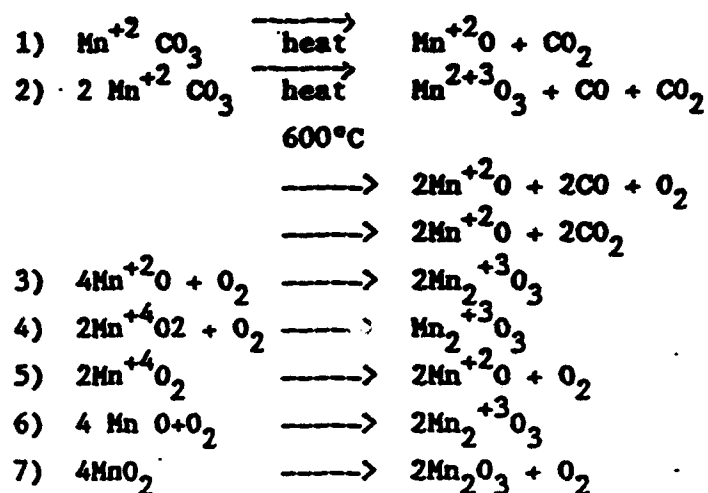
7) $4MnO_2 \longrightarrow 2Mn_2O_3 + O_2$

FIGURE 3-15

Manganese Chemistry (Available oxides/carbonates and
possible solid state chemical reactions)

# EXPERIMENTAL STUDY

## DECOMPOSITION OF MANGANGESE CARBONATE ($MnCO_3$)

Determine the decomposition products of $MnCO_3$ by observing weight loss and color changes in powder heat treated under various conditions.

1) Heat treat a sample of MnCO3 at 600°C for 4 hours in air. Observe the weight loss and color change of the powder.

2) Repeat the first experiment using a flowing oxygen atmosphere. Observe the weight loss and color change for this powder.

3) Using the material from experiment #2 continue heat treatment cycles at 800°C and 1200°C for 4 hours in an air atmosphere. Determine the weight loss for each of these heat treatments.

RESULTS:

| Heat Treatment Cycle | Measured Weight Loss | Color |
|---|---|---|
| #1  600°C/4 hrs AIR | 32.5 % | Black Powder |
| #2  600°C/4 hrs OXYGEN | 32.5 % | Black Powder |
| #3  800°C/4 hrs AIR | 1.2 % | Black Powder |
| 1200°C/4 hrs AIR | 10.1 % | Brown/Black |

Possible Decomposition Reaction for $MnCO_3$:

Calculated Weight Loss

$$2\ MnCO_3 \xrightarrow{600°C} Mn_2O_3 + CO + CO_2 \qquad 31.3\ \%$$

$$Mn_2O_3 \xrightarrow{800°C} Mn_2O_3 \ (\text{No decomposition}) \qquad 0.0\ \%$$

$$2\ Mn_2O_3 \xrightarrow{1200°C} 4\ MnO + O_2 \qquad 10.1\ Z$$

FIGURE 3-16

Some batches of Mn substituted garnets were prepared with a 0.15 weight %
bismuth addition to possibly lower the reaction temperature and thereby retard
the possibility of a valence conversion of the Mn ions. In these batches,
bismuth was added to the mixed oxides before presintering in one case and after
presintering in another. presintering temperatures of 1050°C and 1225°C were
used. No significant changes in the characteristics of the fully sintered
compound were observed from these investigations to indicate a valence change of
the Mn.

## 3.5    MANGANESE SUBSTITUTION IN HYBRID YTTRIUM-GADOLINIUM GARNETS

A mixed yttrium - gadolinium iron garnet (YIG-GdIG) compound ($4\pi M_s$ near 1000
gauss) was selected for the investigation of $Mn^{+3}$ substitution to achieve an
improved stress insensitive material for X-band phaser applications.

The materials studied were based on a 56 2/3% YIG and 43 1/3% GdIG compound.
Assuming a solid solution of these two garnets substituted with $Mn^{+3}$, the
magnetostrictive characteristics presented in Figure 3-17 would be expected.
These data are computed using weighted percentages and Dionne's magnetostrictive
constants presented in Section 2.

With no cobalt (Co) in the structure (Y=0), $\lambda_{111}$ would reach 0 near a $Mn^{+3}$
substitution of 0.2. At this substitution, $\lambda_{100}$ would be a fairly large
positive value of near +16.

To achieve the characteristics of $K_1>0$ and $\lambda_{111}=0$, as discussed in Section 2.2.1
as a stress insensitive condition, $Co^{+2}/Si^{+4}$ can be substituted into this
compound for $Fe^{+3}$. As indicated in Figure 3-17 and 3-18, a $Co^{+2}/Si^{+4}$ amount of
0.0225 would appear sufficient to increase $K_1$ to a slightly positive value with
a $Mn^{+3}$ content for $\lambda_{111}=0$ of near 0.15.

This analysis formed the initial basis for formulating the $Mn^{+3}$ substituted
garnet compounds for preparation and evaluation.
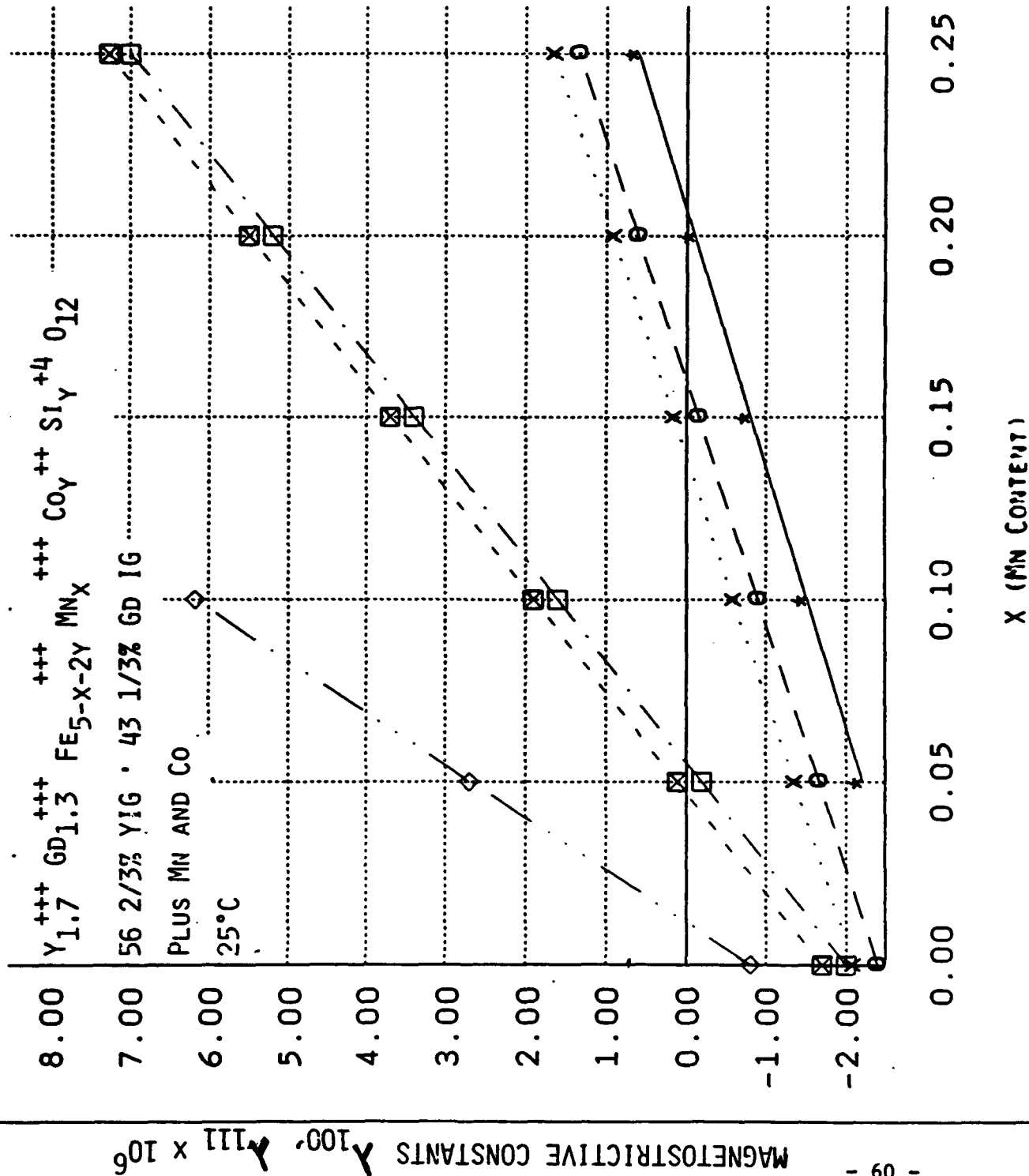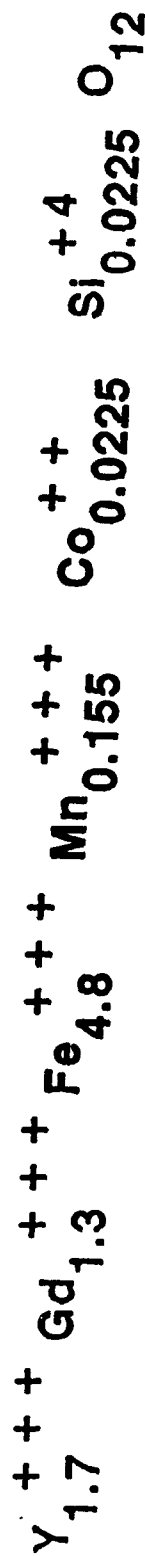
Mn, Co Effects on Magnetostriction

FIGURE 3-17

- 60 -

## STRESS INSENITIVE GARNET COMPOUND

**CONDITIONS:** $K_1 > 0$

$\lambda_{111} = 0$

$Y_{1.7}^{+++} \ Gd_{1.3}^{+++} \ Fe_{4.8}^{+++} \ Mn_{0.155}^{+++} \ Co_{0.0225}^{++} \ Si_{0.0225}^{+4} \ O_{12}$

$\lambda_{111} = 0; \quad \lambda_{100} = +10.1$
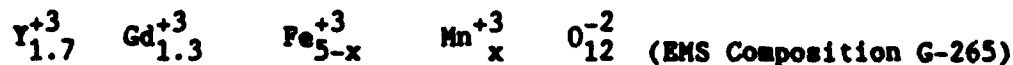
$K_1 = +1 \times 10^3 \ ergs/cm^3$

$K_2 = -3.2 \times 10^3 \ ergs/cm^3$

FIGURE 3-18
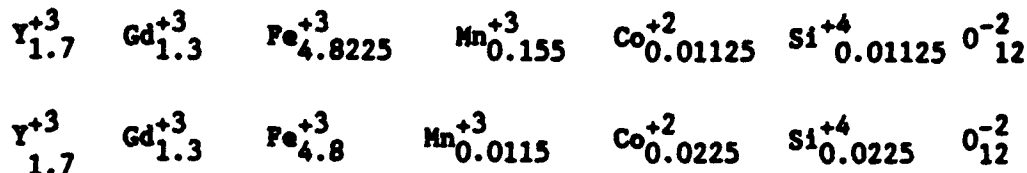
## 4.0    MATERIALS FORMULATED AND PREPARED

### 4.1    MATERIALS FORMULATED

A series of manganese substituted yttrium-gadolinium ion garnets were studied on this program with compositions given by:

$$Y^{+3}_{1.7} \quad Gd^{+3}_{1.3} \quad Fe^{+3}_{5-x} \quad Mn^{+3}_x \quad O^{-2}_{12} \quad \text{(EMS Composition G-265)}$$

Consistent with the discussion of Section 3.5, manganese substitution levels from X=0.09 to X=0.21 were investigated. These compositions are solid solutions of 56 2/3 YIG and 43 1/2% GdIG with $Mn^{+3}$ substituted for $Fe^{+3}$. They are similar to the Trans-Tech commercial product TT G-1002+09Mn, which served as a baseline material.

Some experimental batches of cobalt substituted garnets (as suggested in Section 3.5) were also prepared with composition:

$$Y^{+3}_{1.7} \quad Gd^{+3}_{1.3} \quad Fe^{+3}_{4.8225} \quad Mn^{+3}_{0.155} \quad Co^{+2}_{0.01125} \quad Si^{+4}_{0.01125} \quad O^{-2}_{12}$$

$$Y^{+3}_{1.7} \quad Gd^{+3}_{1.3} \quad Fe^{+3}_{4.8} \quad Mn^{+3}_{0.0115} \quad Co^{+2}_{0.0225} \quad Si^{+4}_{0.0225} \quad O^{-2}_{12}$$

Experimental batches of a pair of cerium doped garnets were also prepared with the following formulation:

$$Y^{+3}_{1-x} \quad Ce^{+3}_x \quad Fe^{+3}_5 \quad O^{-2}_{12} \ , \qquad \text{with } x = 0.025 \text{ and } 0.05$$

The cerium batches were intended to check on earlier reported work on the effects of cerium doping to alleviate magnetostriction problems in garnets.

In addition to these custom materials, several other yttrium gadolinium and yttrium aluminum iron garnets with differing amounts of manganese doping were tested as was a lithium ferrite (spinel) and a magnesium manganese ferrite (TT1-105) sample.

The various garnets had magnetizations of 1780 (YIG,G203-22),1600 (G231-13), 1000 (G293-5), and 800 (G273-12) gauss and are variations on the commercial materials TT G-113, TT G-1600, TT G-1010, and TT G-800 respectively. The lithium ferrite tested is a standard product of the EMS Materials Lab, EL1300 (4$\pi$Ms - 1300 gauss).

## 4.2 MATERIALS PREPARATION

Over the course of this program considerable attention has been paid to the problems associated with proper stoichiometry of the garnets. Single phase garnet materials are only produced for a very narrow compositional field, and the addition of manganese seems to exacerbate this problem. Because the ceramic processes of mixing powders and milling calcined material always involve some iron pick up, allowance must be made in the starting mixtures to allow for some subsequent iron pick-up. Starting iron deficiencies ranging from 1.0 to 3.6 percent were tested, and the results (for a Mn addition of 0.15) are shown in Table 4-1.

Table 4-1  Study of Effect of Iron Stoichiometry on Material Properties

| Iron Deficiency | Density (gms/cc) | Tandm | ke | Tande | 4$\pi$Ms (gauss) | Br (gauss) | Hc (oersteds) |
|---|---|---|---|---|---|---|---|
| 1% | 5.59 | .00429 | 15.0 | .00019 | 1058 | 654 | 1.61 |
| 2% | 5.57 | .00087 | 14.7 | .00012 | 1015 | 654 | 1.58 |
| 2.25% | 5.58 | .00087 | 15.1 | .00012 | 1056 | 771 | 1.13 |
| 2.5% | 5.69 | .00087 | 15.4 | .00012 | 1068 | 717 | 1.29 |
| 3% | 5.67 | .00092 | 15.3 | .00009 | 1045 | 774 | 1.3 |
| 3.6% | 5.72 | .00051 | 15.0 | .00029 | 1010 | 457 | 2.15 |

At the low iron deficiencies, or final high iron content, the garnets have excessively high magnetic loss. This is caused by a second phase that is presumably Mn ferrite or magnetite which both have large values of saturation magnetization ($\sim$ 5000 gauss) and low field losses that extend well up into the X-band region. Magnetic loss is very sensitive to even quite small amounts of such second phases. At a 2.0% iron deficiency in the starting mix the magnetic loss begins to increase.

The various garnets had magnetizations of 1780 (YIG,G203-22),1600 (G231-13), 1000 (G293-5), and 800 (G273-12) gauss and are variations on the commercial materials TT G-113, TT G-1600, TT G-1010, and TT G-800 respectively. The lithium ferrite tested is a standard product of the EMS Materials Lab, EL1300 ($4\pi Ms = 1300$ gauss).

## 4.2    MATERIALS PREPARATION

Over the course of this program considerable attention has been paid to the problems associated with proper stoichiometry of the garnets. Single phase garnet materials are only produced for a very narrow compositional field, and the addition of manganese seems to exacerbate this problem. Because the ceramic processes of mixing powders and milling calcined material always involve some iron pick up, allowance must be made in the starting mixtures to allow for some subsequent iron pick-up. Starting iron deficiencies ranging from 1.0 to 3.6 percent were tested, and the results (for a Mn addition of 0.15) are shown in Table 4-1.

Table 4-1  Study of Effect of Iron Stoichiometry on Material Properties

| Iron Deficiency | Density (gms/cc) | Tandm | ke | Tande | $4\pi Ms$ (gauss) | Br (gauss) | Hc (oersteds) |
|---|---|---|---|---|---|---|---|
| 1% | 5.59 | .00429 | 15.0 | .00019 | 1058 | 654 | 1.61 |
| 2% | 5.57 | .00087 | 14.7 | .00012 | 1015 | 654 | 1.58 |
| 2.25% | 5.58 | .00087 | 15.1 | .00012 | 1056 | 771 | 1.13 |
| 2.5% | 5.69 | .00087 | 15.4 | .00012 | 1068 | 717 | 1.29 |
| 3% | 5.67 | .00092 | 15.3 | .00009 | 1045 | 774 | 1.3 |
| 3.6% | 5.72 | .00051 | 15.0 | .00029 | 1010 | 457 | 2.15 |

At the low iron deficiencies, or final high iron content, the garnets have excessively high magnetic loss. This is caused by a second phase that is presumably Mn ferrite or magnetite which both have large values of saturation magnetization (~ 5000 gauss) and low field losses that extend well up into the X-band region. Magnetic loss is very sensitive to even quite small amounts of such second phases. At a 2.0% iron deficiency in the starting mix the magnetic loss begins to increase.

At high iron deficiencies, or final low iron content, the garnets have low values of remanent magnetization, $B_r$. This is presumably caused by the presence of a second phase of an orthoferrite whose magnetization is very small. These particles act as non-magnetic inclusions and interrupt flux lines, thereby reducing the remanent flux. The onset of serious reduction in $B_r$ values occurs at 3.6% iron deficiency in the starting mix.

High quality materials have been prepared with iron deficiencies in the starting powders of 2.25% to 3.0%. Garnets with Mn contents of 0.09 to 0.15 have been made with low dielectric loss ($\leq 0.00016$), low magnetic loss ($\leq 0.001$), and remanent flux values of $\geq 700$ gauss. For the higher Mn contents (0.17 to 0.21), the remanence drops off.

The preparation of high quality garnets having high Mn contents also requires some adjustment in firing temperature. Negligible differences in properties were found as the firing temperature was varied from 1425 to 1450°C, until relative high Mn contents (>.15) were reached. At the higher Mn contents it was necessary to reduce the firing temperature somewhat to prevent serious loss of remanent flux.

The use of an oxygen atmosphere was standard practice in sintering these materials, but the improvement in properties was barely above the detectable level for most compositions. For those compounds on the acceptable iron rich side of stoichiometry, sintering in an oxygen atmosphere reduced the magnetic loss tangent.

A number of selected samples of the manganese substituted garnets were sent to the Center for Advanced Ceramic Technology at Alfred University for analysis using the energy dispersive spectrocopy (EDS) capabilities of their Scanning Electron Microscope (SEM).

Figure 4-1 shows a backscattered SEM EDS micrograph (magnification 1000X) of a sample of G-265 with 0.12Mn substitution. The micrograph shows the presence of yttrium(Y), iron(Fe), and gadolinium(Gd) in substantial quantities in relative agreement with the composition. The micrograph does not clearly identify the presence of any manganese (Mn). The energy of the Mn peak, if present, is noted on the micrograph and is very close to that of Gd. The EDS detection limit is about 2 atomic percent, and our substitution of Mn in this case was about 1.5 atomic %. In this sample there were very small regions (scattered grains) that exhibited micrographic characteristics showing different ratios of Y,Gd, and Fe indicating a possible need for minor mixing and/or sintering adjustments.

In samples containing large substitutions of Mn such as 0.21, scattered dark grains were evident in the micrographs, and the EDS analysis indicated that these grains contained only Mn and Fe and thus were clearly undesirable. It is believed that samples with Mn substitutions above 0.15 may contain a scattered matrix of these grains and processing to reduce their presence becomes much more difficult.

Table 4-2 lists the six levels of Mn doping prepared in the G-265 family of compounds, based on a solid solution of 56 2/3% YIG and 43 1/3% GdIG. The commercial TT G-1002 with 0.09 Mn is also listed as the baseline material. The measured values of 4πMs of the G-265 compounds are, on the average, slightly higher than G-1002. This may be due to slight differences in the Gd content of the composition. The G-265 compounds also possess slightly higher Br and Hc values. This is believed to be due to microstructure differences. The G-265 compounds possess a smaller and thus more uniform average gain size. Also included in this table are the additional materials tested for stress sensitivity: G203 (a manganese doped YIG), TT G1600 and G231(1600 gauss YGdIG), TT G1010 and G293(1000 gauss YAlIG), TT G800 and G273(800 gauss YGdAlIG), TT1-105(a magnesium manganese spinel), and L141 (a lithium-titanium ferrite).
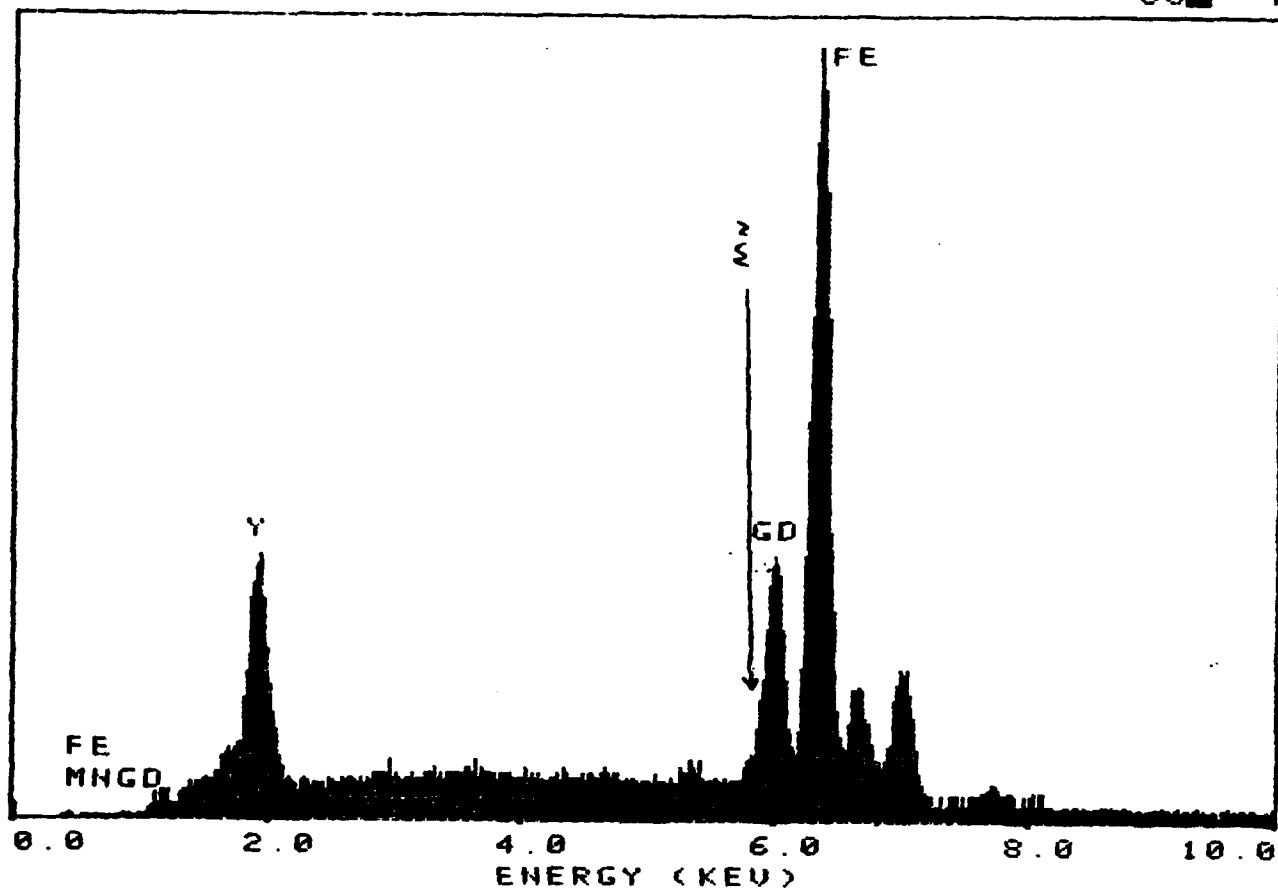
FIGURE 4-1

Energy Dispersive Spectrum of G-265 with 0.12 Mn Substitution
(EDS analysis provided by Alfred University)

| Sample | Mn | Density | Ms | Tandm | tande | ke | Br | Bd | Hc | Dbr | DH | DHK |
|---|---|---|---|---|---|---|---|---|---|---|---|---|
| *TransT1002 | 0.09 | | 1000 | 0.00068 | 0.00009 | 15.7 | 669 | 818 | 1.08 | 0.72 | 114 | 10.3 |
| G265-35 | 0.09 | 5.64 | 1097 | 0.0009 | 0.00006 | 15.4 | 723 | 816 | 1.35 | 0.772 | 137 | 12.2 |
| G265-36 | 0.11 | 5.65 | 1049 | 0.0008 | 0.00006 | 15.4 | 758 | 849 | 1.25 | 0.789 | 170 | 12.1 |
| G265-37 | 0.13 | 5.63 | 1071 | 0.00085 | 0.00006 | 15.3 | 722 | 828 | 1.25 | 0.858 | 145 | 11.8 |
| G265-33 | 0.15 | 5.62 | 1038 | 0.00092 | 0.00009 | 15.3 | 721 | 818 | 1.29 | 0.958 | 128 | 12.2 |
| G265-42 | 0.17 | 5.64 | 1106 | 0.00085 | 0.00025 | 15 | 601 | 730 | 1.5 | 0.935 | 141 | |
| G265-41 | 0.21 | 5.66 | 1013 | 0.00099 | 0.00024 | 15.3 | 645 | 763 | 1.4 | 1 | 119 | 9.63 |
| G203-22 | 0.13 | 5.04 | 1750 | 0.0008 | 0.00006 | 14.7 | 1376 | 1539 | 0.72 | 0.945 | 104 | 1.65 |
| *TT-G1600 | 0.09 | *NM | 1600 | NM | 0.0002 | 15.1 | 986 | 1165 | 0.83 | NM | 50 | 3.8 |
| G231-13 | 0.13 | 5.26 | 1560 | 0.00045 | 0.0002 | 15.0 | 1200 | 1300 | 0.75 | NM | 100 | 4.0 |
| TTG-1010 | 0.09 | NM | 1000 | NM | 0.0002 | 14.7 | 694 | 773 | 0.55 | NM | 40 | 1.4 |
| G293-5 | 0.17 | 5.05 | 1070 | 0.0008 | 0.00014 | 14.5 | 829 | 924 | 0.63 | 0.99 | 52 | 2.1 |
| TTG-800 | 0.09 | *NM | 800 | NM | 0.0002 | 14.7 | 504 | 594 | 0.69 | NM | 55 | 4.3 |
| G273-12 | 0.17 | 5.42 | 825 | NM | 0.00008 | 14.8 | 543 | 643 | 1.44 | NM | 94 | 3.7 |
| TT1-105 | 0 | *NM | 1750 | NM | 0.00025 | 12.2 | 1220 | 1343 | 1.16 | NM | 225 | 2.3 |
| L141 | 0.09 | NM | 1300 | NM | 0.0005 | 17.5 | 875 | 950 | 4.0 | NM | 650 | 3.0 |

*TRANSTECH MATERIALS

NM - NOT MEASURED

TABLE 4-2   TABULATION OF THE PROPERTIES OF MATERIALS EVALUATED

## 4.3     MATERIAL PROPERTIES

The material properties listed were all measured in the EMS materials
laboratory by standard measurement procedures.  Table 4-3 describes
measurement techniques and accuracies.  The abbreviations used to designate
the various properties are given below.

Density (in grams/$cm^3$)

Ms      Saturation magnetization ($4\pi MS$) (in gauss)

Tandm   Magnetic loss tangent

tande   Dielectric loss tangent

ke      Relative permittivity

Br      Remanent magnetic flux (in gauss)

Bd      Drive flux level, when hysteresis is measured (in gauss)

Hc      Coercive field (in oersteds)

Dbr     Ratio of remanent flux at 3000 PSI axial stress to Remanent
        flux at no stress

DH      Resonance linewidth (in oersteds)

DHk     Spinwave linewidth (in oersteds)

## TABLE 4-3

## MATERIAL PROPERTY MEASUREMENTS

| PROPERTY | MEASUREMENT TECHNIQUE | ACCURACY |
|---|---|---|
| Density | Water immersion | $\pm$ 0.02 gm/cc |
| Magnetization, $4\pi Ms$ (Gauss) | Magnetometer | $\pm$ 3 to 5 % |
| Remanent Magnetization, Br (Gauss) | Square Loop Tester | $\pm$ 5 % |
| Coercive Field, Hc (Oe.) | Square Loop Tester | $\pm$ 0.2 Oe. |
| Resonant Linewidth $\Delta H$ (3dB) (Oe.) | X-Band Transmission Cavity | $\pm$ 3 % |
| Spinwave Linewidth $\Delta Hk$ (Oe.) | X-Band Transmission Cavity | $\pm$ 10 % |
| Dielectric Loss Tangent $\tan\delta\varepsilon'$ | X-Band Transmission Cavity ASTM C525-63T | $\pm$ 0.0002 (<0.001) |
| Dielectric Constant $\varepsilon'$ | X-Band Transmission Cavity ASTM C525-63T | $\pm$ 0.3 |
| Magnetic Loss Tangent $\tan\delta m$ | X-Band Transmission Cavity | $\pm$ 0.0002 (<0.001) |
| Stress Sensitivity $\Delta Br$ | Square Loop Tester | |

Stress is applied to the toroid by placing the toroid in fixture and applying a controlled torque to a screw. Axial stress applied in the direction as shown is perpendicular to the direction of magnetization. The amount of torque applied resulted in a compressive force of 3000 psi on the toroid.
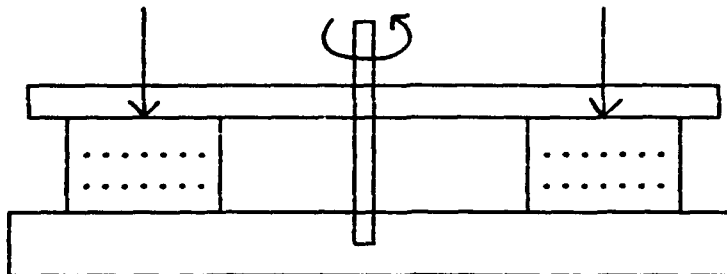
In an attempt to study the effects of processing parameters on oxidation state of the Mn ions (as discussed in Section 3.4) some batches of materials were prepared using an oxygen atmosphere in the calcine stage. These results, shown in Table 4-4, are compared to those obtained when calcining in air. The oxygen calcine ("OxCalc" under "Comments") produced results that do not differ (outside of experimental error) in any property from those of material prepared by the standard ("STD") process.

As a part of the study of manganese chemistry described in Section 3.4, some batches of the 0.15 Mn composition were prepared with preoxidized Mn added before ("Mnprecalc") the calcine step, rather than as a carbonate ($Mn^{+2}$) in the initial mix. In other batches the preoxidized $Mn^{+3}$ was added after the calcine step ("Mnpostcalc") rather than as the carbonate ($Mn^{+2}$) in the initial mixing. Both of these approaches, as seen in Table 4-5, led to somewhat lower densities and markedly lower values of remanent magnetization than obtained in the standard ("STD") process. This result is probably a reflection of less thorough mixing and a less uniform end product, rather than any effect from altering the valence of the Mn ions.

The results of these investigations would appear to support the conclusion that the divalent manganese ions initially mixed as a carbonate do convert to a trivalent state as required by the garnet chemical balance.

## 4.4    EXPERIMENTAL MATERIALS

The cobalt doped garnet materials were prepared in an attempt to achieve the characteristics of $K_1>0$ and $\lambda_{111}=0$ that have been predicted by Dionne, as discussed in Section 3.5, to yield stress insensitivity. Two batches were prepared with somewhat different calcine and firing schedules. The measured properties of these materials are given in Table 4-6 below. In both cases the hysteresis loops are  rather skewed, and the values of $B_r$ are markedly below those of other garnets. The increased values of spin wave linewidth and magnetic loss tangent are expected from the addition of cobalt. With $K_1>0$ the "easy" direction of magnetization becomes the cube edge rather than

| sample# | density | ..Ms.. | Tandm | tandm | ...ke | ....Br | ....Bd | ..Hc.. | ..Dbr.. | ...DH.. | ..DHk | Comments |
|---|---|---|---|---|---|---|---|---|---|---|---|---|
| G265-39A | 5.68 | 999 | 0.00093 | 0.0001 | 15.3 | 751 | 826 | 1.1 | 0.9 | 112 | 9.8 | STD(1100-1450@1/min/O2 |
| G265-39B | 5.58 | 964 | 0.00107 | 0.00015 | 15.2 | 697 | 794 | 1.2 | 0.88 | 121 | 9.3 | STD(1100-1450@1/min/air |
| G265-39C | 5.66 | 1061 | 0.00085 | 0.00009 | 15.2 | 754 | 858 | 1.3 | 0.96 | 101 | 10.3 | STD(1075-1425@1/min/O2 |
| G265-39D | 5.67 | 1047 | 0.00092 | 0.00009 | 15.3 | 774 | 867 | 1.25 | 0.95 | 114 | 9.99 | STD(1075-1425@1/min/air |
| G265-40A | 5.68 | 1028 | 0.00086 | 0.0001 | 15.1 | 724 | 816 | 1.1 | 0.92 | 121 | 9.9 | OxCalc/Std/1100-1450@1/min/O2 |
| G265-40B | 5.59 | 1038 | 0.00114 | 0.0001 | 15.2 | 651 | 776 | 1.3 | 0.85 | 144 | 10 | OxCalc/Std/2100-1450@1/min/air |
| G265-40C | | 1044 | 0.00092 | 0.00009 | 15.3 | 753 | 836 | 1.24 | 0.93 | 109 | 9.76 | OxCalc/Std/1075-1425@1/min/O2 |
| G265-40D | | 973 | | | | 730 | 825 | 1.3 | 0.95 | 113 | 9.43 | OxCalc/Std/1075-1425@1/min/air |

Table 4-4    Results of Study of Effect of Oxygen Calcine Treatment
Conducted on a .15 Mn Composition.

| sample# | density | ..Ms.. | Tandm | tandc | ...ke | ...Br | ...Bd | ..Hc.. | ..Dbr | ..Dh | ..DHk | Comments |
|---|---|---|---|---|---|---|---|---|---|---|---|---|
| G265-39A | 5.68 | 999 | 0.00093 | 0.0001 | 15.3 | 751 | 826 | 1.1 | 0.9 | 112 | 9.8 | STD(1100-1450@1/min/O2 |
| G265-39B | 5.58 | 964 | 0.00107 | 0.00015 | 15.2 | 697 | 794 | 1.2 | 0.88 | 121 | 9.3 | STD(1100-1450@1/min/air |
| G265-39C | 5.66 | 1061 | 0.00085 | 0.00009 | 15.2 | 754 | 858 | 1.3 | 0.96 | 101 | 10.3 | STD(1075-1425@1/min/O2 |
| G265-39D | 5.67 | 1047 | 0.00092 | 0.00009 | 15.3 | 774 | 867 | 1.25 | 0.95 | 114 | 9.99 | STD(1075-1425@1/min/air |
| G265-44A | 5.69 | 1072 | 0.00085 | 0.00018 | 14.9 | 608 | 737 | 1.46 | 0.99 | 144 | 10.65 | Mnpostcalc/1075-1425/AIR |
| G265-44B | 5.62 | 1004 | 0.00078 | 0.00016 | 13.8 | 623 | 756 | 1.59 | 0.93 | 138 | | Mnpostcalc/1075-1425/O2 |
| G265-44C | 5.64 | 1031 | 0.00086 | 0.00018 | 14.7 | 603 | 759 | 1.42 | 0.89 | 125 | 9.89 | Mnpostcalc/1100-1450/O2 |
| G265-45A | 5.65 | 1013 | 0.00078 | 0.00018 | 15.4 | 563 | 714 | 1.77 | 0.955 | 132 | 10.65 | Mnprecalc/1075-1425/O2 |
| G265-45B | 5.65 | 1018 | 0.00085 | 0.00018 | 15.7 | 561 | 709 | 1.59 | 0.945 | 145 | 9.86 | Mnprecalc/1100-1450/O2 |

Table 4-5   Results of Pre-treatment of Mn in a 0.15 Mn substituted G-265

| Sample | Mn | Co(x) | Density | Ms | Tandm | tande | ke | Br | Bd | Hc | Dbr | DH | DHK |
|--------|------|---------|---------|------|-------|--------|------|-----|-----|------|-------|-----|-----|
| G265-66 | 0.155 | 0.01125 | 5.67 | 988 | NM | 0.0005 | 155 | 336 | 532 | 2.1 | 1.037 | 135 | >11 |
| G265-57 | 0.155 | 0.0225 | 5.63 | 1028 | 0.016 | 0.0003 | 15.1 | 348 | 558 | 2.62 | 1.05 | 116 | >11 |

TABLE 4-6  PROPERTIES OF COBALT SUBSTITUTED YGd1G

$$Y_{1.7} \, Gd_{1.3} \, Fe_{4.845-2x} \, Mn_{0.155} \, Co_x \, Si_x \, O_{12}$$
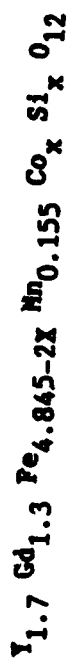
NM - Not Measured

the body diagonal of the cell. With six cube edges versus eight body diagonals, a modest reduction in remanence might be expected, but not the great reduction observed. These results did not warrant further exploration of this family on the current program.

Two cerium doped yttrium iron garnets were prepared to test reported results from the late '60's on the effects of cerium in reducing stress sensitivity in the garnets, much as terbium has been demonstrated to do. Terbium will render a garnet totally impervious to stress, but its magnetic loss is so large that it is of no practical value as a microwave ferrite. The two cerium compounds listed in section 4.1 yielded materials that have only small improvement in stress insensitivity over undoped YIG. At the same time, the magnetic loss tangents and spinwave linewidths increased with the addition of cerium, one of the rare earth elements. This increased loss clearly makes the cerium substitution less desirable than the Mn doping.

## 5.0 STATIC STRESS DATA

## 5.1 INITIAL TESTS

The test fixture discussed in Section 3.3 and illustrated in Figures 3-6 and
3-7 (referred to as the trophy test fixture) was used to measure changes in
the hysteresis characteristics of the materials as a function of applied
stress. The fixture was most useful for studying longitudinal stress
perpendicular to the average direction of the remanent magnetization for
values of stress greater than 1000 PSI. For stress measurements below 1000
PSI, the fixture was modified such that appropriate weights could be placed
on the fixture to provide a constant controlled stress level.

The YIG-TbIG compounds discussed in Section 3.3 were evaluated in this
fixture. Figure 5-1 presents the changes observed in YIG (No TbIG), YIG
(0.167TbIG) and YIG(0.35TbIG) for various stress conditions. Photographs of
the hysteresis curves were presented in Section 3.3. As noted in Figure
5-1, the change in remanence ratio of the YIG (0.167TbIG) compound was very
small up to 4000 PSI for both longitudinal and vertical compressive stress.

Figure 5-2 presents similar data for TTG-1002 (0.09 Mn). The test sample
was a toroid prepared for phaser evaluation. It is observed that the
material exhibits considerable change in the remanence ratio with stress in
all directions; however the material is considerably more sensitive to
longitudinal stress.

## 5.2 STATIC STRESS TESTS ON MANGANESE SUBSTITUTED G-265

The manganese substituted compounds prepared for study were discussed in
Section 4.0 The EMS formulated YIG-GdIG compound is designated as G-265
with the following manganese substitution (0.09 Mn, 0.11 Mn, 0.13 Mn, 0.15
Mn, 0.17 Mn, and 0.21 Mn).

Toroids were prepared of each substitution to dimensions for phase shifter
evaluation. These same toroids were used in the static stress tests.
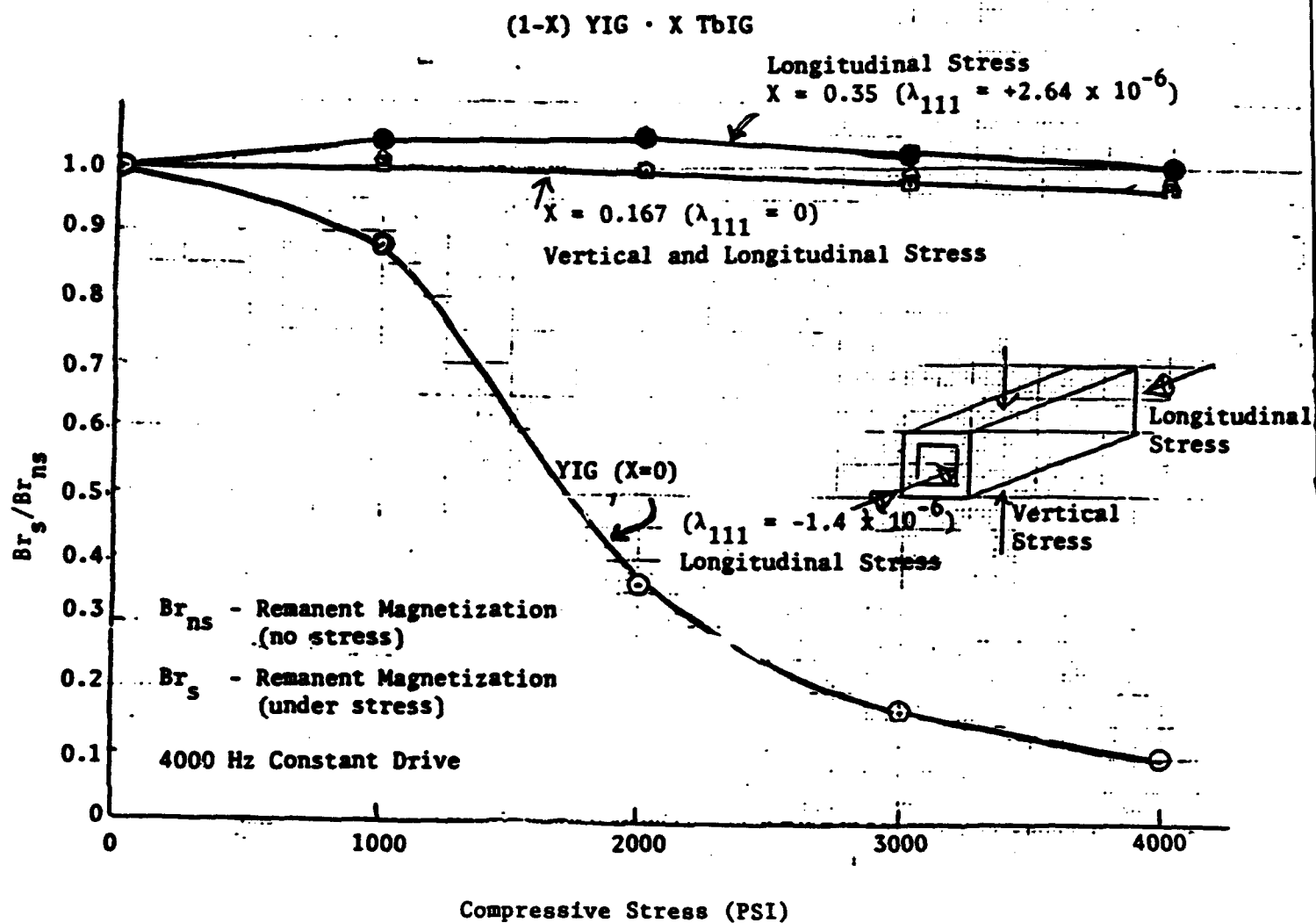
CHANGE IN REMANENCE RATIO WITH STRESS

(YIG - TbIG COMPOUND)

FIGURE 5-1
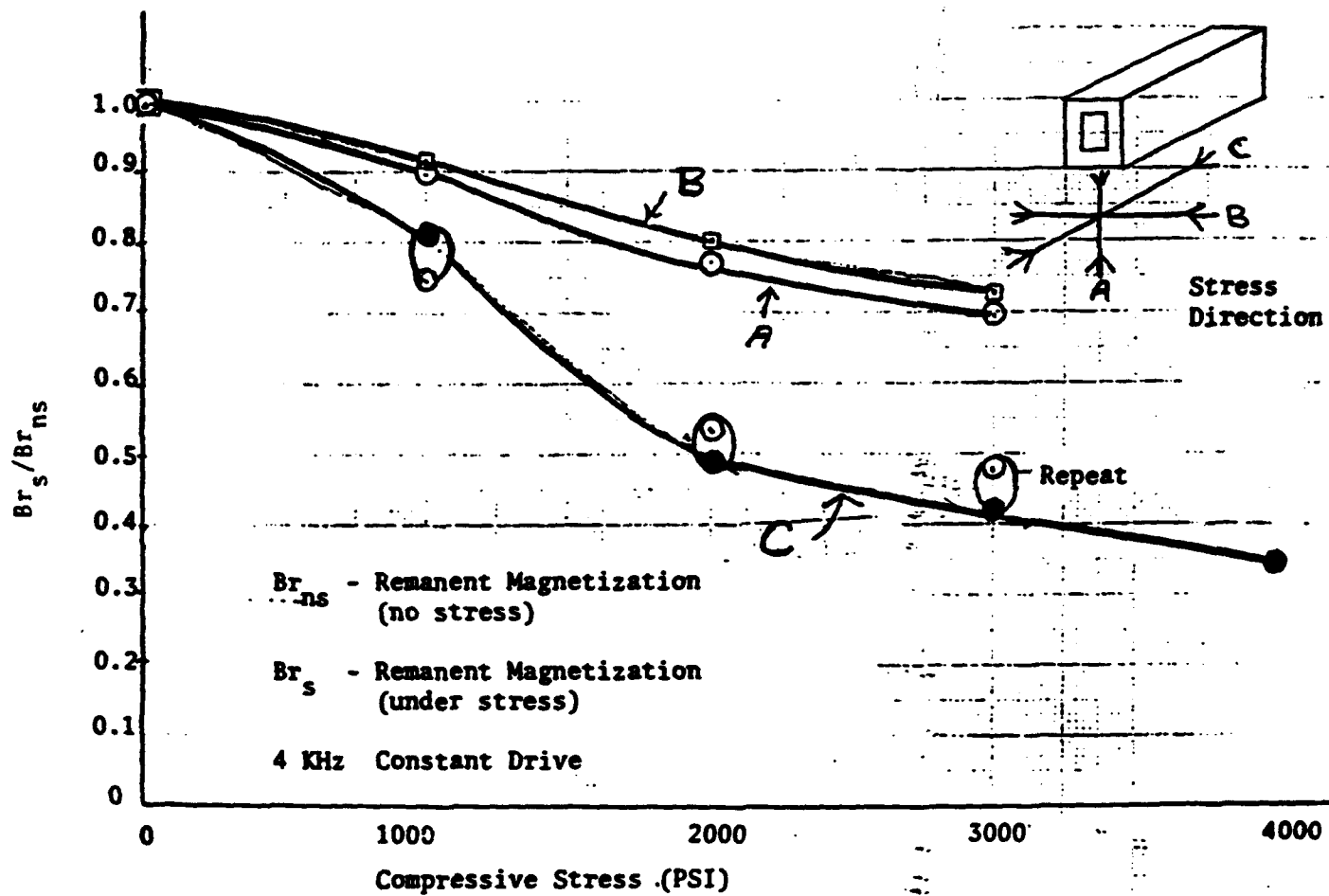
CHANGE IN REMANENCE RATIO WITH STRESS

FOR TTG1002 (0.09 Mn)

FIGURE 5-2

Figures 5-3 through 5-7 present photographs of the hysteresis curves of these materials for longitudinal stress up to 4000 PSI. All of the compounds exhibit same change in the hysteresis curve for stress above 2000 PSI.

The observed change at the 0.17 Mn substitution (Figure 5-7) is very small with some beginning evidence of increasing coercive field with stress, indicating a positive $\lambda_{111}$.

These photographs suggest that above 1000 PSI of longitudinal stress, the toroids may be physically distorting causing the observed changes in the hysteresis curves. Note that the 0.09 Mn and the 0.11 Mn compounds exhibit changes in the hysteresis curves between 0 and 1000 PSI and continue to change up to 4000 PSI. The 0.13 Mn, 0.15 Mn and 0.17 Mn compounds show almost no change in the hysteresis response up to 1000 PSI. Above this stress level some changes in the hysteresis curves are observed. This non-linear response suggests some minor distortion of the sample (such as bending) creating a stress on the sample that is not uni-directional.

The specific data collected on the change in Br (actually Br (stress)/Br (no stress)) with longitudinal compressive stress for all of the Mn substituted G-265 are presented in Figure 5-8. Note the data taken at 1000 PSI (some physical distortion may be present above this level as mentioned previously). At about 0.13 Mn there is no change in Br; below this level, Br decreases and above the 0.13 Mn substitution, the Br increases.

Observations from the comparison of static and phase stress characteristics indicated that the actual stress levels experienced by the material in the phaser structure was considerably less than 1000 PSI. The stress experienced by the material in the soft top phaser housing, both from top to bottom crush and from longitudinal differential expansion with temperature actually appeared to be in the region of 100 PSI (this value of stress appears low compared to readily achievable stress levels of 1000 to 4000

G-265 (0.09 Mn) ILLUSTRATION OF HYSTERESIS CHARACTERISTIC
UNDER LONGITUDINAL COMPRESSIVE STRESS

$\lambda_{100}$ IS POSITIVE
$\lambda_{111}$ IS NEGATIVE
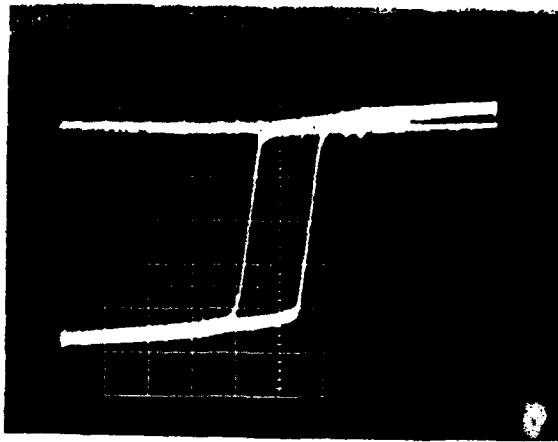


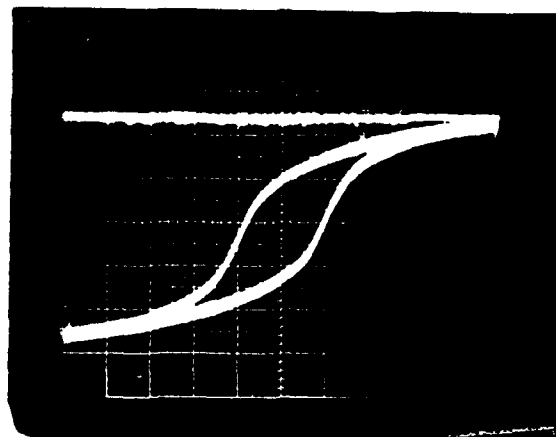.09 Mn NRL 165    0 PSI Axial        .09 Mn NRL 265    1000 PSI Axial
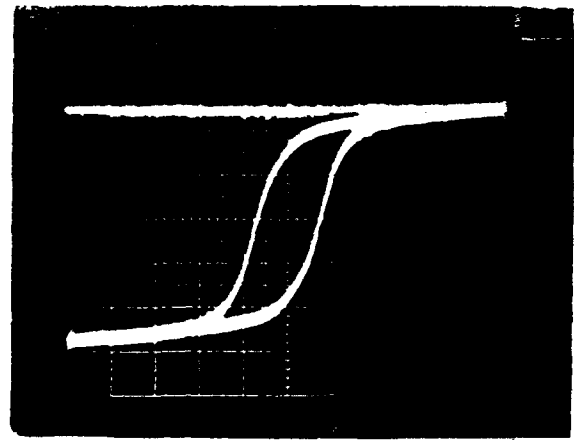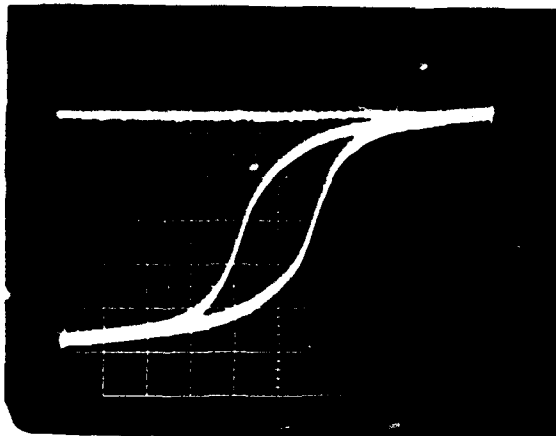
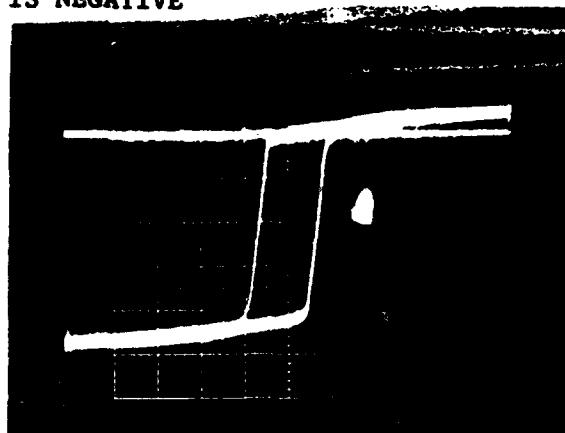.09 Mn NRL 265    2000 PSI Axial        .09 Mn NRL 265    3000 PSI Axial
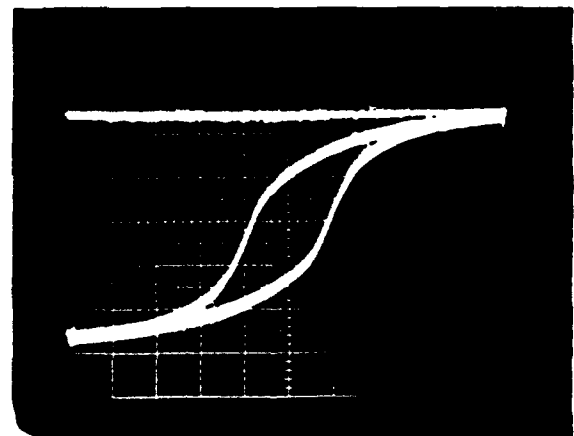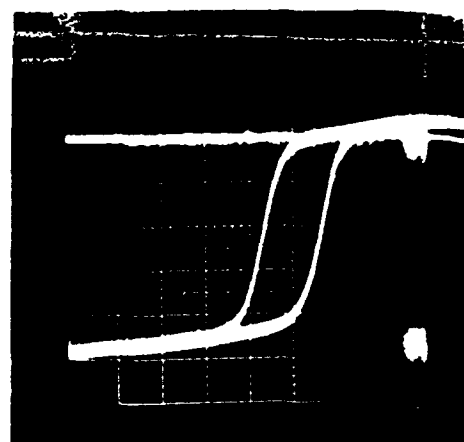
.09 Mn NRL 265    4000 PSI Axial

FIGURE 5-3

- 79 -

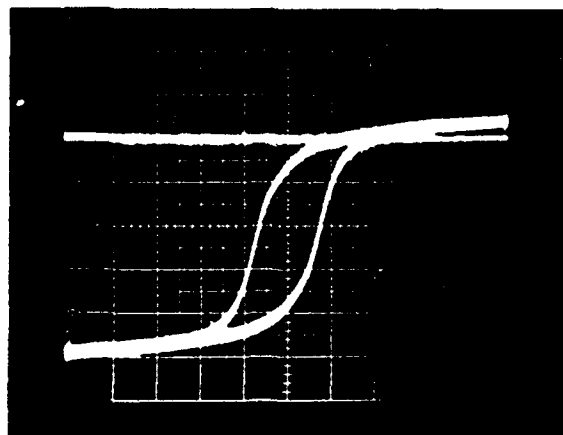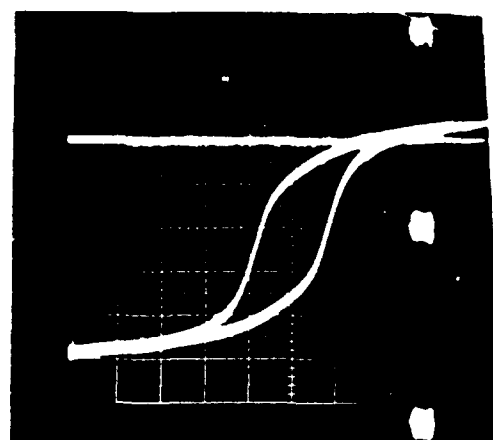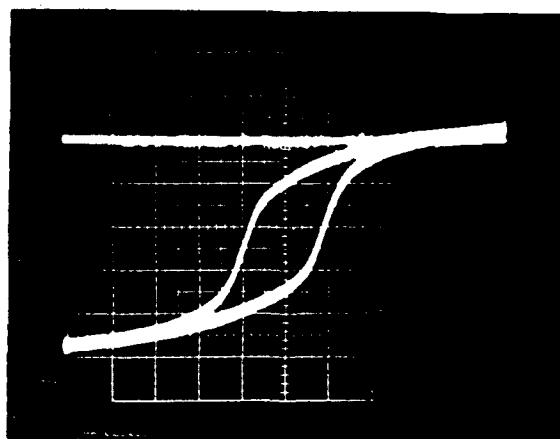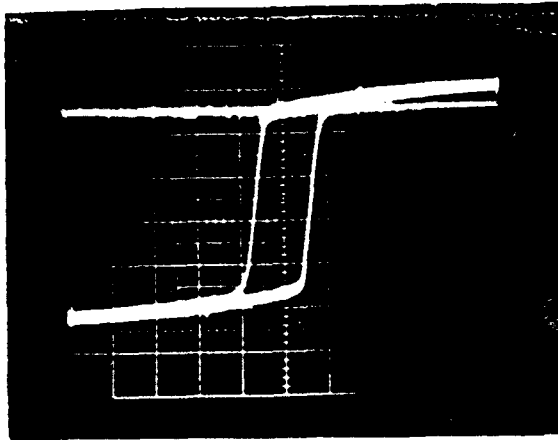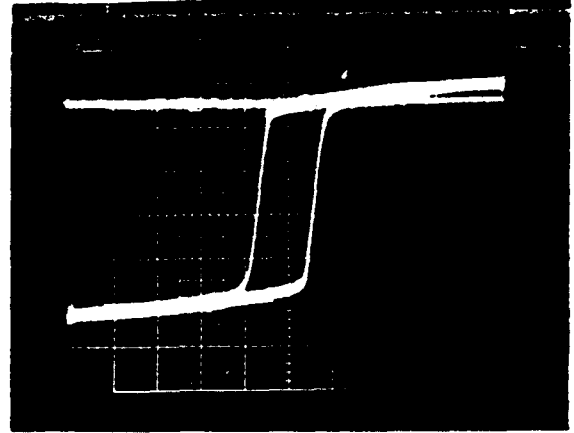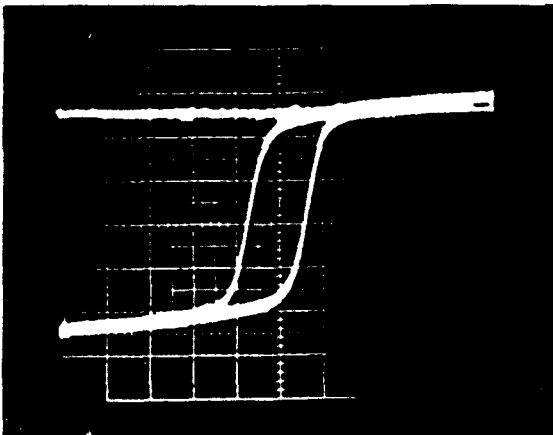G-265 (0.11 Mn) ILLUSTRATION OF HYSTERESIS CHARACTERISTIC UNDER LONGITUDINAL COMPRESSIVE STRESS

$\lambda_{100}$ IS POSITIVE
$\lambda_{111}$ IS NEGATIVE
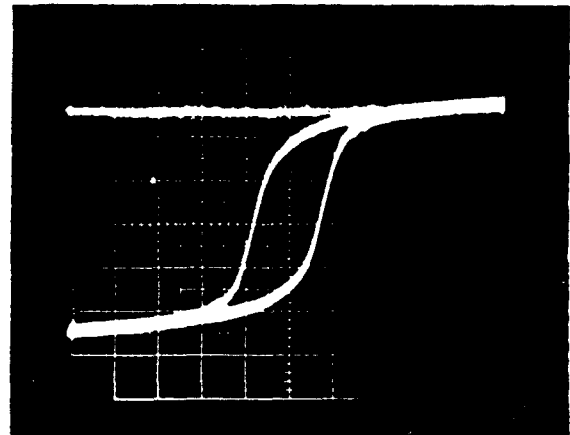


.11 Mn NRL 265      0 PSI Axial
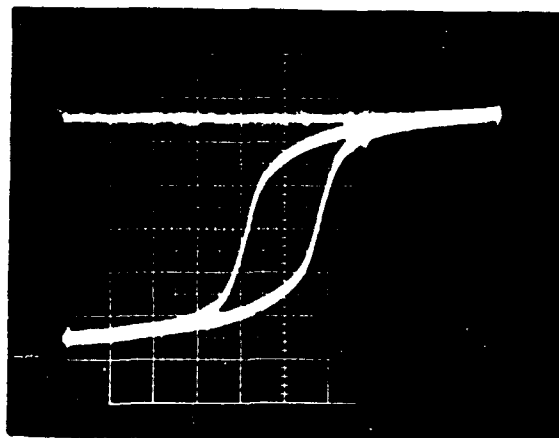
.11 Mn NRL 265      1000 PSI Axial

.11 Mn NRL 265      2000 PSI Axial

.11 Mn NRL 265      3000 PSI Axial
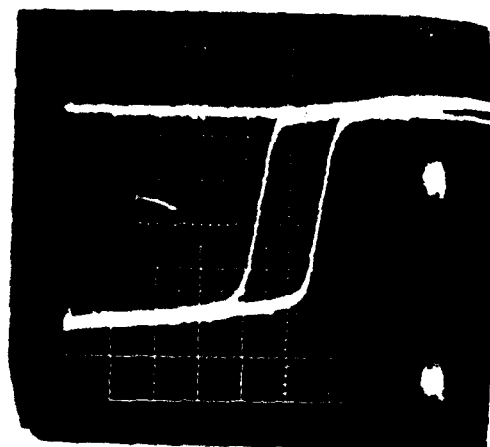
.11 Mn NRL 265      4000 PSI Axial

FIGURE 5-4

G-265 (0.13 Mn) ILLUSTRATION OF HYSTERESIS CHARACTERISTIC UNDER LONGITUDINAL COMPRESSIVE STRESS

$\lambda_{100}$ IS POSITIVE
$\lambda_{111}$ IS NEGATIVE



.13 Mn NRL 265    0 PSI Axial

.13 Mn NRL 265    1000 PSI Axial

.13 Mn NRL 265    2000 PSI Axial

.13 Mn NRL 265    3000 PSI Axial

.13 Mn NRL 265    4000 PSI Axial

FIGURE 5-5

G-265 (0.15 Mn) ILLUSTRATION OF HYSTERESIS CHARACTERISTIC UNDER LONGITUDINAL
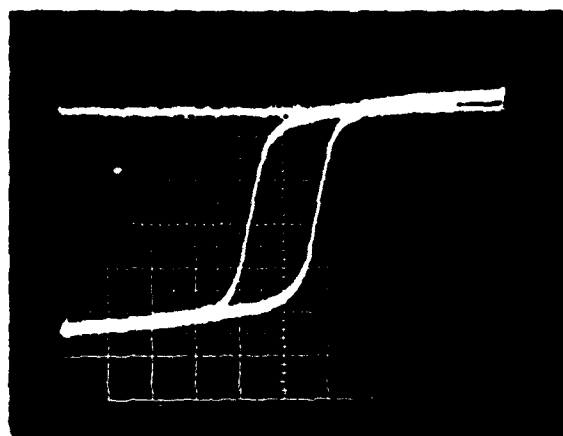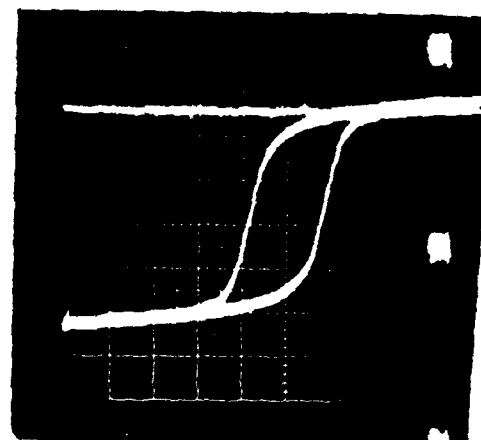COMPRESSIVE STRESS

$\lambda_{100}$ IS POSITIVE
$\lambda_{111} \sim 0$



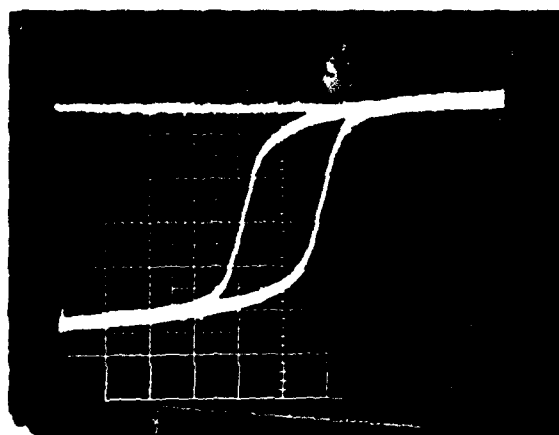.15 Mn NRL 265    0 PSI Axial      .15 Mn NRL 265    1000 PSI Axial

.15 Mn NRL 265    2000 PSI Axial      .15 Mn NRL 265    3000 PSI Axial

.15 Mn NRL 265    4000 PSI Axial

FIGURE 5-6

G-265 (0.17 Mn) ILLUSTRATION OF HYSTERESIS CHARACTERISTIC UNDER LONGITUDINAL COMPRESSIVE STRESS

$\lambda_{100}$ IS POSITIVE
$\lambda_{111} \sim 0+$



.17 Mn NRL 265     0 PSI Axial

.17 Mn NRL 265     1000 PSI Axial

.17 Mn NRL 265     2000 PSI Axial
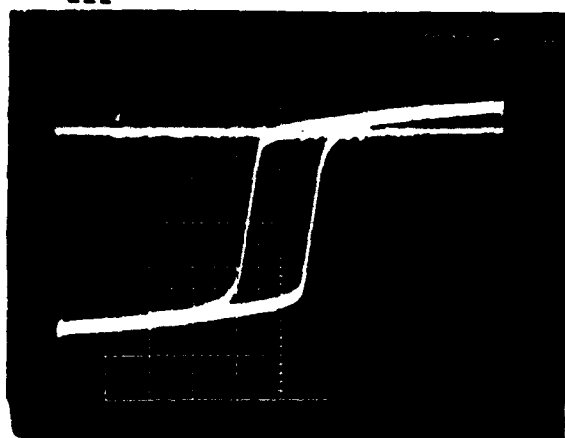
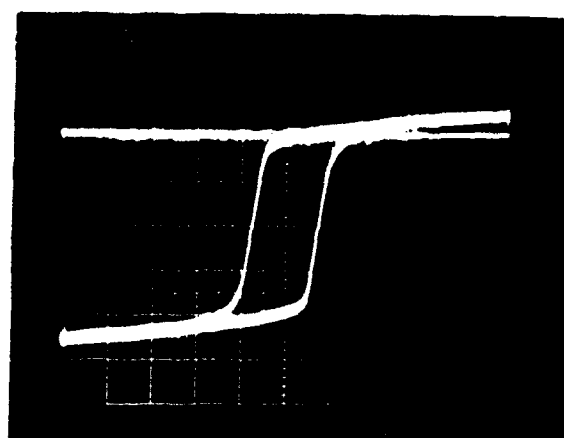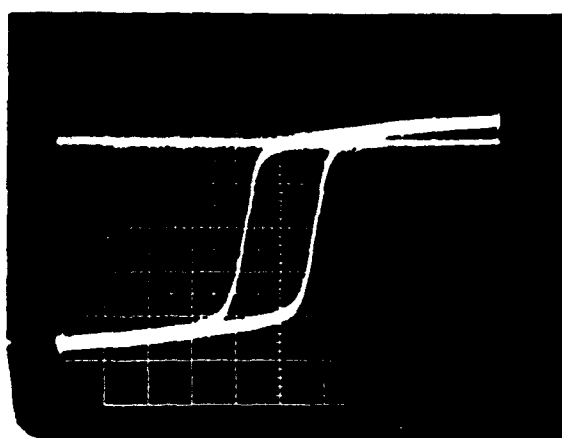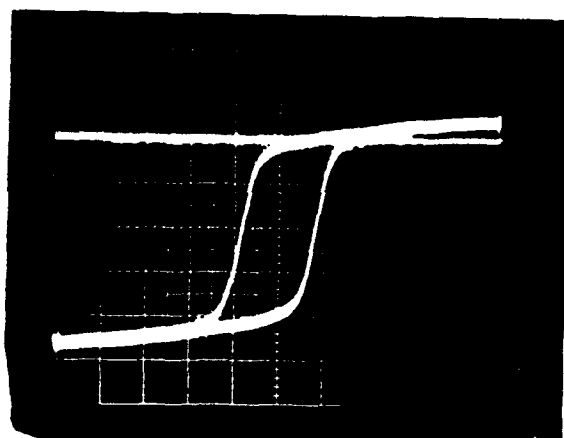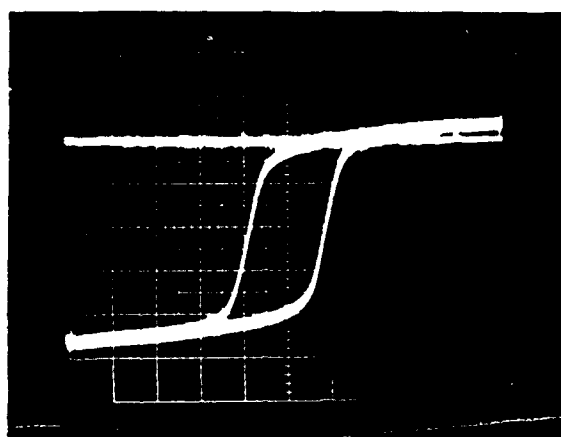.17 Mn NRL 265     3000 PSI Axial

.17 Mn NRL 265     4000 PSI Axial

FIGURE 5-7

- 83 -

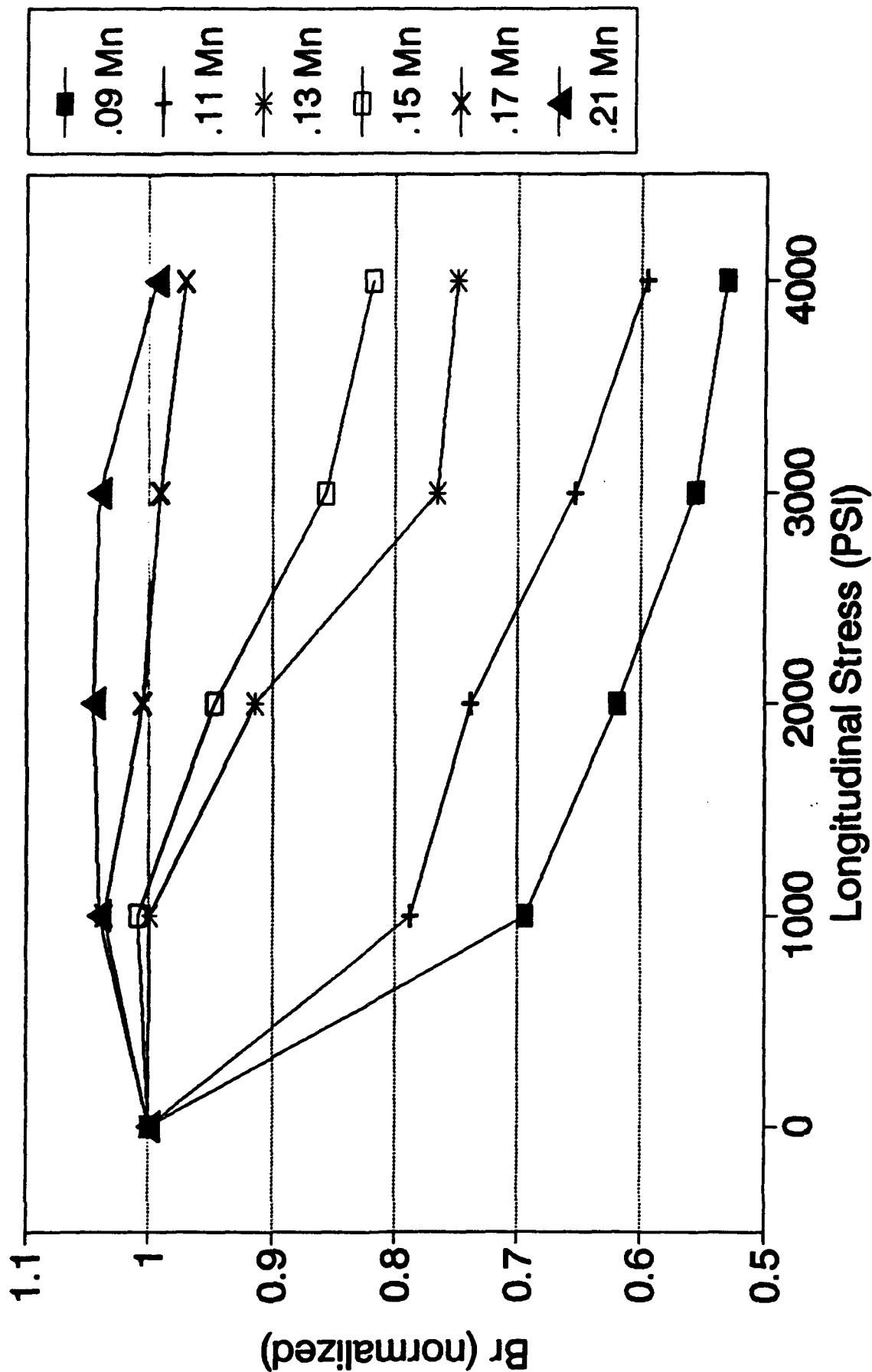Br vs. Longitudinal Stress
EMS G265 / Various Mn Contents

FIGURE 5-8

- 84 -

PSI; however, a 100 pound weight on one square inch is still a considerable stress.) Prior to this observation, no data were available to indicate the actual stress levels experienced by the materials in phaser structures. The test fixture was altered as indicated in Section 5.1, and the materials were more carefully evaluated in the region of 0 to 1000 PSI. The resulting data are presented in Figures 5-9 through 5-14. These figures present the relative measured changes in Br (remanent magnetization) as a function of transverse and longitudinal compressive stress up to values of 1000 PSI for the manganese substituted G-265 compounds. Figure 5-15 presents the transverse compressive stress response for all of the compositions (for comparison) and Figure 5-16 presents similar data for the longitudinal compressive stress response.

For transverse compressive stress, the stress direction (top to bottom) is on the average parallel to the remanent magnetization producing phase shift in the phaser structure. This stress is perpendicular to the average direction of the magnetization in the top and bottom legs of the nearly square toroid. At remanence the magnetic moments are predominately along the 111 crystalographic direction (body diagonal in cubic structure). Figure 3-17 presented the anticipated variation of magnetostrictive constants as a function of Mn in the G-265 garnet compound.

The data presented in Figures 5-9 through 5-16 would indicate the following general characteristics:

Response to transverse compressive stress:

- For the 0.09 Mn substituted compound, a slight increase in Br with stress was observed for low stress levels (up to 400 PSI). Above this stress level, Br decreased. These data could indicate that $\lambda s$ is slightly negative for this Mn substitution; however, the overall transverse variation with stress is lower than any of other Mn substitutions.
- The transverse stress characteristic of all the other Mn substituted compounds are observed to be very similar.

Br vs. Applied Stress
EMS G265 (.09 Mn)

■ Transverse Stress  ● Longitudinal Stress
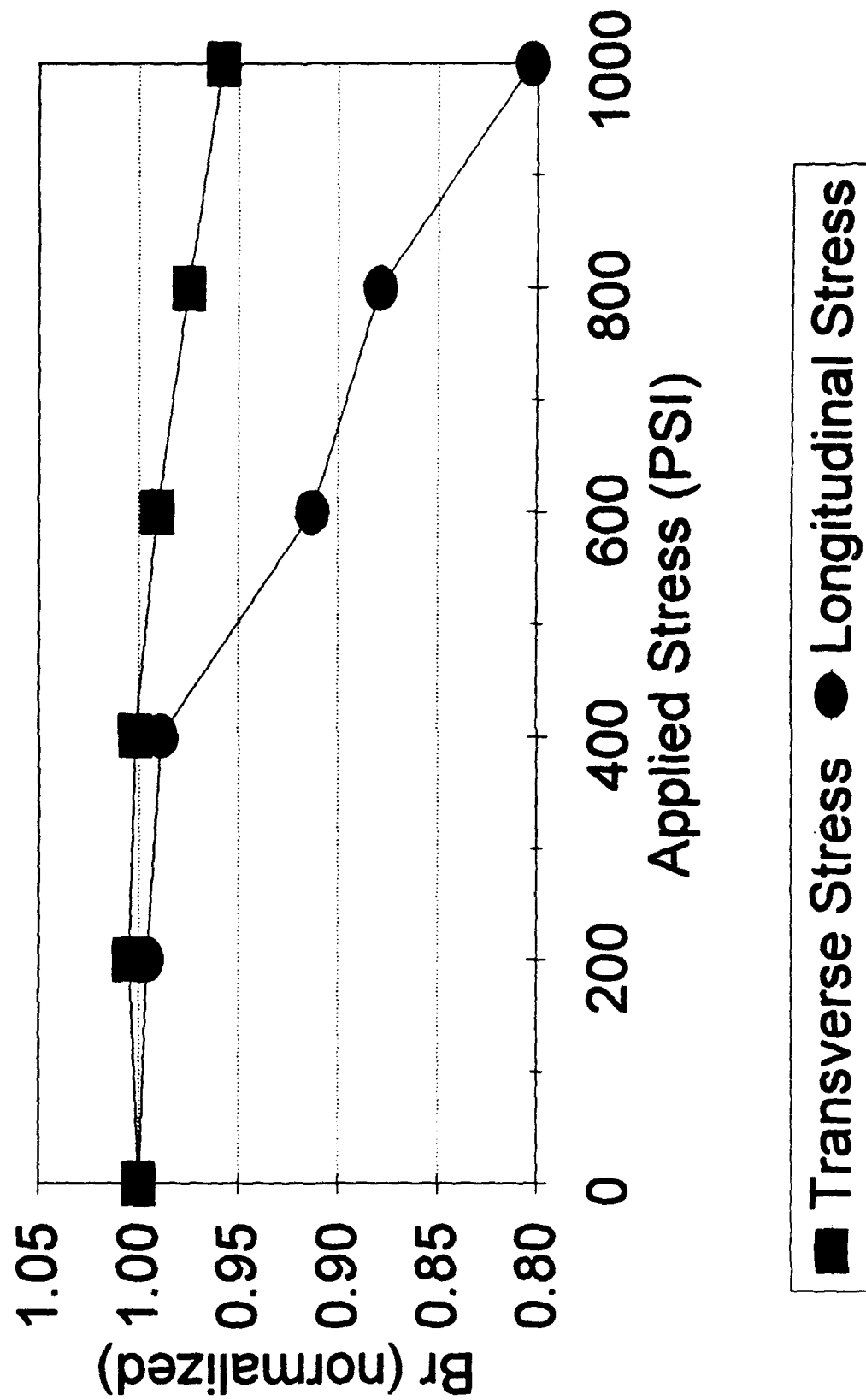
FIGURE 5-9

Br vs. Applied Stress
EMS G265 (.11 Mn)

Br (normalized) vs. Applied Stress (PSI)

■ Transverse Stress  ● Longitudinal Stress

**FIGURE 5-10**

Br vs. Applied Stress
EMS G265 (.13 Mn)

FIGURE 5-11

■ Transverse Stress ● Longitudinal Stress

Br vs. Applied Stress
EMS G265 (.15 Mn)

■ Transverse Stress ● Longitudinal Stress

FIGURE 5-12

Br vs. Applied Stress
EMS G265 (.17 Mn)

Br (normalized)

Applied Stress (PSI)

■ Transverse Stress ● Longitudinal Stress
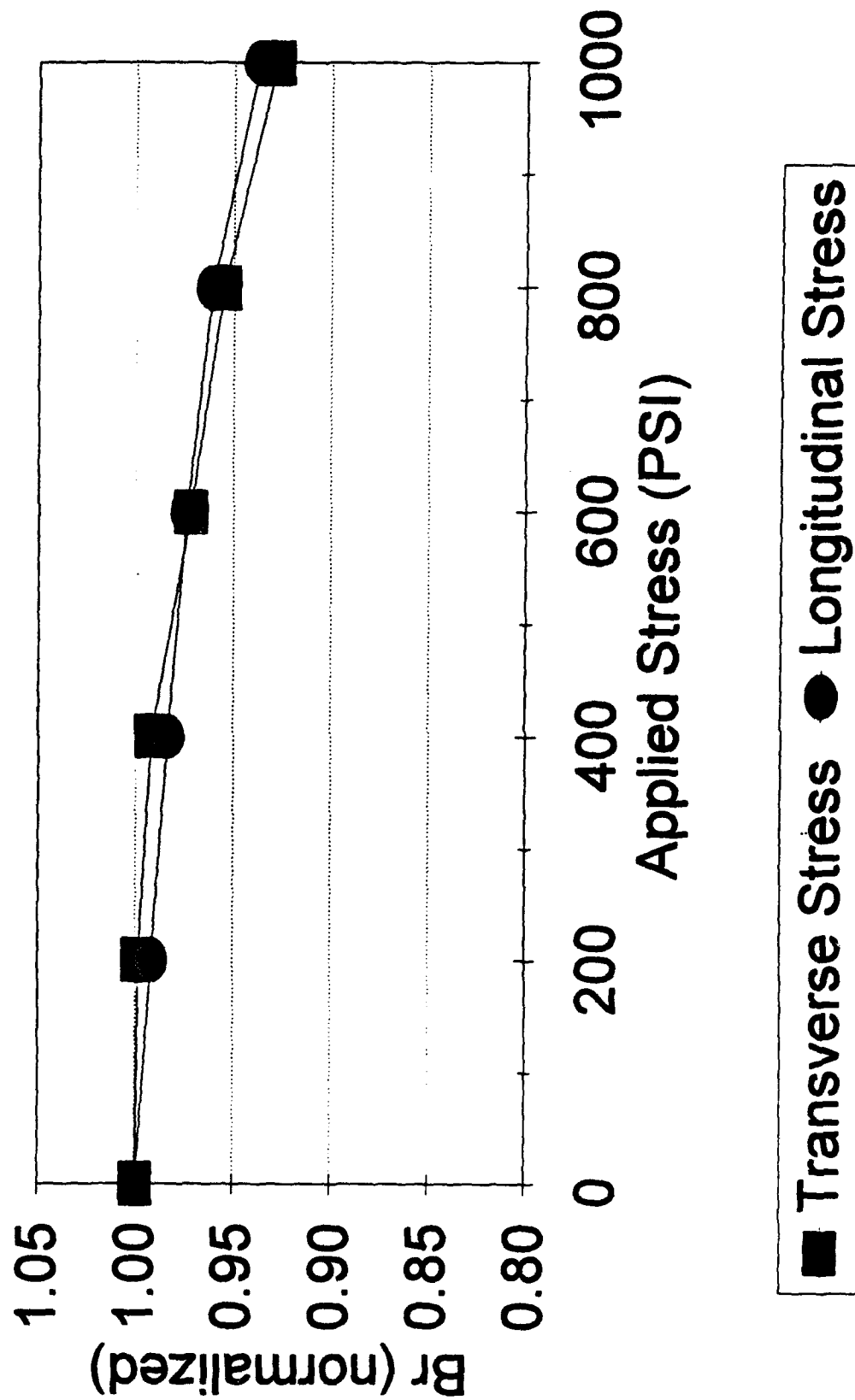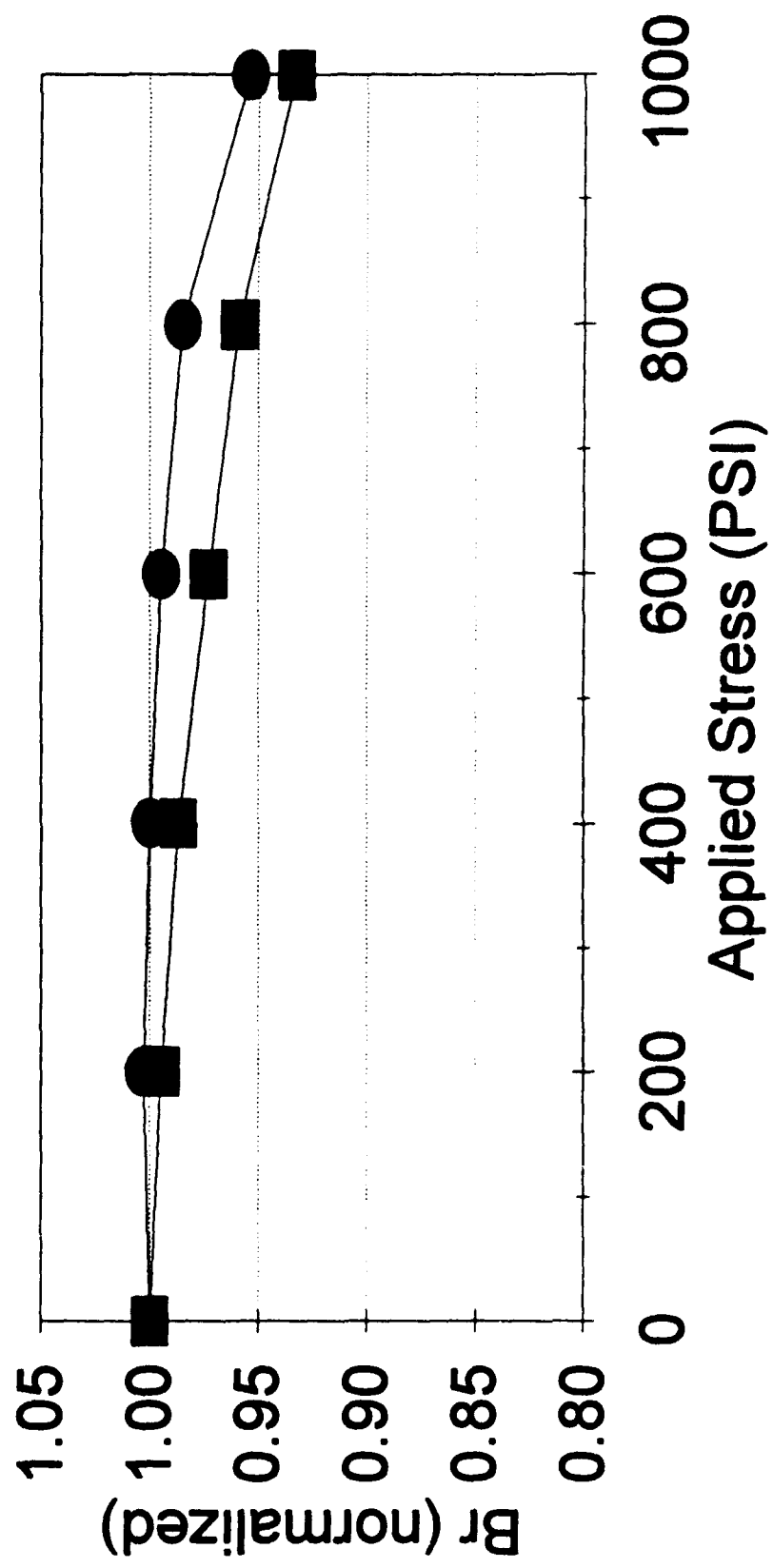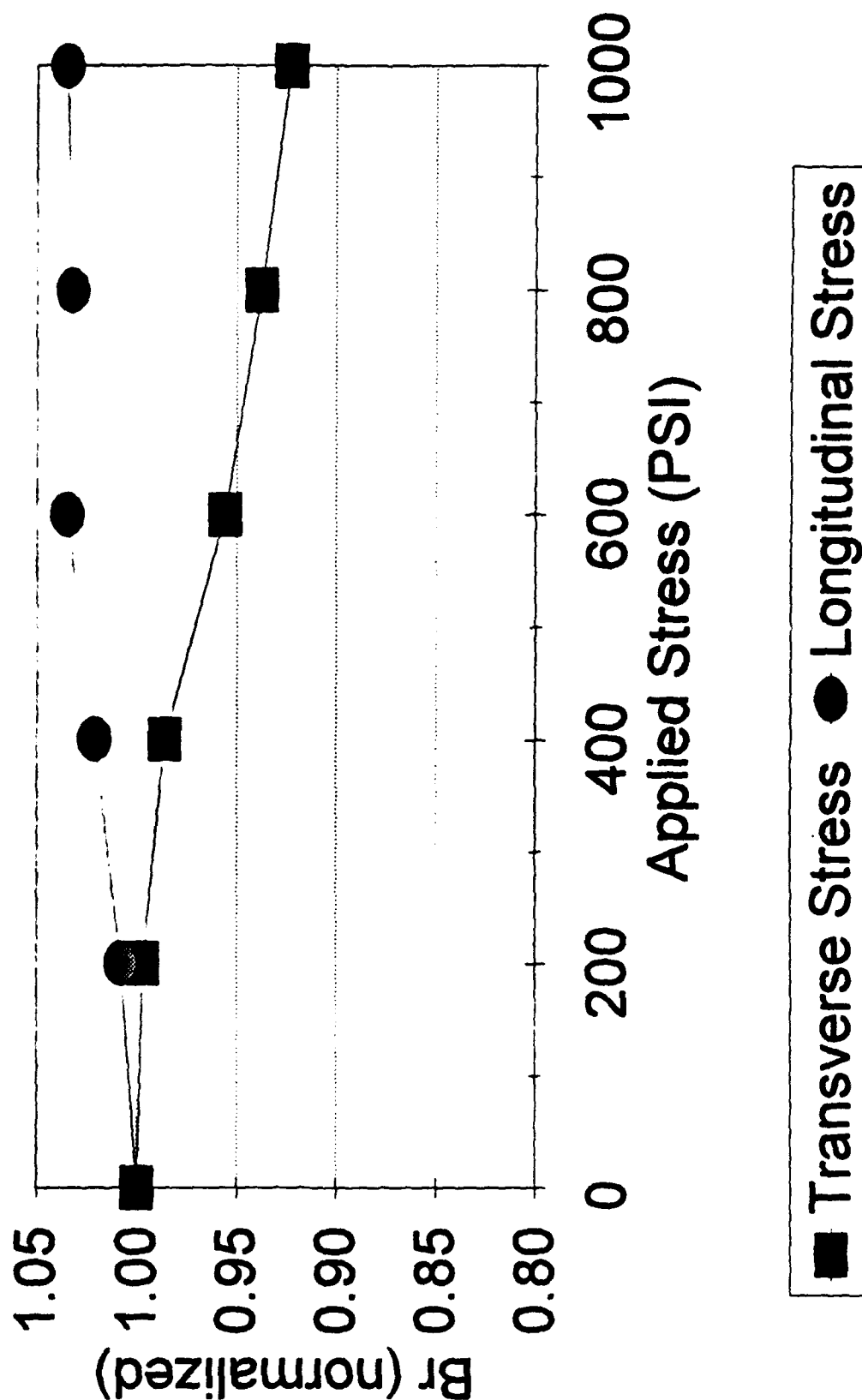
FIGURE 5-13

Br vs. Applied Stress
EMS G265 (.21 Mn)

■ Transverse Stress ● Longitudinal Stress
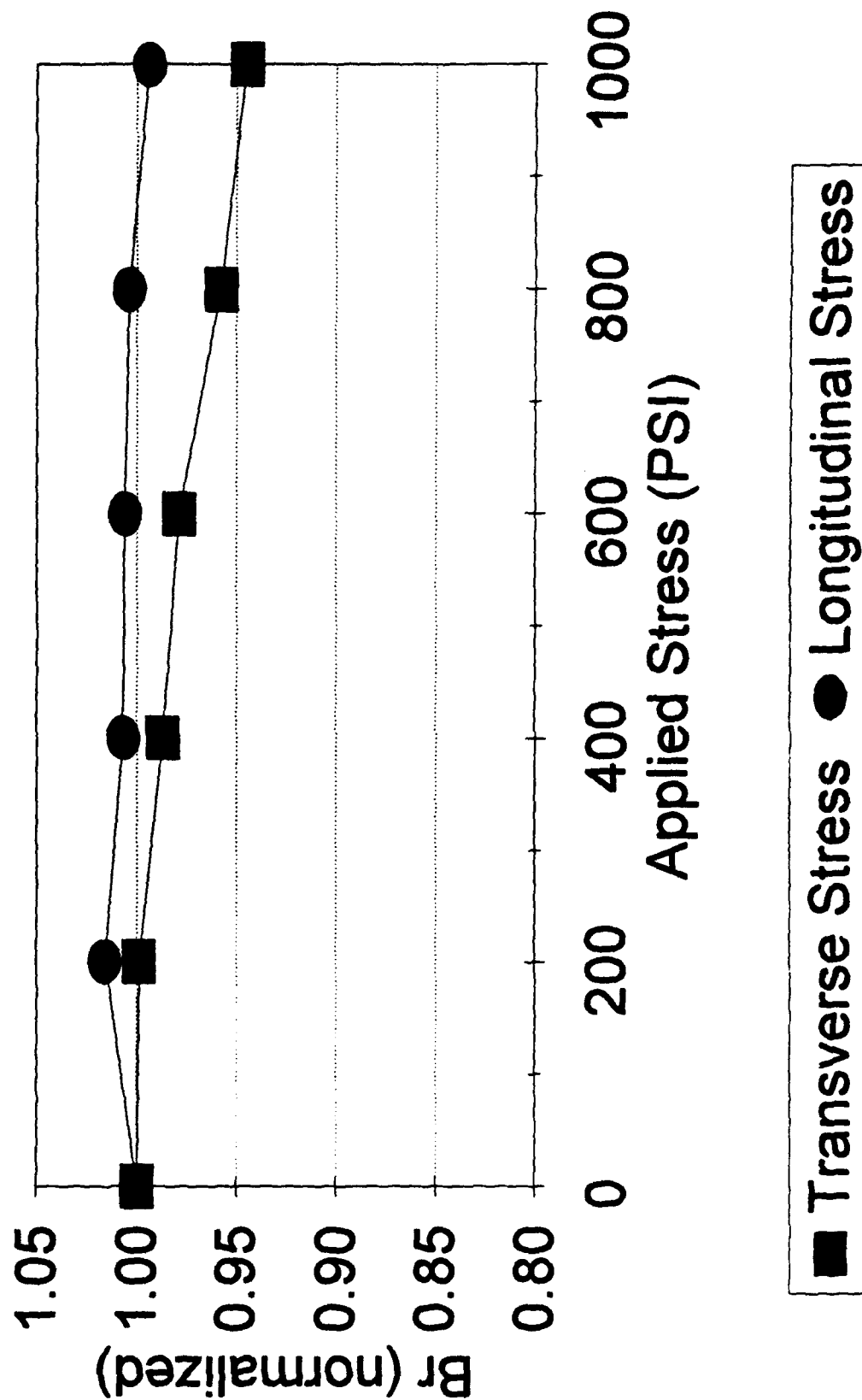
FIGURE 5-16

- 91 -
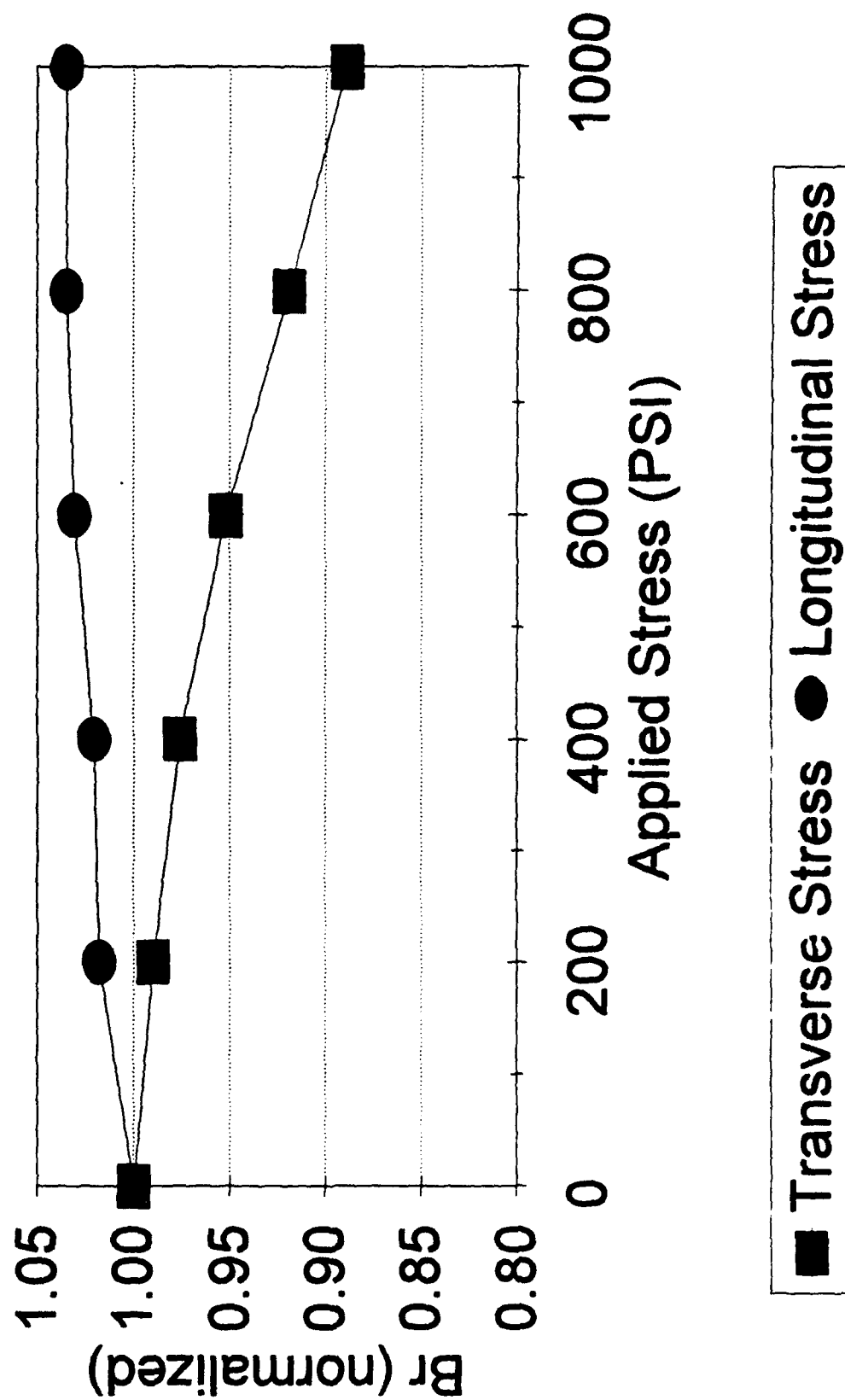
# Br vs. Applied Transverse Stress

Legend:
- ■ G265 (.09)
- ● G265 ( 11)
- ▼ G265 ( 13)
- ⋈ G265 ( 15)
- ▲ G265 (.17)
- ⊠ G265 (.21)

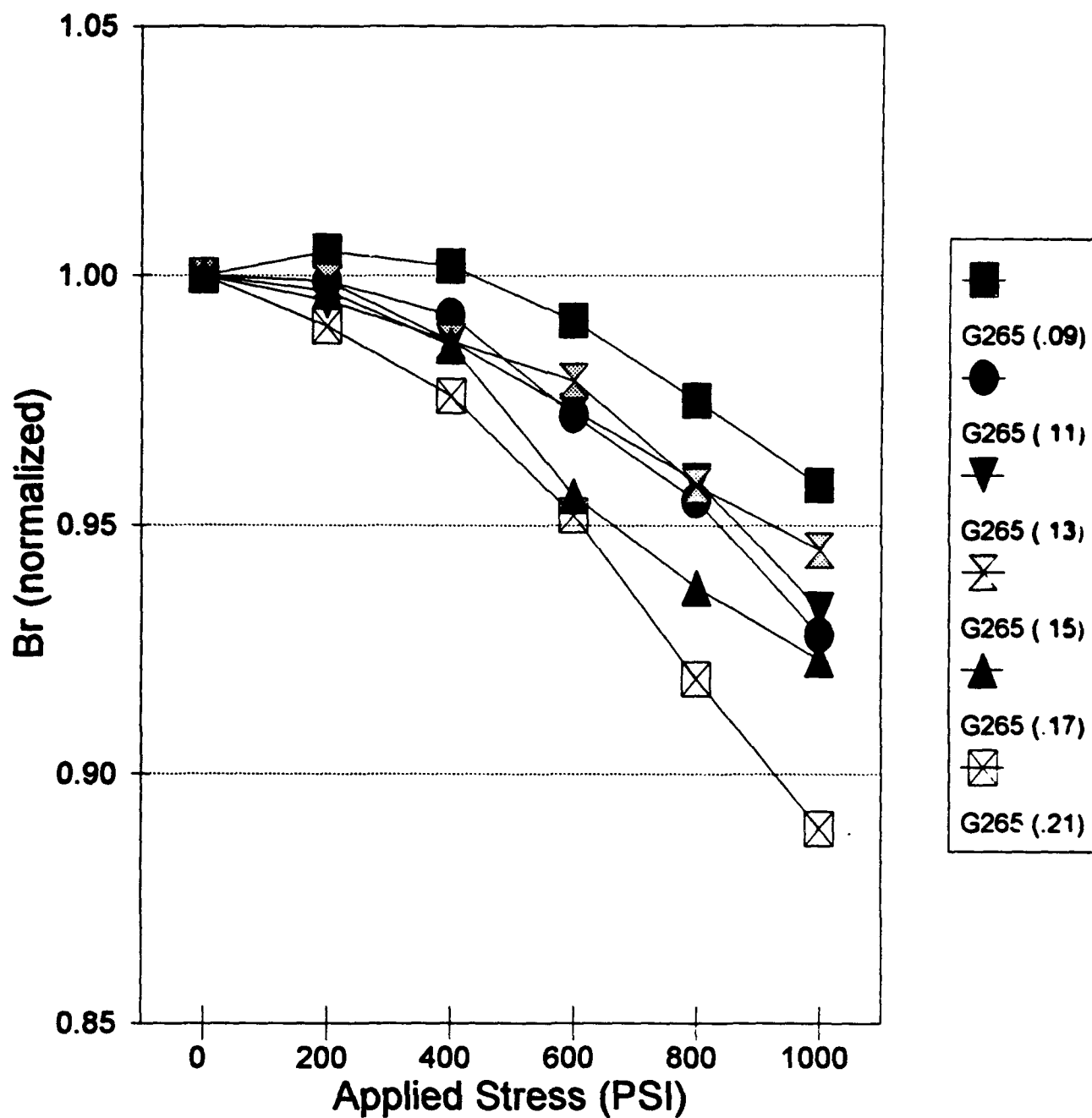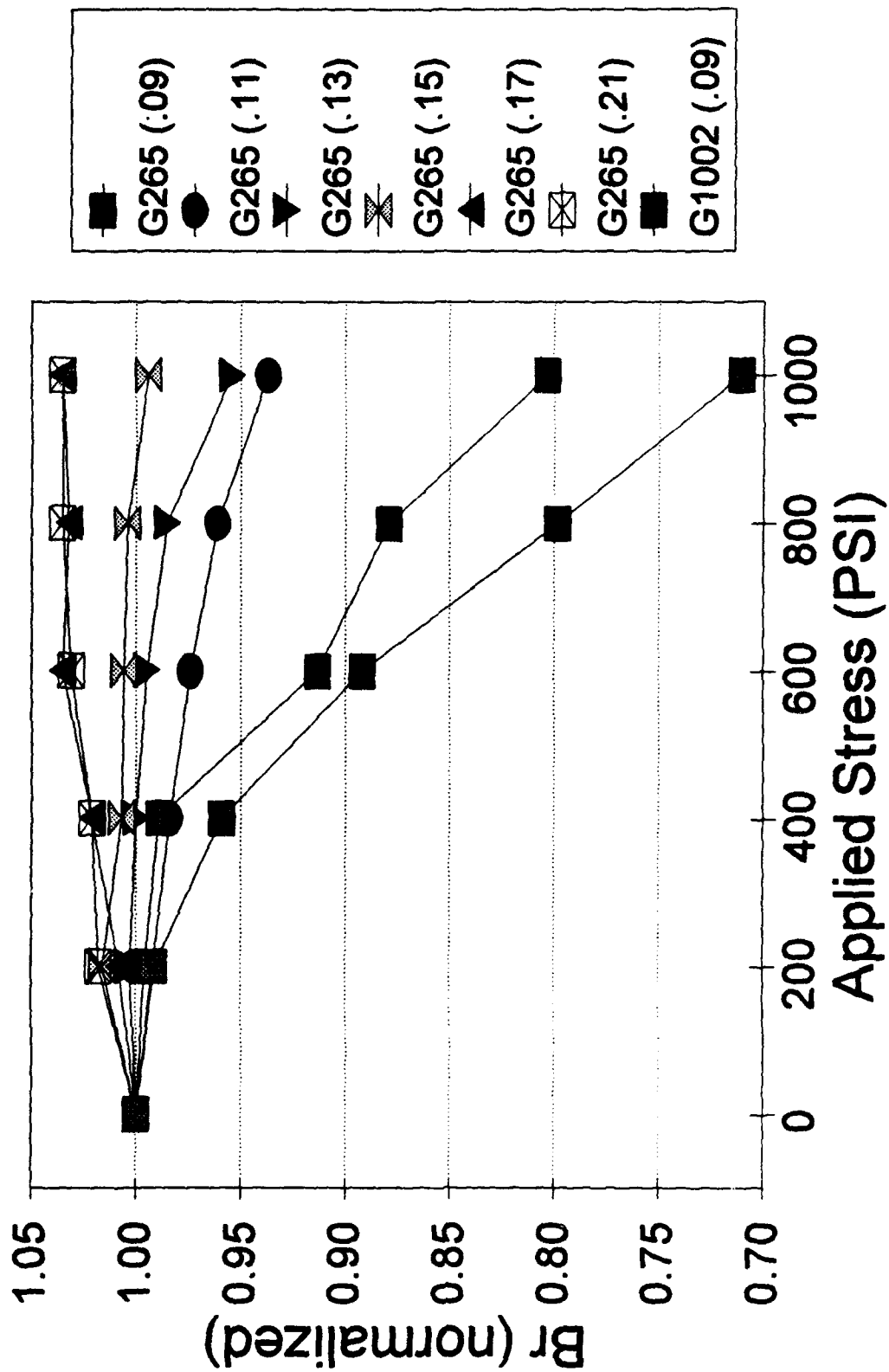FIGURE 5-15

- 92 -

Br vs. Applied Longitudinal Stress

FIGURE 5-16

Response to longitudinal compression stress:

- For remanent state magnetization, the longitudinal compressive stress is perpendicular to the average magnetic moment.
- For the 0.09 Mn substituted compound, the relative Br decreased rapidly with stress. This again would be indicative of a negative $\lambda s$ for this substitution (the magnetization will move toward alignment with the stress and thus lower the remanent magnetization).
- For the 0.11 Mn substituted compound, the longitudinal and transverse stress responses are nearly equal.
- For the 0.13 Mn substitution, the longitudinal stress response exhibits the most stable characteristics up to 500 PSI. This could be indicative of a near zero value of $\lambda s$ for this substitution.
- Above the 0.13 Mn substitution, the relative Br was observed to increase with longitudinal compressive stress. This is indicative of a positive value of $\lambda s$; the magnetization would attempt to align perpendicular to the stress and thus enhance the resultant remanent magnetization. The sensitivity of the observed enhancement is small since remanent values are already fairly high in these compounds and thus cannot be increased very much by favorable resultant magnetostrictive forces.
- Figures 5-17 and 5-18 present the observed stress data from Figures 5-9 through 5-16 in a different form. In these figures the change in relative Br is plotted versus Mn content for different values of stress. Figure 5-17 presents the transverse compression stress response. All of the compounds exhibit some stress effects. The 0.09 Mn substituted compound exhibited the least change in normalized BR with transverse compression stress.
- Figure 5-18 presents the longitudinal compressive stress response as a function of Mn content. These data indicate that very low stress sensitivity would be achieved for Mn substitutions near 0.13 for stress level up to 600 PSI.

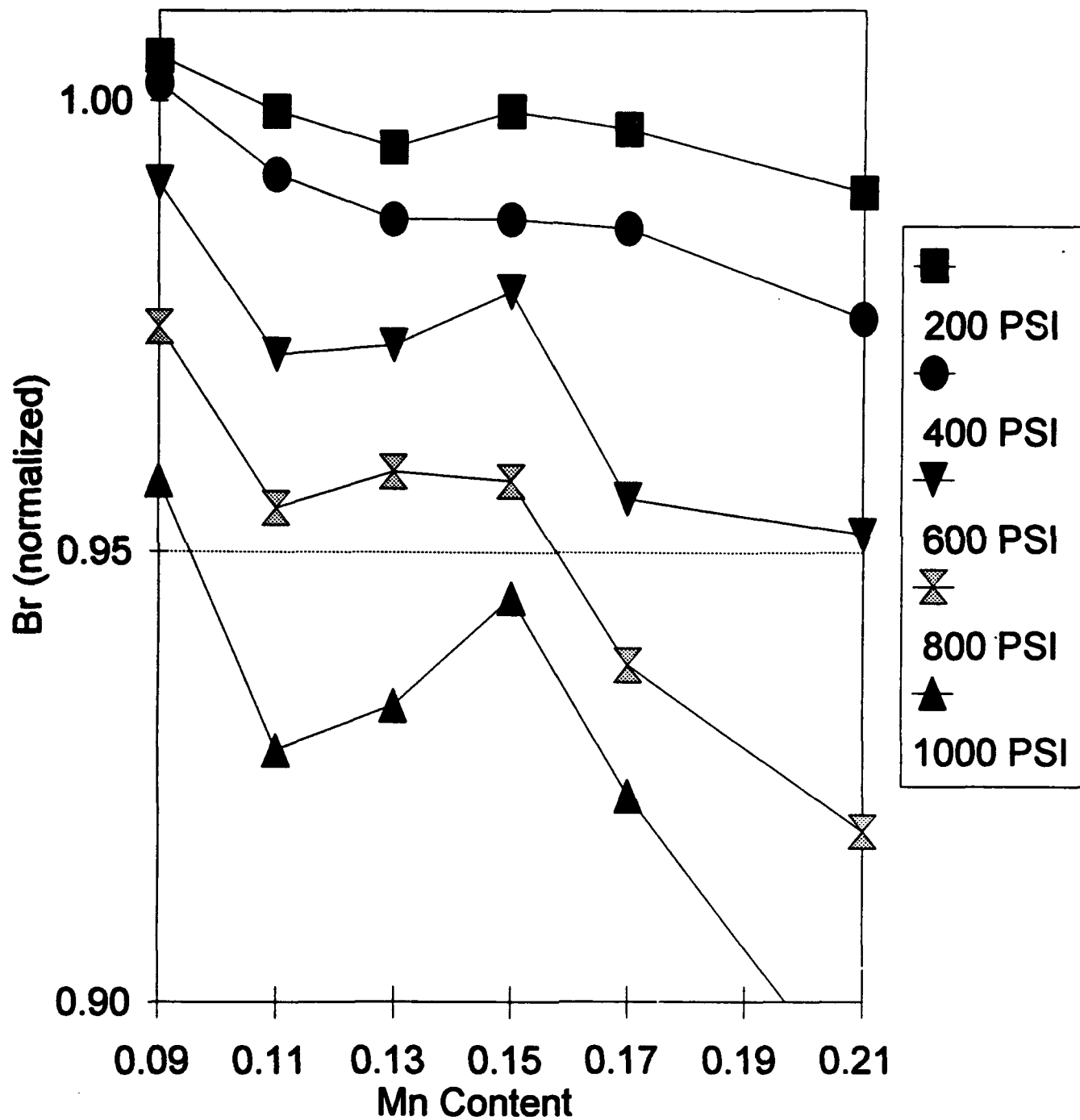# Br vs. Mn Content/Transverse Stress
## EMS G265



FIGURE 5-17

- 95 -

Br vs. Mn Content/Longitudinal Stress
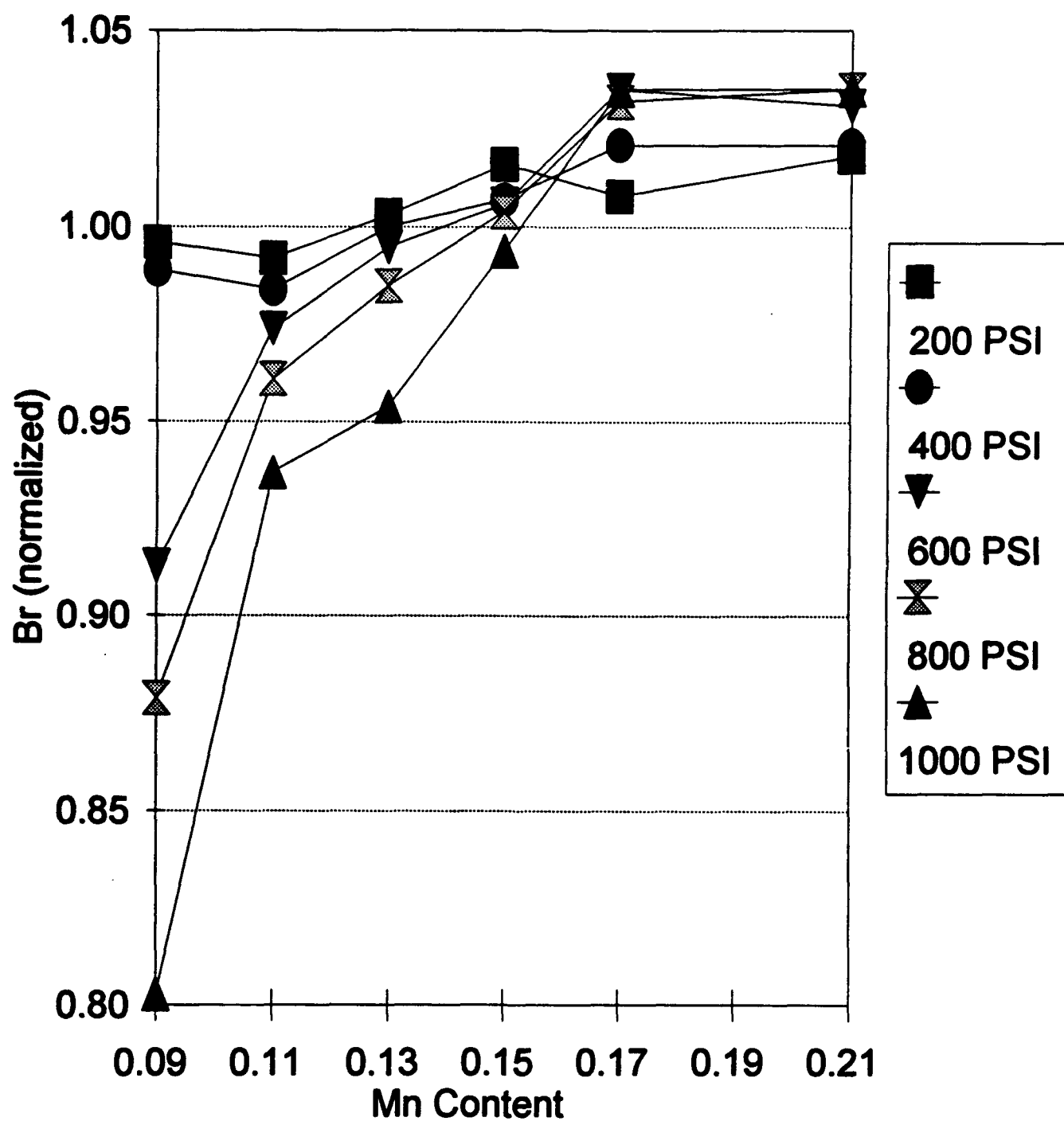EMS G265

FIGURE 5-18

## 6.0    PHASER STRUCTURE TESTS (Phase I)

## 6.1    TEST PROGRAM

The program of measurements on the selected materials are described by the
diagrams in Figure 6-1.  Square phase shifter toroids were matched with a
center dielectric slab to form a phaser unit.  The schedule of measurements
was designed to allow maximum correlation of hysteresis measurements with
phase shift measurements.  This is to our knowledge the first time that B-H
loops have been obtained on actual phaser toroids in waveguide housings
under high power conditions.

Hysteresis measurements were made of the B-H loop properties of phaser
toroids (side 1 and side 2) loosely held in the housing as a function of
temperature from room temperature (~25°C) to 100°C.  The data (shown later)
indicate no hysteresis with temperature, as one would expect.  It was found
that for all of the materials tested, the side 1 and side 2 toroids had
values of Br that tracked within 1% over the full range of temperatures.

Next these toroids were further assembled into the housing for low power RF
tests as a function of temperature.  The drum top (soft top) phase shifter
housing was used to minimize non-repeatable changes resulting from top to
bottom "crush" on the toroids. Hysteresis loops were again measured at each
temperature and differential phase shift was also measured with the toroids
driven by a latch box.  These data show hysteresis with temperature in both
remanent flux and differential phase shift.  The toroids on the two sides of
the structure still had Br values that tracked within 1% over the full range
of temperatures.  The room temperature values of Br measured on toroids
mounted in the housing was about 98 to 99% of the values measured on the
same toroids loose.  From data presented in  Section 5 it can be inferred
that the transverse pressure exerted by the housing is less than 200 PSI.

Finally, the toroids (mounted in the housing) were tested at high RF average
power with water cooling applied to the housing.  Again the B-H loops were
measured while the material was exposed to powers of up to 400 W average.
The differential phase shift was also measured at each power level from 10
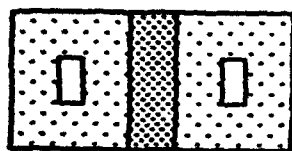
Br Vs TEMPERATURE
NO STRESS; TOROIDS LOOSE
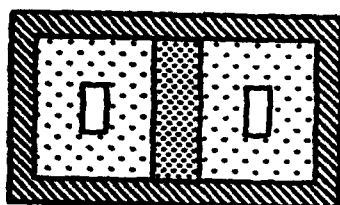
Br AND Δφ Vs TEMPERATURE
TOROIDS CAPTURED IN PHASER
HOUSING

At high rf power

Br AND Δφ Vs RF AVERAGE
POWER AND TEMPERATURE
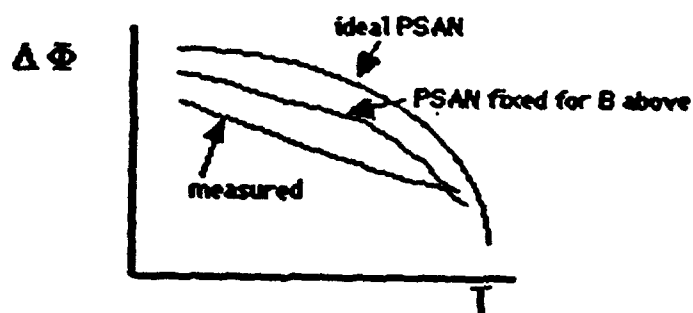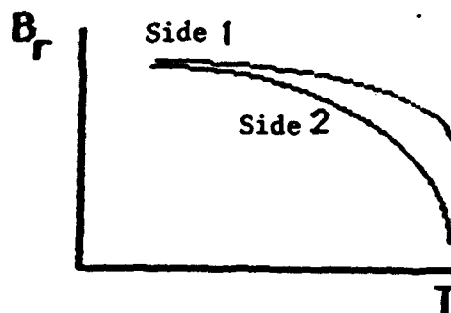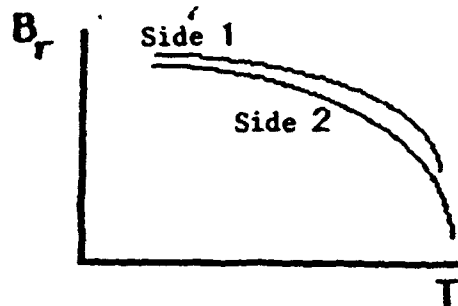
FIGURE 6-1

vatts to 400 vatts and for both increasing and decreasing powers. In these measurements the phaser is controlled by a flux driver, which does not produce as complete svitching of the toroids as does the latch box. This high average RF power resulted in some heating of the ferrite and housing to a maximum temperature of about 32°C against the 16°C heat sink.

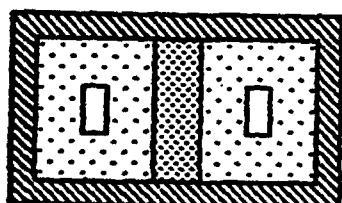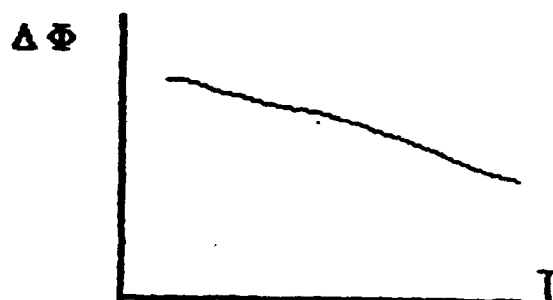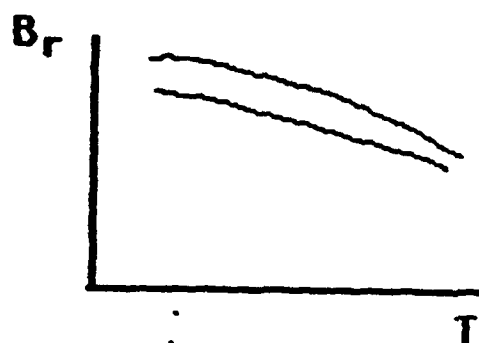Theoretical comparisons of the effects of temperature and power are possible using the EMS generated computer analysis program called PSAN. Having measured values of Br available for each condition of operation alloved these units to be modeled more accurately.

## 6.2    TEMPERATURE DATA

Measurements of remanent magnetization (Br) and differential phase shift (Delta Phi) versus temperature are presented graphically in Figures 6-2 through 6-15. Seven (7) materials vere tested, namely Trans-Tech's G-1002 (.09 Mn) and EMS G-265 (.09 Mn, .11 Mn, .13 Mn, .15 Mn, .17 Mn, and .21 Mn). For each material Br is plotted as a function of temperature both for toroids in a housing and for loose toroids. As expected the loose toroid data shovs no hysteresis effects and is plotted for reference. The second plot for each material is a lov power differential phase measurement with the Br measurement repeated to shov hov phase shift and remnant magnetization track one another. In each case the data are plotted on a normalized scale so that the materials may be compared easily. The differential phase shift for each material tested vas near 115 degrees at 25°C. Note that the Trans-Tech G-1002 (.09 Mn) material is on a slightly different scale than the other materials due to its larger magnitude of hysteresis. Additionally, arrows are included on each plot to indicate the sense of the hysteresis (clockwise or counterclockwise).

Figure 6-2 shovs the clockwise sense hysteresis of Br for the Trans-Tech G-1002 (.09 Mn) material. Figure 6-3 shovs differential phase hysteresis of the same sense and magnitude ($\approx$ 20%) as for Br of this material.

Figure 6-4 shovs that EMS G-265 (.09 Mn) material has clockwise hysteresis just as the Trans-Tech material did, but with a much reduced magnitude (less than 1% relative to loose toroid data). Figure 6-5 shovs that phase and Br measurements track closely.

- 99 -

Br vs. Temperature
TT-G1002 (.09 Mn)

**Legend:**
- Toroid Loose
- Toroid in Housing

Temperature (deg C)

Br (normalized)

FIGURE 6-2

- 100 -

Phase & Br vs. Temperature
TT G1002 (.09 Mn)
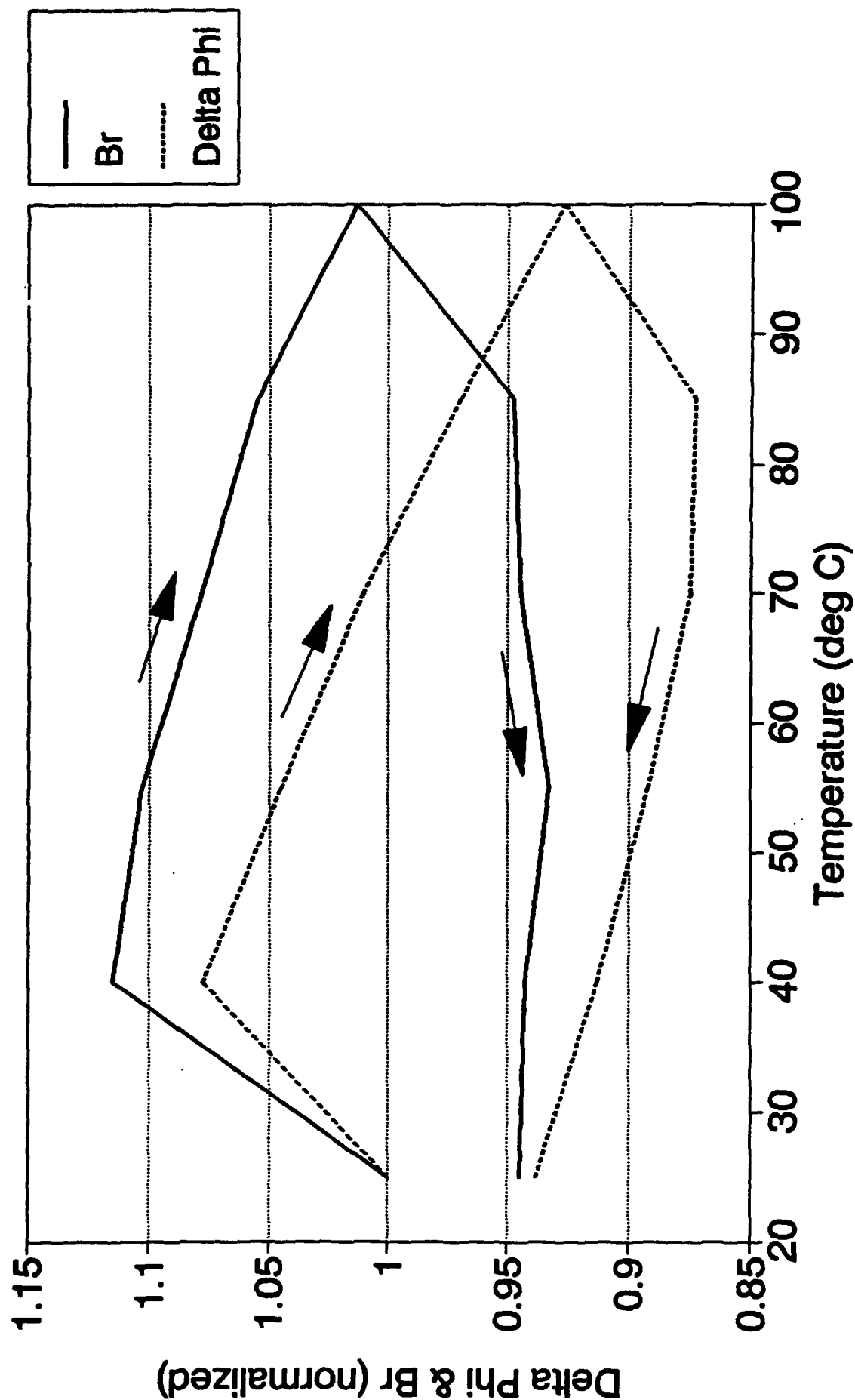
FIGURE 6-3

Br vs. Temperature
EMS G265-35 (.09 Mn)

Toroid Loose
Toroid in Housing

Br (normalized)
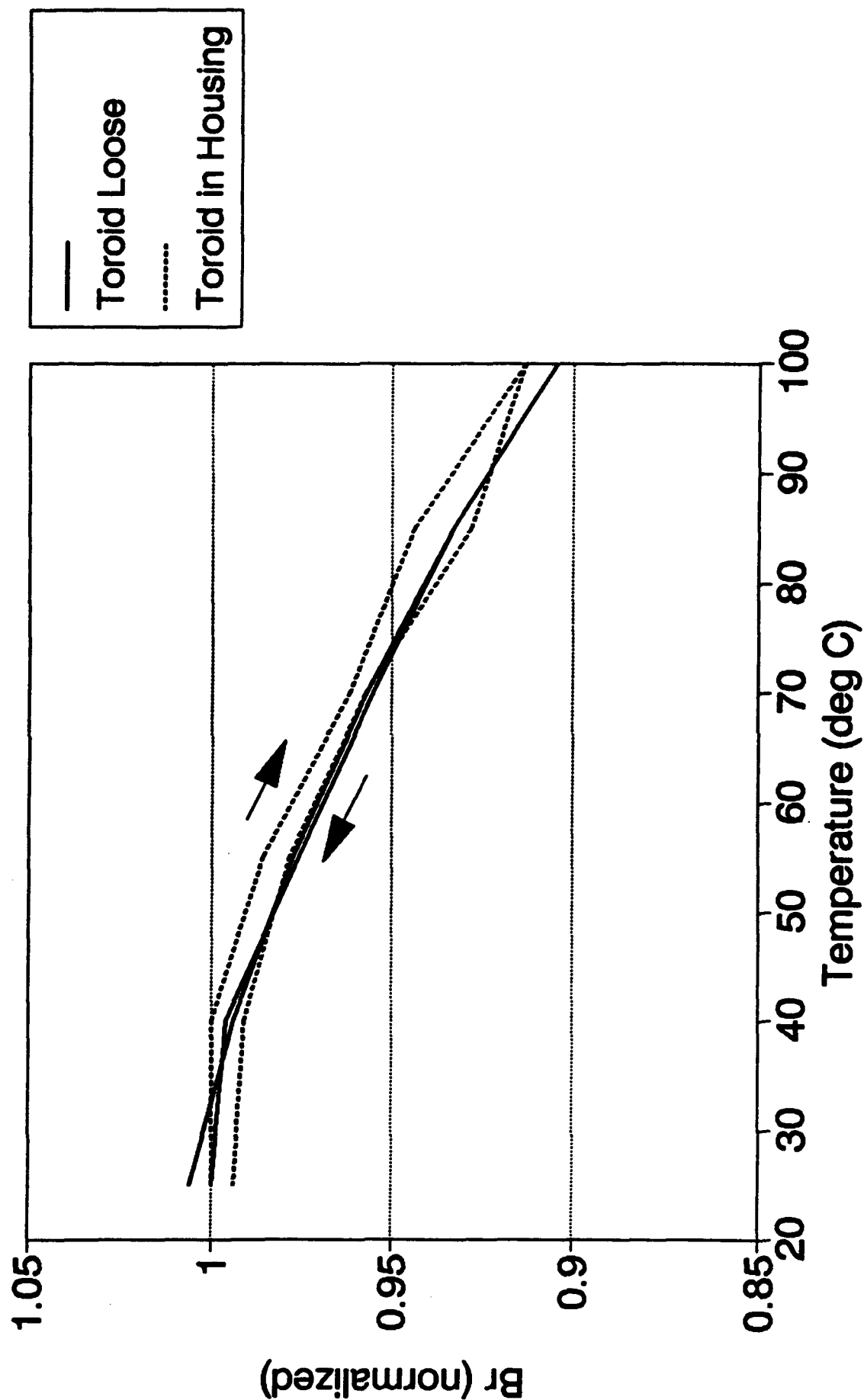
Temperature (deg C)

FIGURE 6-4

Phase & Br vs. Temperature
EMS G265-35 (.09 Mn)

FIGURE 6-5

- 103 -
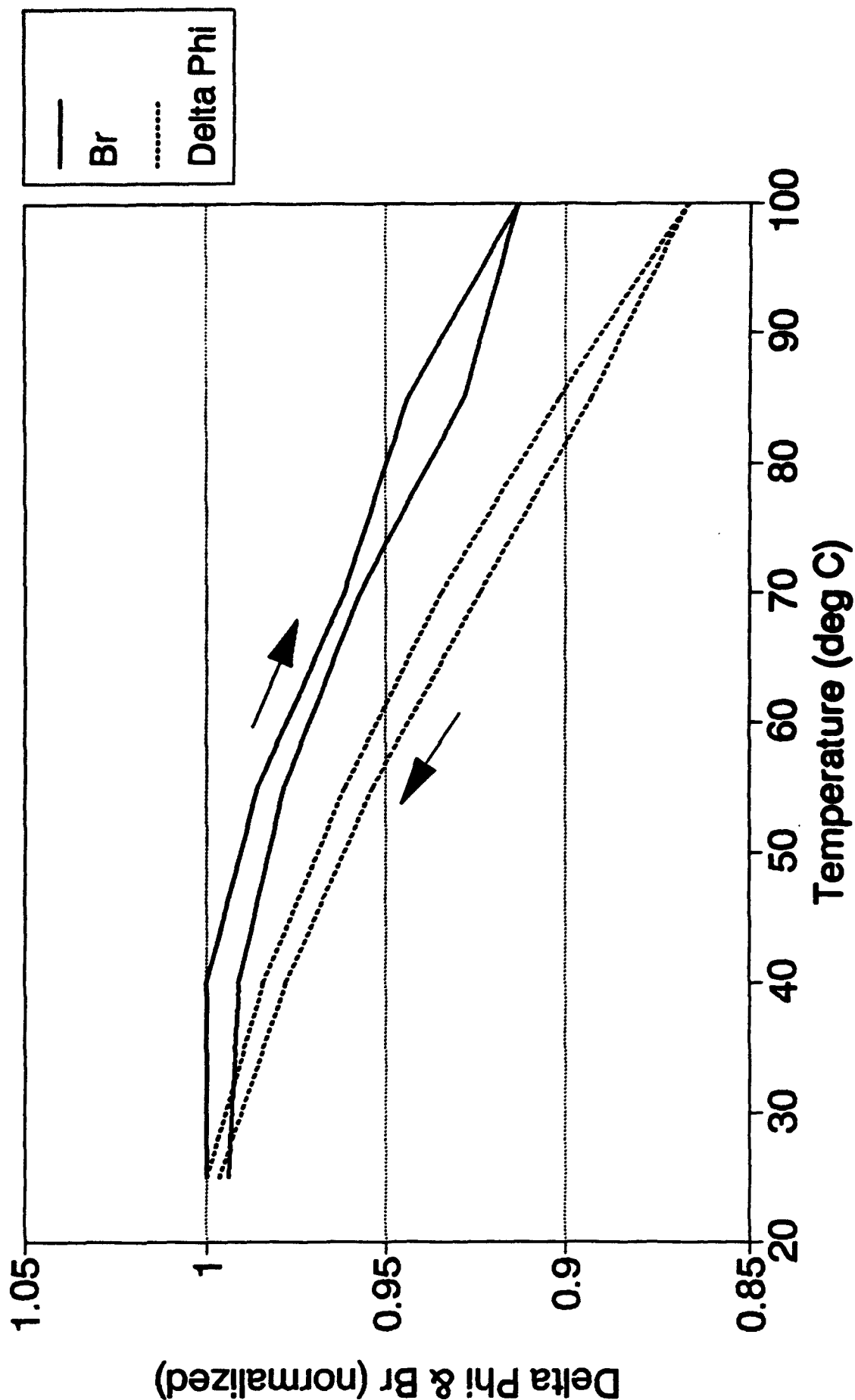
Figures 6-6 and 6-7 show hysteresis results for the EMS G-265 (.11 Mn) material that has the same sense (clockwise) and nearly the same magnitude of hysteresis as that of the EMS G-265 (.09 Mn) material.

Figures 6-8 and 6-9 show results for the EMS G-265 (.13 Mn) material which indicate very little hysteresis of either Br or Delta Phi. The small amount of hysteresis (much less than 1%) that is displayed has a counter clockwise sense. This is significant because, as will be seen later, all materials measured with higher than 0.13 Mn content have significant counterclockwise hysteresis of phase and remnant magnetization. These results indicate a stress insensitive compensation point for a Mn+3 substitution level near 0.13.

Figures 6-10 and 6-11 show the counter clockwise hysteresis of Br and Delta Phi for the EMS G-265 (.15 Mn) material. The magnitude of the hysteresis is only slightly larger than that of the .11 Mn material (which is on the opposite side of the compensation point).

Figures 6-12 and 6-13 show the counterclockwise hysteresis of Br and Delta Phi for the EMS G-265 (.17 Mn) material. The magnitude of the hysteresis ($\approx$ 4%) is much larger than that of materials with lower Mn dopings.

Figures 6-14 and 6-15 show the counterclockwise hysteresis of Br and Delta Phi for the EMS G-265 (.21 Mn) material with magnitude near 5%.

## 6.3    THERMAL HYSTERESIS

The thermal hysteresis seen in Figures 6-2 through 6-15 is a major problem for high power ferrite phase shifters, power dividers and switches. It is believed to be caused by differential expansion of the ferrite and metallic waveguide housing and by a resulting longitudinal stress on the ferrite toroids. An interpretation of this effect is given below.

Br vs. Temperature
EMS G265-36 (.11 Mn)

Toroid Loose
Toroid in Housing

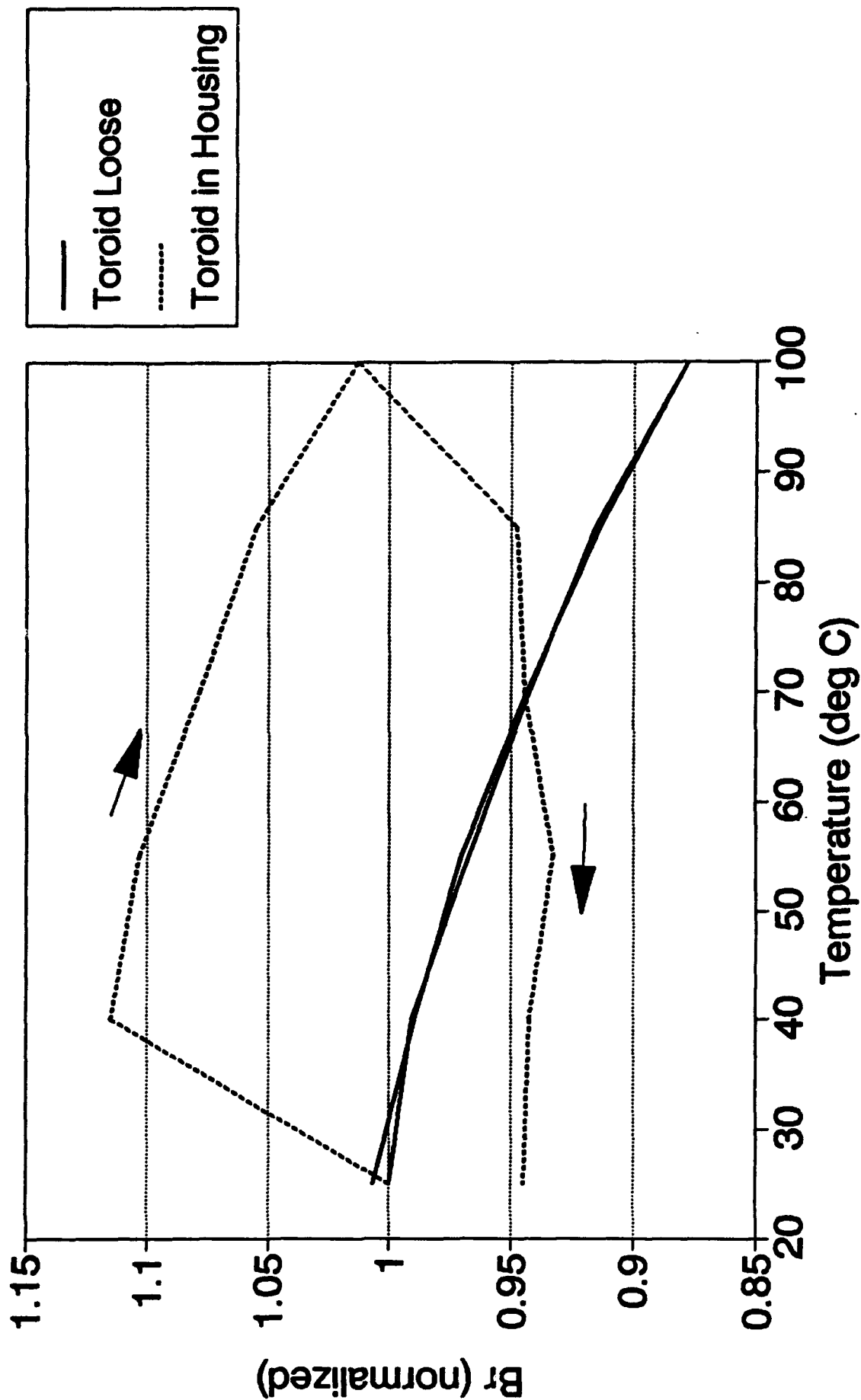Br (normalized)
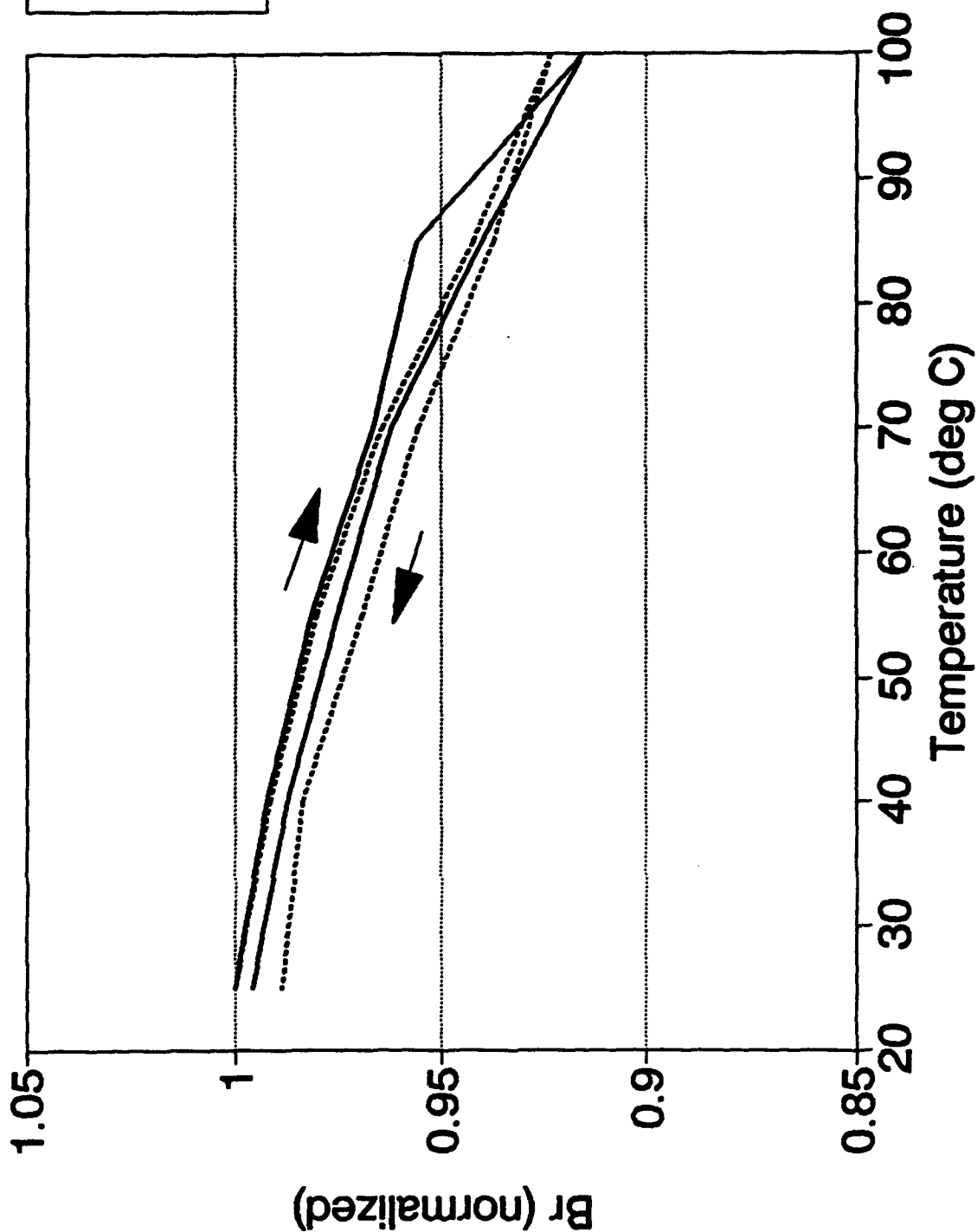
Temperature (deg C)

FIGURE 6-6

Phase & Br vs. Temperature
EMS G265-36 (.11 Mn)
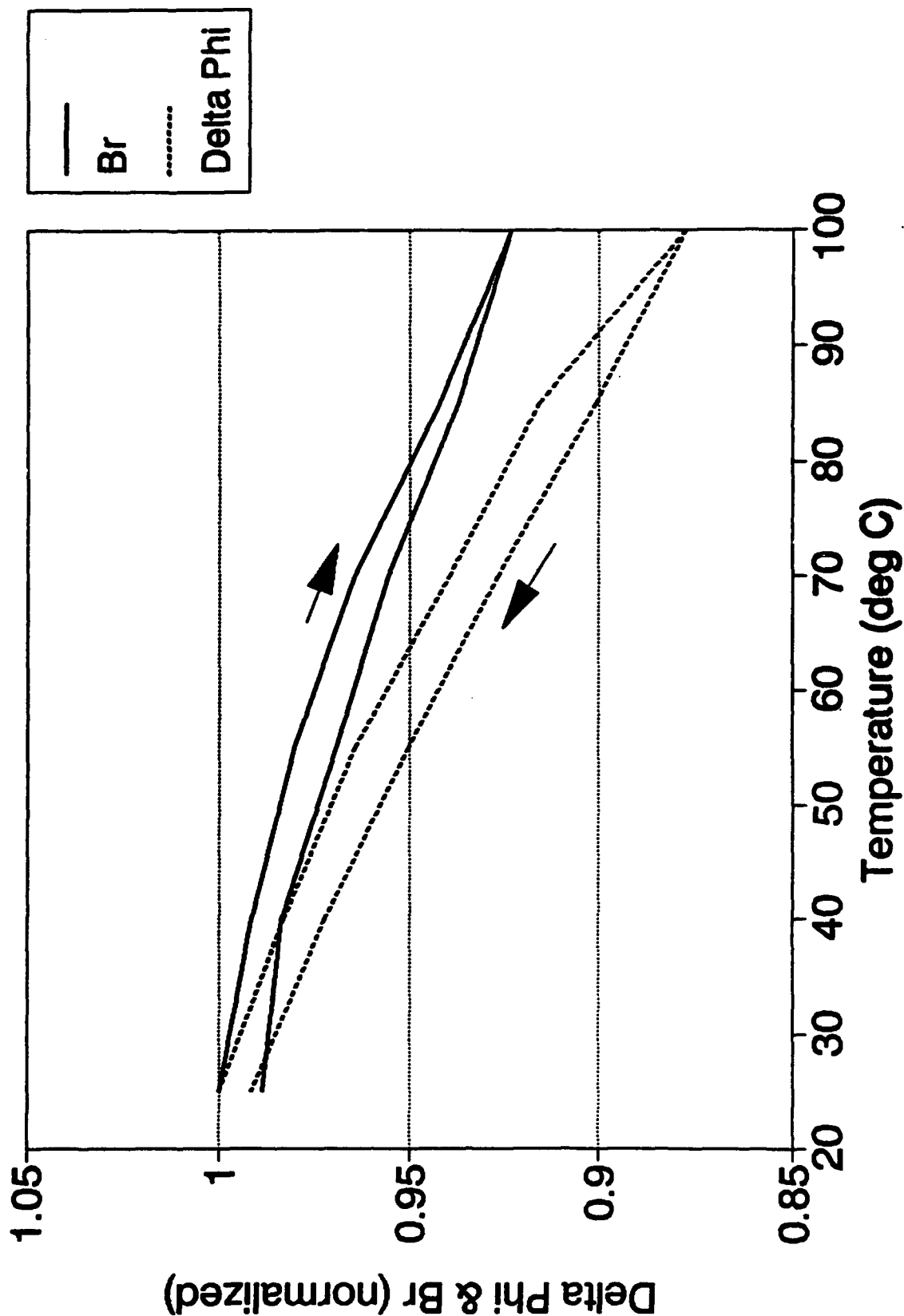
FIGURE 6-7

Br vs. Temperature
EMS G265-37 (.13 Mn)
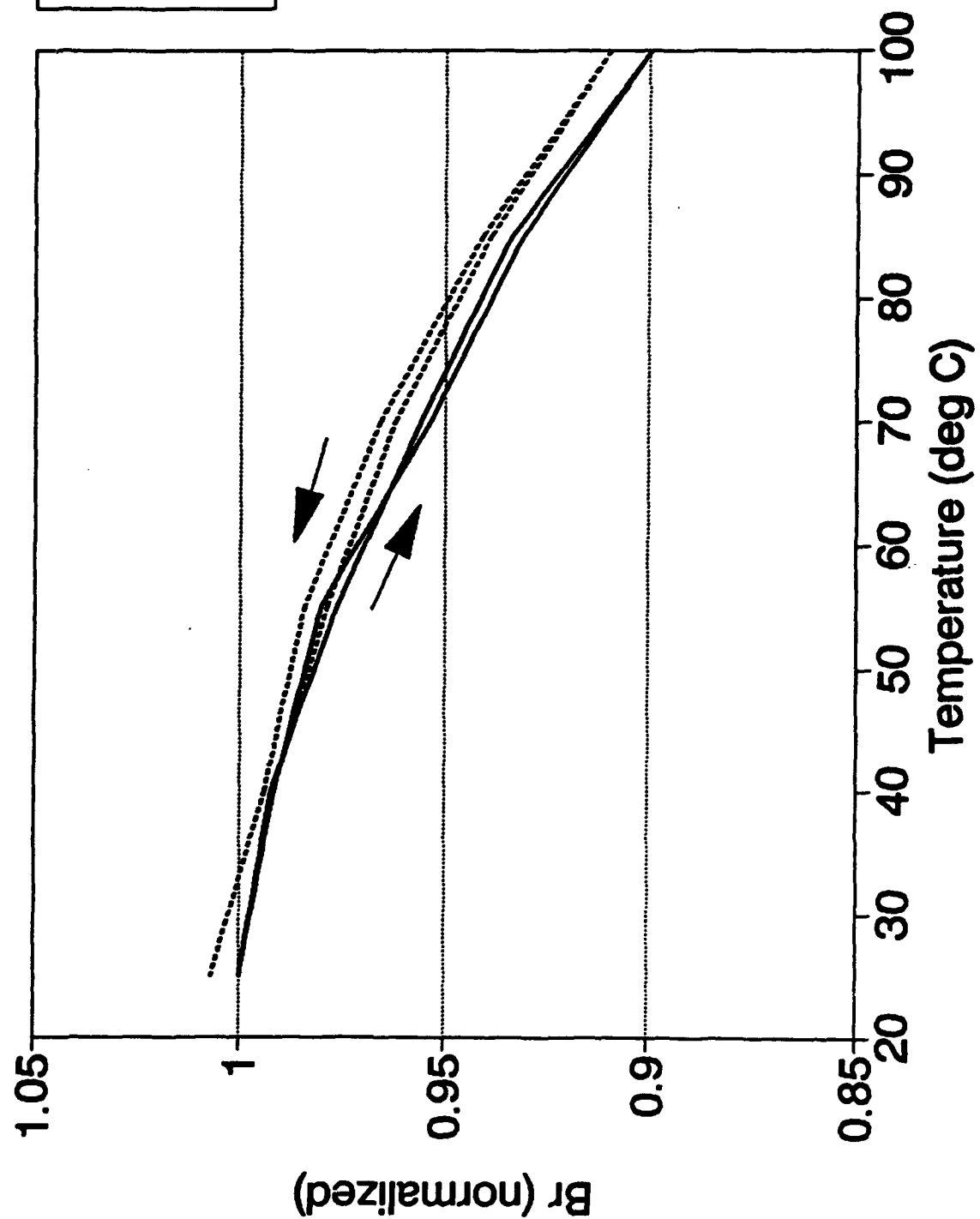
FIGURE 6-8

Phase & Br vs. Temperature
EMS G265-37 (.13 Mn)
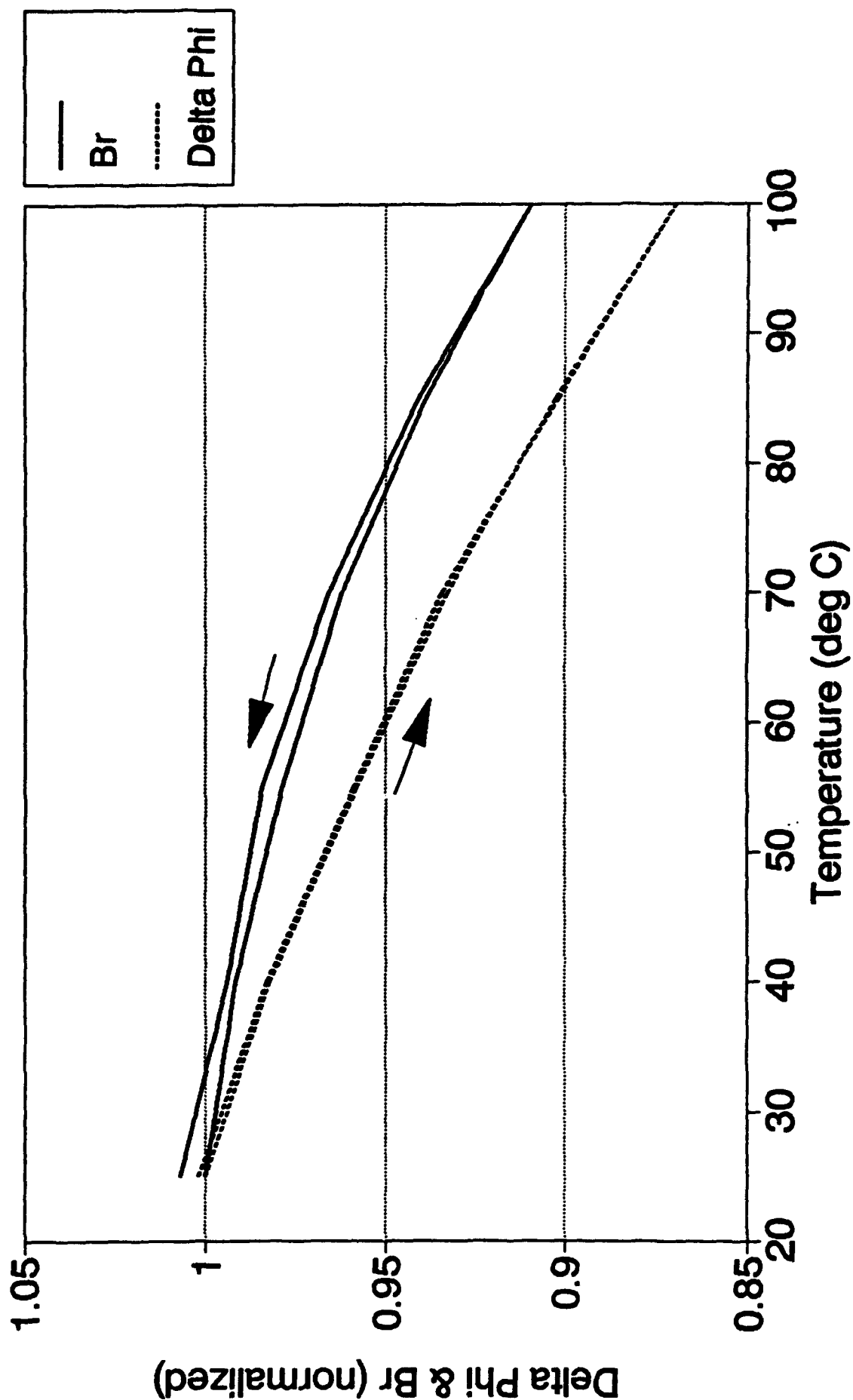
FIGURE 6-9

Br vs. Temperature
EMS G265-33 (.15 Mn)
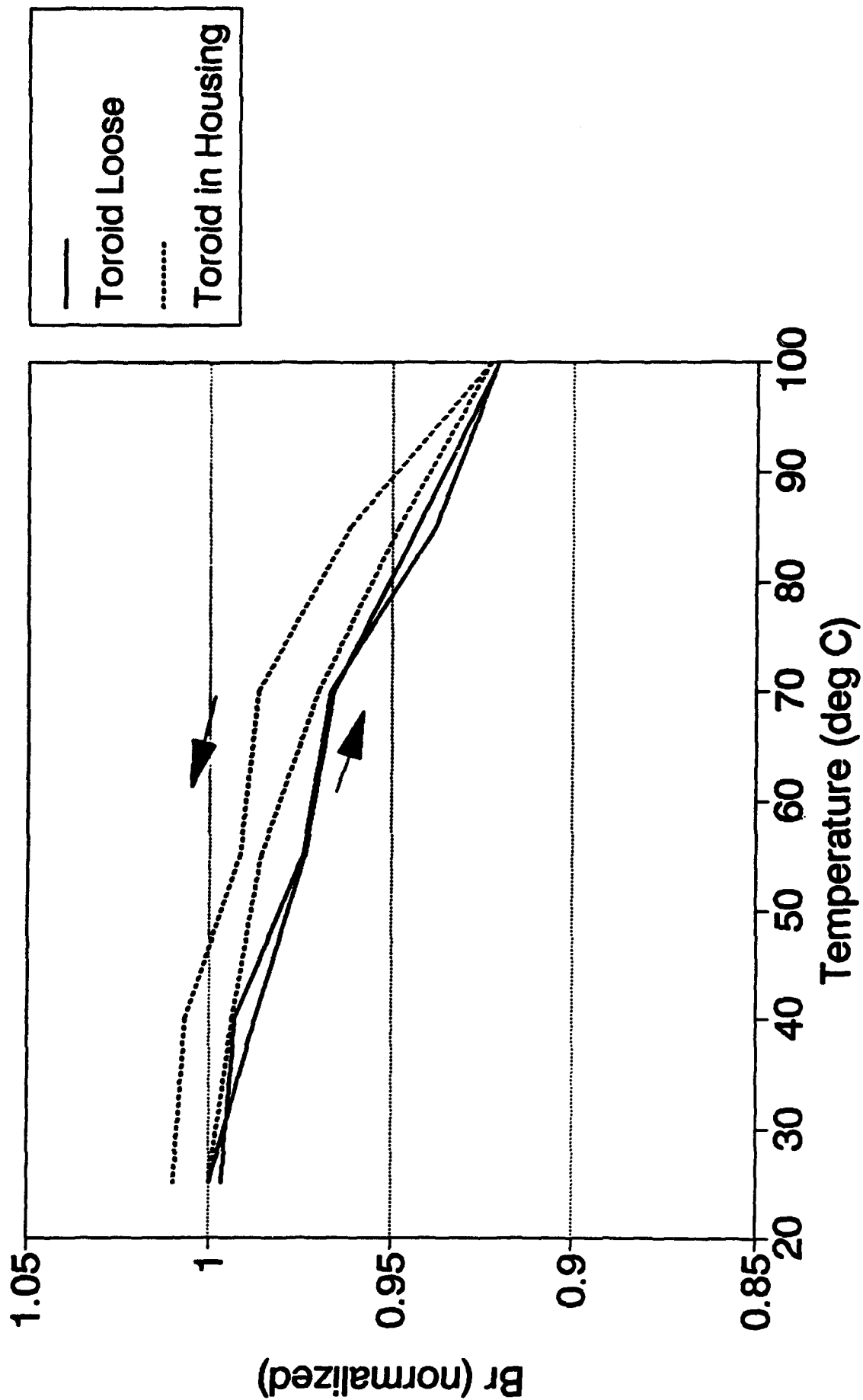
FIGURE 6-10

Phase & Br vs. Temperature
EMS G265-33 (.15 Mn)
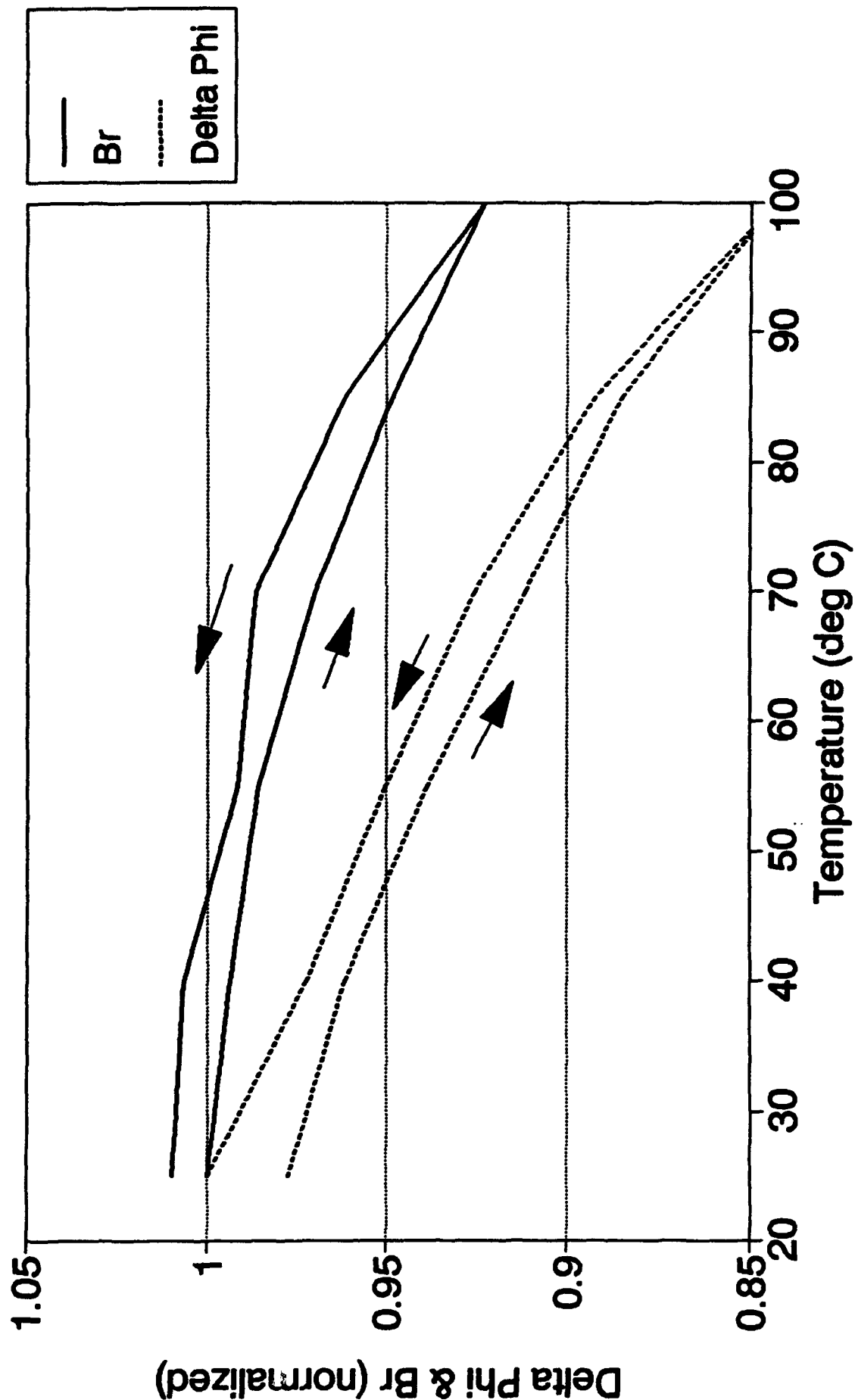
FIGURE 6-11

Br vs. Temperature
EMS G265-42 (.17 Mn)

Toroid Loose
Toroid in Housing

Temperature (deg C)

Br (normalized)
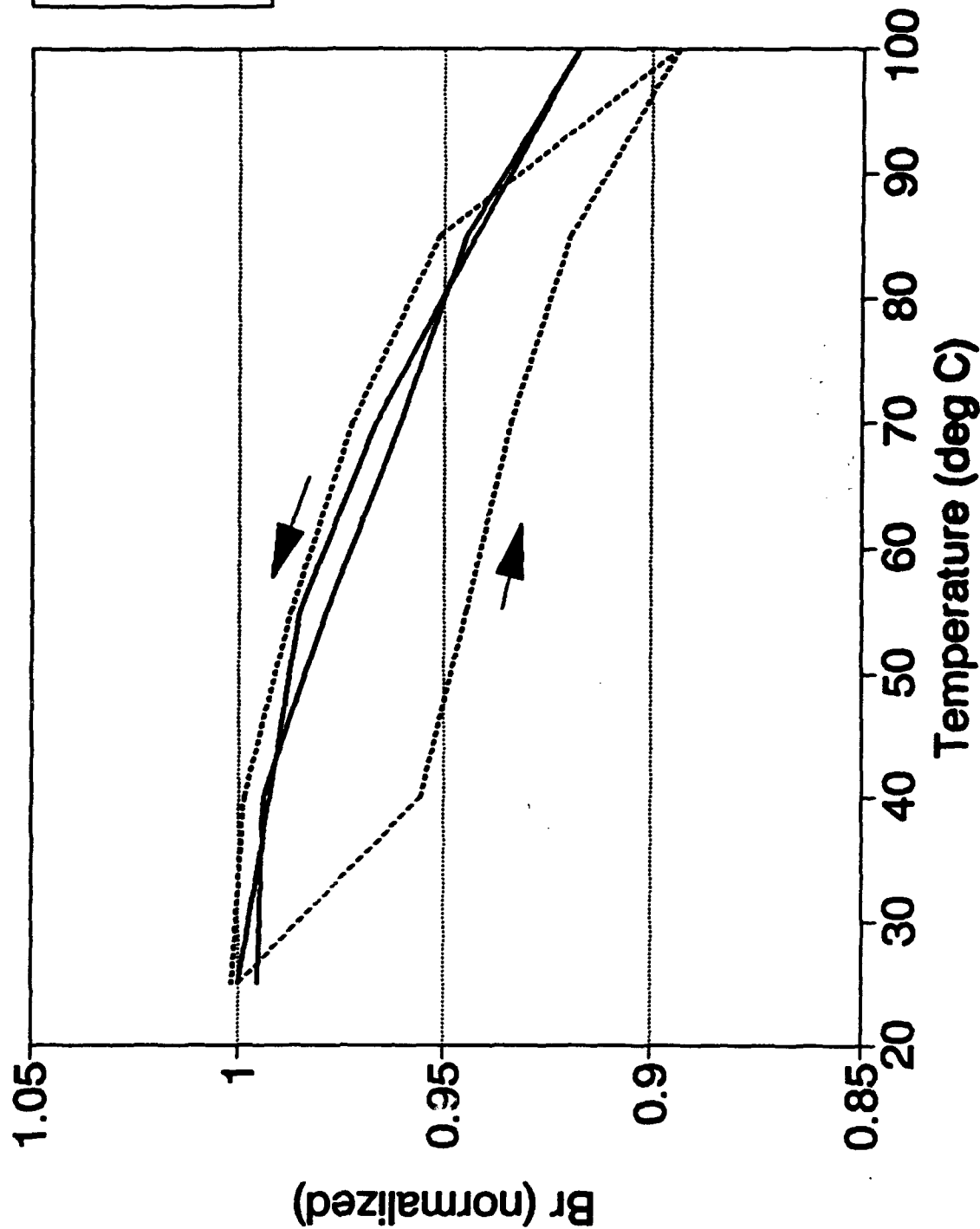
FIGURE 6-12

Phase & Br vs. Temperature
EMS G265-42 (.17 Mn)

FIGURE 6-13

Delta Phi & Br (normalized)

Temperature (deg C)

Br
Delta Phi

Br vs. Temperature
EMS G265-41 (.21 Mn)

Toroid Loose
Toroid in Housing
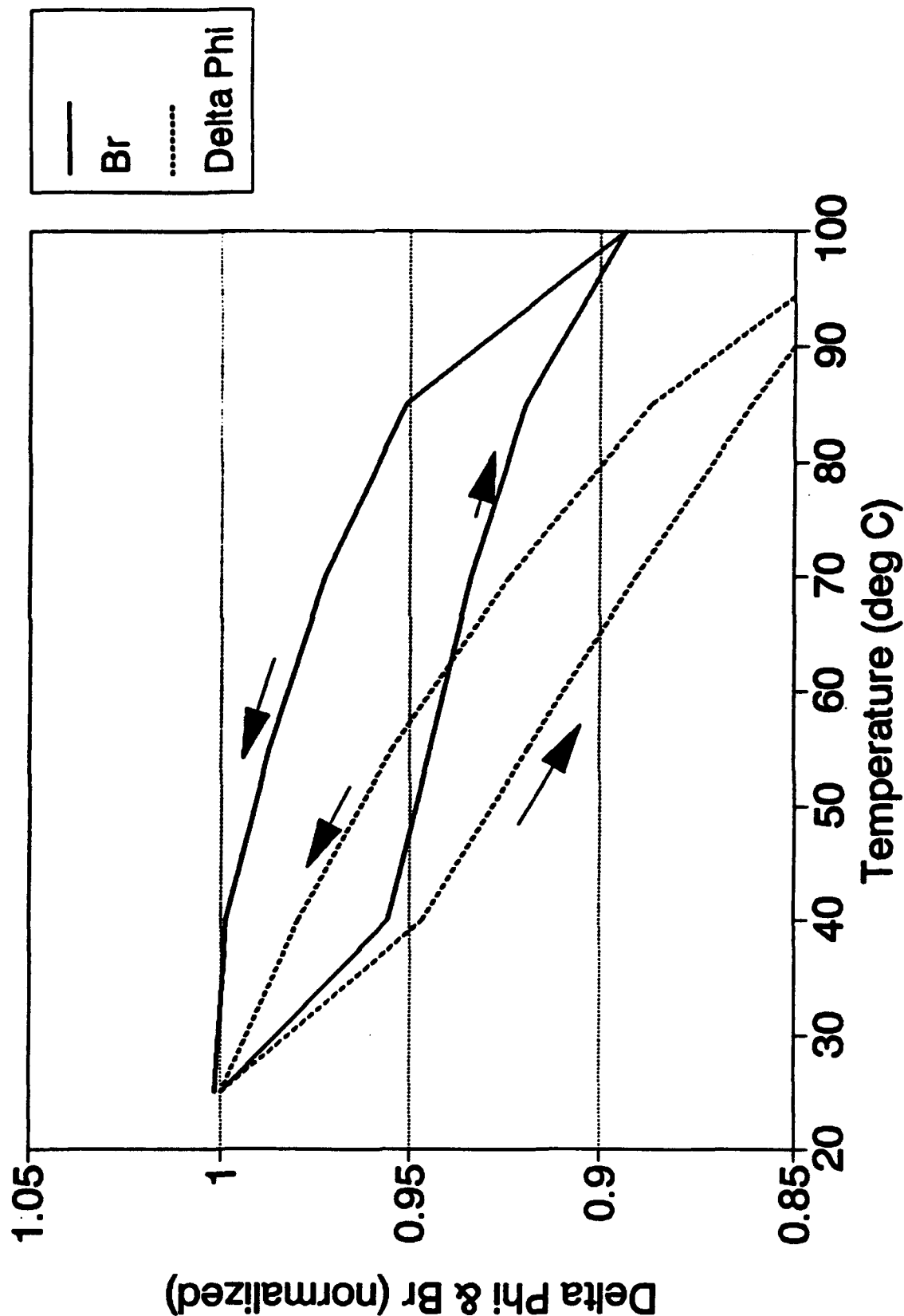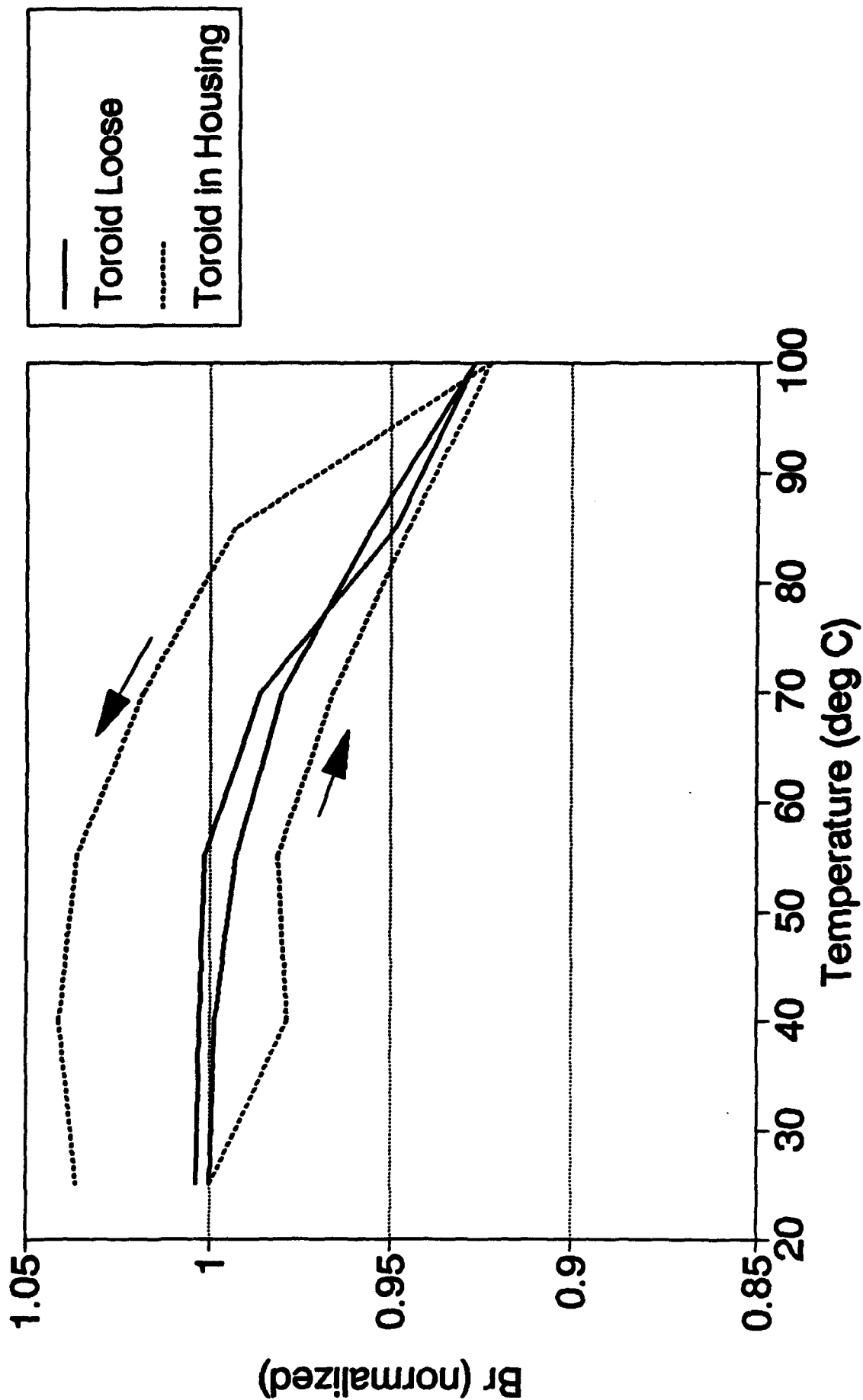
FIGURE 6-14

Phase & Br vs. Temperature
EMS G265-41 (.21 Mn)

FIGURE 6-15

- 114 -
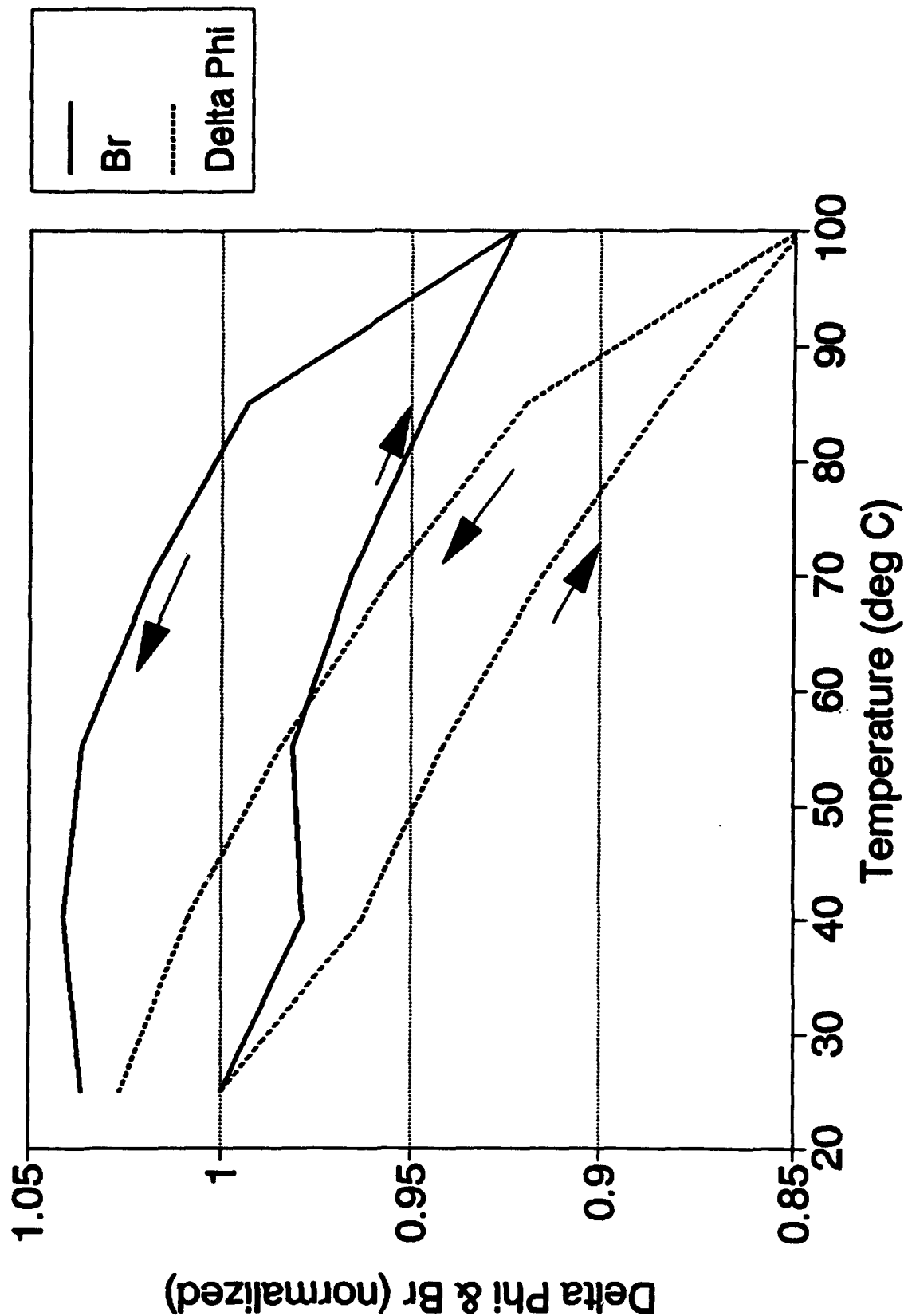
The ferrite and dielectric parts are not bonded to the waveguide, but rather held in place by friction between mating surfaces as enhanced by a transverse pressure from top to bottom of the waveguide structure. When assembled at room temperature the ferrite and dielectric parts rest against the waveguide bed with no longitudinal stress and some modest transverse stress due to the coverplate or metal sheet. As the temperature is increased, the housing (aluminum in this case) expands more than does the ferrite. Friction forces between the ferrite and the aluminum housing then cause the ferrite to be pulled longitudinally as the temperature rises. The ferrite experiences a tensile stress. This strain in the ferrite can be relieved by the ferrite slipping or creeping along the surface of the waveguide. Such creeping will occur when the longitudinal stress at the surface of the ferrite exceeds the frictional forces that tend to drag the ferrite along with the expanding aluminum. Thus with continuous increases in temperature the ferrite will always be under longitudinal tensile stress, and some relief of this stress will also occur continuously by the creeping. The amount of longitudinal stress that occurs will be dependent on those factors that determine friction forces: the coefficient of friction between ferrite and aluminum (and therefore surface finish of both parts) and the transverse force or pressure that bears the ferrite against the aluminum.

When the temperature begins to decrease, the aluminum housing shrinks faster than does the ferrite, and the ferrite experiences a longitudinal compression. On this decreasing temperature cycle, creeping will again occur whenever the longitudinal stress exceeds the frictional force. The net result is that the ferrite is always under longitudinal compression as the temperature is lowered.

Several experiments were done to check this hypothesis. In one, ferrites were semi-rigidly bonded to an aluminum plate, and in a second, very small cycles in temperature were used.

When the 0.09 Mn substituted garnet was heated to 100°C in the housing (and free to creep along the waveguide surface) the measured decrease in remanent magnetization was to 90.5% of its room temperature value. When the same toroid was bonded to an aluminum block by Scotchweld to reduce creeping and heated to

100°C the remanent magnetization decreased to 88% of its room temperature value. By not allowing as much creeping to occur, the total stress is increased, as evidenced by the greater decrease in remanence. It was also observed that the thermal hysteresis in remanent magnetization is reduced in the case of the toroid bonded to the metal. Scotchweld is a moderately malleable bond, so that relative motion of the ferrite and metal parts was still possible in this experiment.

In the second experiment, the temperature of the ferrite was cycled over a small temperature range, 5°, and it was observed that the hysteresis has nearly the same amplitude as that seen for full 80° temperature cycles. This shows that the effect results from the direction of change in temperature, not from the total change in temperature. Stresses from the total change in temperature are relieved by creeping after some threshold stress is reached. This threshold is determined by friction and therefore, by surface finish and transverse pressure.

For Mn substitutions of 0.11 or less the clockwise thermal hysteresis indicates that a longitudinal tension increases the remanent flux or that the effect in magnetostrictive coefficient is negative. For Mn substitution of greater than 0.13 the observed counter clockwise thermal hysteresis indicates that a longitudinal tension decreases the remanent flux or that the magnetostrictive coefficient is positive.

It should perhaps be mentioned that the ferrite creeping does not represent a net migration of the ferrite toroid down the waveguide. The center of the toroid presumably stays fixed and both ends move along the metal with increasing and decreasing temperatures.

## 6.4   HIGH AVERAGE POWER DATA

Results of the high average power tests are presented in Figures 6-16 through 6-22. The seven materials tested are the same as those used in the temperature tests of Section 6.2. CW power levels from 10 Watts to 400 Watts were used as indicated on each plot. Corresponding temperature due to RF heating is

# Br & Phase vs. Temperature (RF Heating)
## TT G1002 (.09 Mn)
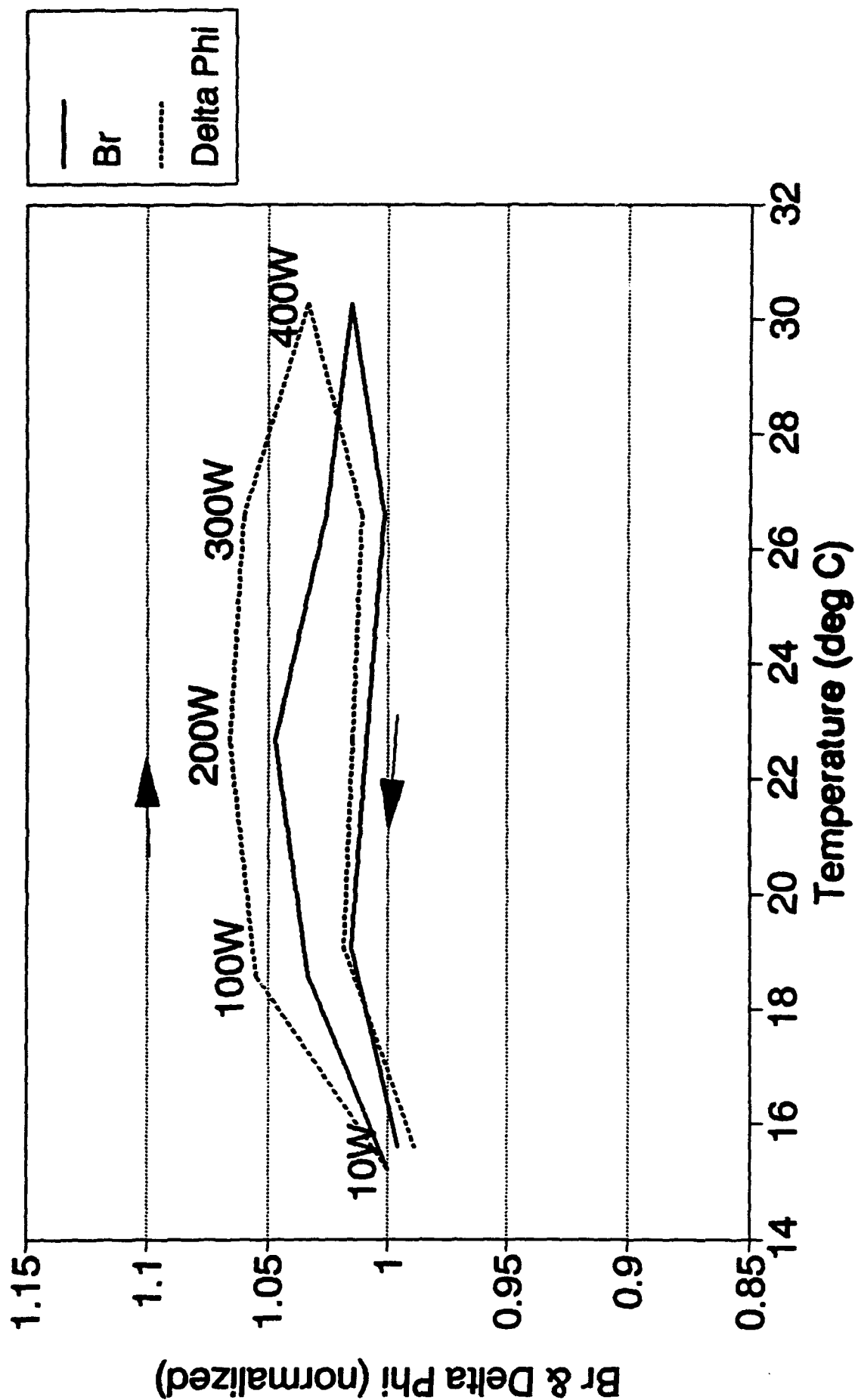


FIGURE 6 16

Br & Phase vs. Temperature (RF Heating)
EMS G265-35 (.09 Mn)
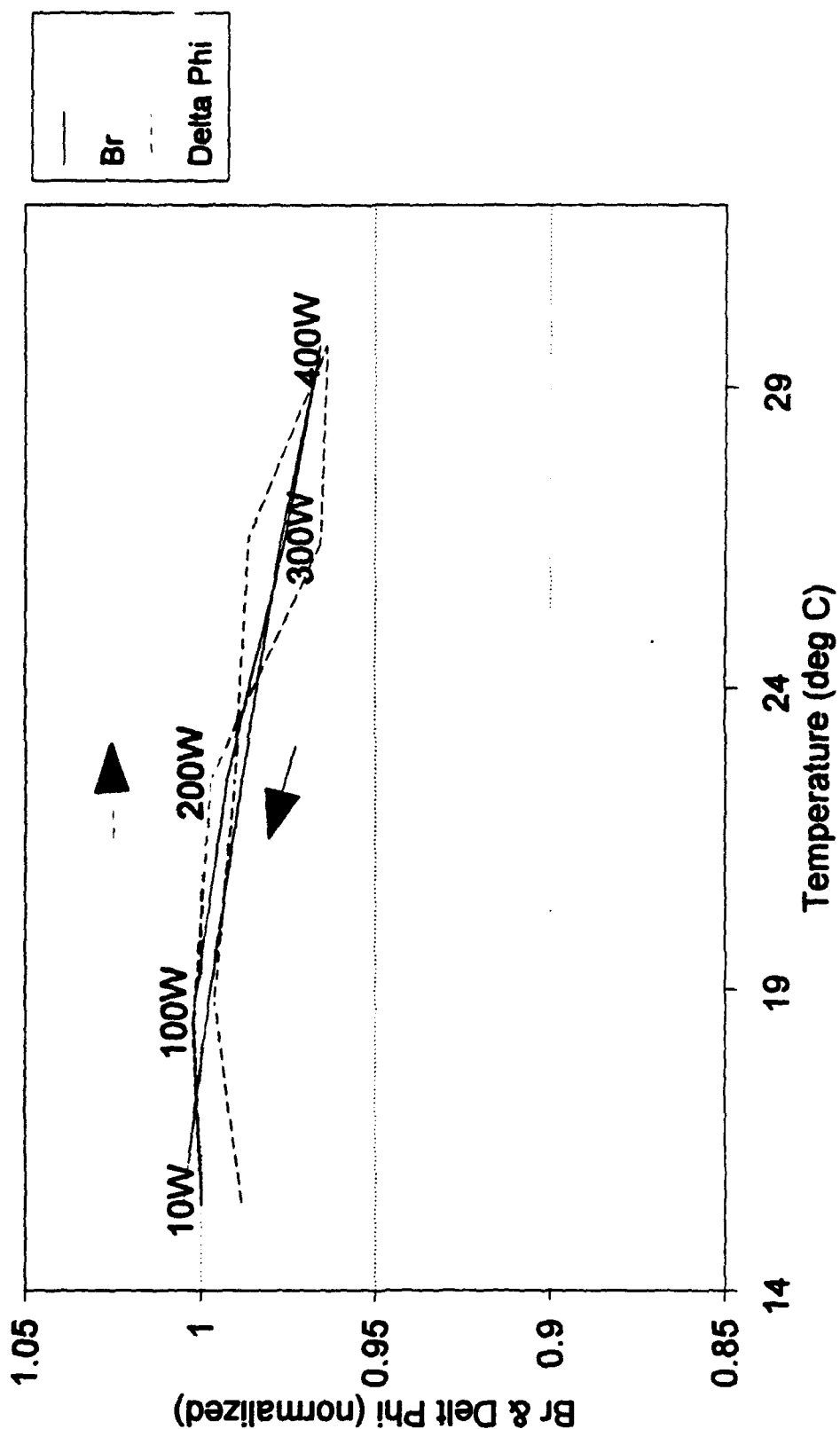
FIGURE 6-17

Br & Phase vs. Temperature (RF Heating)
EMS G265-36 (.11 Mn)
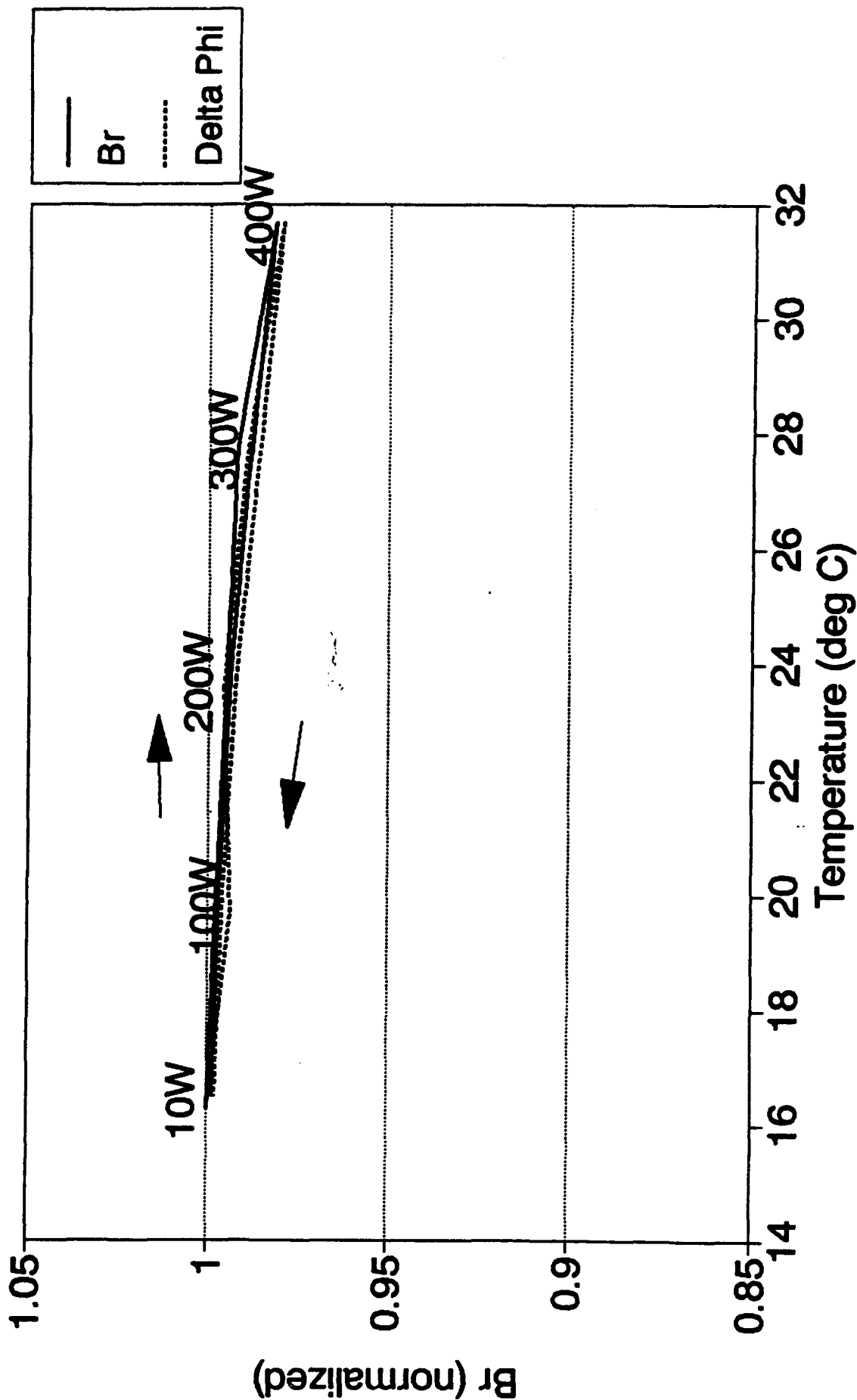
FIGURE 6-18

Br & Phase vs. Temperature (RF Heating)
EMS G265-37 (.13 Mn)
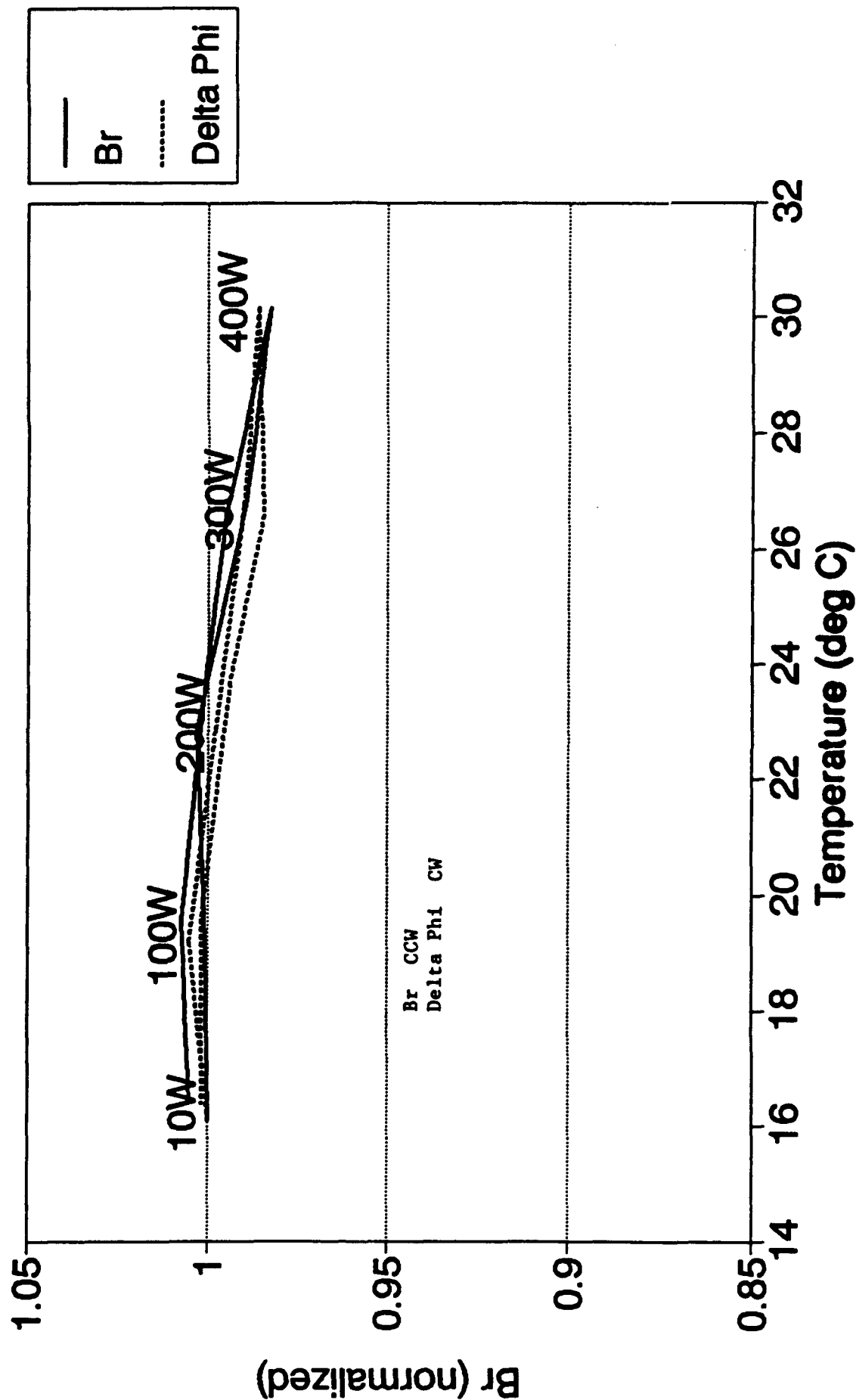
FIGURE 6.10

# Br & Phase vs. Temperature (RF Heating)
## EMS G265-33 (.15 Mn)
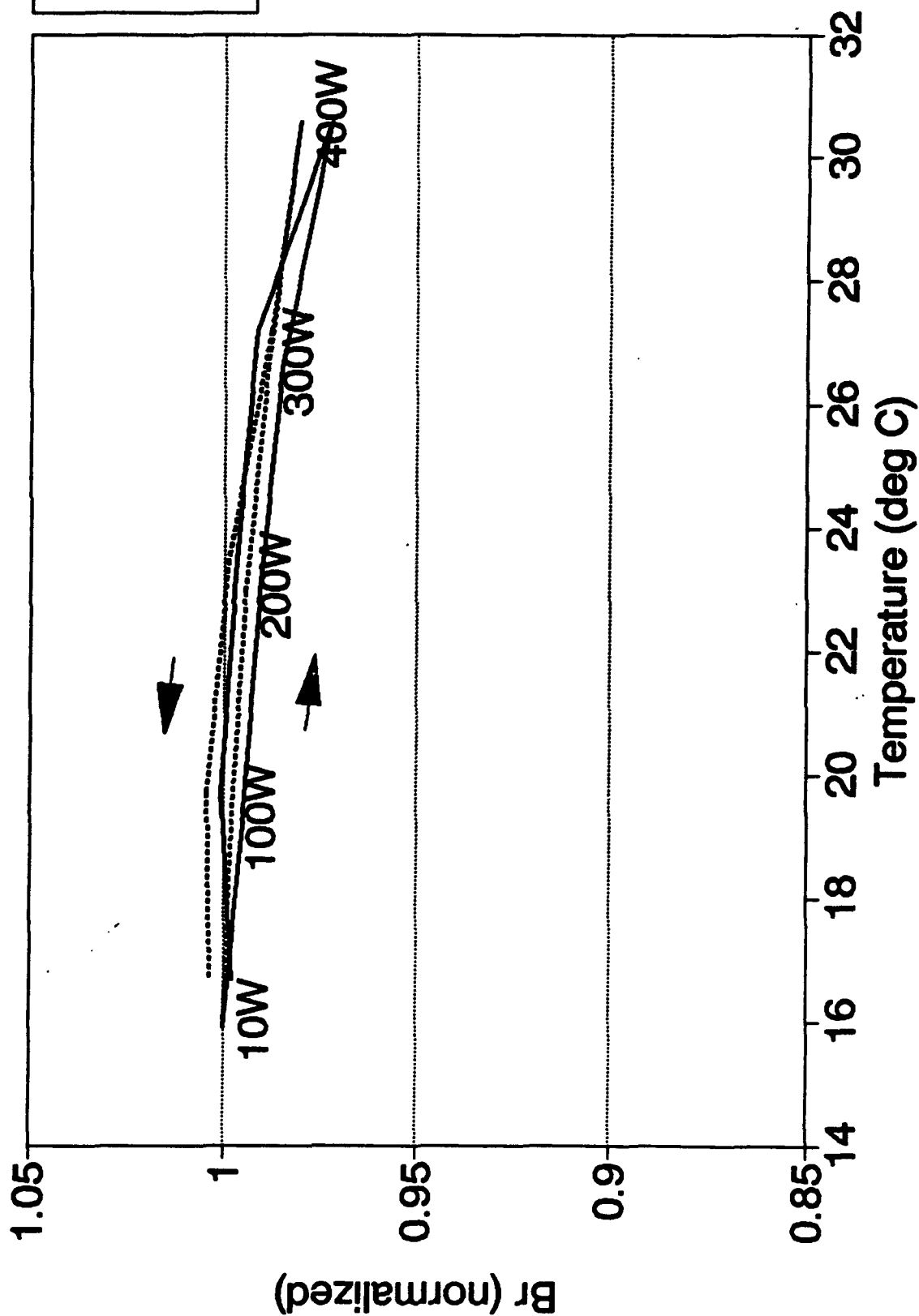


**FIGURE 6-20**

# Br & Phase vs. Temperature (RF Heating)
## EMS G265-42 (.17 Mn)
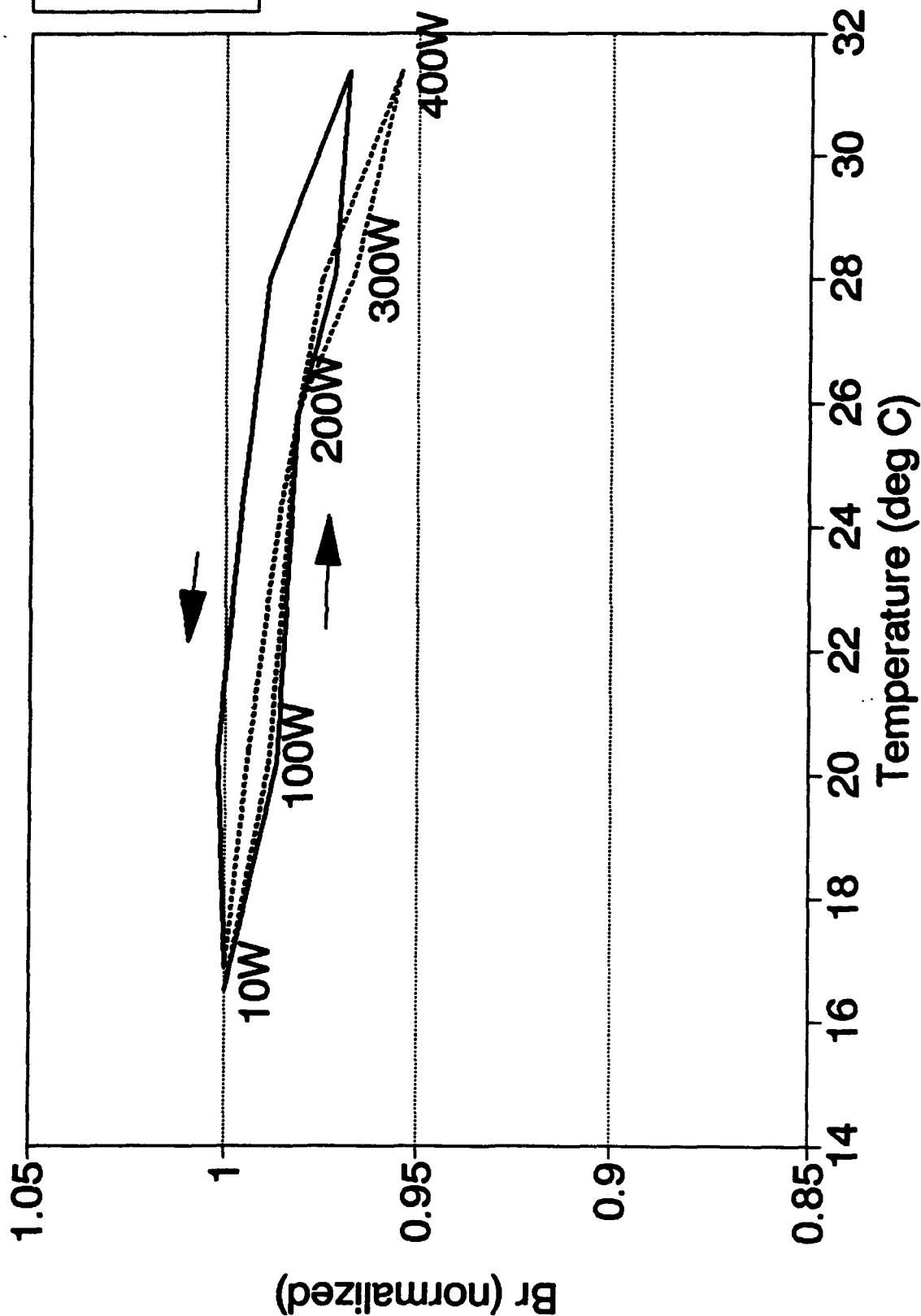


**FIGURE 6-21**

Br & Phase vs. Temperature (RF Heating)
EMS G265-41 (.21 Mn)
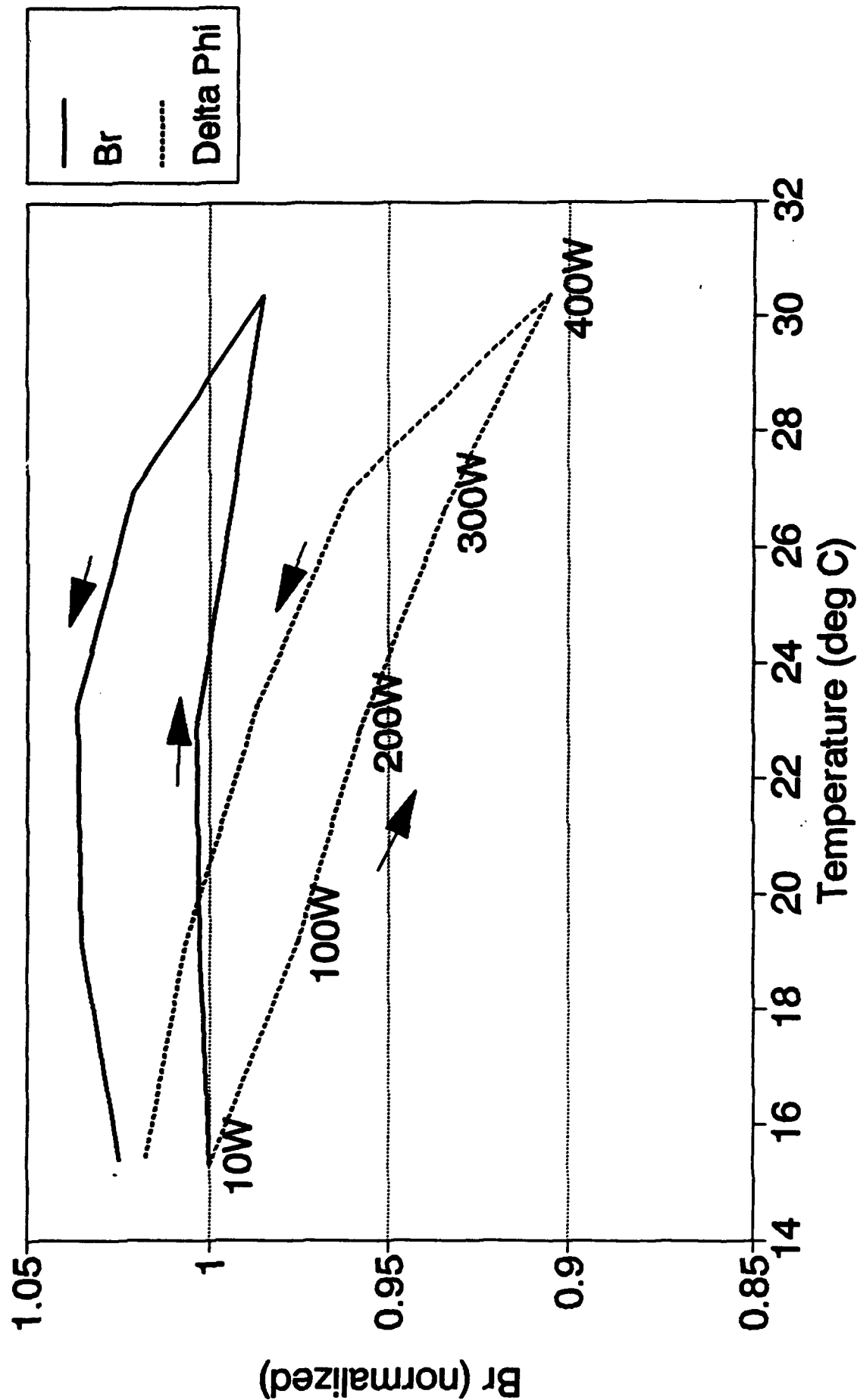
FIGURE 6-22

represented on the x-axis. The temperature was measured (and monitored) from a thermistor mounted to the thin walled drum top part of the housing just above the ferrite section in the center of the waveguide. All plots are on a normalized scale with the scale for the Trans-Tech G-1002 (0.09 Mn) material being slightly different due to its greater hysteresis. As before in the temperature data, arrows on the plots are used to indicate the sense of the hysteresis (clockwise or counterclockwise). For each material, both remanent magnetization (Br) and differential phase shift (Delta Phi) are plotted on the same graph.

Figure 6-16 shows that, as in the temperature testing, the Trans-Tech G-1002 (0.09 Mn) material also exhibits considerable hysteresis with RF heating. The sense of the hysteresis is clockwise with a magnitude ≈ 6%.

Figure 6-17 shows that over the measured range of RF power, very little hysteresis is detectable for the EMS G-265 (0.09 Mn ) material. For comparison, it should be noted that this range of temperatures for the RF heating test (15°C to 30°C) is small compared to the range of temperatures used in the temperature tests (25°C to 100°C) of section 6.2. Therefore, in general much less hysteresis is seen in the RF heating data than in the temperature test data.

Similar to the 0.09 Mn material, Figures 6-18 and 6-19 show that very little hysteresis is associated with either the EMS G-265 (.11 Mn) of the EMS G-265 (.13 Mn) materials.

The data for the EMS G-265 (0.13 Mn) material of Figure 6-20 is significant because, as in the temperature data, all materials with higher than 0.13 Mn content have a counterclockwise sense of hysteresis. Again, it appears that a compensation point exists near the 0.13 Mn substitution.

Figures 6-20 through 6-22 show the measured magnitude of the Br and phase hysteresis to be increasing with the higher Mn content of the EMS G-265 (0.15 Mn), EMS G-265(0.17 Mn), and EMS G-265 (0.21 Mn) materials respectively. For the 0.21 Mn doping the hysteresis reaches a magnitude of about 4%. In each case the hysteresis is counterclockwise.

As noted in the figures, the temperature of the test phaser varied from near 15°C at low power (temperature resulting from tap water flowing through the mounting plate) to about 32°C measured at the 400 watt level (with the same cooling of mounting plate). Over this temperature and power range, the G-265 material with 0.09 Mn, 0.11 Mn, 0.13 Mn, and 0.15 Mn substitutions performed almost equally well. Large changes in ambient temperatures would effect data as noted in Figures 6-4 through 6-11. Figure 6-23 (a through i) present typical experimental data collected for the high power measurements.

As noted in these data, 128 phase states were measured at each power level. Thirty-two of these states were printed for each power level to investigate the stability of partially switched states. Figure 6-24 is a plot of change with power level for partial switched phase states. These results are typical of all the materials tested. The partially switched states show hysteresis responses that appear to be percentage wise constant within experimental error.

HIPOWER TEST RESULTS                    FIGURE 6-23 (a)

10 Apr 1992
11:06:10


370/.13MN


TESTED AT  9.99    WATTS                 G265 -37D/.13 Mn

MEASURED INSERTION LOSS=   .55 dB
 TEMP MEASURED ON DUT=    16.0789390692
 TOTAL DELTA PHASE   =    98.6952
 128   STATES MEASURED

| STATE | | DEGREES |
|---|---|---|
| STATE | 0 | .0236 DEGREES |
| STATE | 128 | 2.4353 DEGREES |
| STATE | 256 | 5.8275 DEGREES |
| STATE | 384 | 8.5032 DEGREES |
| STATE | 512 | 9.86 DEGREES |
| STATE | 640 | 13.3332 DEGREES |
| STATE | 768 | 16.3039 DEGREES |
| STATE | 896 | 20.848 DEGREES |
| STATE | 1024 | 22.6985 DEGREES |
| STATE | 1152 | 25.235 DEGREES |
| STATE | 1280 | 27.1166 DEGREES |
| STATE | 1408 | 29.3719 DEGREES |
| STATE | 1536 | 31.7695 DEGREES |
| STATE | 1664 | 32.272 DEGREES |
| STATE | 1792 | 34.2508 DEGREES |
| STATE | 1920 | 39.4567 DEGREES |
| STATE | 2048 | 44.9412 DEGREES |
| STATE | 2176 | 48.2636 DEGREES |
| STATE | 2304 | 51.1002 DEGREES |
| STATE | 2432 | 54.1755 DEGREES |
| STATE | 2560 | 54.7646 DEGREES |
| STATE | 2688 | 58.153 DEGREES |
| STATE | 2816 | 62.1893 DEGREES |
| STATE | 2944 | 66.1625 DEGREES |
| STATE | 3072 | 69.327 DEGREES |
| STATE | 3200 | 73.3723 DEGREES |
| STATE | 3328 | 76.7207 DEGREES |
| STATE | 3456 | 79.177 DEGREES |
| STATE | 3584 | 85.7702 DEGREES |
| STATE | 3712 | 90.2775 DEGREES |
| STATE | 3840 | 93.3236 DEGREES |
| STATE | 3968 | 99.1585 DEGREES |
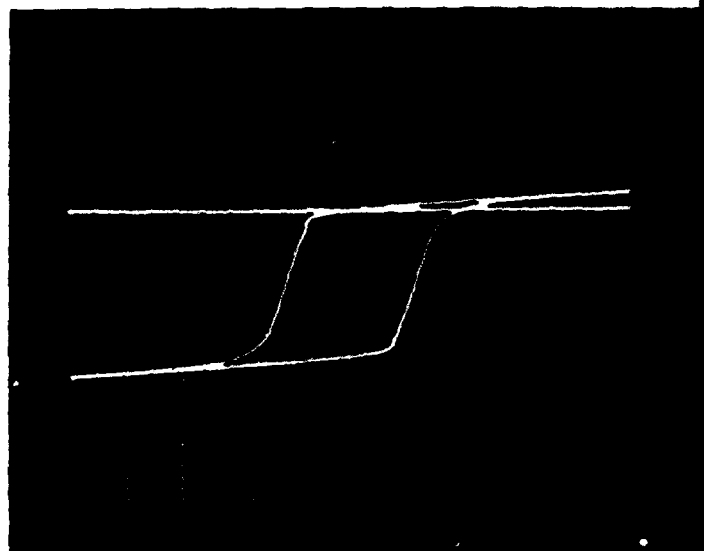
1110 10 APR 92                          1332.6°

BrAvg = 1332.67 in Millivolts

NRL MATERIAL STUDY

HIPOWER TEST RESULTS                    FIGURE 6-23 (b)

10 Apr 1992
11:27:05


37D/.13MN


TESTED AT  97.3   WATTS                 G265- 37D/.13·Mn                  100W

MEASURED INSERTION LOSS=    .53 dB
 TEMP MEASURED ON DUT=   19.1539986035
 TOTAL DELTA PHASE    =   99.2122
 128   STATES MEASURED
STATE      0       .1864    DEGREES
STATE     128      .2137    DEGREES
STATE     256     5.4431    DEGREES
STATE     384     8.4267    DEGREES
STATE     512     9.6348    DEGREES
STATE     640    12.9396    DEGREES
STATE     768    16.115     DEGREES
STATE     896    20.5391    DEGREES
STATE    1024    22.3576    DEGREES
STATE    1152    24.6363    DEGREES
STATE    1280    26.5158    DEGREES
STATE    1408    28.7138    DEGREES
STATE    1536    31.1541    DEGREES
STATE    1664    34.2209    DEGREES
STATE    1792    37.3569    DEGREES       428 10 APR 92                     1333.67
STATE    1920    41.0827    DEGREES
STATE    2048    44.3229    DEGREES
STATE    2176    47.5889    DEGREES
STATE    2304    50.435   DEGREES         BrAvg = 1333.67  in Millivolts
STATE    2432    53.6011    DEGREES
STATE    2560    54.2    DEGREES
STATE    2688    57.6614    DEGREES
STATE    2816    61.6592    DEGREES
STATE    2944    65.2377    DEGREES
STATE    3072    68.0237    DEGREES
STATE    3200    73.2216    DEGREES
STATE    3328    76.2593    DEGREES
STATE    3456    81.3484    DEGREES
STATE    3584    86.1661    DEGREES
STATE    3712    90.8777    DEGREES
STATE    3840    94.3796    DEGREES
STATE    3968   100.1216    DEGREES

HIPOWER TEST RESULTS                              FIGURE 6-23 (c)

10 Apr 1992
11:48:53


37D/.13MN


TESTED AT  199.4   WATTS

MEASURED INSERTION LOSS=    .52 dB              G265 -37D/.13 Mn                    200W
 TEMP MEASURED ON DUT=    22.8728227587
 TOTAL DELTA PHASE    =    98.5227
 128   STATES MEASURED
STATE    0      .1932   DEGREES
STATE    128     .5547   DEGREES
STATE    256    5.4895   DEGREES
STATE    384    7.9082   DEGREES
STATE    512    9.0003   DEGREES
STATE    640    11.5098  DEGREES
STATE    768    14.7419  DEGREES
STATE    896    19.0392  DEGREES
STATE    1024   20.7443  DEGREES
STATE    1152   23.0107  DEGREES
STATE    1280   24.3223  DEGREES
STATE    1408   26.2757  DEGREES
STATE    1536   28.5746  DEGREES
STATE    1664   31.3581  DEGREES          1151 10 APR 92                        1337.33
STATE    1792   35.3842  DEGREES
STATE    1920   38.5961  DEGREES
STATE    2048   41.8918  DEGREES          Br Avg = 1337.33  in Millivolts
STATE    2176   45.239   DEGREES
STATE    2304   48.1034  DEGREES
STATE    2432   51.2023  DEGREES
STATE    2560   51.7893  DEGREES
STATE    2688   55.3132  DEGREES
STATE    2816   59.3356  DEGREES
STATE    2944   63.5372  DEGREES
STATE    3072   67.4732  DEGREES
STATE    3200   71.161   DEGREES
STATE    3328   75.1647  DEGREES
STATE    3456   79.6644  DEGREES
STATE    3584   84.7049  DEGREES
STATE    3712   89.6172  DEGREES
STATE    3840   94.4  DEGREES
STATE    3968   97.8403  DEGREES

NRL MATERIAL STUDY

HIPOWER TEST RESULTS

FIGURE 6-23 (d)

10 Apr 1992
12:05:32

37D/.13MN

TESTED AT  305.8  WATTS

MEASURED INSERTION LOSS=    .52 dB
 TEMP MEASURED ON DUT=   26.8241621678
 TOTAL DELTA PHASE    =   97.7171
 128   STATES MEASURED

| STATE | | | |
|-------|------|---------|---------|
| STATE | 0 | .3819 | DEGREES |
| STATE | 128 | .9434 | DEGREES |
| STATE | 256 | 5.4841 | DEGREES |
| STATE | 384 | 7.5478 | DEGREES |
| STATE | 512 | 8.5721 | DEGREES |
| STATE | 640 | 10.3613 | DEGREES |
| STATE | 768 | 13.6365 | DEGREES |
| STATE | 896 | 17.7026 | DEGREES |
| STATE | 1024 | 19.2025 | DEGREES |
| STATE | 1152 | 21.2297 | DEGREES |
| STATE | 1280 | 22.9668 | DEGREES |
| STATE | 1408 | 24.9353 | DEGREES |
| STATE | 1536 | 27.2202 | DEGREES |
| STATE | 1664 | 30.1011 | DEGREES |
| STATE | 1792 | 33.1412 | DEGREES |
| STATE | 1920 | 36.3358 | DEGREES |
| STATE | 2048 | 39.8442 | DEGREES |
| STATE | 2176 | 42.7996 | DEGREES |
| STATE | 2304 | 45.7926 | DEGREES |
| STATE | 2432 | 48.9511 | DEGREES |
| STATE | 2560 | 49.5777 | DEGREES |
| STATE | 2688 | 53.1978 | DEGREES |
| STATE | 2816 | 57.2896 | DEGREES |
| STATE | 2944 | 61.5869 | DEGREES |
| STATE | 3072 | 65.7565 | DEGREES |
| STATE | 3200 | 69.6423 | DEGREES |
| STATE | 3328 | 73.8238 | DEGREES |
| STATE | 3456 | 78.1226 | DEGREES |
| STATE | 3584 | 81.272 | DEGREES |
| STATE | 3712 | 88.8982 | DEGREES |
| STATE | 3840 | 93.8076 | DEGREES |
| STATE | 3968 | 98.0067 | DEGREES |

G265-37D/.13 Mn                          300W
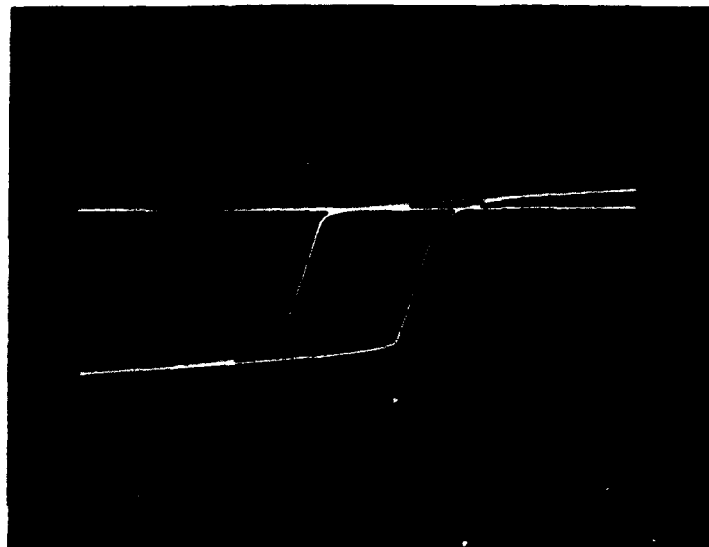


1207 10 APR 92                          1319.0

Br Avg = 1319.0 in Millivolts

NRL MATERIAL STUDY

HIPOWER TEST RESULTS

FIGURE 6-23 (e)

10 Apr 1992
12:24:12

37D/.13MN

TESTED AT 395.3 WATTS

MEASURED INSERTION LOSS= .51 dB
 TEMP MEASURED ON DUT= 30.15762554
 TOTAL DELTA PHASE = 97.2764
 128 STATES MEASURED

| STATE | 0 | .0622 | DEGREES |
|---|---|---|---|
| STATE | 128 | 3.5505 | DEGREES |
| STATE | 256 | 4.7353 | DEGREES |
| STATE | 384 | 6.6435 | DEGREES |
| STATE | 512 | 7.5482 | DEGREES |
| STATE | 640 | 9.081 | DEGREES |
| STATE | 768 | 12.2577 | DEGREES |
| STATE | 896 | 15.8431 | DEGREES |
| STATE | 1024 | 17.3742 | DEGREES |
| STATE | 1152 | 19.2932 | DEGREES |
| STATE | 1280 | 21.0341 | DEGREES |
| STATE | 1408 | 22.9259 | DEGREES |
| STATE | 1536 | 25.128 | DEGREES |
| STATE | 1664 | 27.945 | DEGREES |
| STATE | 1792 | 30.9498 | DEGREES |
| STATE | 1920 | 34.4056 | DEGREES |
| STATE | 2048 | 37.5667 | DEGREES |
| STATE | 2176 | 40.809 | DEGREES |
| STATE | 2304 | 43.5957 | DEGREES |
| STATE | 2432 | 46.5839 | DEGREES |
| STATE | 2560 | 50.4703 | DEGREES |
| STATE | 2688 | 54.6296 | DEGREES |
| STATE | 2816 | 58.8495 | DEGREES |
| STATE | 2944 | 63.0027 | DEGREES |
| STATE | 3072 | 66.9984 | DEGREES |
| STATE | 3200 | 68.0615 | DEGREES |
| STATE | 3328 | 72.3803 | DEGREES |
| STATE | 3456 | 77.2612 | DEGREES |
| STATE | 3584 | 82.6892 | DEGREES |
| STATE | 3712 | 87.862 | DEGREES |
| STATE | 3840 | 91.6164 | DEGREES |
| STATE | 3968 | 97.9365 | DEGREES |

G265-37D/.13 Mn                    400W



1226   10 APR 92                 1309.67
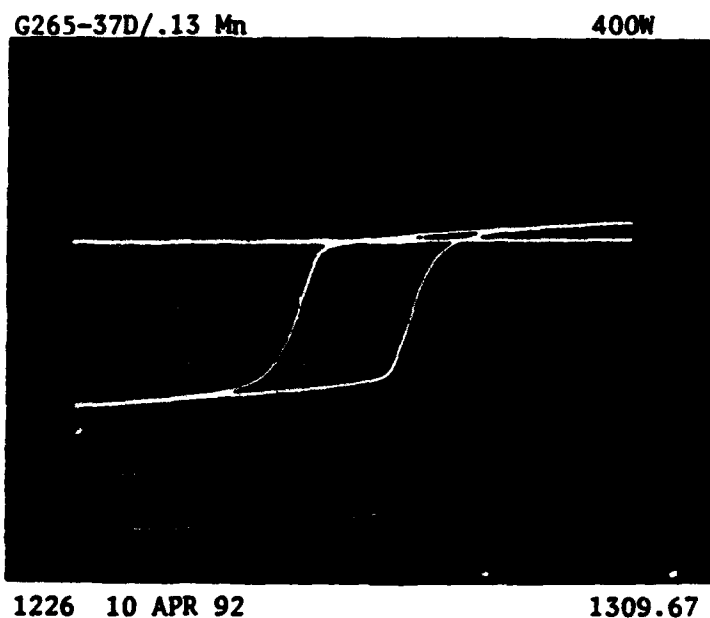
Br Avg = 1309.67 in Millivolts

NRL MATERIAL STUDY

HIPOWER TEST RESULTS

FIGURE 6-23 (f)

10 Apr 1992
12:44:25

37D/.13MN

TESTED AT  293.5   WATTS

MEASURED INSERTION LOSS=   .52 dB
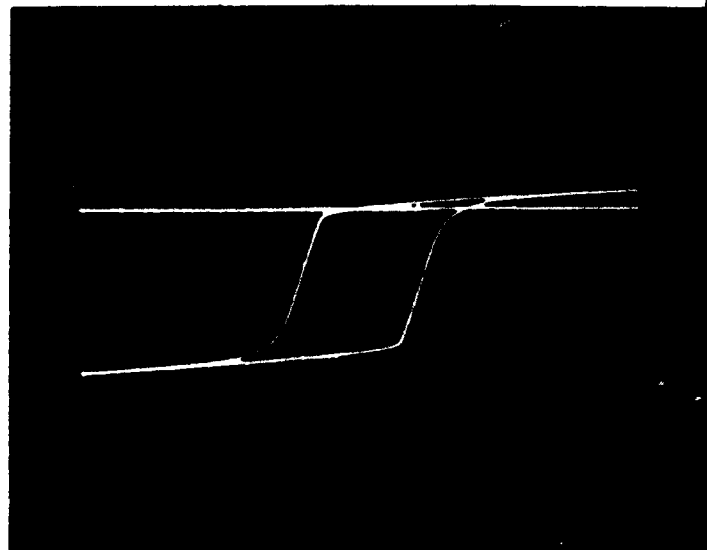 TEMP MEASURED ON DUT=   26.6072032902
 TOTAL DELTA PHASE   =   97.2372
 128   STATES MEASURED

| STATE | | | |
|-------|------|---------|---------|
| STATE | 0 | .0176 | DEGREES |
| STATE | 128 | .1766 | DEGREES |
| STATE | 256 | 4.9514 | DEGREES |
| STATE | 384 | 7.1226 | DEGREES |
| STATE | 512 | 8.1732 | DEGREES |
| STATE | 640 | 9.8289 | DEGREES |
| STATE | 768 | 13.1085 | DEGREES |
| STATE | 896 | 16.9183 | DEGREES |
| STATE | 1024 | 18.4485 | DEGREES |
| STATE | 1152 | 20.4382 | DEGREES |
| STATE | 1280 | 22.0242 | DEGREES |
| STATE | 1408 | 24.0362 | DEGREES |
| STATE | 1536 | 26.303 | DEGREES |
| STATE | 1664 | 28.7271 | DEGREES |
| STATE | 1792 | 32.2045 | DEGREES |
| STATE | 1920 | 35.5636 | DEGREES |
| STATE | 2048 | 38.7248 | DEGREES |
| STATE | 2176 | 41.8256 | DEGREES |
| STATE | 2304 | 44.6619 | DEGREES |
| STATE | 2432 | 47.8477 | DEGREES |
| STATE | 2560 | 48.4499 | DEGREES |
| STATE | 2688 | 51.9643 | DEGREES |
| STATE | 2816 | 56.208 | DEGREES |
| STATE | 2944 | 60.5585 | DEGREES |
| STATE | 3072 | 63.2056 | DEGREES |
| STATE | 3200 | 68.5922 | DEGREES |
| STATE | 3328 | 72.0693 | DEGREES |
| STATE | 3456 | 74.7204 | DEGREES |
| STATE | 3584 | 82.7522 | DEGREES |
| STATE | 3712 | 87.9706 | DEGREES |
| STATE | 3840 | 92.9312 | DEGREES |
| STATE | 3968 | 97.3436 | DEGREES |



G265- 37D/.13 Mn                          300W

1227  10 APR 92                          1326.0

Br Avg = 1326.0 in Millivolts

NRL MATERIAL STUDY

HIPOWER TEST RESULTS

FIGURE 6-23 (g)

10 Apr 1992
13:22:04

37D/.13MN

TESTED AT  198.6   WATTS

MEASURED INSERTION LOSS=   .53 dB
 TEMP MEASURED ON DUT=   23.1770465798
 TOTAL DELTA PHASE    =   98.1333
 128   STATES MEASURED

| STATE | | | |
|-------|------|---------|---------|
| STATE | 0    | .0619   | DEGREES |
| STATE | 128  | .3231   | DEGREES |
| STATE | 256  | 5.3907  | DEGREES |
| STATE | 384  | 7.2577  | DEGREES |
| STATE | 512  | 8.5019  | DEGREES |
| STATE | 640  | 10.804  | DEGREES |
| STATE | 768  | 14.1839 | DEGREES |
| STATE | 896  | 18.4225 | DEGREES |
| STATE | 1024 | 20.0137 | DEGREES |
| STATE | 1152 | 22.329  | DEGREES |
| STATE | 1280 | 23.8632 | DEGREES |
| STATE | 1408 | 26.0969 | DEGREES |
| STATE | 1536 | 28.4644 | DEGREES |
| STATE | 1664 | 31.4083 | DEGREES |
| STATE | 1792 | 34.4412 | DEGREES |
| STATE | 1920 | 37.9527 | DEGREES |
| STATE | 2048 | 41.0032 | DEGREES |
| STATE | 2176 | 44.2042 | DEGREES |
| STATE | 2304 | 47.2945 | DEGREES |
| STATE | 2432 | 50.2227 | DEGREES |
| STATE | 2560 | 50.9586 | DEGREES |
| STATE | 2688 | 54.2471 | DEGREES |
| STATE | 2816 | 58.382  | DEGREES |
| STATE | 2944 | 59.8012 | DEGREES |
| STATE | 3072 | 66.4999 | DEGREES |
| STATE | 3200 | 70.5573 | DEGREES |
| STATE | 3328 | 74.2997 | DEGREES |
| STATE | 3456 | 76.7075 | DEGREES |
| STATE | 3584 | 83.8976 | DEGREES |
| STATE | 3712 | 89.178  | DEGREES |
| STATE | 3840 | 92.4176 | DEGREES |
| STATE | 3968 | 98.8672 | DEGREES |

G265-37D/.13 Mn                    200W



1325   10 APR 92                   1334.0

Br Avg = 1334.0  in Millivolts

NRL MATERIAL STUDY

HIPOWER TEST RESULTS

FIGURE 6-23 (h)

10 Apr 1992
14:04:11

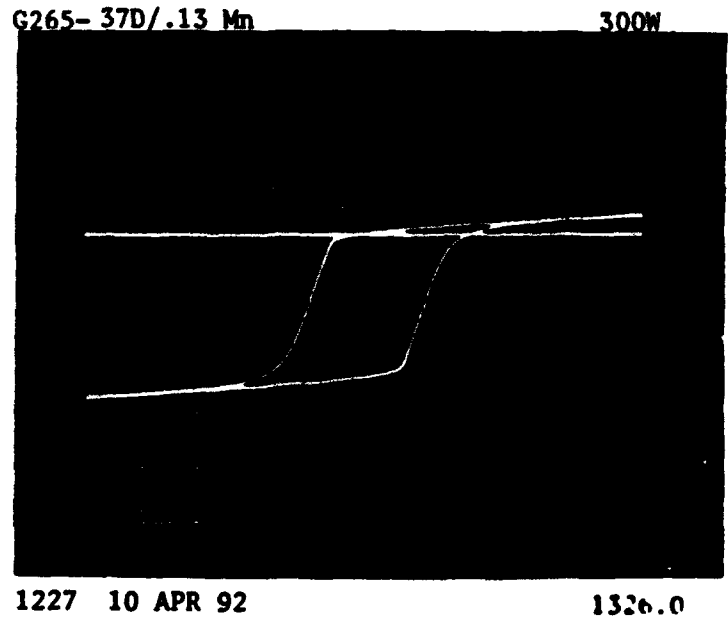37D/.13MN

TESTED AT 101.8 WATTS

MEASURED INSERTION LOSS= .53 dB
 TEMP MEASURED ON DUT= 19.598300683
 TOTAL DELTA PHASE = 98.8752
 128 STATES MEASURED

| STATE | | | |
|---|---|---|---|
| STATE | 0 | .2356 | DEGREES |
| STATE | 128 | 2.7806 | DEGREES |
| STATE | 256 | 5.4168 | DEGREES |
| STATE | 384 | 7.7503 | DEGREES |
| STATE | 512 | 9.1099 | DEGREES |
| STATE | 640 | 12.2444 | DEGREES |
| STATE | 768 | 15.2726 | DEGREES |
| STATE | 896 | 19.5125 | DEGREES |
| STATE | 1024 | 21.3525 | DEGREES |
| STATE | 1152 | 23.5642 | DEGREES |
| STATE | 1280 | 25.4014 | DEGREES |
| STATE | 1408 | 27.4305 | DEGREES |
| STATE | 1536 | 29.9885 | DEGREES |
| STATE | 1664 | 32.9442 | DEGREES |
| STATE | 1792 | 36.0559 | DEGREES |
| STATE | 1920 | 39.3938 | DEGREES |
| STATE | 2048 | 42.695 | DEGREES |
| STATE | 2176 | 46.176 | DEGREES |
| STATE | 2304 | 48.9624 | DEGREES |
| STATE | 2432 | 51.8504 | DEGREES |
| STATE | 2560 | 55.2565 | DEGREES |
| STATE | 2688 | 59.2577 | DEGREES |
| STATE | 2816 | 63.5319 | DEGREES |
| STATE | 2944 | 67.4134 | DEGREES |
| STATE | 3072 | 70.8505 | DEGREES |
| STATE | 3200 | 74.6055 | DEGREES |
| STATE | 3328 | 79.1105 | DEGREES |
| STATE | 3456 | 83.9008 | DEGREES |
| STATE | 3584 | 88.6346 | DEGREES |
| STATE | 3712 | 93.0889 | DEGREES |
| STATE | 3840 | 97.6057 | DEGREES |
| STATE | 3968 | 102.4434 | DEGREES |

G265-37D/.13 Mn                                    100W



1407   10 APR 92                               1342.67

Br Avg = 1342.67  in Millivolts

NRL MATERIAL STUDY

HIPOWER TEST RESULTS                    FIGURE 6-23 (i)

10 Apr 1992
14:31:00

37D/.13MN

TESTED AT  9.78   WATTS
                                        G265- 37D/.13 Mn                    10W
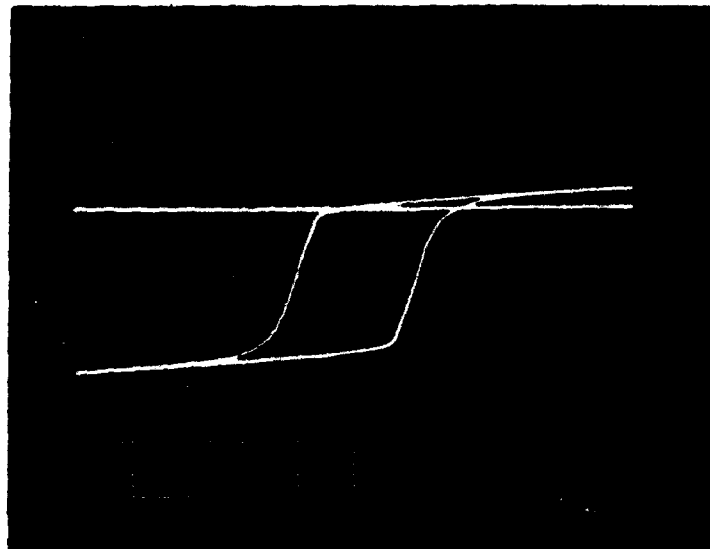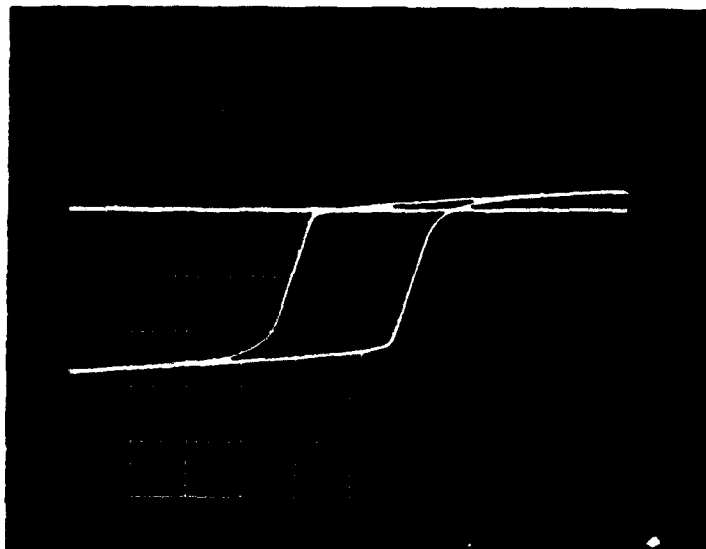MEASURED INSERTION LOSS=   .55 dB
  TEMP MEASURED ON DUT=   16.4302363404
  TOTAL DELTA PHASE   =   98.8742
  128   STATES MEASURED
STATE      0      .5596   DEGREES
STATE     128     .4711    DEGREES
STATE     256    4.8946    DEGREES
STATE     384    8.1802    DEGREES
STATE     512    9.408   DEGREES
STATE     640    12.7564   DEGREES
STATE     768    15.8078   DEGREES
STATE     896    20.2316   DEGREES
STATE     1024    22.1845    DEGREES
STATE     1152    24.6308    DEGREES
STATE     1280    26.5123    DEGREES
STATE     1408    28.7948    DEGREES
STATE     1536    31.2353    DEGREES
STATE     1664    34.1013    DEGREES
STATE     1792    37.6405    DEGREES
STATE     1920    41.0965    DEGREES
STATE     2048    44.3423    DEGREES
STATE     2176    47.4988    DEGREES
STATE     2304    50.4951    DEGREES
STATE     2432    53.6071    DEGREES
STATE     2560    57.1218    DEGREES
STATE     2688    60.6376    DEGREES
STATE     2816    64.5867    DEGREES
STATE     2944    68.6564    DEGREES
STATE     3072    72.1749    DEGREES
STATE     3200    75.8442    DEGREES
STATE     3328    79.7041    DEGREES
STATE     3456    84.2391    DEGREES
STATE     3584    88.7195    DEGREES
STATE     3712    93.4999    DEGREES
STATE     3840    97.9788    DEGREES
STATE     3968    102.6739    DEGREES
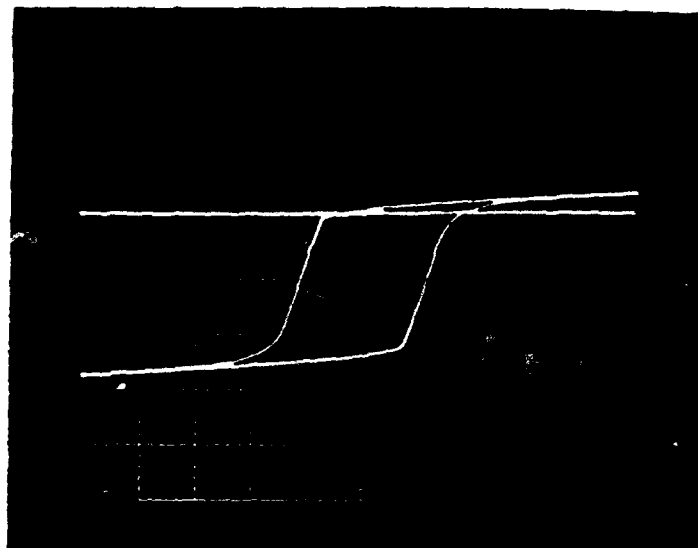


1433   10 APR 92                                        1339.67

Br Avg = 1339.67 in Millivolts

# Phase vs. Temperature (RF Heating)
## EMS G265-37 (.13 Mn)



**FIGURE 6-24**

## 7.0 STATIC TESTS AND PHASER DATA (PHASE II)

### 7.1 STATIC TESTS

A number of test fixtures were evaluated toward achieving a static test fixture (no Rf) that could be used to evaluate the stress characteristics of the materials in an environment similar to that actually experienced in a waveguide phase shifter structure. Capturing this material in the phaser structure generally produces some stress (such as top-to-bottom crush in a waveguide structure; a very tight f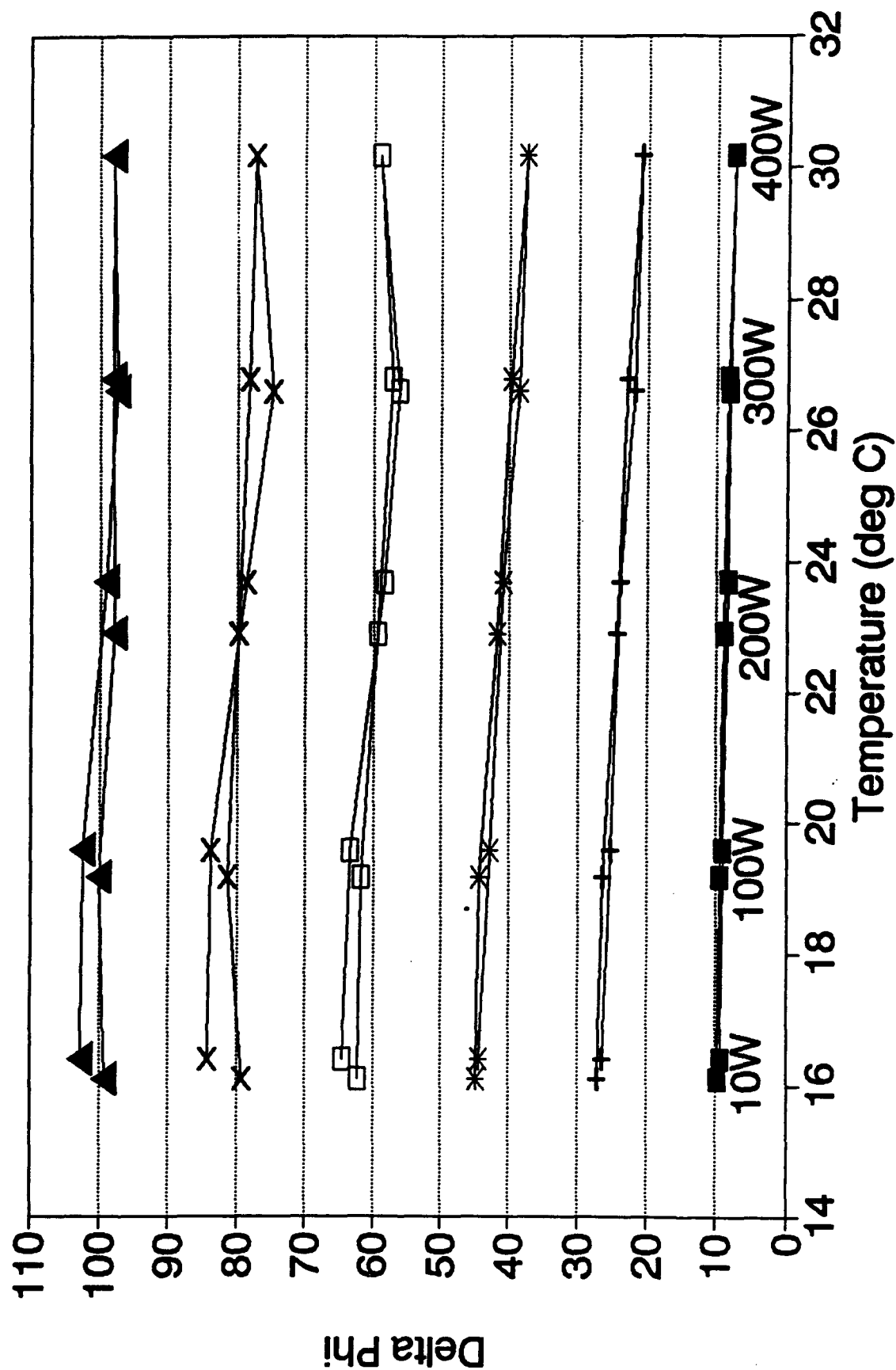it is required to provide acceptable microwave performance). Once captured in this waveguide Rf structure, the material may experience additional stress as a function of temperature (and/or Rf power) due to the different thermal expansion characteristics of the ferrite material and the metallic Rf structure in which (waveguide) or on which (metallic carrier/substrate) the material is housed.

The material can thus potentially experience many of the stresses pictorially presented and defined in Figure 3-5. In a phase shifter structure the material most often will be experiencing a multi-directional stress environment.

Characterizing the material in a uni-directional stress environment (relative to the magnetization) would be a valuable evaluation of the stress sensitivity. The test fixture and data presented in Section 5 provided some characterization of this type. It is believed that high stress levels may distort the sample and result in uni-directional pressure producing a multi-directional stress. Most materials were observed to be more stress sensitive to bending, twisting or bowing stresses (resultant stresses that are not uni-directional relative to the magnetization).

The applied stresses and the resultant stress sensitivity of the material cannot be directly equated to the crystallographic magnetostrictive constants, $\lambda_{111}$, $\lambda_{100}$, or $\lambda s$, as presented in Figure 3-17, since uni-directional stress and uni-directional magnetization cannot be achieved

in a polycrystalline material in a remanent magnetization state. However some reasonable correlation with the value of magnetostrictive constants should be achieved that will allow for predicting stress sensitivity in phaser structures from static measurements and evaluations.

Fixtures evaluated that applied pressure to the toroidal material samples via some type of threaded (screw) mechanism appeared to creep when temperatures cycled. Data was very difficult to reproduce.

The test fixture referred to as the phaser simulator test fixture (PSTF) and described in Section 3.3 (see Figure 3-13) was the best structure for static evaluations of the stress sensitivity of material. Good correlation of results was obtained with phase data on the same material in phase shifter housings.

As indicated in Section 5, the pressure (stress) actually applied to and experienced by the ferrite toroids in a waveguide phaser was initially unknown. Data were thus collected at different stress levels; correlations of the data collected indicates that stress levels near 100 PSI are typical for soft top waveguide phaser structures. Static stress data reported in this section using the PSTF includes results observed up to 500 PSI applied stress.

The manganese (Mn) substituted yttrium gadolinium garnets (composition G-265) as previously discussed were the initial materials evaluated. Data presented in Section 5 and 6 strongly suggests that a Mn substitution of 0.11 to 0.13 appeared to provide the least stress sensitive composition.

Normalized Br versus temperature data (25°C to 100°C) for each of the manganese substituted G-265 garnet compounds studied are presented in Figure 7-1. These data show a temperature hysteresis as discussed in Section 6.0. The hysteresis is clockwise (CW) for Mn substitutions of 0.09 and 0.11 and counterclockwise (CCW) for substitution of 0.13, 0.15, 0.17 and 0.21. The CW/CCW change in direction of the hysteresis with temperature is related to a change from minus to plus of the magnetostrictive characteristics.

# Br vs. Temperature
## 100 PSI Transverse Stress
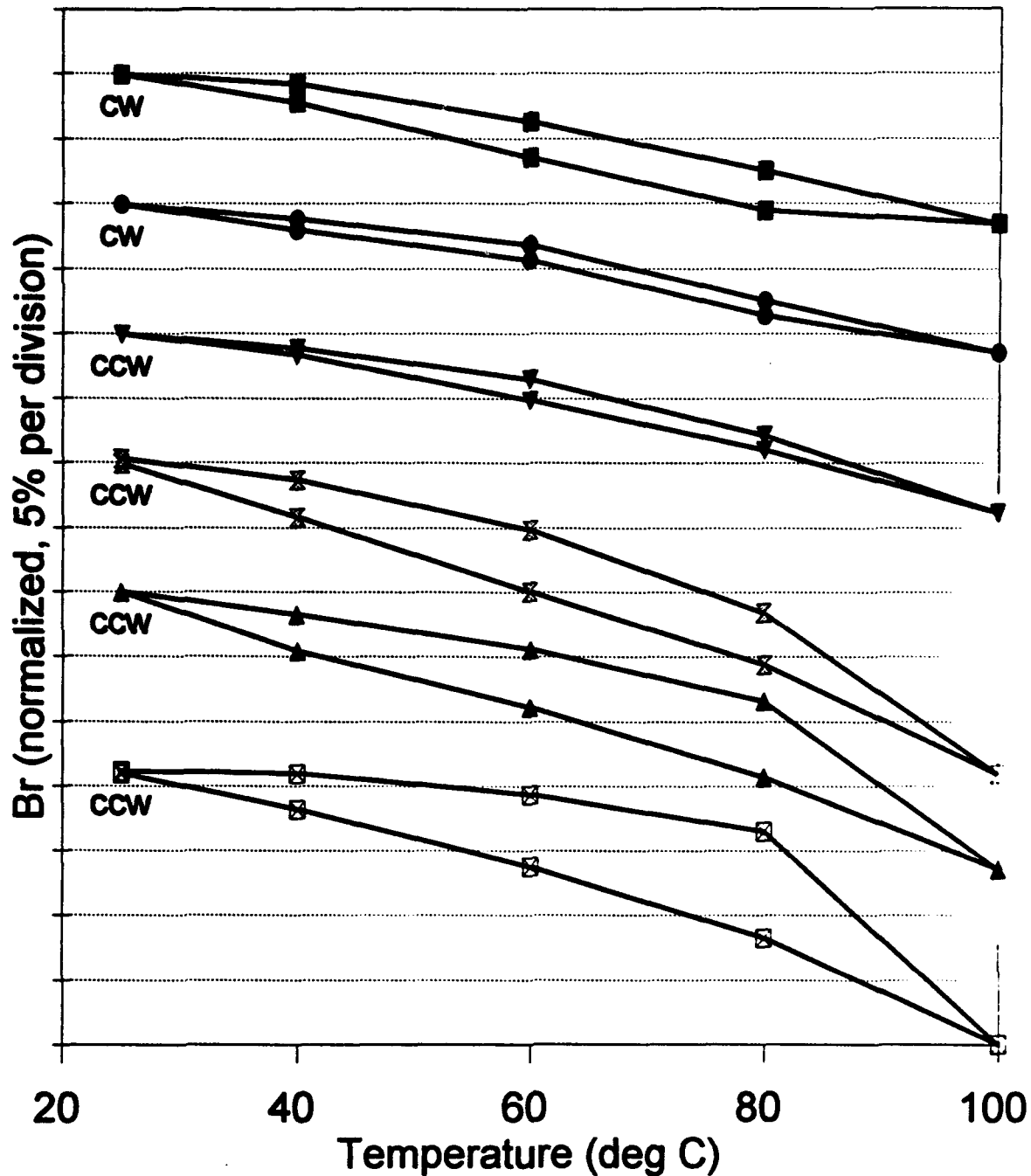


**FIGURE 7-1**   NORMALIZED Br VERSUS TEMPERATURE FOR Mn SUBSTITUTED G-265 IN THE PHASER SIMULATOR TEST FIXTURE AT 100 PSI TRANSVERSE COMPRESSIVE STRESS

In these data the toroids were captured in the PSTF with a top to bottom crush (transverse stress) of 100 PSI. Minor changes in the hysteresis responses were observed and noted for this applied constant stress. In the legs of the toroid under stress, the remanent magnetization (Br) is on the average parallel to this transverse stress; as the temperature is increased the metallic fixture expands more (higher coefficient of expansion) than does the garnet material and this results in a longitudinal tensional stress (pulling) on the toroid. If the average magnetostrictive constant is negative for the material, the magnetostrictive forces would tend to support enhanced magnetization alignment perpendicular to this stress. This would be in the direction to increase remanent magnetization. Since magnetization in these garnets intrinsically decreases with increased temperature, the resultant Br is lower due to the higher temperature but slightly enhanced due to the stress. This process continues up to the maximum test temperature (100°C in this case). During this period, the toroid and the housing creep or slip (as described in Section 6.3) and when the temperature cycle is reversed (100°C to 25°C), the toroid experiences a longitudinal compressive stress. For a negative average magnetostrictive constant, the resultant magnetostrictive forces would tend to support alignment of the magnetization with the stress and under this condition, reduce the net remanent magnetization. The result is a clockwise temperature hysteresis like that observed for the 0.09 Mn substituted G-265.

If the average magnetostrictive constant is positive, the reverse of the previous observation would occur and a counterclockwise temperature hysteresis would be observed. A material with near zero average magnetostrictive properties would exhibit small, if any, temperature hysteresis. The "parrot beak" shape of the curves between 80°C and 100°C turns up for CW and down for CCW hysteresis due to the single data point at the point of temperature reversal (100°C).

It is recognized that the transverse stress on the toroid (top to bottom crush) may also be changing with temperature and thus contributes to the observed data. This transverse stress variation with temperature was computed to be less than ± 5PSI over the temperature range of 25°C to 100°C.

The data presented in Figure 7-1 indicates that minimum stress sensitivity in this structure with its associated stresses occurs for a Mn substitution of 0.11 to 0.13. This supports the conclusion reached for the static stress data presented in Figure 5-9.

These same compounds were also evaluated in the PSTF at 200 PSI transverse stress and the data are presented in Figure 7-2. These data would suggest that the best stress insensitive material is shifted slightly toward the 0.11Mn substituted composition.

Many of the other materials listed in Table 4-2 were also evaluated in the PSTF at 100 PSI transverse stress. These data are presented in Figures 7-3, 7-4, 7-5 and 7-6.

The responses presented in Figure 7-3 show three pairs of materials that are similar in basic composition but with different manufacturers and different Mn substitutions. G-231-13AB is an EMS processed composition that is very similar to Trans-Tech TTG-1600. The EMS composition contains 0.13Mn and the Trans-Tech G-1600 has 0.09Mn. The Trans-Tech 0.09Mn compound exhibits a clockwise temperature hysteresis and the 0.13Mn EMS compound has considerable less hysteresis in a CCW direction.

The EMS G293-5 is a similar compound to Trans-Tech G1010. The G293-5 has 0.17Mn substitution and the G1010 has 0.09Mn. These two responses, one CW (0.09) and one CCW (0.17), appear to exhibit temperature hysteresis of nearly the same magnitude suggesting a stress compensated composition in the region of 0.12 to 0.13Mn.

The G-273-12 (0.17Mn) and TT G800 (0.09) have $4\pi Ms$ values near 800 gauss but may be somewhat different in basic composition. The temperature hysteresis characteristics are similar to that observed for the other 0.09 (CW) and 0.17Mn (CCW) compounds.

Figure 7-4 is a lithium-titanium ferrite with a $4\pi Ms$ near 1300 gauss. These data are presented for reference only.
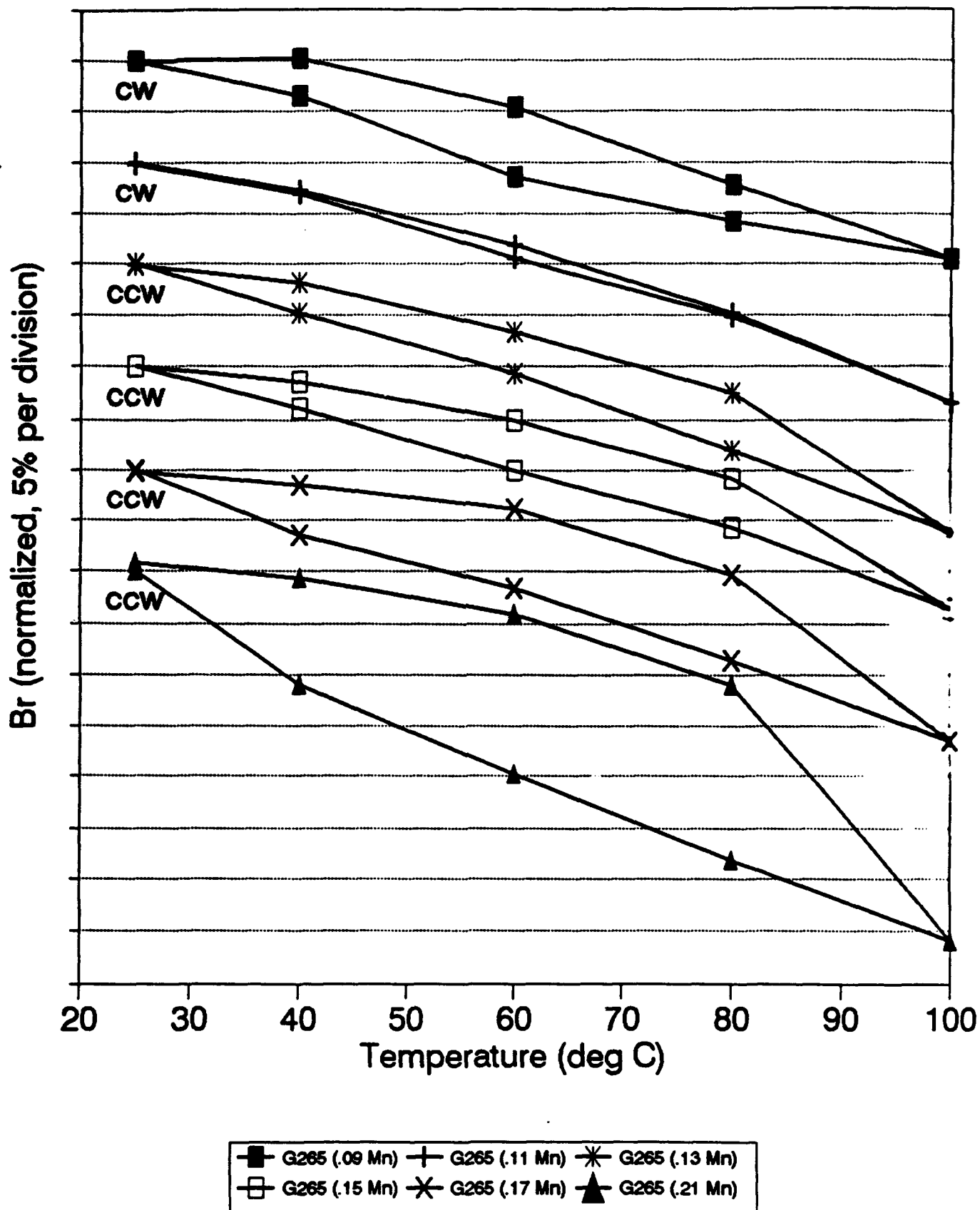
**FIGURE 7-2** NORMALIZED Br VERSUS TEMPERATURE FOR Mn SUBSTITUTED G-265 IN THE PHASER SIMULATOR TEST FIXTURE AT 200 PSI TRANSVERSE COMPRESSIVE STRESS

# Br vs. Temperature
## 100 PSI Transverse Stress

**FIGURE 7-3** NORMALIZED Br VERSUS TEMPERATURE FOR VARIOUS Mn SUBSTITUTED GARNET MATERIALS IN PSTF AT 100 PSI TRANSVERSE COMPRESSIVE STRESS

# Br vs. Temperature
## 100 PSI Transverse Stress

Br (normalized, 5% per division)

Temperature (deg C)

L141

FIGURE 7-4    NORMALIZED Br VERSUS TEMPERATURE FOR LITHIUM-TITANIUM FERRITE
IN THE PSTF AT 100 PSI TRANSVERSE COMPRESSIVE STRESS

# Br vs. Temperature
## 100 PSI Transverse Stress

Br (normalized, 5% per division)

Temperature (deg C)

■ G2021  ● G2022

CW

CW

FIGURE 7-5   NORMALIZED Br VERSUS TEMPERATURE FOR CERIUM SUBSTITUTED YIG
IN PSTF AT 100 PSI TRANSVERSE COMPRESSIVE STRESS

- 144 -

# Br vs. Temperature
## 100 PSI Transverse Stress



G-352   YIG
G-354   YIG (16.7%TbIG)
G-356   YIG (35%TbIG)

FIGURE 7-6   NORMALIZED Br VERSUS TEMPERATURE FOR YIG/TbIG IN PSTF AT 100
PSI TRANSVERSE COMPRESSIVE STRESS

Figure 7-5 presents the data on the cerium substituted YIG (composition presented in Section 4.0). Neither of the compounds exhibit characteristics indicating that cerium can be used to reduce the stress sensitivity of YIG. Of interest in this data is a mini-temperature cycle at 60°C to 55°C and back up to 60°C. The Br data collected are indicated on the graph (Figure 7-5) which shows that the Br would cycle around the hysteresis response.

Figure 7-6 shows the data collected on samples of the YIG (Tb) garnets discussed in Section 2.0 and Figures 2-7 and 2-8. These compounds are not suitable for phaser applications, but the 16.7% TbIG · 83.3% YIG (G-354) exhibits excellent stress insensitive characteristics. At this stress level, the pure YIG (G352) exhibited considerably better characteristics than expected. Note the data for G-356 which indicates that magnetostrictive influence (forces) on the remanent magnetization can completely offset the normal decline of remanent magnetization with temperature. In this case the Br increased with temperature under the influence of the stress experienced by the toroidal sample.

Some of these same materials were evaluated using a transverse stress of 200PSI and these data are presented in Figure 7-7. At this stress level some of the materials, particularly the Trans-Tech 0.09Mn substituted compounds, exhibited an initial increase in Br. This response is not inconsistent with the previous data and associated conclusions.
Figure 7-8 compares directly the stress response of the EMS G265 (0.09Mn) with the Trans-Tech TT G1002 (0.09Mn). A considerable temperature hysteresis is observed for both of these compounds indicating stress sensitive characteristic in the PSTF. The microstructures of these two materials are different based on the measured coercive field. The TT G1002 has coercive field about one-half as large as the EMS G265 as a result primarily of microstructure (grain size). In this case, the magnetostrictive influence on the magnetization would be greater in a material with lower coercive field. This is believed to be reason for the difference in the temperature hysteresis response of these two compounds.

# Br vs. Temperature
## 200 PSI Transverse Stress



Legend:
- o  G-203(0.13 Mn) CCW
- □  G-231(0.13 Mn) CCW
- ■  G-1600(0.09 Mn) CW
- ▽  G-800(0.09 Mn) CW
- ▼  G-273(0.17 Mn) CCW

◆ G-293(0.17 Mn) CCW

◇ G-1010(0.09 Mn) CW

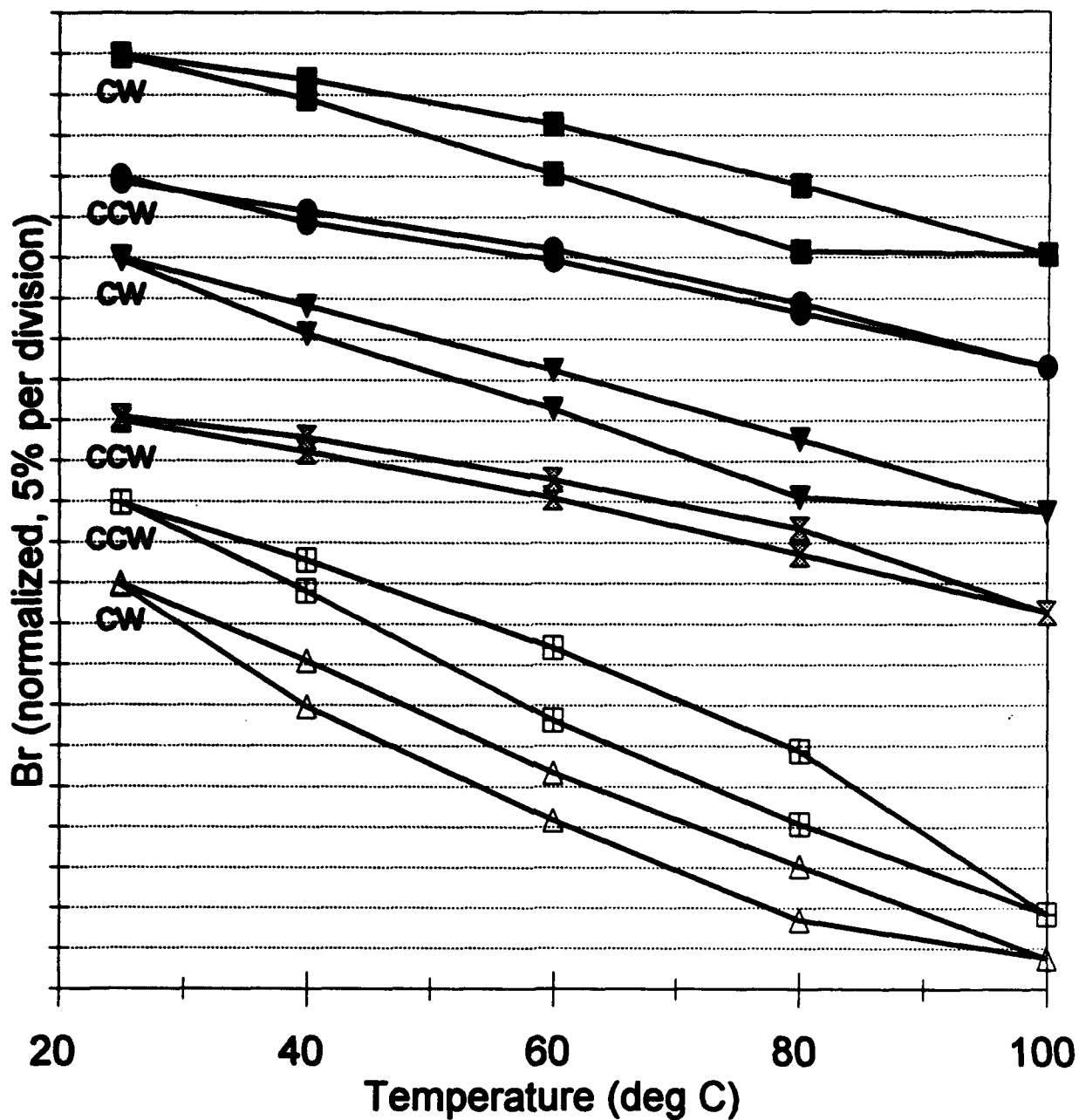Br (normalized, 5% per division)

Temperature (deg C)

FIGURE 7-7    NORMALIZED Br VERSUS TEMPERATURE FOR VARIOUS Mn SUBSTITUTED
GARNET MATERIALS IN THE PSTF AT 200 PSI TRANSVERSE
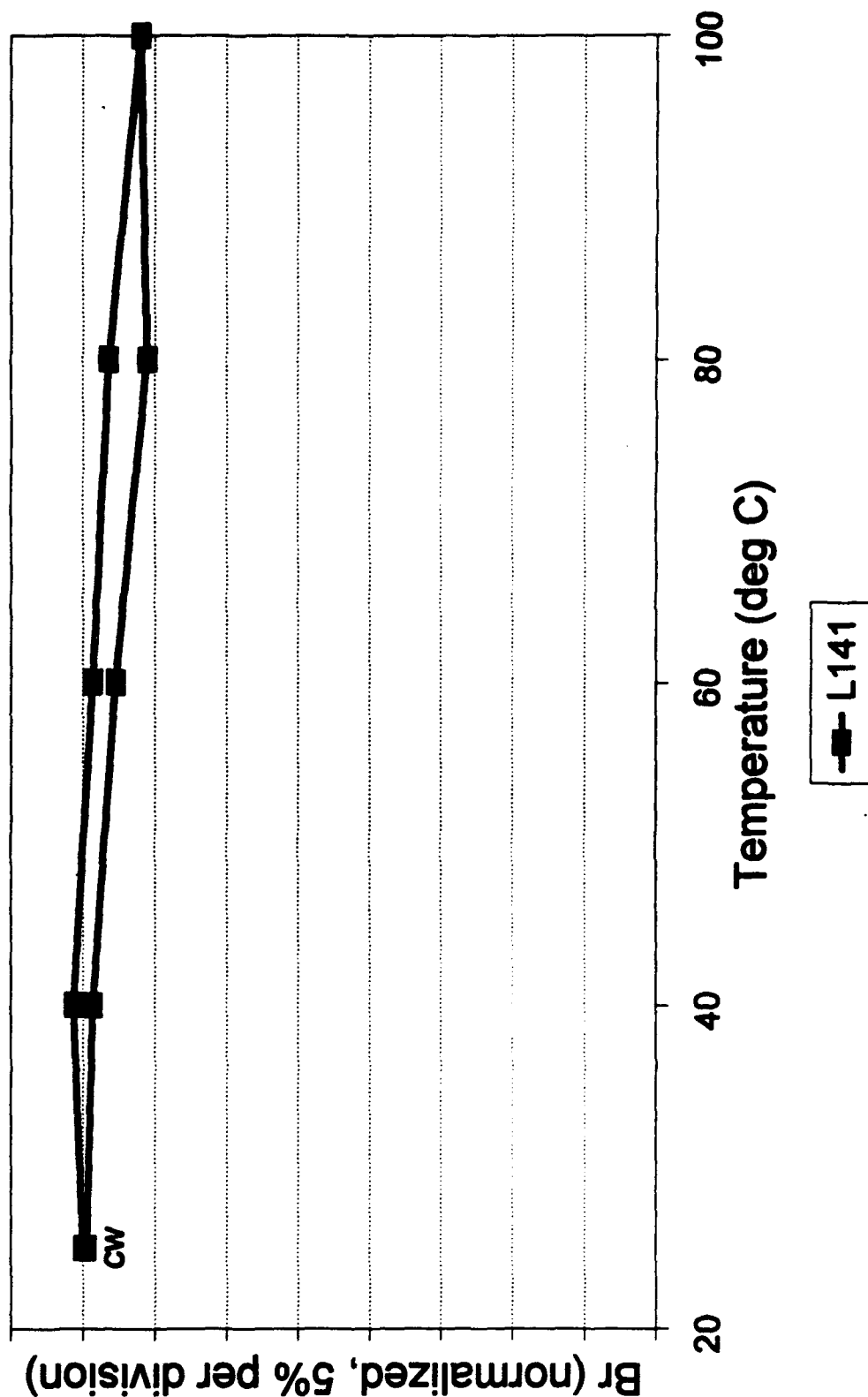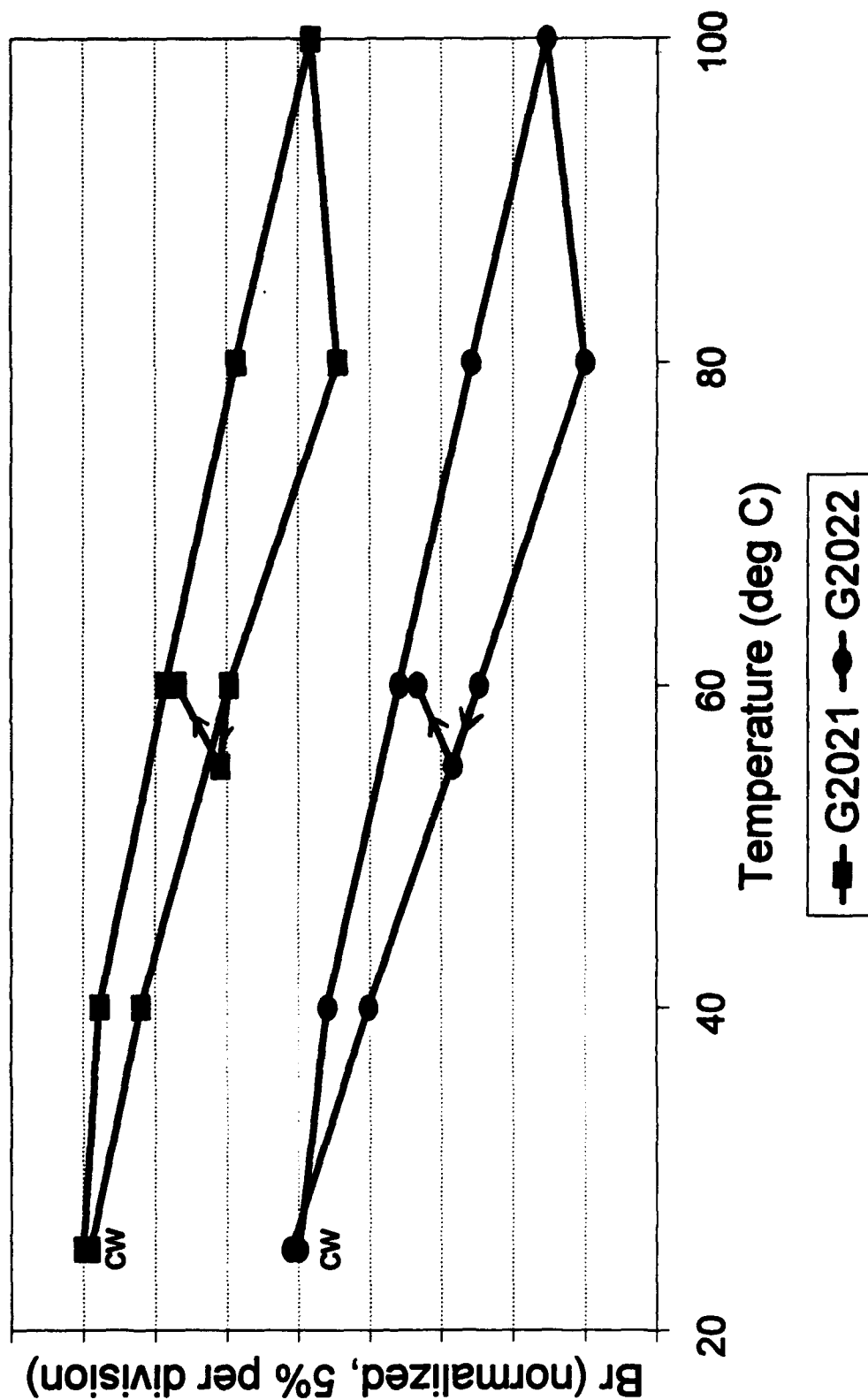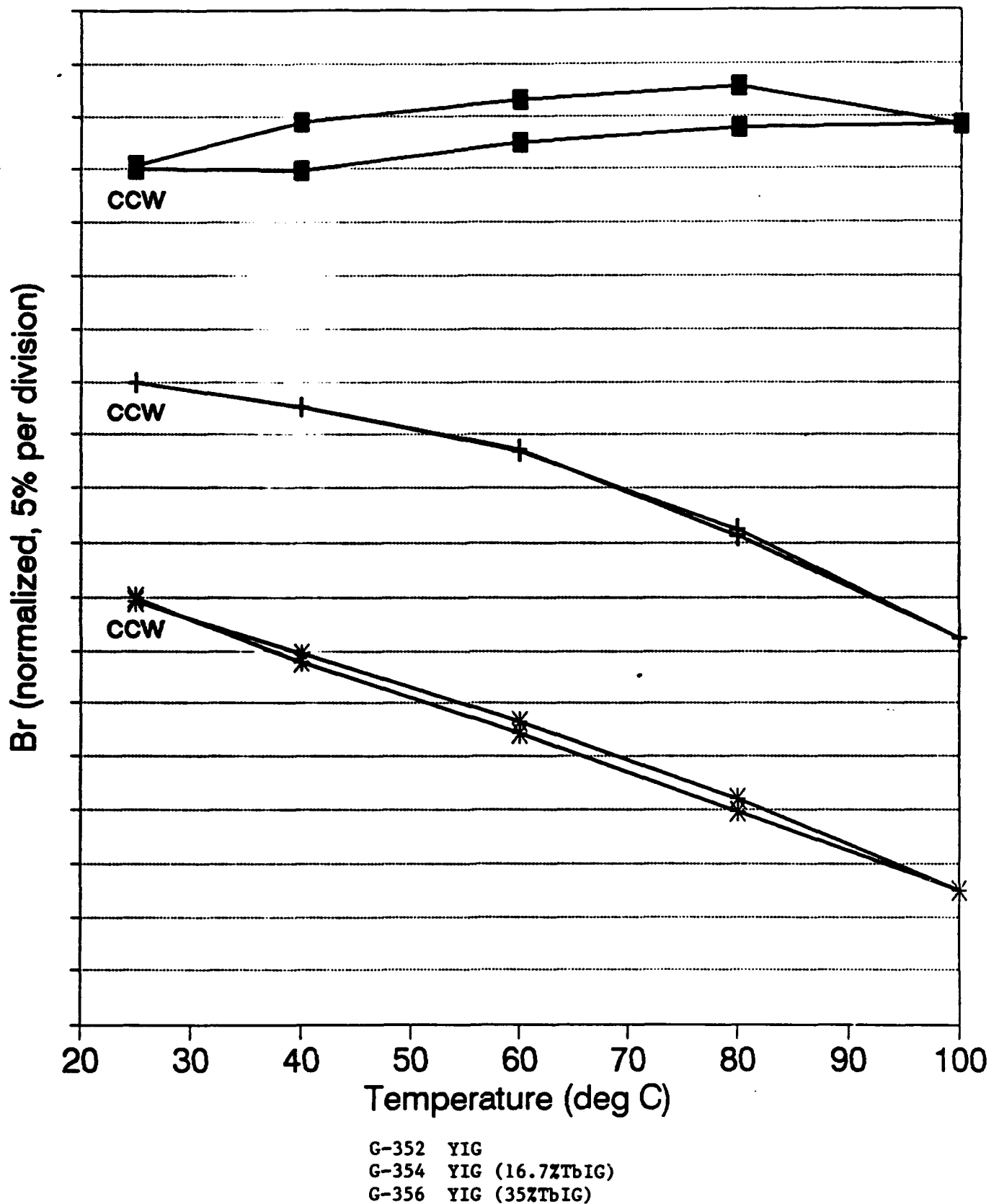COMPRESSIVE STRESS

# Br vs. Temperature
## 200 PSI Transverse Stress



Legend: G265 (0.09 Mn)   + TT G1002 (0.09Mn)

FIGURE 7-8   NORMALIZED Br VERSUS TEMPERATURE FOR 0.09 Mn SUBSTITUTED G-265
AND TT G-1002 IN PSTF AT 200 PSI TRANSVERSE COMPRESSIVE STRESS

Some compounds were evaluated at 300PSI transverse stress and these data are presented in Figure 7-9.

Initially, some data were collected at transverse stress levels of 500 to 600 PSI. At this level some of the test samples broke or had small sections sheared off the ends during temperature cycling. For completeness, some of the data on toroids that survived are presented in Figure 7-10. This is believed to be a transverse stress level considerably higher than that typically encountered in soft top phaser structures.

The magnesium-manganese ferrite materials such as Trans-Tech TT1-105 have been identified as materials that exhibit essentially no sensitivity to stress, and if the garnet materials could be formulated to possess similar stress insensitive characteristics, they would offer improved performance in phase shifter structures.

Figure 7-11 compares the stress sensitivity characteristic of some of the Mn substituted garnet compounds generated during this development program with that of TT 1-105. The 0.11Mn to 0.13Mn substituted hybrid YIG compounds exhibit stress sensitivity comparable to that of TT 1-105. The yttrium-gadolinium iron garnets (YGdIG) like G-265 have less intrinsic temperature sensitivity of saturation and remanent magnetization than the magnesium manganese ferrite as shown in this figure which is advantageous to many applications.

7.2    DATA IN PHASER HOUSING

The previous data presented in Section 7.1 were collected in the PSTF using single toroids of approximately one-inch length. This fixture characterized the relative Br versus temperature of the various materials in a simulated phase shifter configuration. The fixture was designed to evaluate the stress sensitivity of materials in a static (non-Rf) environment sufficiently well to predict performance in actual dual toroid waveguide phaser structures.

# Br vs. Temperature
# 300 PSI Transverse Stress
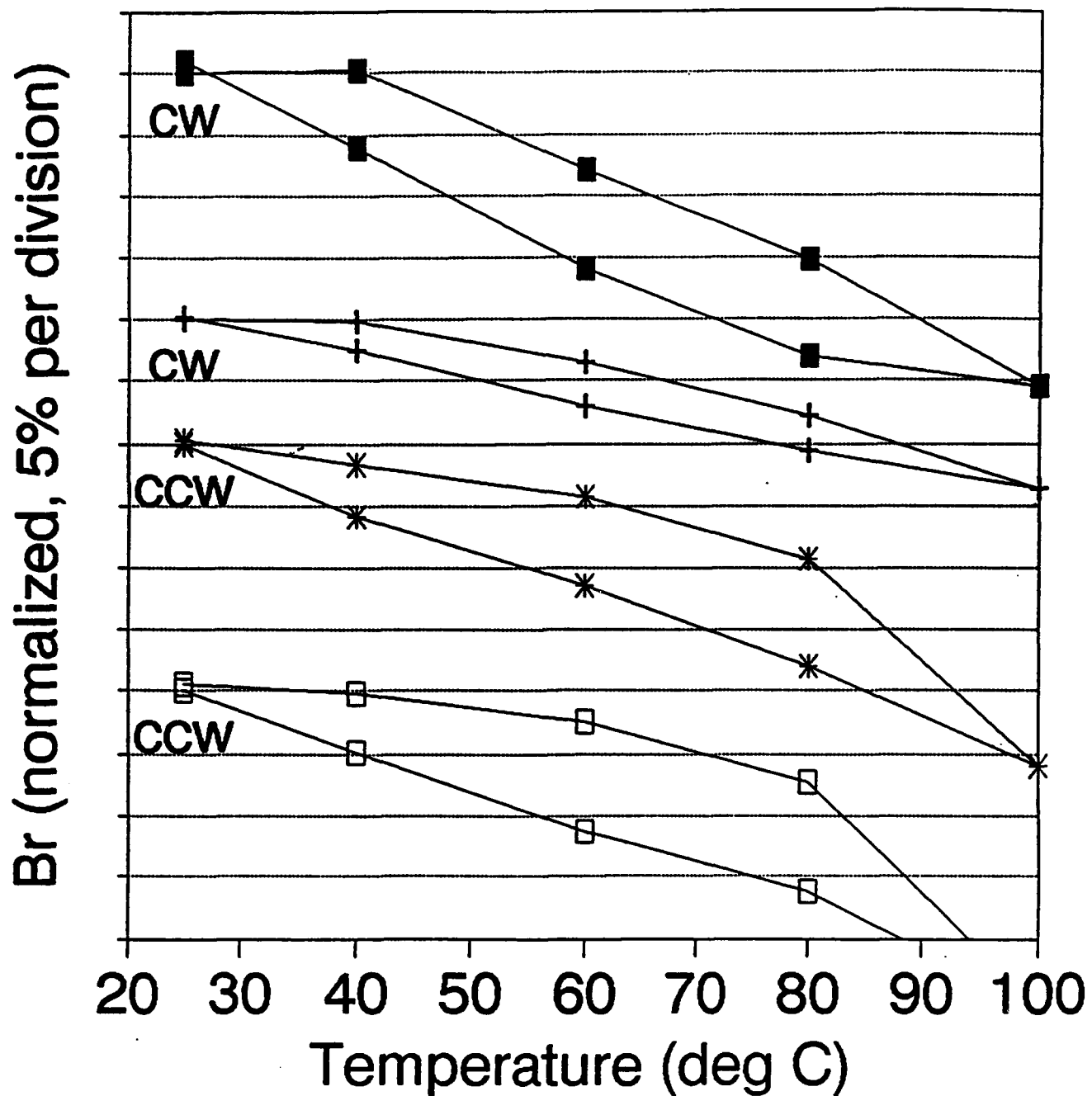


**FIGURE 7-9    NORMALIZED Br VERSUS TEMPERATURE FOR VARIOUS Mn SUBSTITUTED GARNETS IN PSTF AT 300 PSI TRANSVERSE COMPRESSIVE STRESS**
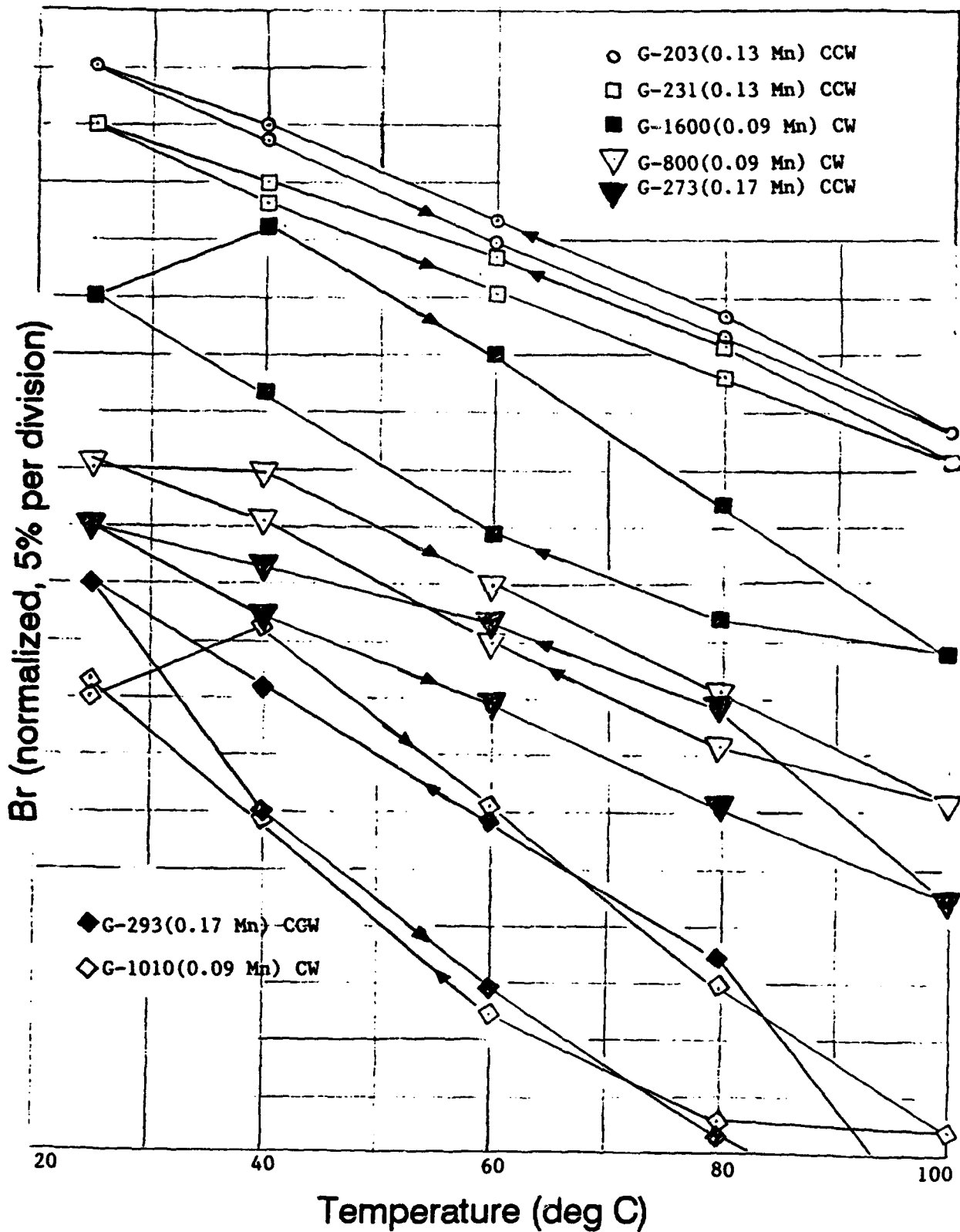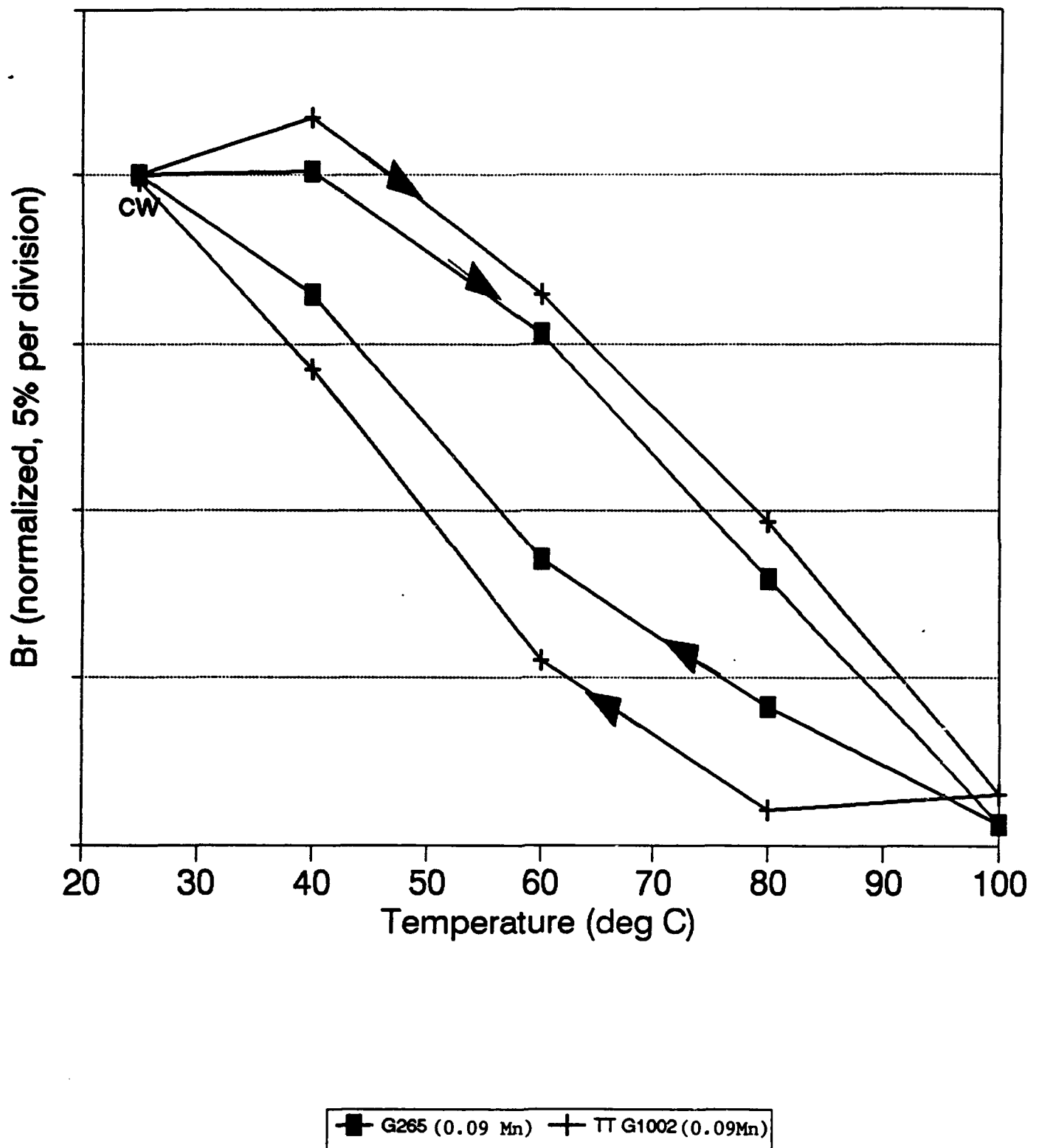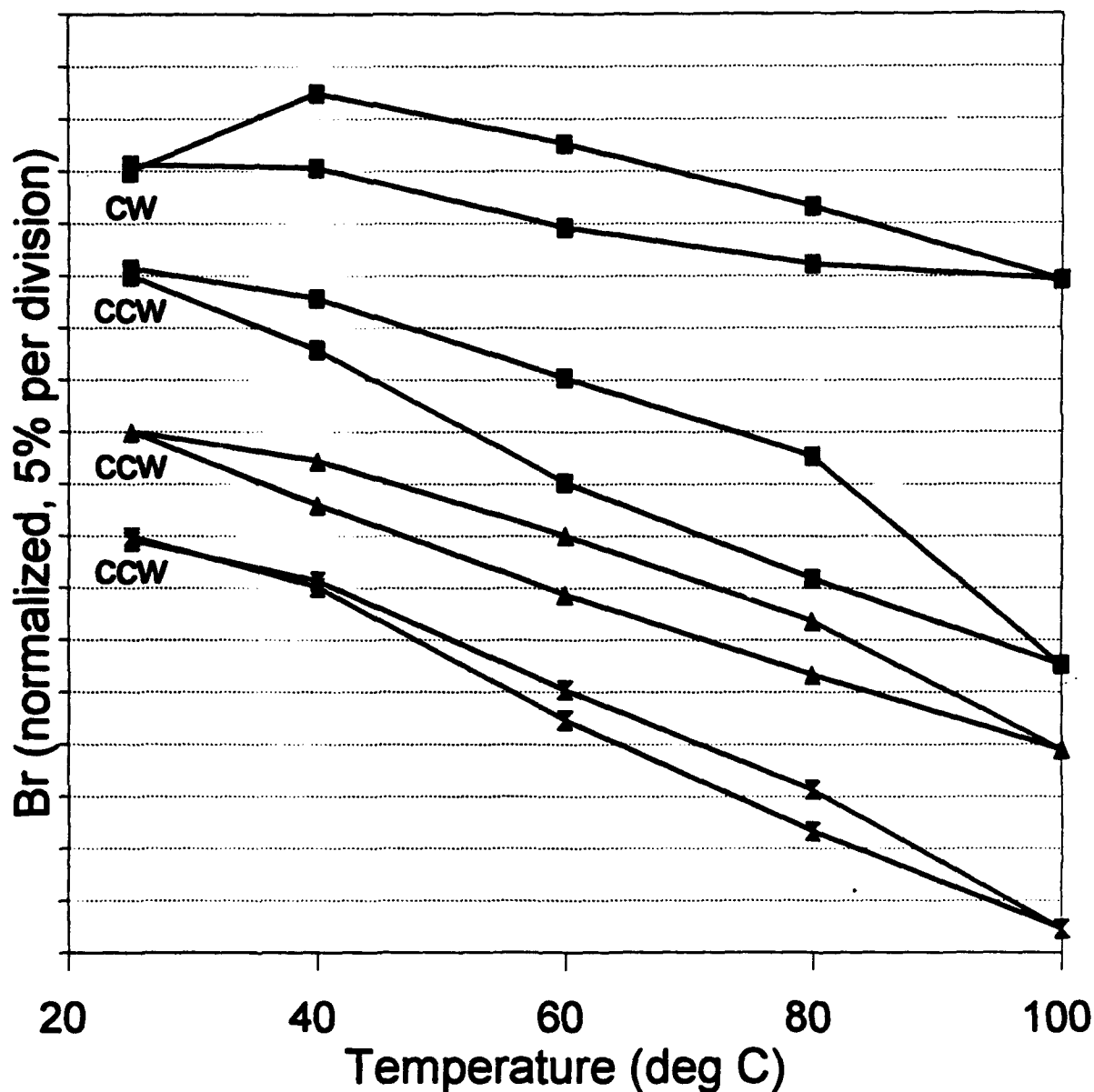
FIGURE 7-10 NORMALIZED Br VERSUS TEMPERATURE FOR VARIOUS Mn SUBSTITUTED GARNET MATERIALS IN PSTF AT 550 PSI TRANSVERSE COMPRESSIVE STRESS

# Br vs. Temperature
## 100 PSI Transverse Stress
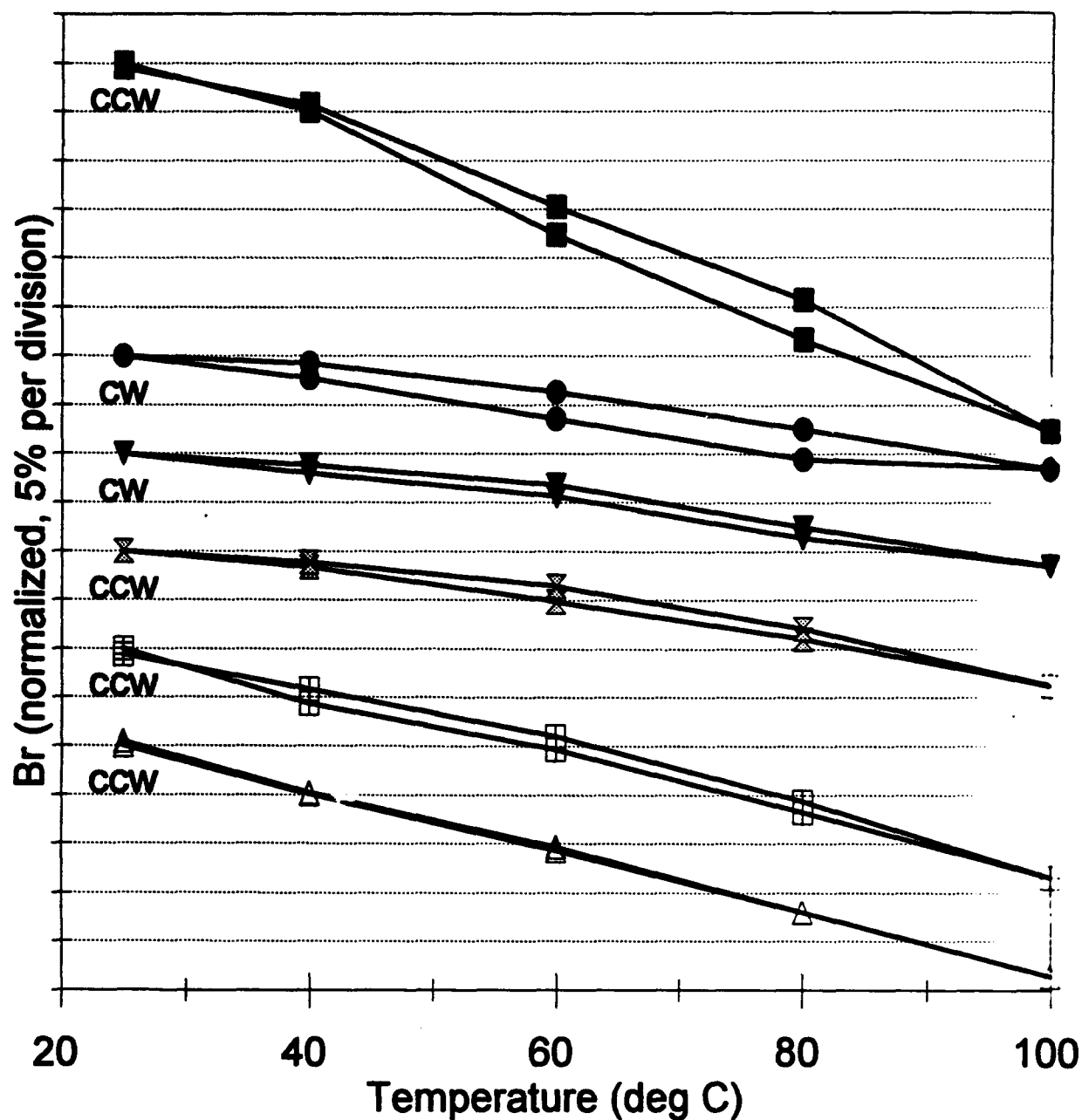


FIGURE 7-11  NORMALIZED Br VERSUS TEMPERATURE FOR VARIOUS Mn SUBSTITUTED GARNETS COMPARED TO TT1-105 Mg-Mn FERRITE IN THE PSTF AT 100 PSI TRANSVERSE COMPRESSIVE STRESS

Data presented in this section were collected to correlate and compare data taken in the PSTF with that observed in actual dual toroid phase shifter housing. The two structural environments differ in the following aspects:

- The PSTF primarily was designed to evaluate single toroids; however, the structure was constructed large enough to accommodate a dual toroid structure and some data have been collected on the fully assembled dual toroid phaser configuration.

- The PSTF provides a more rigid stress to the toroid. While the stress is generated by compression of the rubber in both structures, the rubber/metal stack-up above the toroid in the PSTF is a much thicker aluminum plate. In the phaser housing the re-designed soft top structure uses a 4 mil aluminum sheet (foil) between the compressed rubber and the dual toroid ferrite structure.

- In the dual toroid configuration, as used in the phaser, the dielectric center core will provide some stress resistance (or relief) for the ferrite material as compared to the single toroid in the PSTF.

- The PSTF is expected to provide an environment that is more responsive to stress than that experienced in the dual toroid phaser housings. Stress points and "creep" may however be somewhat different in the two structures.

The static and phase data from the previous sections indicate that the garnet compounds exhibiting the least stress sensitivity are those with 0.11 and 0.13 manganese substitutions. Previous to these studies, 0.09 manganese substitution in garnets had primarily been used for phase shifter applications to reduce stress sensitivities and to improve Br.

Tests in the phaser housing thus focused on the evaluations of these compounds.

Data presented in this section were collected to correlate and compare data taken in the PSTF with that observed in actual dual toroid phase shifter housing. The two structural environments differ in the following aspects:

. The PSTF primarily was designed to evaluate single toroids; however, the structure was constructed large enough to accommodate a dual toroid structure and some data have been collected on the fully assembled dual toroid phaser configuration.

. The PSTF provides a more rigid stress to the toroid. While the stress is generated by compression of the rubber in both structures, the rubber/metal stack-up above the toroid in the PSTF is a much thicker aluminum plate. In the phaser housing the re-designed soft top structure uses a 4 mil aluminum sheet (foil) between the compressed rubber and the dual toroid ferrite structure.

. In the dual toroid configuration, as used in the phaser, the dielectric center core will provide some stress resistance (or relief) for the ferrite material as compared to the single toroid in the PSTF.

. The PSTF is expected to provide an environment that is more responsive to stress than that experienced in the dual toroid phaser housings. Stress points and "creep" may however be somewhat different in the two structures.

The static and phase data from the previous sections indicate that the garnet compounds exhibiting the least stress sensitivity are those with 0.11 and 0.13 manganese substitutions. Previous to these studies, 0.09 manganese substitution in garnets had primarily been used for phase shifter applications to reduce stress sensitivities and to improve Br.

Tests in the phaser housing thus focused on the evaluations of these compounds.

- 153 -

Figure 7-12 presents stress response data (Br versus temperature at 100 PSI) on the 0.09 Mn substituted G-265 compound as a single toroid (1" length) in the PSTF, as a complete dual toroid structure including the dielectric center slab in the PSTF and as a dual toroid structure in the phase shifter housing. There are minor variations in the data; however, the static tests in the PSTF on the single one inch toroid provides a very good evaluation of the expected stress response in the phaser housing.

Figure 7-13 presents similar data on the 0.11 Mn substituted G-265 compound. Again, the data collected in the PSTF correlates well with the data observed from the phaser housing.

Figure 7-14 presents the data collected on the 0.13 Mn substituted G-265 compound. This material was used in the phaser supplied at the end of Phase I.) The data include the Br versus temperature response of a single toroid in the PSTF and a dual toroid in the phaser housing (3.84 inches of material). Again the data from the PSTF correlates well with the data collected in the phaser housing.

The Br versus temperature data collected on the G-265 (0.11Mn) and the G-265 (0.13 Mn) compounds in the phaser housing are presented on the same graph in Figure 7-15 to compare responses since these compounds exhibit the least sensitivity to stress. Consistent with the data presented in Section 7.1, the 0.11 Mn substituted compound has a small clockwise Br vs. temperature hysteresis and the 0.13 Mn substituted compound exhibits a small counter-clockwise response. The phase shifter housing in this case is a soft top (4 mil aluminum foil) waveguide structure with removable matching transitions to double ridged WR-650 waveguides. This is the same structure as that used for the delivered demonstration phase shifter at the end of Phase II.
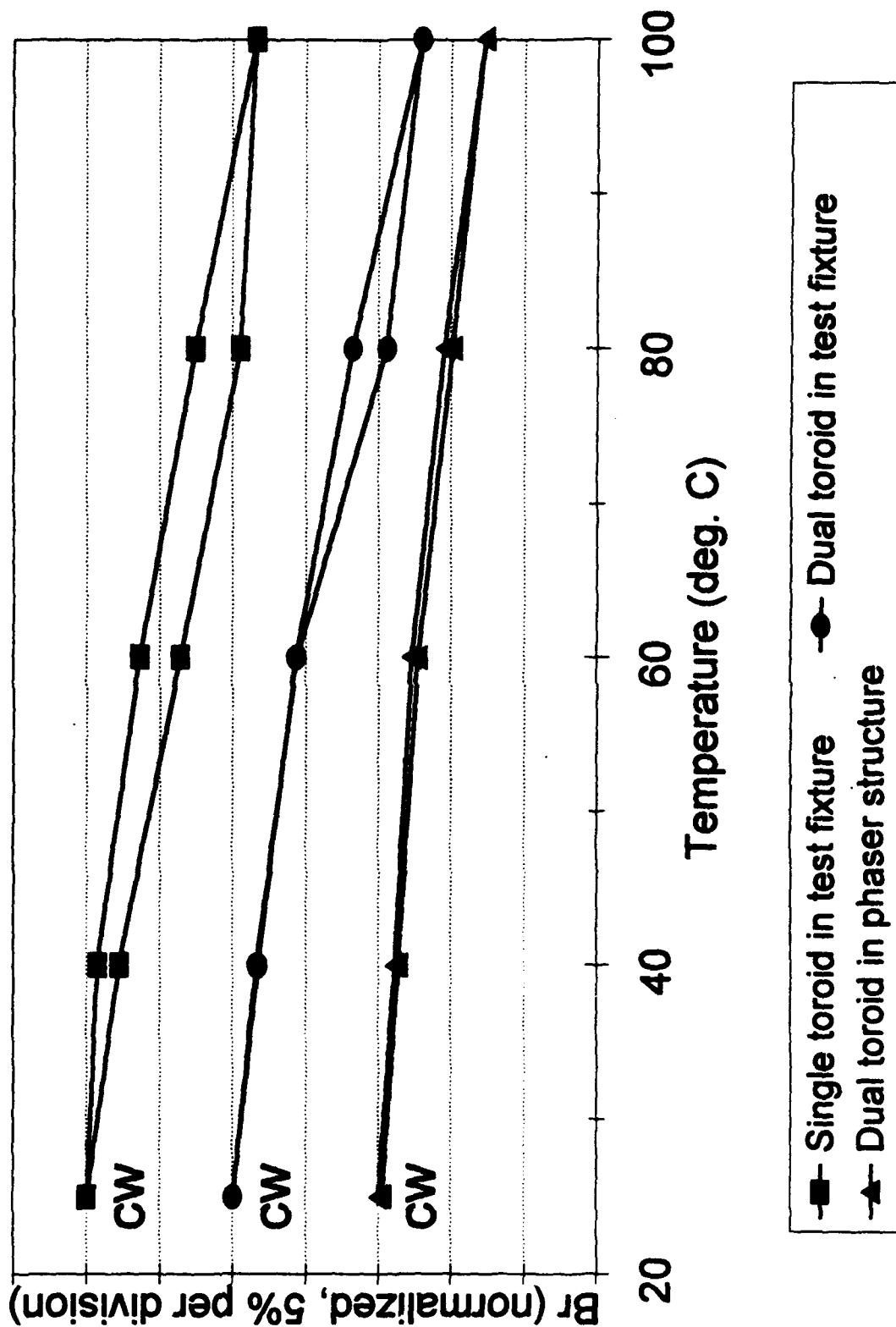
FIGURE 7-12 COMPARISON OF Br VERSUS TEMPERATURE EVALUATION OF SINGLE TOROID AND DUAL TOROID IN TEST FIXTURE WITH DUAL TOROID IN PHASER STRUCTURE

## Br vs. Temperature, EMS G265 (.11 Mn), 100 PSI Transverse Stress

Temperature (deg. C)

Br (normalized, 5% per division)

CW

CCW

■ Single toroid in test fixture    ● Dual toroid in phaser housing
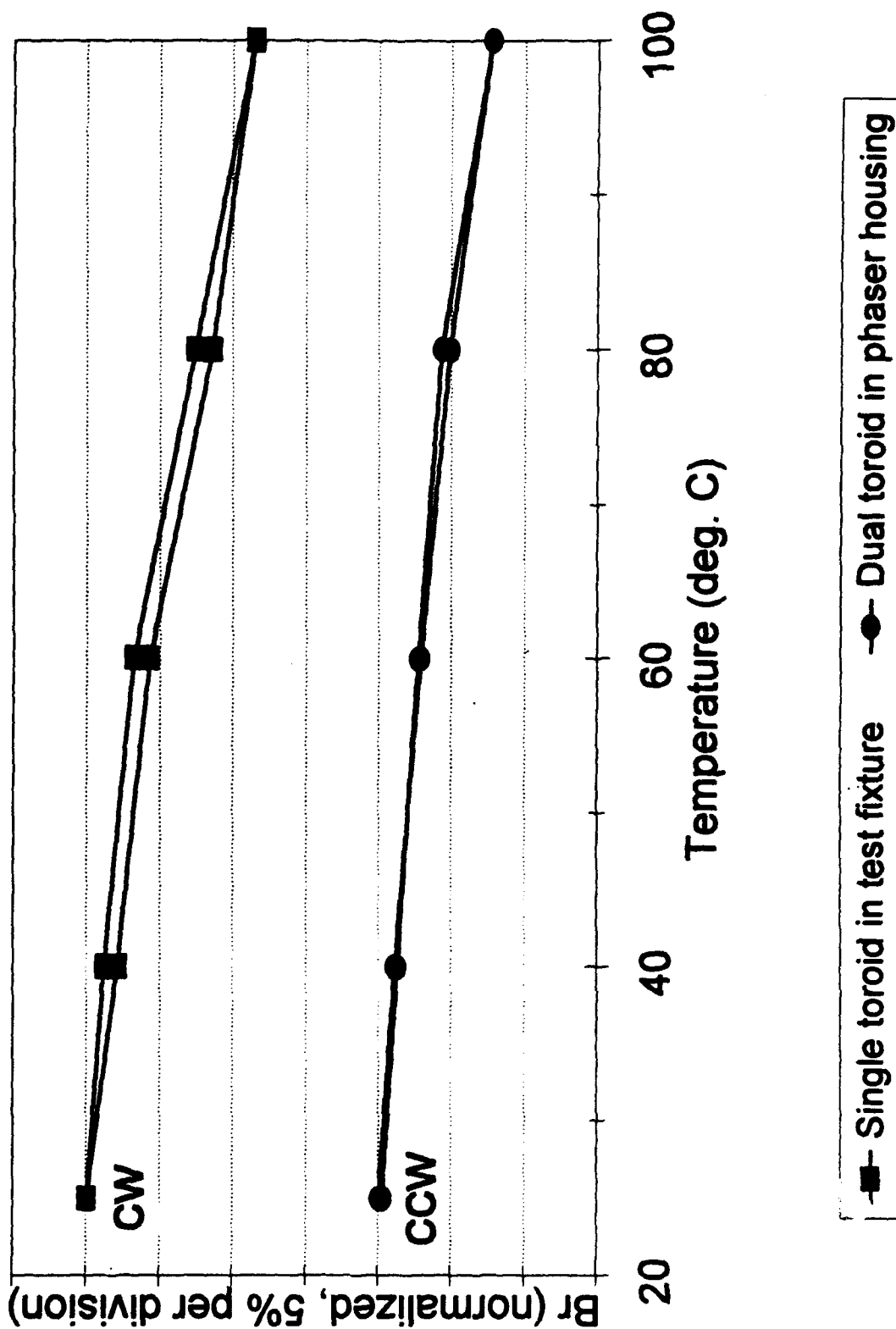
FIGURE 7-13   COMPARISON OF Br VERSUS TEMPERATURE CHARACTERISTICS OF
G265 (0.11 mn) IN TEST FIXTURE (SINGLE TOROID) WITH DUAL
TOROID STRUCTURE IN PHASER HOUSING

Br vs. Temperature, EMS G265 (.13 Mn),
100 PSI Transverse Stress

■ Single toroid in test fixture    ● Dual toroid in phaser housing
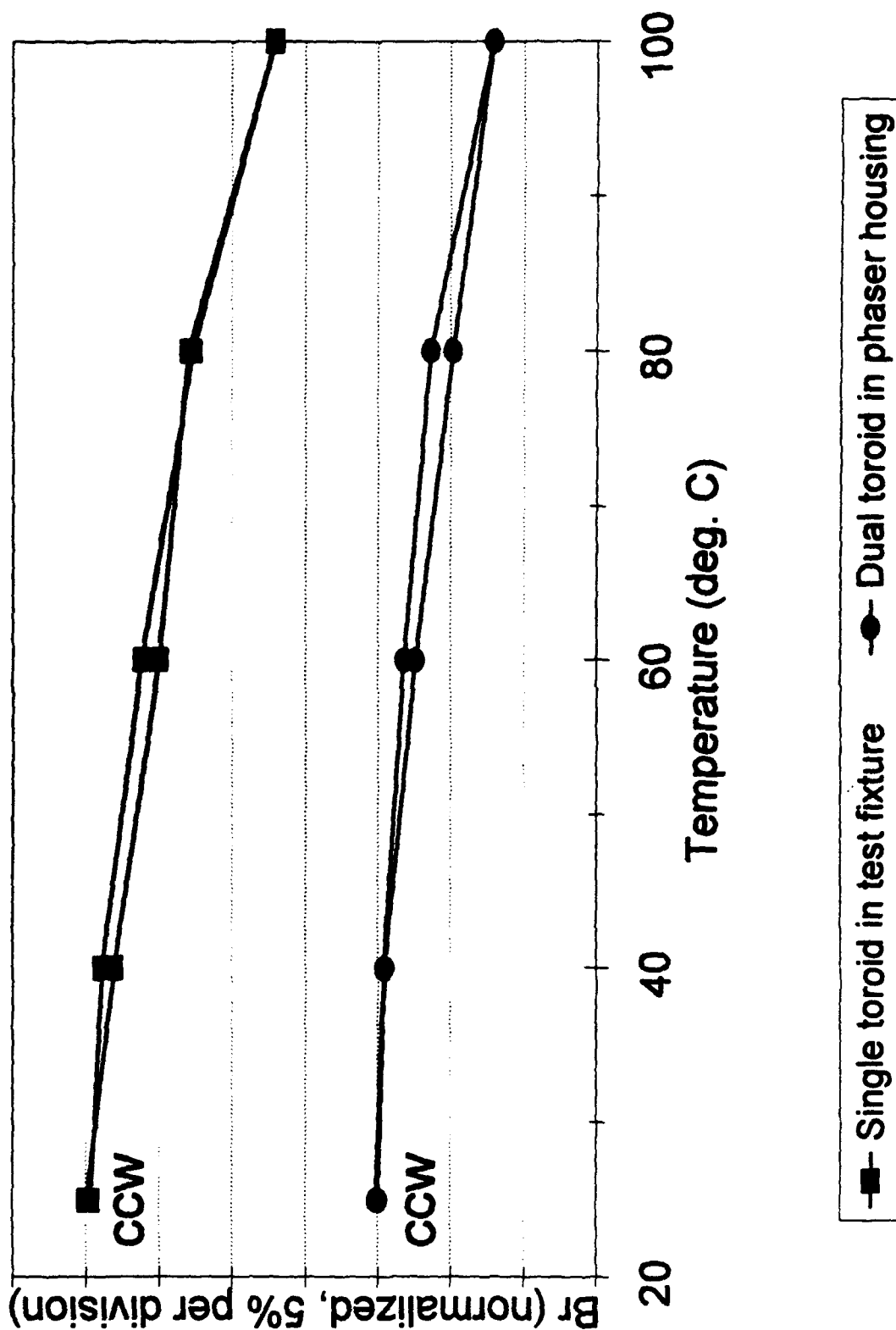
FIGURE 7-14   COMPARISON OF Br VERSUS TEMPERATURE CHARACTERISTICS OF
G265(0.13 Mn) IN TEST FIXTURE (SINGLE TOROID) WITH DUAL
TOROID STRUCTURE IN PHASER HOUSING

# Br vs. Temperature
# In Phase Shifter Housing

**Temperature (deg C)**

**Br (normalized, 5% per division)**

CW

CCW

G265 (.11 Mn) — G265 (.13 Mn)
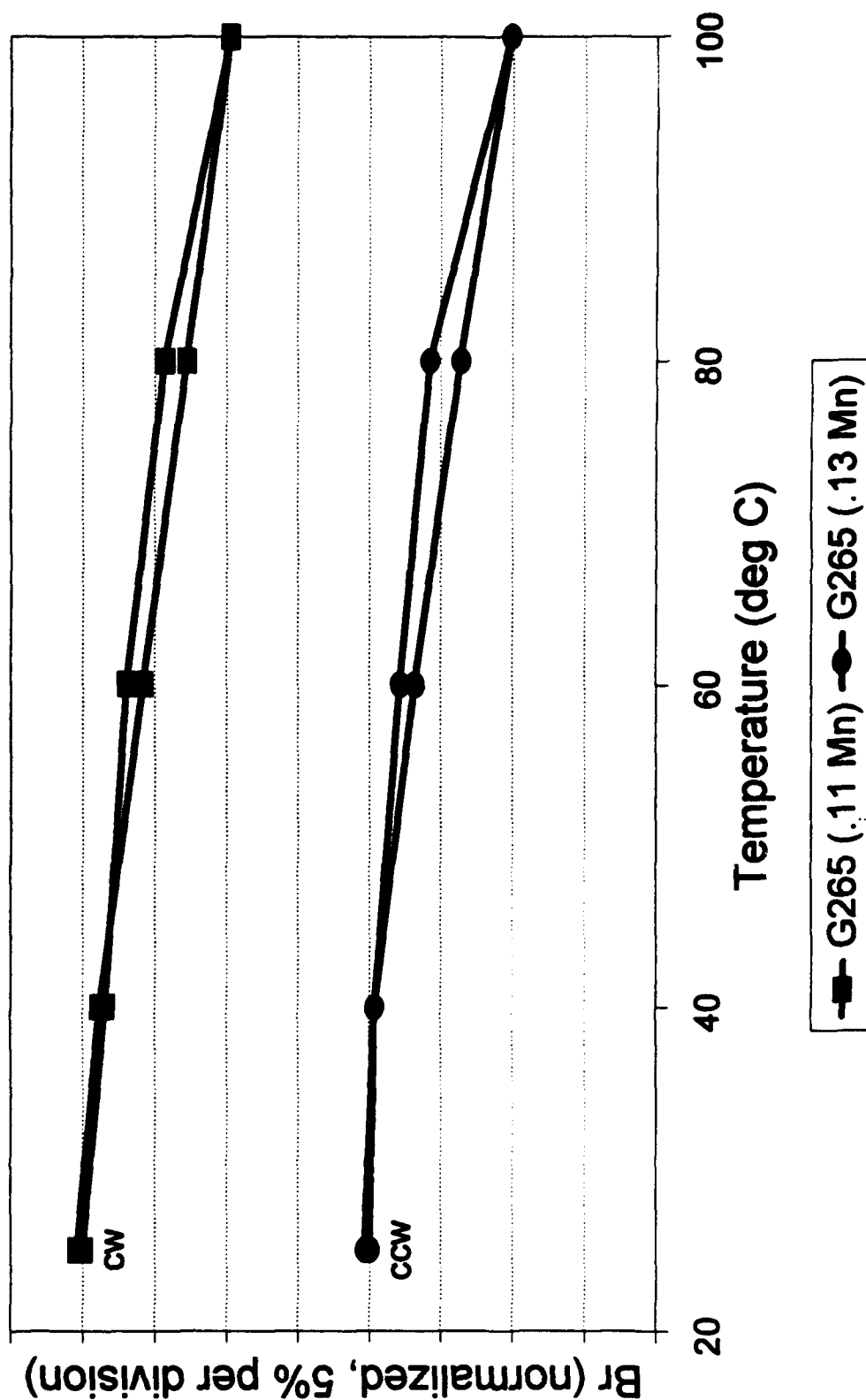
FIGURE 7-15

Normalized Br vs temperature for 0.11 and 0.13 Mn substituted G-265 in dual
toroid phaser housing

Figure 7-16 presents the normalized Br and differential phase shift data measured on the 0.11 Mn substituted compound (G 265-83) in the finalized phase shifter structure. The structure provided 111 degrees of differential phase shift at 25°C, and 94° at the maximum temperature of 100°C. The material was 3.84" long in this design structured for high average power applications as measured during Phase I (see Section 6.). The Rf performance of this phaser is shown in Figure 7-17 with an insertion loss of about 0.6 dB over the 7 to 11 GHz region.

Similar Rf performance data are presented in Figure 7-18 for the 0.13 Mn substituted compound (G 265-70). The performance of these two compounds are very similar with a hysteresis in differential phase with temperature of not more than 0.7° over the temperature range from 25°C to 100°C in a structure providing 111° to 94° total differential phase shift (<0.8% phase stress sensitivity) and suitable for acceptable Rf performance up to the tested power of 400 Watts CW.

## Br and Phase vs. Temperature EMS G265 (.11 Mn)
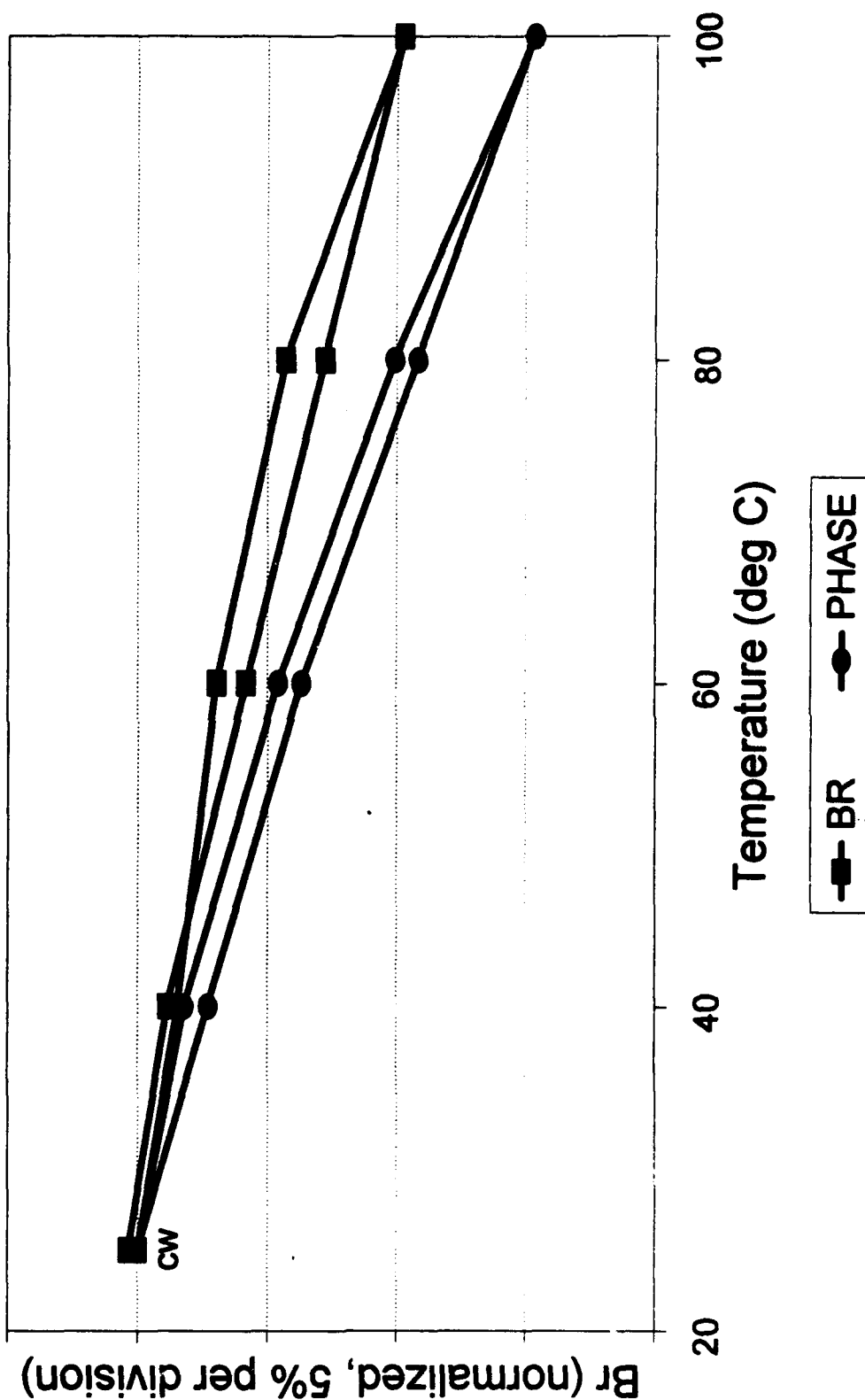
FIGURE 7-16

Normalized Br and Phase shift versus temperature for G-265  (0.11 Mn)  in dual toroid
high power phaser configuration
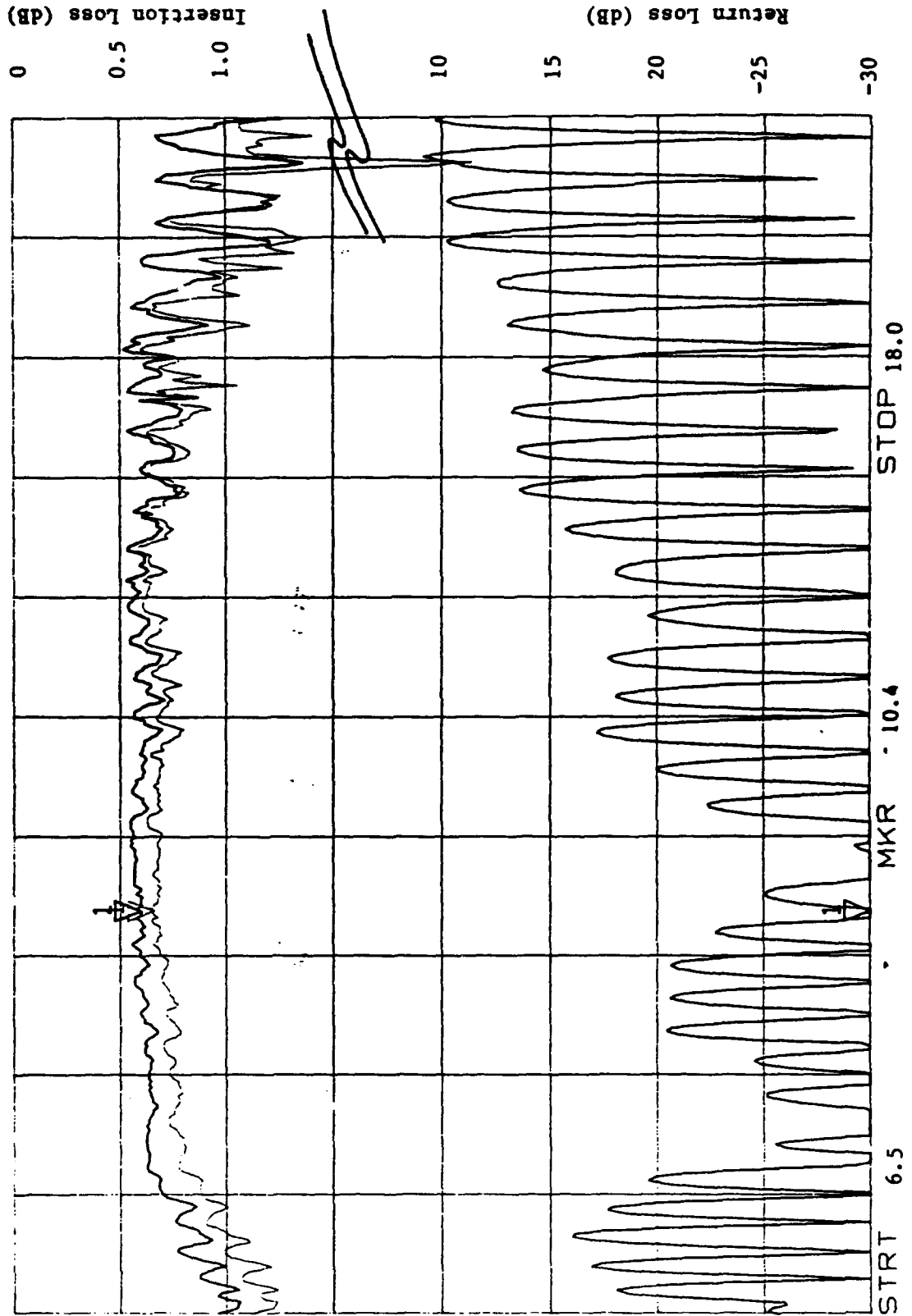
FIGURE 7-17 LOW POWER RF PERFORMANCE CHARACTERISTICS OF DUAL
TOROID PHASER USING G-265-83C(0.11Mn)
(DELIVERED DEMONSTRATION MODEL)
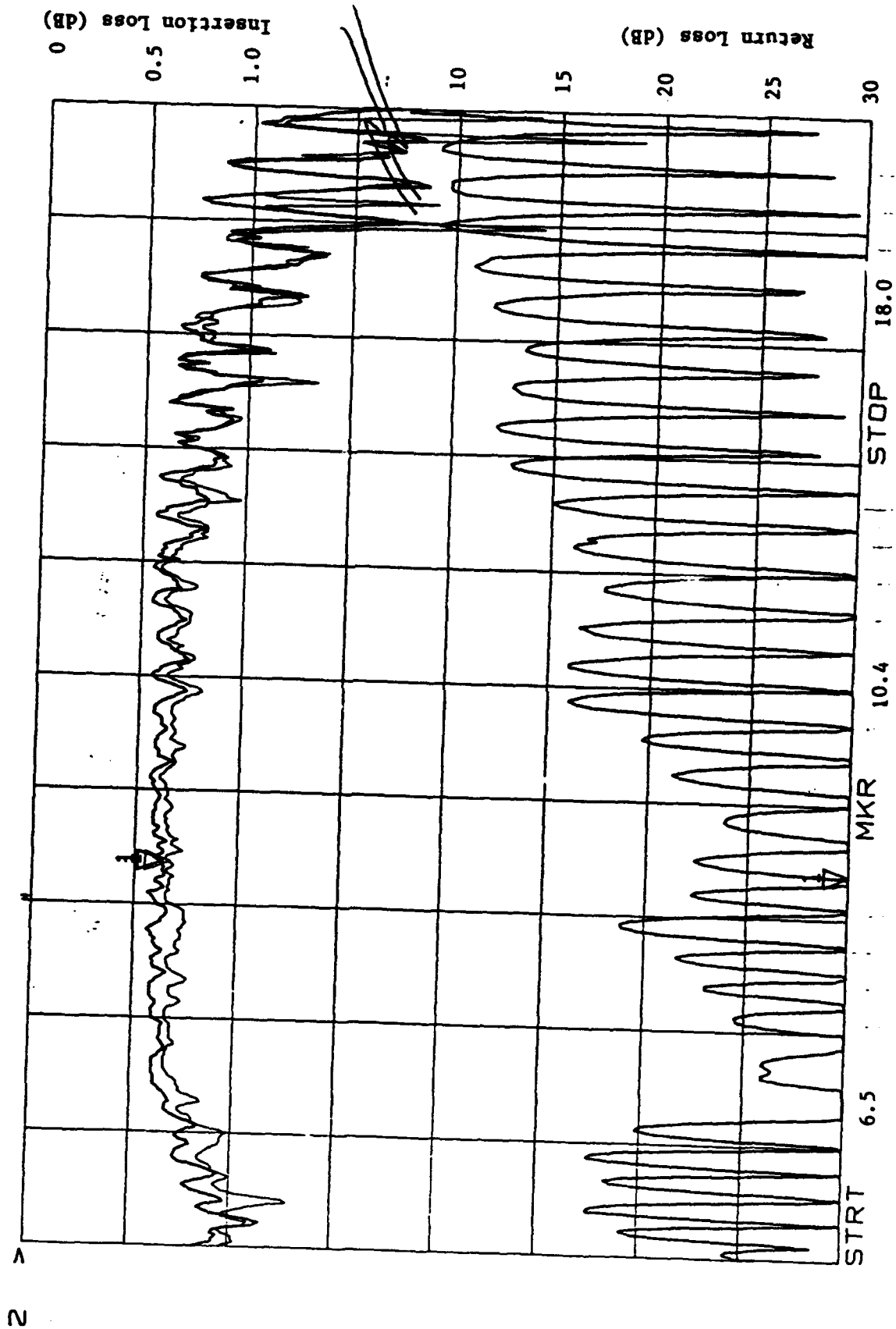
FIGURE 7-18  LOW POWER RF PERFORMANCE OF DUAL TOROID PHASER
G-265-70g(0.13 Mn)

# 8.0    COMPUTER AIDED ANALYTICAL STUDIES

## 8.1    THERMAL ANALYSIS

The phase shifter design used as a test bed in Phase I and as the delivered unit of Phase II is relatively inefficient from an electromagnetic standpoint. It has an overall cross section of 0.365 by 0.172 inches and is 3.84 inches long. This design produces only 28 degrees of phase shift per inch of ferrite length. Because of this inefficient design, the insertion loss is greater (0.6 dB) than it could be in the 90 degree phase shifter. The design uses a center rib of S-145 material whose relative permittivity is 10.0, lower than that of the ferrite ($\varepsilon_r$ = 16), and therefore the Rf fields are not concentrated in the vicinity of the dielectric rib. The rather large length of the device leads to somewhat large ohmic loss in the waveguide that is largely responsible for the 0.6 dB total insertion loss.

A second, more electrically efficient design, was explored in the second phase of this program. This design is based on the use of a dielectric rib of D-19 with a larger relative permittivity ($\varepsilon_r$ = 19). The overall dimensions of this second design are 0.307 by 0.161 inches with a length of 2.20 inches. The field concentration effects caused by the higher permittivity of the dielectric yield more phase shift per unit length (50°/inch), and therefore less ohmic loss in the waveguide and a lower predicted insertion loss (0.4 dB vs. 0.6 dB for the original unit).

Using the COSMOS/M FEA models (with 128 elements and 160 nodes) both units were analyzed for their heat dissipation characteristics and the predicted rise in temperature in the ferrite under average high power loading. The analysis was run first assuming that heat sinking occurs only along the bottom of the unit, and again assuming that heat sinking is effected along both top and bottom surfaces. Because of probable air gaps at the sides and the long thermal path to the sides, no appreciable heat loss is expected there. In the actual units significant heat sinking is expected only along the bottom surface because the top plate is a thin (0.004 inches) sheet with no coolant flow adjacent to it. The bottom of the waveguide housing has coolant (maintained at 16°C) flowing through it.

Based on the results of an electromagnetic analysis (PSAN) of field distributions in the phasers, the power dissipation is assumed to occur 48% in the dielectric rib, 20.8% in the inner leg of each ferrite toroid, 8% in the top and bottom areas around the hole in the toroids, and 2.4% in the two outer two legs of the ferrite toroids.

The results of this thermal study are shown in Figure 8-1 through Figure 8-8. In every case it is assumed that 400 watts of average power is incident on the phasers with 0.6 dB and 0.4 dB of insertion loss, as previously stated. Figures 8-1 and 8-2 show contours of constant temperature for the larger and smaller cross section designs, respectively, under the assumption that heat sinking exists at the bottom surface only. A one mil (0.001") air gap is assumed to exist between the rib and the toroid on either side. In these units the ferrite toroids are not bonded to the dielectric rib, and therefore a small air gap is assumed.

The larger S-145 design has a predicted temperature rise of 15.7°C with 400 watts of incident power, and the smaller D-16 design has a rise of 60.7°C. This striking difference is caused by the facts that the thermal conductivity of the S-145 is seventeen times larger than that of D-19 (0.17 vs. 0.01 $cal/cm^2/cm/sec/°C$) and the heat dissipation of the larger unit occurs in a larger volume and since the added loss of the larger unit is in the metallic walls, this loss does not significantly affect the ferrite temperature.

Figures 8-3 and 8-4 show comparable results when it is assumed that no air gap exists between the center rib and the ferrite toroids. Now the predicted temperature rise is 9.0°C for the S-145 design and about 50°C for the D-19 unit. Without an air gap between ferrite and dielectric rib the dielectric provides an enhanced thermal conducting path to the heat sink. These results are summarized in Table 8-1.

THERMAL Step=1

Temp
31.7
30.2
28.6
27.0
25.4
23.9
22.3
20.7
19.1
17.6
16.0
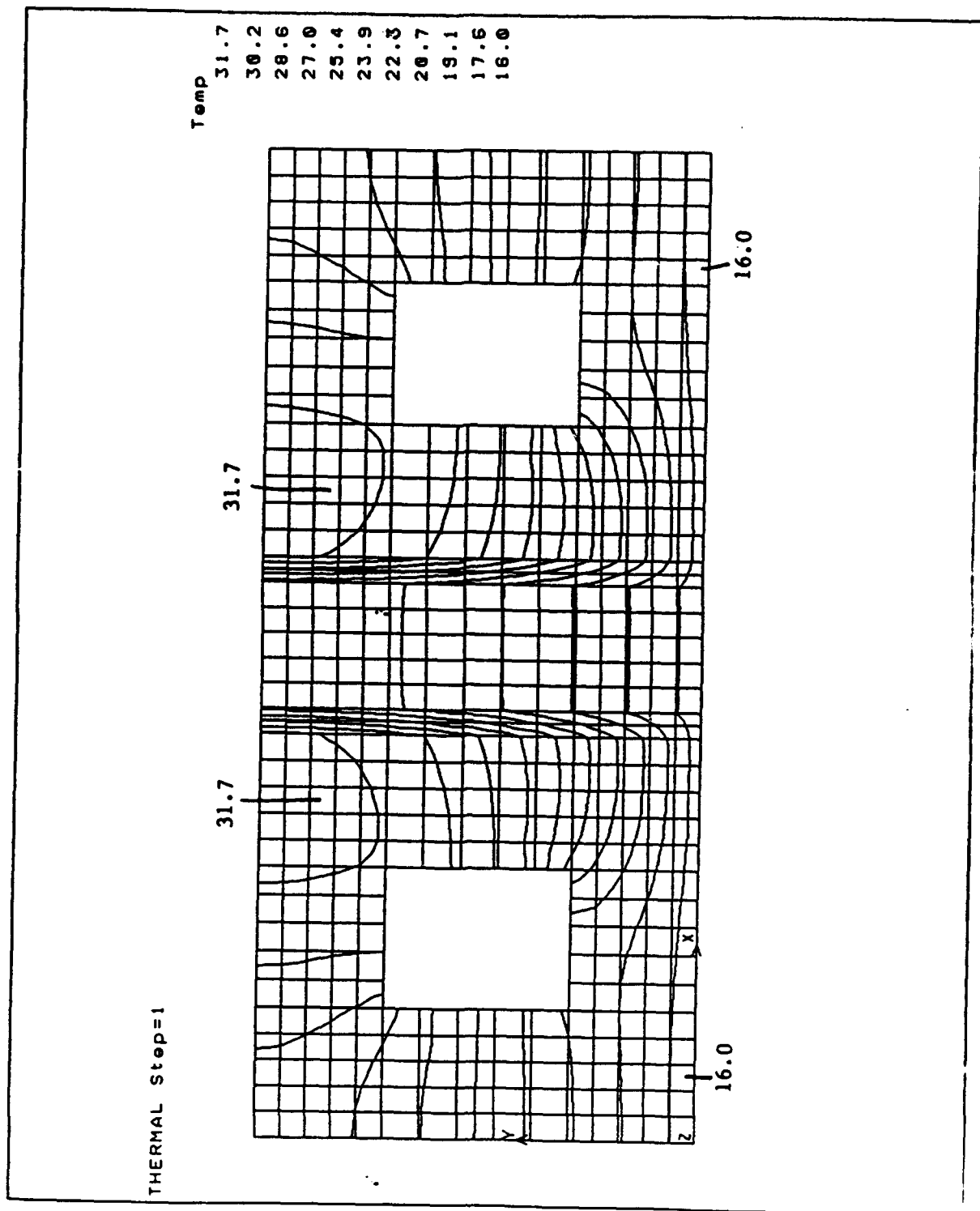
FIGURE 8-1  ISOTHERMS FOR THE SIAS BASED PHASE WITH A ONE MIL AIR GAP AND BOTTOM ONLY HEAT SINKING.
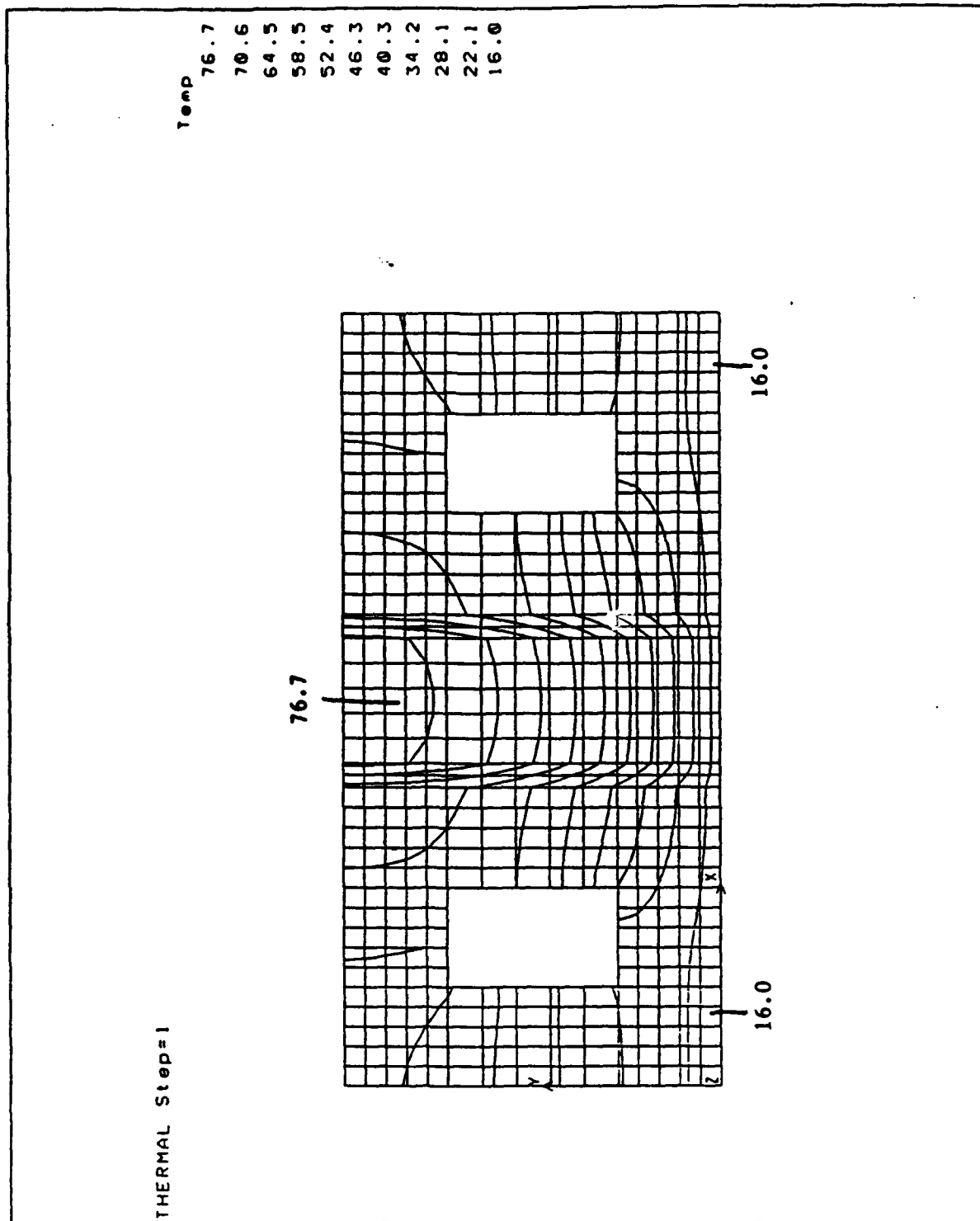
FIGURE 8-2   ISOTHERMS FOR THE D-10 BASED PHASER WITH A ONE MIL AIR GAP
AND BOTTOM ONLY HEAT SINKING.

THERMAL Step=1
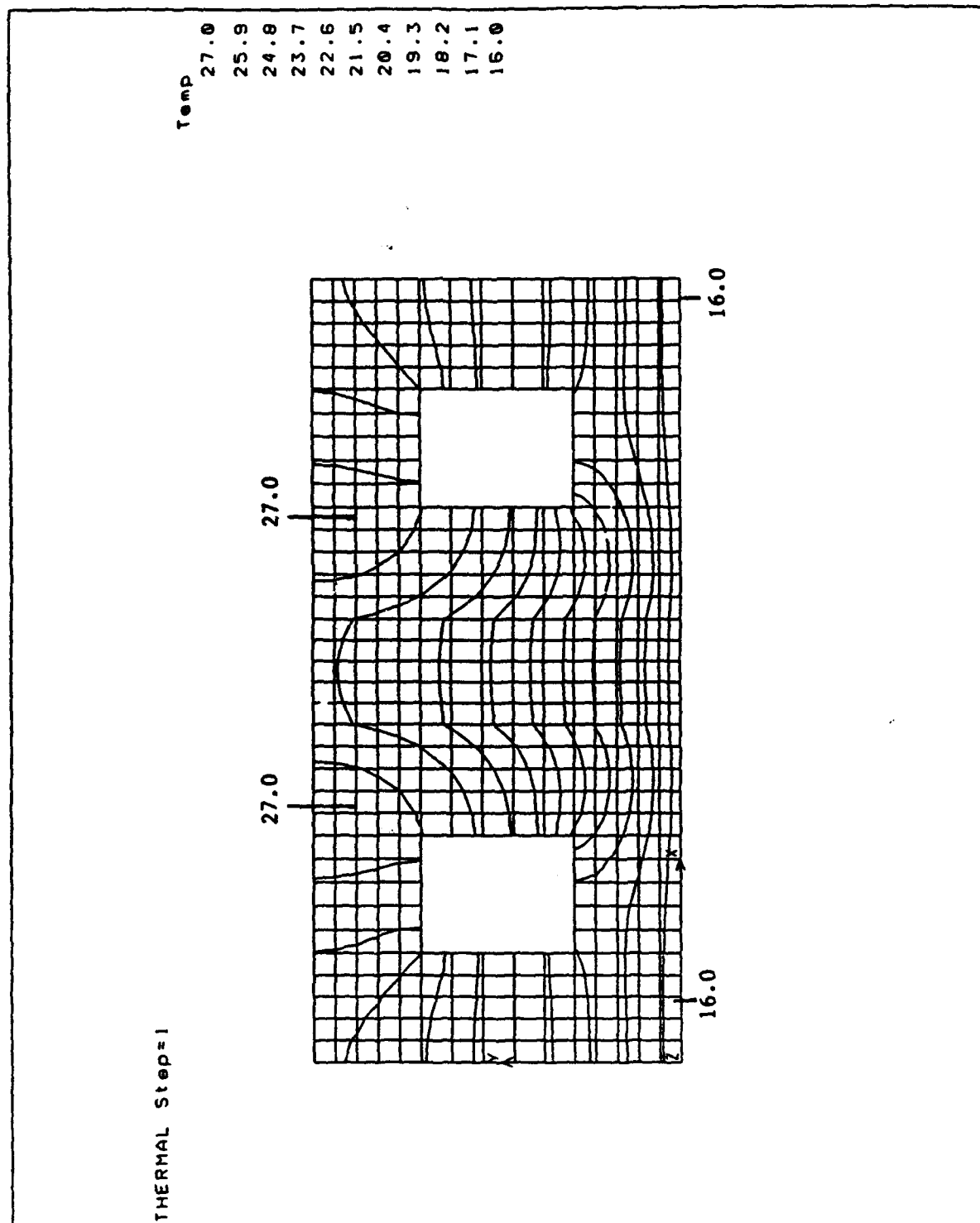
FIGURE 8-3   ISOTHERMS FOR THE SI45 BASED PHASER WITH NO AIR GAP
AND BOTTOM ONLY HEAT SINKING.

FIGURE 8-4   ISOTHERMS FOR THE D19 BASED PHASER WITH NO AIR GAP AND BOTTOM ONLY HEAT SINKING.
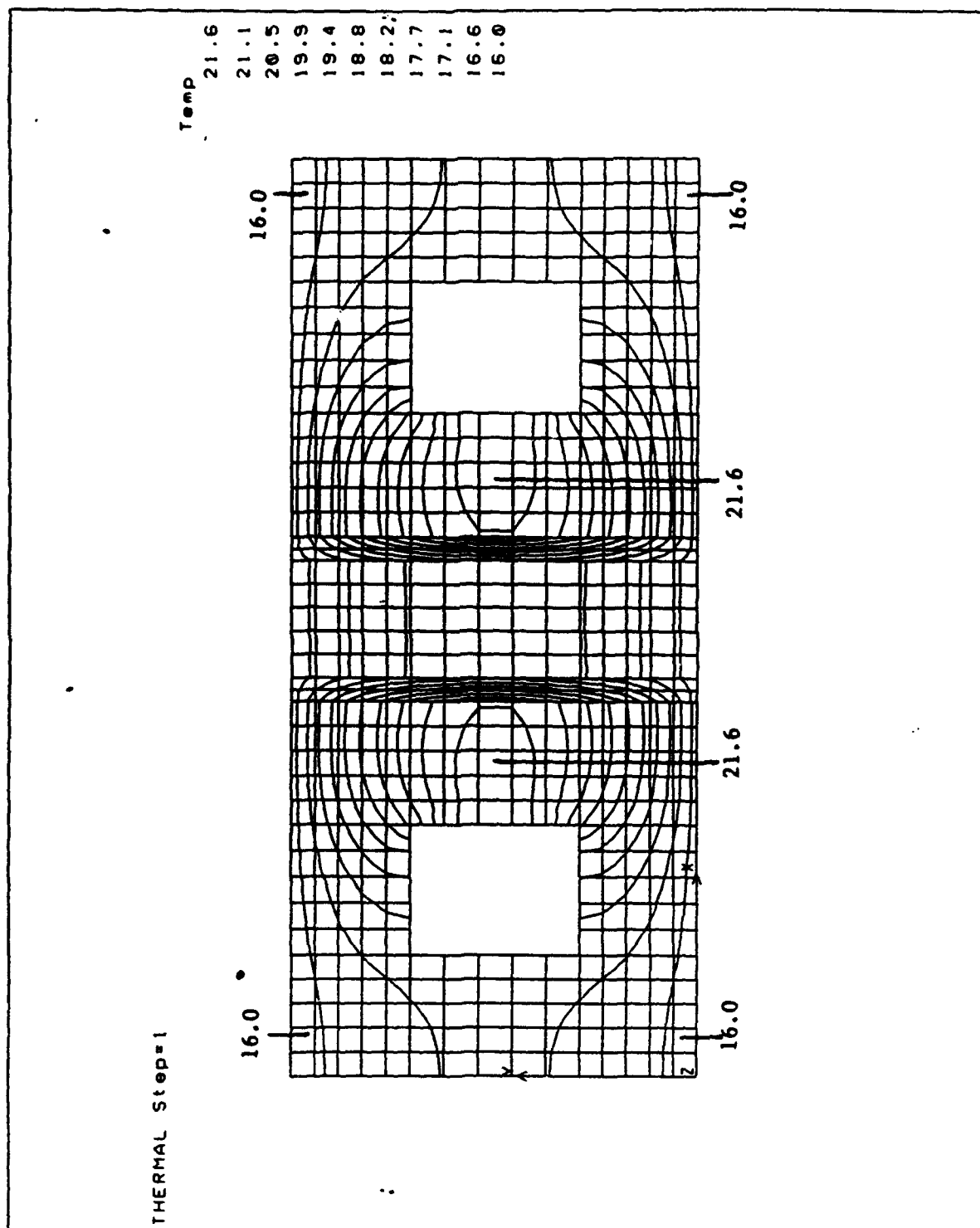
FIGURE 8-5   ISOTHERMS FOR THE S145 BASED DEISGN WITH A ONE MIL AIR GAP AND BOTH TOP AND BOTTOM HEAT SINKING.

FIGURE 8-6 ISOTHERMS FOR THE D19 BASED DESIGN WITH A ONE MIL AIR GAP AND BOTH TOP AND BOTTOM HEAT SINKING.

THERMAL Step=1

Temp
19.7
19.4
19.0
18.6
18.2
17.9
17.5
17.1
16.7
16.4
16.0

FIGURE 8-7    ISOTHERMS FOR THE SIGS BASED PHASES WITH NO AIR GAP AND BOTH
TOP AND BOTTOM HEAT SINKIN..

- 171 -

THERMAL Step=1

Temp
31.7
30.2
28.6
27.0
25.4
23.9
22.3
20.7
19.1
17.6
16.0

16.0

16.0

31.7

16.0

16.0
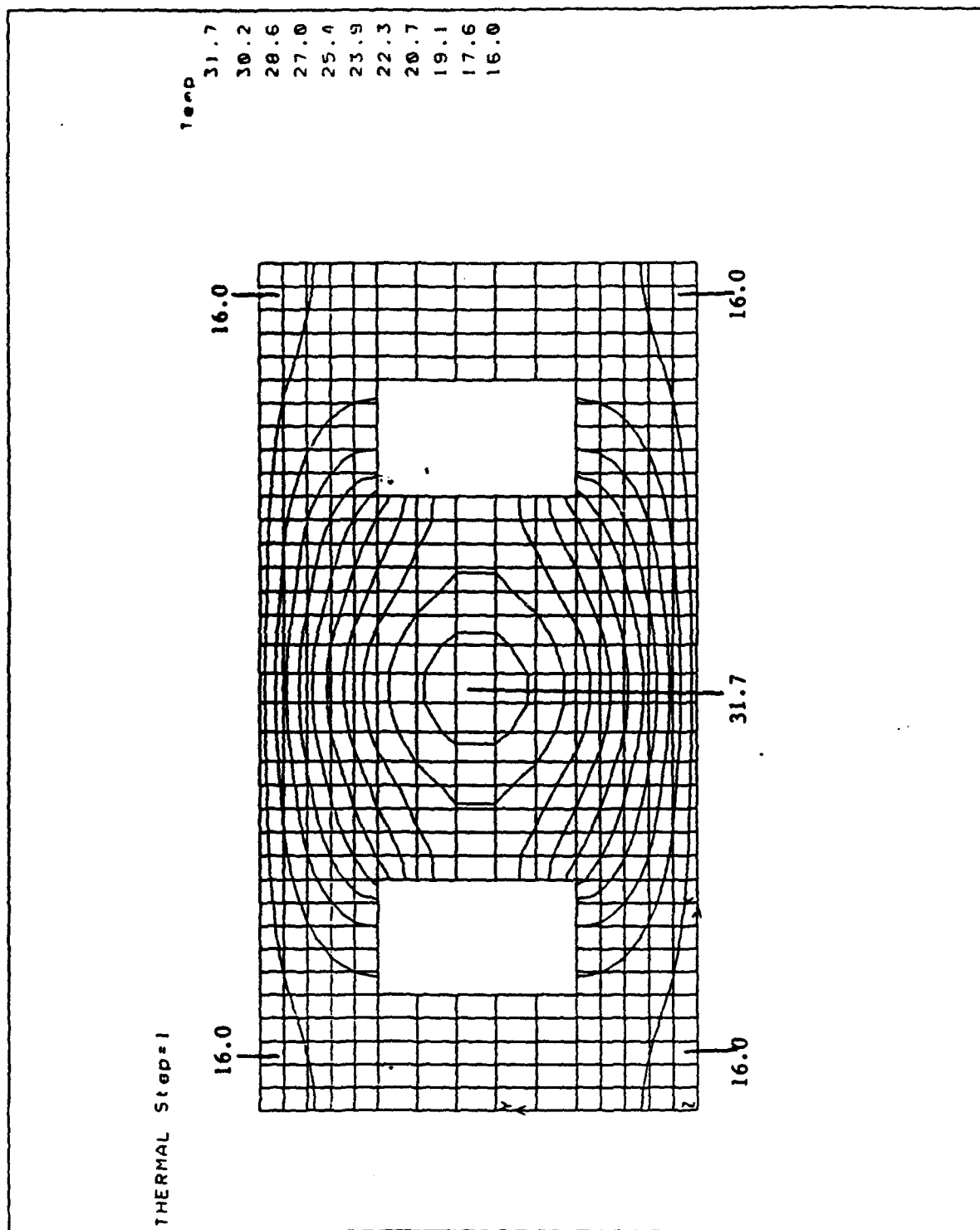
FIGURE 8-8   ISOTHERMS FOR THE D19 BASED PHASE WITH NO AIR GAP AND BOTH
BOTTOM AND TOP HEAT SINKING

## Table 8-1

### Predicted Maximum Temperature Rise in the Ferrite
### Input average power of 400 watts
### (Bottom heat sinking only)

| Unit | One mil air gap | No air gap |
|------|-----------------|------------|
| S-145 | 15.7°C | 9.0°C |
| D-19 | 90.°C | 50.°C |

Figures 8-5 through 8-8 show results obtained when it is assumed that heat sinking occurs at both top and bottom surfaces. Now the predicted maximum rise in temperature for the various configurations is as listed below (Table 8-2).

## Table 8-2

### Predicted Maximum Temperature Rise in the Ferrite
### Input average power of 400 watts
### (Top and bottom heat sinks)

| Unit | 0.001 inch air gap | no air gap |
|------|--------------------|------------|
| S-145 | 5.6°C | 3.7°C |
| D-19 | 21°C | 15.7°C |

In Phase I the S-145 unit was tested at an input average power level of 400 watts, and the temperature rise measured by a sensor mounted at the top of the housing was 16°C.  In Table 8-1 the predicted rise (assuming a one mil air gap) for 400 watts of average power is 15.7°C, in excellent agreement with the observed 16°C rise.

These results showed that the electrically inefficient design is superior for handling high average powers, and further testing was continued on the S-145 based unit.

## 8.2     ELECTROMAGNETIC ANALYSIS

The proprietary EMS computer aided analysis program (PSAN) has been used to interpret experimentally measured results in an attempt to separate purely thermally induced changes in phaser performance from those caused by stress effects.

Any practical device operating at high average power will experience an increase in operating temperature. In a ferrite device this may result in a loss of saturation and remanent magnetizations which may degrade phaser performance. In a unit excited by a "smart" flux driver, the driver may be calibrated for temperature changes in magnetization. But the driver assumes that a given amount of flux is available at given temperature. It is further necessary that the ferrite have sufficient flux available at the highest temperature to provide the required phase shift. Driver compensation is possible only if the phaser is exercised. A phaser that remains in a quiescent state cannot be driver compensated. Furthermore, if stress effects cause a change in available remanent flux at a fixed temperature, the driver has no way of correcting. Stress effects may cause the B-H loop shape to change so that the fall-back of the magnetization from the drive state is altered. This change in fall-back characteristic is also not compensated by the driver.

As indicated above, in addition to purely thermal effects, external or internal stress may also cause a loss of remanent flux and phase shift. Moreover, change in stress conditions may cause a ferrite toroid to assume different remanent states at the same temperature. This stress induced thermal hysteresis was reported in earlier work at EMS for NRL and was a key element of the phase I results. The observed thermal hysteresis was discussed in some detail in Sections 6.3 and 7.1.

- 174 -

## 8.2.1  PSAN Studies

In order to separate pure temperature effects from those also involving
stress, measurements were made of hysteresis (B-H) loops and phase shift
under both uniform temperature conditions and average power induced elevated
(and therefore non-uniform) temperature conditions.  These results can then
be compared to the predictions of the PSAN model which has built into its
library the uniform temperature characteristics of ferrites, dielectrics,
and conductors.

PSAN also allows the engineer to study such things as the effects of
vertical air gaps between the center dielectric rib and the ferrite toroids,
or between the toroids and the waveguide wall.

## 8.2.2  Uniform Temperature Studies

Dual toroid phasers have been tested under uniform temperature conditions
from room temperature (25°C) to 100°C.  While the toroids were in place in
the housing their B-H loops were measured at each temperature and the phase
shift measured.  Simultaneous measurement of hysteresis and phase shift
characteristics allows a comparison of phase shift with remanent flux under
identical conditions.  These measured B-H properties can be compared
(scaled) with similar data taken as a function of temperature on the same
square toroids loose, outside the housing and on round toroids used for
calibration.

The round toroid data is taken as a standard measurement in the materials
laboratory.  Through the use of calibration standards and geometric
measurements the voltage readings obtained can be converted to drive and
remanent flux values.  Round toroids are thin walled and circular and their
uniform cross section provides for uniform flux.

The square toroids used in phase shifters have saturated, uniform
magnetization (flux) in their legs, but non-uniform magnetization in their

corners where the cross section is larger, and the flux bends around the curve. The hysteresograph used outputs voltages, not flux values, so these readings must be converted to flux (gauss) based on the data from round toroids of the same material.

When placed in the phaser housing the square toroids may be under significant stress, and their B-H properties may be modified. Again voltage readings from the hysteresograph can be converted to actual flux values to be used in the PSAN program that calculates phase shift.

The PSAN program has a corner correction that models the curved flux path that occurs at the corners of the round toroid where the magnetization is not perpendicular to the Rf magnetic fields.

A sample set of data is shown in Table 8-3. These readings were taken on the 0.11 Mn, G-265, material.

Table 8-3

Comparison of Theoretical and Experimental Values of Phase Shifter

| Temperature | Round toroid | Square toroid (loose) | Square toroid (in-house) | PSAN | Measured Data |
|---|---|---|---|---|---|
| (°C) | (gauss) | (volts / gauss) | (volts / gauss) | (degrees) | (degrees) |
| 25 | 758 | 1.692 / 758 | 1.676 / 751 | 112.2 | 109.2 |
| 40 | | 1.679 / 752 | 1.662 / 745 | 111.3 | 107 |
| 55 | | 1.661 / 744 | 1.643 / 736 | 109.9 | 105.3 |
| 70 | | 1.636 / 733 | 1.617 / 724 | 108.1 | 102.6 |
| 85 | | 1.618 / 725 | 1.579 / 707 | 105.4 | 100. |
| 100 | | 1.549 / 694 | 1.547 / 693 | 103.2 | 95.8 |

The PSAN calculated values were obtained assuming a perfect fit between the ferrite toroids and the dielectric rib. If one assumes that there is a half mil air gap there (0.0005"), then the phase shift is reduced by a factor of 0.971. This would provide perfect agreement between the calculated and observed values of 109 degrees at 25°C.

It is seen in the data of Table 8-3 (and in graphs drawn elsewhere) that the observed phase shift falls off more rapidly with increasing temperature than does Br or calculated values of phase shift. The observed decrease in Br from 25°C to 100°C is by a factor of 0.923. The PSAN predicted decrease in phase shift is by a factor of 0.919, and the observed decrease in phase shift is by a factor of 0.877.

Three possible causes for this (small) discrepancy in predicted and observed phase shift values can be imagined.

1. Air gaps in the structure that increase with increasing temperature.

2. Stresses induced by changes in temperature that cause the material to have a non-uniform remanence.

3. Changes in permittivity with temperature that are outside the values contained in the PSAN library.

Each of these has been explored to some extent, as will be described below.

Air Gaps

The ferrite and dielectric elements of the phaser are held by friction between the top and bottom plates of the waveguide housing. They are not bonded together, because they have different coefficients of thermal expansion and bonding would therefore introduce additional mechanical stress with changes in temperature. The ferrite and metal parts also have

- 177 -

different expansion coefficients, and therefore as the temperature is increased the width of the waveguide increases by more than does the transverse dimensions of the dielectric and ferrite parts. Since the dielectric is centered in the waveguide, it will remain centered as the temperature is increased and the waveguide grows with increasing temperature. The ferrites on either side will be pulled along with the expanding metal that presses against it. The net result is that a small air gap will open between the ferrite toroids and the dielectric center rib. Air gaps at this location always decrease the amount of phase shift in the structure.

The PSAN program was used to model this effect, and the results are shown in Figure 8-9. This graph shows the normalized phase shift as a function of the width of the air gaps that are assumed to exist on either side between the ferrite and the dielectric center rib. A one mil (.001") air gap will reduce the total phase shift to 95.3% of the phase shift available with no air gap. Over this small range of air gaps the reduction is linear with the dimensions of the air gap. To fully account for the reduction in phase shift seen at 100°C the air gaps would have to grow to 0.0008". Based on the dimensions of the housing and the coefficients of expansion of the metal and ferrite, one would expect the air gaps to be about 0.0002" at 100°C. While the air gaps no doubt contribute to the decrease in phase shift, they do not seem to fully explain the observed decrease.

## Thermally Induced Stresses

Since the ferrite and metal have different expansion coefficients, it is also reasonable to expect that non-uniform mechanical stresses may occur in the ferrite. Magnetostrictive effects could then lead to a non-uniform remanence in the ferrite. The total remanent flux is measured in the housing, but we do not know that it is uniform. One might suppose that the outer portion is under greater stress and therefore has less flux than the inner portion.
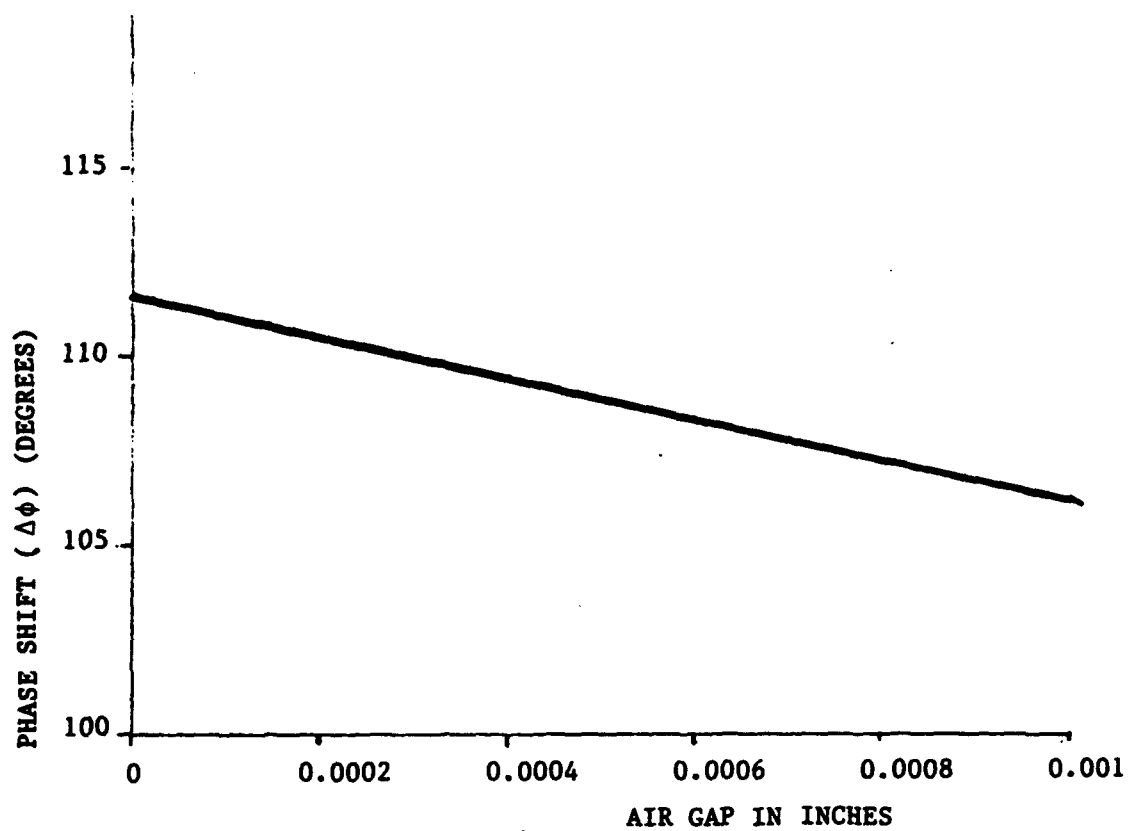
FIGURE 8-9   EFFECT OF AIR GAPS ON DIFFERENTIAL PHASE SHIFT

The effects of a nonuniform remanence was studied using the PSAN program by modeling the ferrite toroid as two concentric toroids having different values of remanent flux while maintaining the total flux constant. Two equal area regions of the toroid were used, one with a remanence of 738 gauss and the other with 600 gauss. The average flux then remained at 669 gauss. Figure 8-10 shows a representation of this model. Two cases were analyzed. (Case A): When the inner shell has a reduced Br value (600g) and the outer shell (nearest the dielectric) had an increased Br (738g), the total phase shift is predicted to decrease by 2.9%. (Case B): When the situation is reversed so that the inner region has the higher Br value, the total phase shift is predicted to increase by 2.7% over that of a uniform toroid with a 669 gauss remanence.

These results are somewhat surprising as one would normally expect that the largest phase shift would occur for the case of having the highest flux nearest the dielectric rib. The observed results arise because in the S145 design the dielectric loading is so light that the region of circular polarization lies well within the ferrite toroids.

The waveguide housing construction is such that one would expect the stress to be largest near the center of the housing, at the dielectric rib. The ferrite toroid would then experience more stress at its outer shell (Case B above). The predicted effects do not agree with those observed experimentally (actual phase shift falls off rather than increases) and the magnitude of the change in Mr required is much larger than one would reasonably expect. It can be concluded that this effect does not explain the greater decrease in phase shift than in Br as temperature increases.

Uncatalogued Changes in $\varepsilon_r$ with Temperature

PSAN has a library of "known" temperature coefficients of $\varepsilon_r$ for both ferrites and dielectrics. If the ferrite (or dielectric) has a true coefficient different from that in the library, that would lead to an
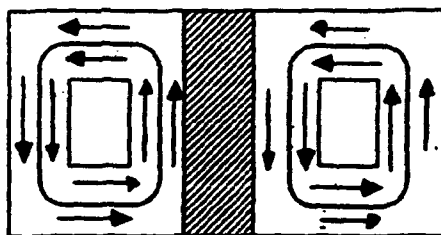
FIG. 8.10    Dual Toroids showing non-uniform remanent flux

unpredicted change in phase shift. By assuming different coefficients of $\varepsilon_r$, we can examine how large the coefficient would have to be to explain the observed effect. The results are tabulated below where the assumed temperature coefficient of $\varepsilon_r$ is listed along with the resultant change in phase shift as temperature is raised from 25°C to 100°C.

| $\delta\varepsilon/\delta T$ (ppm) | % change in $\Delta\phi$ |
|---|---|
| 170 | -10.3 |
| 510 | -11.4 |
| 940 | -12.8 |

These changes are also based on the library change in $B_r$ as a function of temperature. The 170 value is the commonly accepted value for garnets. A change of 940 ppm would be required to explain the measured results in phase shift. This is an unreasonably large coefficient, and thus the dependence of $\varepsilon_r$ on temperature it is not believed to be the cause of the roll-off in phase shift.

In summary, the uniform temperature results do not show evidence of additional, non-uniform stress effects and are modeled with good accuracy by the PSAN program. It does appear that small air gaps are opened up between the dielectric and the ferrite at elevated temperatures. These air gaps cause some reduction of available phase shift.

8.2.2 High Average Power

Data taken during Phase I on the performance of phasers at high average power levels are shown in Section 6, Figures 6-16 to 6-22. Both the computer aided thermal analysis and the experimental data indicate that the hottest parts of

the ferrite will reach a temperature of about 31°C against a heat sink temperature of 16°C for an input power level of 400 watts. As seen in Figure 8-1 the temperature profile in the ferrite is quite non-uniform. Since the total remanent flux is limited by the weakest link in the flux path, the remanence of the toroid might be expected to be that of a toroid uniformly heated to 31.7°C, unless the non-uniform temperatures produced by average power heating cause further reduction in flux due to stress. By the same argument the measured phase shift should also be that of toroids uniformly heated to 31.7°C.

Table 8-4 lists fractional changes in $B_r$ and phase shift as the input average power is increased from 10 to 400 watts for the several materials studied.

Table 8-4

Fractional changes in remanence and phase shift with average power

| Material | Mn | $B_r(400)/B_r(10)$ | $\Delta\Phi(400)/\Delta\Phi(10)$ |
|---|---|---|---|
| TT G1002 | .09 | 1.02 | 1.04 |
| G-265-35 | .09 | 0.97 | 0.968 |
| G-265-36 | .11 | 0.98 | 0.97 |
| G-265-37 | .13 | 0.982 | 0.985 |
| G-265-33 | .15 | 0.972 | 0.979 |
| G-265-42 | .17 | 0.968 | 0.951 |
| G-265-41 | .21 | 0.985 | 0.917 |

With the exception of the last two entries (0.17 and 0.21 Mn) all phase shift data track the remanent flux data to within one percent. Since these measurements are made with different drivers (in one case the driver for the hysteresis tester and in the other a flux driver) this is quite good agreement.

One question remaining is whether the decrease in both flux and phase shift is greater for induced heating by Rf power than it would be for uniform heating. Since the increase in temperature is only 15°C, the effects seen are small. Comparison of uniform and Rf heating is made more difficult by the fact that the

15° rise caused by Rf heating is against a lower base (16°) than was used for the uniform heating tests (25°C). Table 8-5 lists the fractional decrease in $B_r$ measured in a 15° change in uniform temperature (from 25° to 40°) and the fractional decrease resulting from a 15°C change caused by Rf power (from 16° to 31°).

TABLE 8-5

COMPARISON OF CHANGES IN $B_R$ CAUSED BY UNIFORM AND RF HEATING

| MATERIAL | Mn | $B_r(40°)/B_r(25°)$ uniform heating | $B_r(31°)/B_r(16°)$ Rf heating |
|----------|-----|------------------------------------|-------------------------------|
| TT G-1002 | 0.09 | 1.115 | 1.04 |
| G265-35 | 0.09 | 1.0 | 0.97 |
| G-265-36 | 0.11 | 0.992 | 0.98 |
| G-265-37 | 0.13 | 0.992 | 0.982 |
| G-265-33 | 0.15 | 0.994 | 0.972 |
| G-265-42 | 0.17 | 0.956 | 0.968 |
| G-265-41 | 0.21 | 0.979 | 0.985 |

It appears that the decrease in remanent flux is somewhat greater in the case of Rf heating for Mn contents of 0.15 or less. This observation clearly does not hold for the two higher Mn doping levels. Based on the temperature dependence of the saturation magnetization ($4\pi M_s$) one would expect less change at the lower range of temperatures (16° to 31°) than at the higher range (25° to 45°). In view of this fact, the small differences in roll off of $B_r$ are more significant. The non-uniform heating and the attendant differential expansion of the top and bottom parts of the toriod would be expected to produce transverse stress. One could argue that we are, in fact, seeing a greater decrease in $B_r$ due to these transverse stress effects for the lower Mn bearing samples, and that at the two highest Mn contents the transverse stress actually augments the remanent flux, as one might expect for a positive value of $\lambda_{111}$. These observed effects are, however, so small that drawing such conclusions from this data is highly speculative.

At best one can observe that there is not much additional degradation in remanent flux caused by the non-uniform Rf heating in these materials, and that the small effects observed are consistent with other observations on the signs of the various magnetostrictive coefficients.

# 9.0 SUMMARY OF RESULTS AND SIGNIFICANT OBSERVATIONS

## 9.1 MATERIAL FABRICATION

No major problems were experienced in fabricating the manganese substituted garnet compounds studied during the program. Processing parameters were adjusted to achieve optimization in the ceramic, electrical and magnetic characteristics of the compounds. A very good quality microwave polycrystalline material was achieved.

Some variations in the processing were implemented as a function of manganese (Mn) substitution. A firing temperature of 1440°C was found to be optimum for most of the G-265 (56 2/3%YIG · 43 1/3%GdIG) compositions; however at the higher Mn substitutions (0.15 and greater) slightly lower firing temperature (1425°C) provided improved characteristics.

Studies were made to define the range of iron content (starting iron content deficiency) supportive to achieving single phase garnet structures. For the processing used, the iron deficiency range from 2.25% to 3.0% appeared acceptable. Br values, on the average, appeared better toward the iron rich side of the garnet compositional range.

Properties (particularly Br values) of the various Mn substituted compounds appeared to be more sensitive to final firing (sintering) temperature than expected. This observation could be related to insufficient mixing (grain to grain composition) or the presence of the manganese and its influence on the sintering process. Firing in an oxygen environment, while not always used, provided some improvement in property reproducibility particularly for the higher firing temperature.

The microstructure of the compounds was monitored toward achieving uniformity in grain size. Good hysteresis properties were achieved.

Coercive fields near 1.5 oersteds were typical indicating an average grain structure somewhat smaller than the comparable garnet compounds possessing coercive fields of one oersted or less.

Manganese (Mn) chemistry was investigated to provide assurance that $Mn^{+3}$ was entering the garnet structure. The starting carbonate ($Mn^{+2}CO_3$) appeared to be converted to $Mn_2^{+3}O_3$ (by color and weight change) above 600°C; above 1000°C, a small hint of brown color was noted, perhaps indicating some decomposing of $Mn_2O_3$. Weight change suggested some formation of MnO.

However, varying the mixing procedure (adding Mn after presintering, for example) and presintering and firing temperatures did not produce any measurable changes in the properties of the compounds as related to potential changes in the Mn content or valence. All investigations and resultant data indicate that $Mn^{+3}$ is the prime manganese ion captured in the structure.

Analytical evaluation via the energy dispressive spectrocopy capabilities of scanning electron micrographs did not identify any phase variational problems associated with the various Mn substitutions. The sensitivity of this technique was not adequate to provide useful information indicating the level of Mn substitution achieved.

The conversion of the total manganese substituted to the $Mn^{+3}$ ion in the finalized garnet structure cannot be experimentally/analytically verified; however, the stress sensitivity characteristics of the resultant compounds to mixed Mn content was very evident. Differences in stress sensitivity were readily observed for changes in Mn of 0.02 per formula unit (1% change in the Fe-Mn cation content).

## 9.2     STATIC STRESS TESTS

A very adequate static stress fixture, referred to as the phaser simulator test fixture (PSTF), was generated that provides static stress sensitive evaluation (No Rf) of materials as a function of pressure and temperature.

Stress sensitive data from this static test fixture correlates well with the data collected from waveguide dual toroid phase shifters. The PSTF can be used to evaluate the stress characteristics of toroidal ferrite material adequately to predict performance associated with the stress environment of phase shifter designs.

Static test structures generated and evaluated which utilized threaded screw mechanisms to generate stress (pressure) did not provide reproducible performance particularly for stress levels below 1000 PSI.

Hysteresis properties of toroids appear to be very sensitive to some stress conditions such as deformation of the structure by bending or twisting or multi-mode deforming created by applying too much (or non-uniform) stress.

Longitudinal (axial stress perpendicular to the remanent magnetization) and transverse (parallel to the remanent magnetization in the phase active legs of toroids in waveguide structures) stress tests were conducted. Transverse stress occurs primarily from the top-to-bottom crush required in the phaser for acceptable Rf performance. Longitudinal stress is primarily the resultant of differences in thermal expansion coefficients between the ferrite magnetic material and the metallic Rf structures in which the material is captured. Longitudinal stress effects present the most troublesome design and performance problems.

Non-uniform heating of the toroidal material as a function of Rf power may also produce some difficult stress related problems. The center section of the dual toroid structure may become hotter than the outer return legs. Both thermal analysis and measured data, however, indicate that such differences in temperature are small at average powers of 400 watts. High average power Rf tests have also indicated that the apparent stress effects observed are more closely related to general temperature effects than to differential heating within the toroid.

For the toroid structures tested, stress levels above 1000 PSI appear to begin to alter the hysteresis properties by deformation. The range of

transverse stress (pressure) utilized (or experienced) in typical waveguide phase shifter designs was not known prior to this study effort. Data collected from static stress tests when compared to phaser housing tests, indicate that typical pressures utilized are in the range of 100 PSI.

In stress sensitive toroidal structures, any stress supportive to reducing the remanent magnetization is readily observed; a stress supportive to enhancing the remanent magnetization is weakly observed, most often by observing no change in the remanent states while the coercive field is observed to slightly increase.

Mn substitutions are <u>very valuable</u> in reducing the stress sensitivity of the garnet compounds. In the compounds studied, substitution of 0.09 Mn per formula unit, as used in a similar commercially available compound (Trans-Tech G-1002), does not appear to be optimized for minimizing longitudinal stress sensitivity. Our data indicate that a larger Mn substitution is significantly better (0.11 to 0.13 Mn per formula unit).

The data collected indicates the 0.09 Mn substitutions are more near optimum for transverse stress as claimed by the supplier.

For longitudinal compressive stress, data indicate that $\frac{Br(Stress)}{Br(No\text{-}Stress)}$ equals approximately one (stress insensitive) for a Mn substitution of 0.13 and stress values up to 500 PSI.

Mn substitutions in the range of 0.11 to 0.13 appear to provide materials exhibiting the best stress insensitive characteristics in waveguide phase shifter structures.

The stress sensitivity of these materials is dependent on the magnitude of the magnetostrictive forces (characteristics) relative to other forces (fields) interacting with the magnetization. For example, in the same composition where the coercive field is changed via microstructure (changing and controlling grain size), the structures possessing larger coercive field

(smaller grain size) would exhibit less change in hysteresis characteristics with stress. Similar responses are observed in materials with lower Br values due to localized demagnetizing effects (higher porosity and/or lower density, for example). Mn substitutions to reduce or compensate magnetostrictive forces are much more valuable in higher quality ceramics where the effective field associated with magnetocrystalline anisotropy is the dominate influence on the remanent magnetization.

As noted in the data presented in Section 7, a hysteresis was observed in the Br versus temperature response of the materials as evaluated in the PSTF. The magnitude of the temperature hysteresis was dependent on Mn content. Varying the Mn content from 0.09 to 0.21 reversed the direction of the observed temperature hysteresis from clockwise (CW) to counter clockwise (CCW). All 0.09 Mn substituted materials exhibited CW temperature hysteresis characteristics and all 0.15 and higher Mn substituted compounds exhibited CCW responses. Most data on the 0.11 Mn substituted compounds exhibited slight CW hysteresis responses with the 0.13 Mn exhibiting slight CCW. The observed temperature hysteresis was somewhat dependent on transverse compressive stress. For transverse stress levels near 100 PSI, almost no hysteresis was observed for these compounds which strongly indicated that magnetostrictive compensation was being achieved.

Analysis of hybrid YIG compounds other than the G-265 composition indicated similar magnetostrictive constants so that similar $Mn^{+3}$ substitution should provide improved characteristics in these compositions also. YIG with 0.13 Mn substitution was prepared and found to have minimal stress sensitivity similar to the G265 with 0.13 Mn.

The magnetostrictive constants and thus the stress sensitivity of the garnet materials (and other ferrimagnetic compounds) are known to vary with temperature. As noted in Table 2-1, the reported magnetostrictive constants of YIG and GdIG decrease with increasing temperature but at a relatively slow rate. The change, however, is significant and should be noted even though the data collected during these investigations do not indicate any strong evidence suggesting a difference in stress sensitivity at different temperatures.

Magnesium-manganese ferrite materials, such as Trans-Tech TT 1-105, exhibit very stable hysteresis characteristics with stress. This compound was evaluated during this program and exhibited good, expected characteristics. The improved stress insensitive garnet compounds, G-265 (0.11Mn) and G-265 (0.13Mn), exhibited characteristics very similar to this Mg-Mn ferrite.

## 9.3    PHASER HOUSING STRESS TESTS

With the materials assembled into the phase shifter structure, a hysteresis in $B_r$ and phase shift was observed as a function of temperature. This hysteresis changed direction from clockwise to counter-clockwise for Mn substitution below 0.11 and above 0.13 respectively. The hysteresis in the phase shift response corresponded to that of Br. Best performance was observed for the 0.11 and 0.13 Mn substitutions. The direction of the temperature hysteresis, when evident, reversed direction from CW to CCW between these Mn substitutions. These compounds exhibited very small changes in $B_r$ due to top-to-bottom "crush" when captured in phaser housings (transverse stress was estimated to be near 100 PSI). No hysteresis in $B_r$ versus temperature was observed for "loose" toroids. For comparable stress levels, the Br versus temperature hysteresis characteristics in the dual toroid phaser housing structure were reduced in magnitude compared to similar tests on single toroids in the PSTF. This apparently results from the presence of the dielectric center core in the dual toroid structure which provides some stress support to the ferrite toroids.

The data appear to be consistent with stress resulting from differences in expansion coefficients of the metallic housing and garnet material. Magnetostrictive related hysteresis in phase shift as a function of temperature has been reduced from 10° for Trans-Tech G-1002(0.09 Mn) to less than 1° for the 0.11 or 0.13 Mn substituted G-265 garnet compound over the temperature range of 25°C to 100°C in actual phaser structures designed for high power operation.

The data presented in Section 6 was collected during Phase I of the Program and utilized a "drum" top phaser structure as a test structure. The G-1002

(0.09 Mn) exhibited a very large temperature hysteresis in this structure (Figures 6-2 and 6-3). Considerable improvement in characteristics were observed in the data for G-265 (0.09 Mn) in this same test structure. A clockwise temperature hysteresis was observed for both materials in Br and phase but the magnitude was greatly reduced for the G-265 (0.09 Mn) (from 15% to 2%). The G-1002 (0.09 Mn) appeared to be considerably more sensitive to longitudinal and transverse stresses than the G-265 (0.09 Mn). Microstructure of these two materials are different with the G-265 possessing a smaller and more uniform grain structure. The higher coercive field of the G-265 (1.5 oersteds compared to 0.9 oersteds for G-1002) would support the observed response but the magnitude of the difference was surprising and unexpected.

These same materials were re-evaluated during Phase II in the PSTF test structure at 200 PSI and the results are presented in Figure 7-8. The stress characteristics of the G-265 (0.09 Mn) were observed to be somewhat better than the G-1002 but difference in stress sensitivity can more readily be assessed and accepted as due microstructure.

The response to stress of the 0.11 Mn and 0.13 Mn substituted G-265 compounds, however, exhibited added improvement compared to the G-265 (0.09 Mn) including a dramatic reversal of the temperature hysteresis characteristics from cv to ccv. This reversal clearly suggests the optimum Mn content for minimum stress sensitivity in the phaser structure.

## 9.4    HIGH AVERAGE RF POWER TESTS

These tests were conducted to evaluate stress resulting from differences in heating of inner and outer legs of the toroid. The measured data did not present any discernible evidence of change in performance due to induced stress resulting from differential heating. The operational temperature of the phaser changed from +15 to +32°C for a change in incident Rf power from 10 to 400 WATTS CW, respectively. Phase shift and $B_r$ exhibited a hysteresis over this range of power and corresponding temperature change. Best results were obtained for Mn substitution in the range 0.11 to 0.13. Hysteresis in the phase and $B_r$ data are consistent with that observed in temperature tests alone with no high power Rf.

Hysteresis with power/temperature (range noted above) was observed to be less than 0.5° for Mn substitutions of 0.11 and 0.13.

## 9.5 STRUCTURAL CONSIDERATIONS TO REDUCE STRESS SENSITIVITY

RF structure used in these studies was a "soft top" housing where transverse stress on the ferrite structure results from controlled compression of silicon rubber. To reduce stress effects, RF housings should be designed to provide minimum constraint on the material. A dual toroid, plated structure with some improved mechanical packaging would appear to be a design approach possessing minimum constraint features.

Typical dual toroid soft top waveguide phaser structures presently require a transverse stress on the ferrite structure in the range of 100 PSI. Waveguide dual toroid structures will be less affected by stress than single toroid designs.

## 9.6 WHAT IS THE IMPACT OF THE DATA COLLECTED ON ORIGINAL PLANS, EXPECTATIONS AND/OR PROJECTIONS?

Original plans included preparing and evaluating $Mn^{+3}$ substituted garnet compounds up to $Mn^{+3}$ substitution of 0.21 per formula unit in $Y_{1.7} Gd_{1.3} Fe_{5-x} Mn_x O_{12}$ and to characterize the stress sensitivity of these compounds as a function of Mn content. A 56 2/3% YIG · 43 1/3% GdIG compound (G-265) was selected as the composition for study. This compound possesses a $4\pi M_s$ value of approximately 1100 gauss and was similar to TT G-1002 in overall characteristics. The TT G-1002 with 0.09 Mn had been used in previous high power waveguide phaser structures but had exhibited considerable stress sensitivity with temperature. The 0.09 Mn substitution was considered best to reduce magnetostrictive sensitivity to stresses parallel to the magnetization such as the top-to-bottom crush in waveguide phasers. Experimental data on the temperature characteristics of phasers indicated detrimental changes in phase with temperature due to stress sensitive (magnetostrictive) properties of the material. Such temperature generated stresses appear to be more perpendicular to the remanent magnetization than parallel.

Information reported in the published literature [4,10] regarding magnetostrictive characteristics of $Mn^{+3}$ in garnets suggested that larger amounts of $Mn^{+3}$ would perhaps be valuable in achieving improved performance in the stress environment of waveguide phase shifters.

The studies conducted on this program have revealed that $Mn^{+3}$ substitutions in the range of 0.11 to 0.13 produce compounds that provide stress insensitive performance in waveguide phasers. The phase reproducibility with temperature cycling can be an order of magnitude improved in some garnet compounds. The stress characteristics achieved were observed to be very sensitive to $Mn^{+3}$ content.

The original analytical evaluation also recognized published studies (by Dionne) [4] that suggested that materials possessing $\lambda_{111}=0$ with $K_1>0$ would yield stress insensitive characteristics. The effects of $Co^{+2}$ substituted into the garnet structure together with $Mn^{+3}$ appeared promising toward achieving such characteristics. The original plans thus included the examination of substituting $Co^{+2}/Si^{+4}$ into the garnet structure for $Fe^{+3}$ together with $Mn^{+3}$ to achieve the characteristics of $K_1>0$ and $\lambda_{111}=0$.

After studying the $Mn^{+3}$ substitution the following compositions were prepared for evaluation:

$$Y^{+3}_{1.7} \ Gd^{+3}_{1.3} \ Fe^{+3}_{4.845-2x} \ Mn^{+3}_{0.155} \ Co^{+2}_{x} \ Si^{+4}_{x} \ O^{-2}_{12}$$
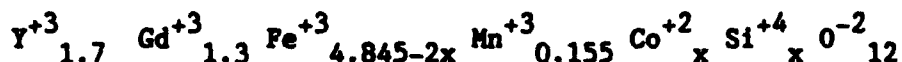
for x = 0.0225 and 0.01125

In both cases the resultant hysteresis curves were rather skewed and the values of Br were markedly below those of other garnets. Longitudinal stress did produce a measurable increase in Br indicating a positive $\lambda_{111}$ characteristic. It is entirely likely that the conditions desired, namely $K_1>0$ and $\lambda_{111}=0$, were not achieved; however the hysteresis characteristics observed did not appear to warrant further exploration of this family of compounds since reasonably good stress insensitive compounds were being obtained from only $Mn^{+3}$ substitutions. Furthermore, the cobalt substitution increased the magnetic loss tangents of these garnets.

G. Dionne, MIT(LL) has reported [2,3,4] results of his investigations of $Mn^{+3}$ substitutions in YIG including his measured data on magnetostrictive constants ($\lambda_{111}$ and $\lambda_{100}$) measured on single crystal samples (Figure 2-9). His results from measurements of magnetostrictive constants indicate that $Mn^{+3}$ substitution has the following characteristics:

| | $\lambda_{100}$ | $\lambda_{111}$ | $\lambda_S$ |
|---|---|---|---|
| Effect of one Mn $^{+3}$ ion Substitution Per Formula Unit in YIG | $+69 \times 10^{-6}$ | $+14 \times 10^{-6}$ | $+36 \times 10^{-6}$ |
| Magnetostrictive Constants of YIG | $-1.3 \times 10^{-6}$ | $-2.8 \times 10^{-6}$ | $-2.2 \times 10^{-6}$ |

His measured results on polycrystalline garnets providing stress insensitive remanence were as follows:

$$\frac{\partial R_{||}}{\partial \sigma} = 0 \text{ for } Mn^{+3} \text{ substitution of 0.09 and stress parallel to M;}$$

$$\frac{\partial R_{\perp}}{\partial \sigma} = 0 \text{ For } Mn^{+3} \text{ substitution of 0.17 and stress perpendicular to M.}$$

Dionne's theory predicted 0.05 and 0.065 respectively for $Mn^{+3}$ substitution based on measured single crystal magnetostrictive constants and his independent grain model for anisotropy stress energy.

Using the measured single crystal $\lambda_{111}$ values (Dionne's data) and adjusting $\lambda_{100}$ to match the stress insensitive polycrystalline results (Dionne's data), the effects of one $Mn^{+3}$ ion substitution per formula unit would be as follows:

| $\lambda_{100}$ | $\lambda_{111}$ | $\lambda_S$ |
|---|---|---|
| $+21 \times 10^{-6}$ | $+14 \times 10^{-6}$ | $+16.8 \times 10^{-6}$ |

The above computation produces a $\lambda_{100}$ considerably different from that computed from Dionne's measured single crystal data.

If $\underline{\delta R} \perp$ is computed using the above values for $Mn^{+3}$, then $\underline{\delta R} \perp$ vanishes for
$\quad \delta\sigma$ $\quad\quad\quad\quad\quad\quad\quad\quad\quad\quad\quad\quad\quad\quad\quad\quad\quad\quad\quad\quad \delta\sigma$
for $Mn^{+3}$ substitution of 0.122 with stress perpendicular to M. This value
is also a reasonable fit to Dionne's experimental polycrystalline data (see
Figure 2-10).

If the above magnetostrictive effects of $Mn^{+3}$ are used and applied to the
G-265 compound studied during this program, the predicted results are shown
in Figure 9-1.

These results indicate:

$$\frac{\partial R_{||}}{\delta\sigma_{||}} = 0 \text{ for } Mn^{+3} \text{ substitution of 0.073 and stress parallel to M;}$$

$$\frac{\partial R\perp}{\delta\sigma} = 0 \text{ for } 0.11 \ Mn^{+3} \text{ substitution.}$$

Also, $\lambda_s = 0$ for a $Mn^{+3}$ substitution of 0.122

These predictions are in good agreement with the experimental data
collected. The change in the direction of the observed temperature
hysteresis from CW to CCW for $Mn^{+3}$ substitutions of 0.11 and 0.13
respectively, indicate a change in the magnetostrictive characteristic
within this range. This range is indicated in Figure 9-1 and is consistent
with the predicted conditions of $\underline{\delta R} \perp = 0$ and $\lambda s = 0$, which could
$\quad\quad\quad\quad\quad\quad\quad\quad\quad\quad\quad\quad\quad\quad\quad \delta\sigma$
account the observed reversal in direction of the temperature hysteresis.
Other investigators [10] have also reported significant reduction in the
variation of remanent phase shift with external stress for manganese
substitutions of 0.15.

During the program other garnet compositions were prepared to further
evaluate these predictions and observations. $Mn^{+3}$ substitutions of 0.13 in
YIG (G203-22 with $4\pi M_s = 1780$ gauss) as well as in a YIG-GdIG (G231-13 with
$4\pi M_s = 1600$ gauss) produced compositions with equally low stress sensitivity.
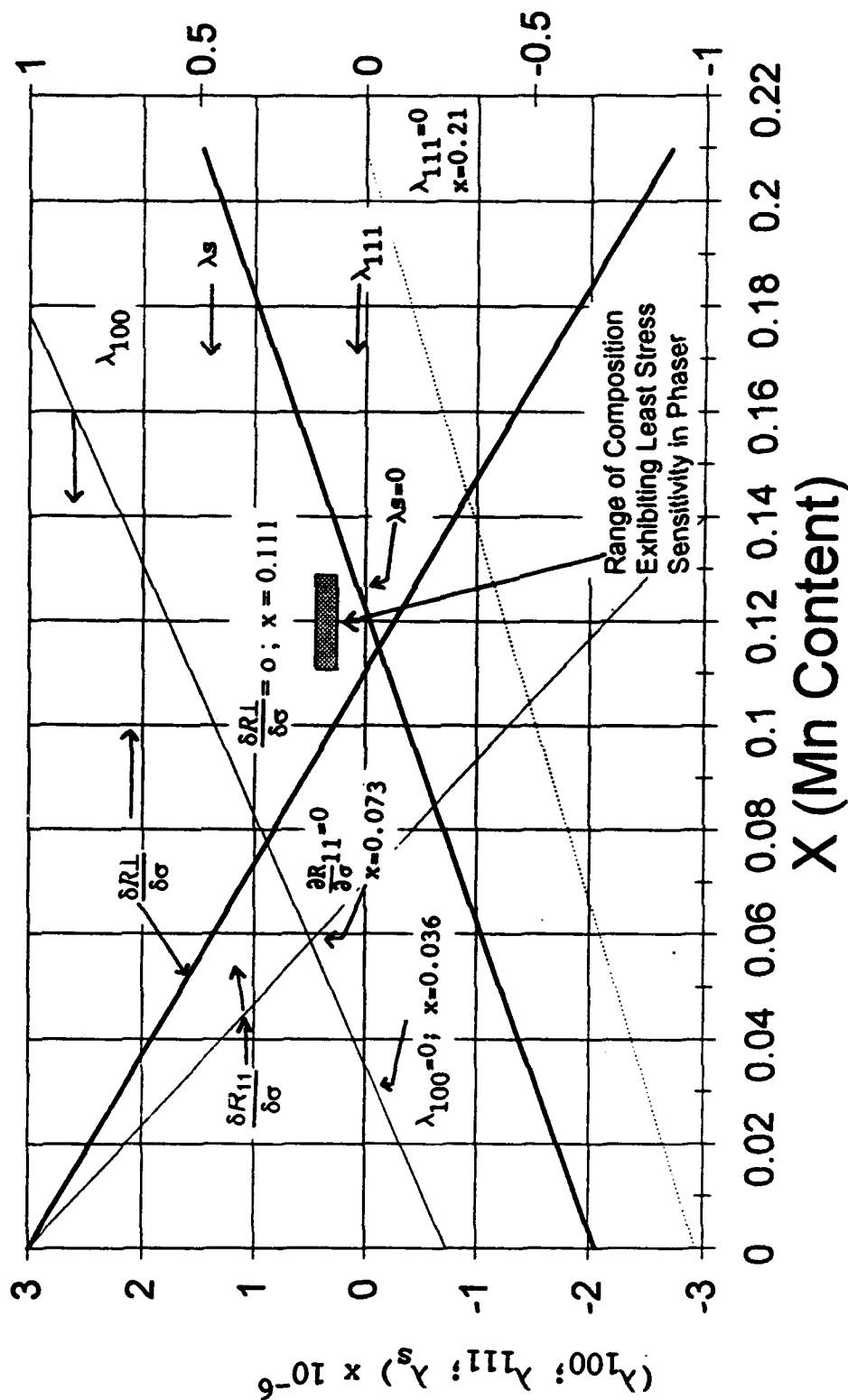
FIGURE 9-1 MAGNETOSTRICTIVE CHARACTERISTICS OF G-265

The predicted optimum value of $Mn^{+3}$ to minimize stress sensitivity will vary with composition. The predicted values are presented in Figure 9-2 for the yttrium-gadolinium iron mixed garnets. The G-265 composition is noted.

Similar predictions can be generated for the yttrium-aluminum iron or yttrium gallium iron garnets by using the measured and reported data for gallium substituted YIG presented in Table 2-2. Aluminum and gallium substitutions in hybrid YIG compounds are very similar. Aluminum is very similar to gallium in structure and predominately locates on the same lattice site (24d) in the garnet structure, so this substitution produces almost identical effects on the magnetic and microwave properties of polycrystalline garnets.[11]

These predictions, therefore, assume that aluminum and gallium would yield very similar magnetostrictive characteristics. Figure 9-3 shows calculated results for these compounds.

The investigations, data collected, and results obtained during this program are expected to be very valuable to the generation of future high power, high precision ferrite phase shifters and the embedded impact these components have on switches and power dividers. The reduction achieved in stress sensitivity will also provide reduced costs via improved phaser structures and the reduced phase sensitivity to stress (pressure) associated with the assembly and manufacturing procedures required.
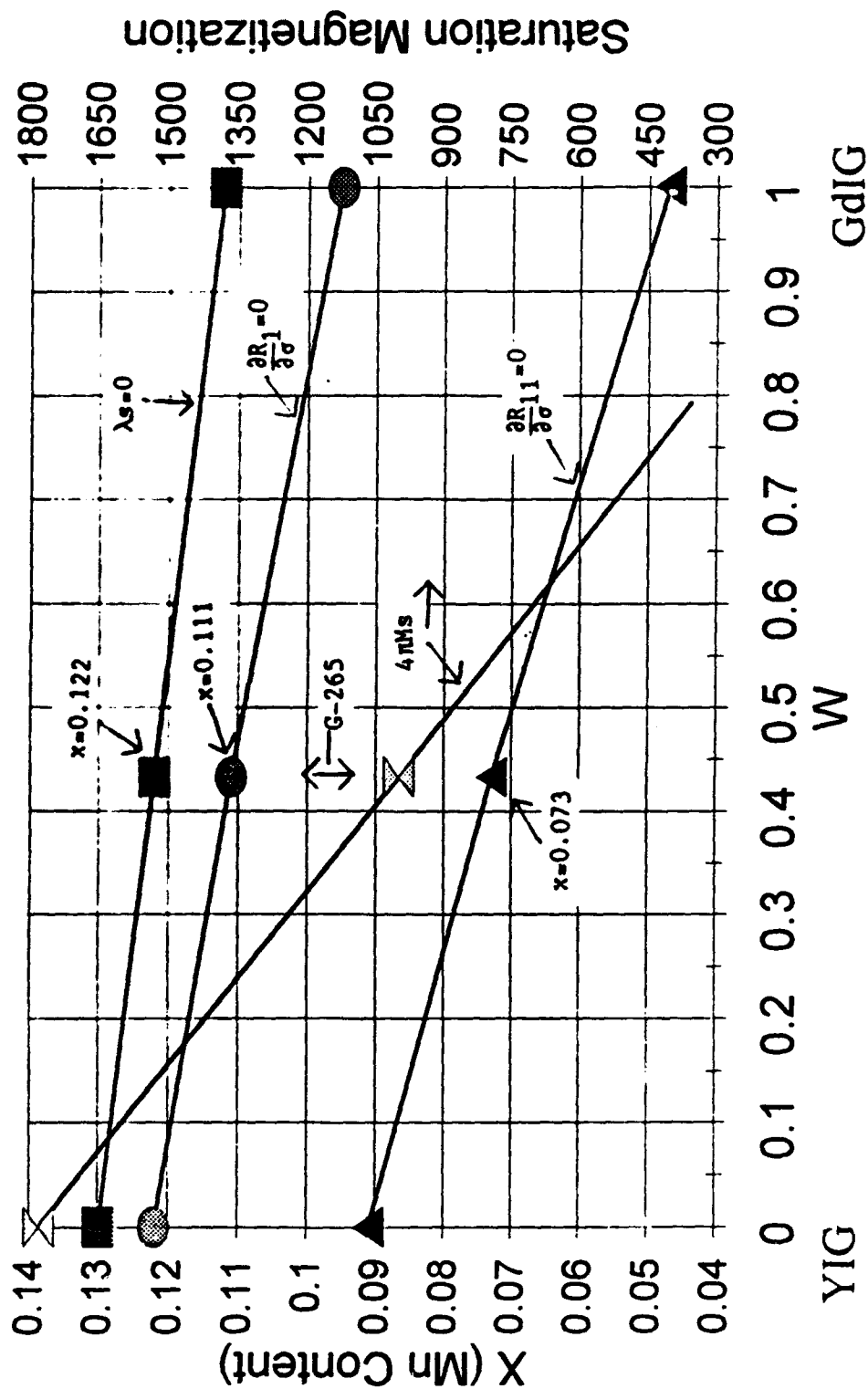
FIGURE 9-2    PREDICTED Mn SUBSTITUTION FOR STRESS REDUCTION FOR YIG-Gd1G
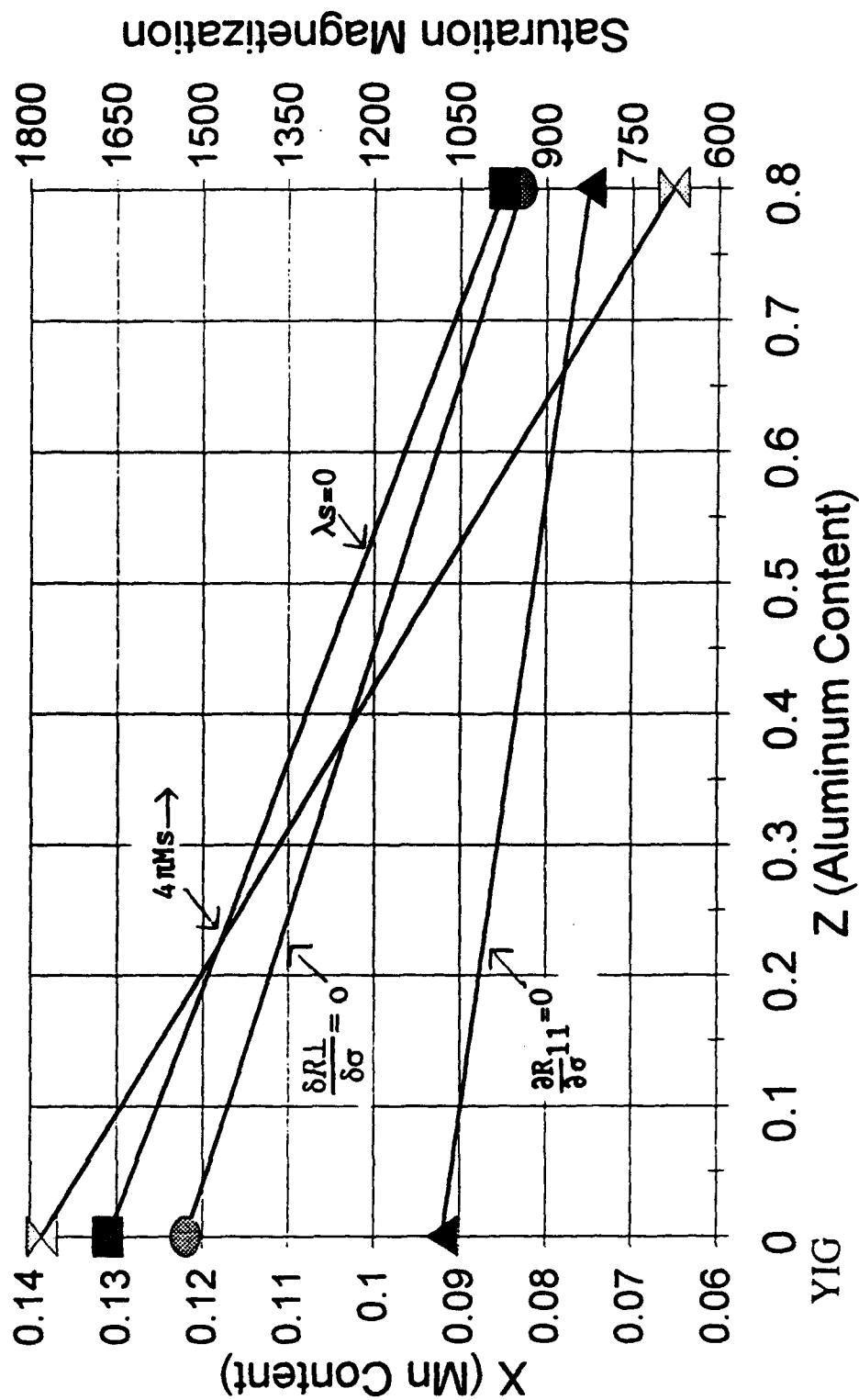
FIGURE 9-3   PREDICTED Mn SUBSTITUTIONS FOR STRESS REDUCTION IN YTTRIUM-ALUMINUM IRON GARNETS

# 10.0    REFERENCES

1.   S. Chikazumi, _Physics of Magnetism_. New York: Wiley, Chapter 12, pp 250-251.

2.   G. F. Dionne and P. J. Paul, _Materials Research Bulletin_, Vol 4, 1969, pp 171-178.

3.   Gerald F. Dionne, IEEE Trans on Mag, _Vol MAG-5_, No. 3, September, 1969, pp 596-600.

4.   Gerald F. Dionne, 1971 Intermag Conference, _IEEE Trans on Mag_, September 1971, pp 715-718.

5.   Iida, S., private communication.

6.   Sperry Microwave Electronics Co., Technical Report RADC Contract No. AF30(602)3490 "Advanced Ferrimagnetic Materials Applied to Digital Phase Shifters" August, 1965.

7.   G. F. Dionne, P. J. Paul, and R. G. West, J. Appl. Physics $\underline{41}$, 1411 (1970).

8.   H. J. VanHook and G. F. Dionne, _AIP Conference Proceedings #24_, p. 487, (Conf. on Magnetism and Magnetic Materials) 1974.

9.   G. F. Dionne, J. Appl. Phys. $\underline{50}$ #6, June 1979.

10.  Andrew S. Hudson, J. Snieder, and J. W. F. Dorleyn, _IEEE Trans. on Microwave Theory and Techniques_, Jan. 1971, p 119.

11.  Gordon R. Harrison and L. R. Hodges, Jr., "Microwave Properties of Polycrystalline Hybrid Garnets", Journal of The American Ceramic Society, Vol. 4, No. 6, May, 1961, pp 214-220.

# Ferrite Phase shifters Using Stress Insensitive Material

## DISTRIBUTION LIST

| | # Copies |
|---|---|
| Advisory Group on Electron Devices<br>201 Varick St., 9th Floor<br>New York, NY  10014 | 3 |
| Commander<br>Air Force Avionics Laboratory<br>AFWAL/ETM<br>Attn: T. Kemmerly<br>Wright Patterson Air Force Base, OH  45433 | 1 |
| Commander<br>U. S. Army ERADCOM<br>Attn: DELET-M, Mr. V. C. Gelnovatch<br>Fort Monmouth, NJ  07703 | 1 |
| Commanding Officer<br>Naval Research Laboratory<br>Attn:  Dr. J. Lawrence, Code 5740<br>Washington, DC  20375-55320 | 2 |
| Commanding Officer<br>Naval Research Laboratory<br>Attn: Dr. Denis C.Webb, Code 6850<br>Washington, DC  20375-5347 | 11 |
| Defense Logistics Agency<br>Defense Technical Information Center<br>Attn: DDAB<br>Cameron Station<br>Alexandria, VA  22314 | 2 |
| Microwave Applications Group<br>Attn:  Mr. William Hord<br>3030 Industrial Parkway<br>Santa Maria, CA  93455 | 1 |
| MIT Lincoln Laboratories<br>Attn:  Dr. Gerry Dionne<br>244 Wood Street<br>Lexington, MA  02173-9108 | 1 |
| Office of Naval Research<br>Attn: Dr. Ingham A. Mack, Code 224<br>800 N. Quincy Street<br>Arlington, VA  22217-5000 | 1 |
| Trans Tech, Inc.<br>Attn:  Mr. Russ West<br>5220 Adamstown Road<br>Adamstown, MD  21710 | 1 |

Westinghouse Research Labs                                    **# Copies**
Attn: Dr. J. D. Adam                                              1
MS 501-2W23
1310 Beulah road
Pittsburgh, PA  155235-5098